

Univerzita Karlova

1. lékařská fakulta

Studijní program: Biomedicína

Studijní obor: Biochemie a patobiochemie



UNIVERZITA KARLOVA
1. lékařská fakulta

Mgr. Barbora Vorlová, MSc

Příprava a charakterizace myší s vyřazeným genem pro glutamátcarboxypeptidasu II

Generation and Characterization of Glutamate Carboxypeptidase II
(GCPII)-Deficient Mice

Disertační práce

Vedoucí závěrečné práce/Školitel: RNDr. Pavel Šácha, Ph.D.

Praha, 2018

Prohlášení:

Prohlašuji, že jsem závěrečnou práci zpracovala samostatně a že jsem řádně uvedla a citovala všechny použité prameny a literaturu. Současně prohlašuji, že práce nebyla využita k získání jiného nebo stejného titulu.

Souhlasím s trvalým uložením elektronické verze mé práce v databázi systému meziuniverzitního projektu Theses.cz za účelem soustavné kontroly podobnosti kvalifikačních prací.

V Praze, 10. 9. 2018

Barbora Vorlová

Identifikační záznam:

VORLOVÁ, Barbora. Příprava a charakterizace myší s vyřazeným genem pro glutamátcarboxypeptidasu II. [Generation and Characterization of Glutamate Carboxypeptidase II (GCPII)-Deficient Mice]. Praha, 2018. 136 stran, 3 přílohy. Disertační práce. Univerzita Karlova, 1. lékařská fakulta, Ústav organické chemie a biochemie AV ČR, v.v.i.. Vedoucí závěrečné práce: RNDr. Pavel Šácha, Ph.D.

Identification record:

VORLOVÁ, Barbora. Generation and Characterization of Glutamate Carboxypeptidase II (GCPII)-Deficient Mice. [Příprava a charakterizace myší s vyřazeným genem pro glutamátcarboxypeptidasu II]. Prague, 2018. 136 pages, 3 appendices. PhD Thesis. Charles University in Prague, First Faculty of Medicine, Institute of Organic Chemistry and Biochemistry of the CAS. Supervisor: RNDr. Pavel Šácha, Ph.D.

ABSTRACT

Glutamate carboxypeptidase II (GCPII) is a transmembrane glycoprotein, which consists of short intracellular and transmembrane domains, and a large extracellular domain possessing carboxypeptidase activity. In the human body, GCPII fulfils a neuromodulatory function in the brain and facilitates folate absorption in the small intestine. In addition to the brain and small intestine, high level of GCPII is also present in the prostate and kidney. However, GCPII function in these tissues has not been determined yet. To study the role of GCPII in detail, several research groups attempted to inactivate GCPII encoding gene *Folh1* in mice. Surprisingly, the experiments led to rather conflicting results ranging from embryonic lethality to generation of viable GCPII-deficient mice without any obvious phenotype. This dissertation project aimed to dissect the discrepancy using alternative strategy for gene modification.

For this purpose, we designed TALENs that specifically targeted exon 11 of *Folh1* gene and manipulated mouse zygotes of C57BL/6NCrl genetic background. We analysed all genetically modified mice of F0 generation for presence of TALEN-mediated mutations and established 5 different GCPII-mutant mouse colonies from founder mice that altogether carried 2 frame-shift mutations and 3 small in-frame deletions. We thoroughly characterized all 5 colonies and found out that GCPII is not expressed in any of mice homozygous for *Folh1*-mutant variant. We were thus able to generate viable GCPII-deficient mice that breed normally and do not show any overt phenotype.

Produced GCPII-deficient mice were utilized for investigation of potential role of GCPII in the urogenital system. It was revealed that aged GCPII-deficient mice possess increased propensity to enlarged seminal vesicles, though the origin of this dilation is yet to be determined. In contrast, kidneys from aged GCPII-deficient mice did not display any pathological abnormalities and targeted metabolomics of mouse urine showed only 3 out of 193 measured metabolites discriminating GCPII-deficient and wild type mice.

In addition to dissecting the discrepancy found in the literature by showing that GCPII-deficient mice are viable, this dissertation project may set the direction for revealing the GCPII function in reproduction. Strikingly, supposed unimportance of GCPII for kidney function may open the door for GCPII-targeted anti-cancer treatment.

KEY WORDS: GCPII, PSMA, *Folh1*, GCPII-deficient mice, knockout mice, TALEN, enlarged seminal vesicles, urogenital system, kidney, urine metabolomics, NAAG, folate

ABSTRAKT

Glutamátkarboxypeptidasa II (GCPII) je transmembránový glykoprotein skládající se z krátké intracelulární a transmembránové domény a velké extracelulární domény, která vykazuje karboxypeptidasovou aktivitu. GCPII se podílí na neuromodulaci v mozku a absorpci folátů v tenkém střevě. Kromě těchto tkání se GCPII též vyskytuje v prostatě a ledvinách. Zde je ale její role neznámá. Za účelem zjištění funkce GCPII se několik vědeckých skupin pokusilo inaktivovat gen *Folh1* (kódující GCPII) v myši. Tyto experimenty však vedly k rozporuplným výsledkům. Zatímco dvě studie ukázaly, že inaktivace genu *Folh1* v myši vede k embryonální letalitě, jiné dvě studie publikovaly, že i po zmíněné inaktivaci jsou myši stále viabilní a navíc nevykazují žádný výrazný fenotyp. Cílem tohoto projektu bylo pokusit se připravit a charakterizovat myši s inaktivovaným *Folh1* genem pomocí alternativní metody genetické modifikace.

Za tímto účelem byly vytvořeny TALENy, které specificky cílily 11. exon genu *Folh1* v myších zygotách genetického pozadí C57BL/6NCrl. Narozená mláďata generace F0 byla analyzována pro přítomnost mutací v rámci genu *Folh1* a myši, které dohromady nesly 5 různých delecí, byly vybrány pro vytvoření mutantních linií. Linie, které nesly mutantní varianty genu *Folh1* na obou alelách, neobsahovaly detekovatelnou hladinu GCPII. Bylo potvrzeno, že myši s vyřazeným genem pro GCPII jsou viabilní, nemají reprodukční problémy a obecně nevykazují žádný výrazný fenotyp.

Modifikované myši byly použity pro zkoumání funkce GCPII v urogenitálním systému. Bylo zjištěno, že starší myši s vyřazeným genem pro GCPII mají zvýšený sklon k obstrukci semenných váčků. Zdroj tohoto fenotypu se ale nepodařilo objasnit. Ledviny starších modifikovaných myši nevykazovaly patologické změny a metabolická analýza moči poukázala pouze na 3 ze 193 možných metabolitů, jejichž hladiny se u modifikovaných myši a myši divokého typu významně lišily.

Kromě prokázání, že myši s vyřazeným genem pro GCPII jsou viabilní, by tento disertační projekt mohl napomoci k odhalení potenciální role GCPII v reprodukci. Pravděpodobný omezený vliv GCPII na funkci ledvin by poté mohl být užitečný pro vývoj protirakovinových léků cílených na GCPII.

KLÍČOVÁ SLOVA: GCPII, PSMA, *Folh1*, myši s vyřazeným genem pro GCPII, geneticky modifikované myši, TALEN, zvětšené semenné váčky, urogenitální systém, ledviny, metabolická analýza moči, NAAG, folát

ACKNOWLEDGEMENTS

I would like to express my deepest gratitude to my two supervisors – PhD supervisor Pavel Šácha and head of the lab Honza Konvalinka. I would like to thank Pavel for designing the dissertation project and introducing me to the GCPII world. I would also like to thank him for many discussions over the obstacles of the project, giving me valuable advices and critical proof reading of the thesis. I would like to thank Honza for accepting me as a member of his research group and introducing me into the science world. His professional as well as personal support has always meant a great deal to me. I am grateful for great amount of very valuable advices, high moral standards in science and a feeling that he is always ready to help when one needs it the most.

There are three people, without whom I would never get to the point of writing my thesis and they truly deserve my deepest gratitude – Franta Sedlák, Karolína Šrámková and Monika Sivá. I would like to thank Franta for helping me all the way through, for willingness to discuss each and every obstacle and detail of my project and for tons of experiments he performed and results he gathered in order to make this story complete. From more personal point of view, I would like to thank him for being such a supportive and always-trying-to-help-getting-over-my-PhD-crisis friend. I would like to thank Karolína for all the work she did in order to help me to gather enough data to publish my first author paper. I would also like to thank her for the enthusiasm and never ending support in moments, when I was so close to giving up.

I would like to thank Moni for literally everything. I was such a lucky girl meeting one of my closest friends and a real soul mate in the lab. I am thankful for all the discussions we had regarding our projects and possibility to share all my ups and downs with her anytime. I would like to thank her for always doing more than her best to figure out how to get me from yet another PhD crisis. I truly cannot imagine how the life will be without seeing her on a daily basis; I will miss our lunches and coffee breaks as well as all the crazy and cheering moments we regularly experienced.

I would also like to acknowledge all collaborators, who participated in the dissertation project. I thank Dr. Petr Kašpárek and Dr. Radislav Sedláček for preparing the GCPII-mutant mice, Dr. Marek Malý for statistical analysis of seminal vesicles enlargement, Dr. Tomáš Olejář for histopathology of the seminal vesicles and kidneys, Dr. David Friedecký, Radana Karlíková and their colleagues for metabolomic analysis and help with interpretation of the data and prof. Josef Zámečník for providing the human epididymis samples.

Huge thanks belong to all present or past lab colleagues, who have created a friendly atmosphere and great working environment. Namely, I would like to thank students Karča Janoušková, Martin Pehr and Lenka Šimonová for helping me with number of experiments. I would like to thank Tom Knedlík, Vašek Navrátil and Honza Tykvart for helping me orient myself in the GCPII world and giving me great amount of valuable advices. I want to acknowledge Míša Svoboda for helping me with some figures and critical proof reading of my PhD Thesis Summary. I would also like to thank Peťulka Dvořáková for mutual support and many “srackaland” conversions, which helped me to stay on the track. Last, but definitely not least, I would like to express my gratitude to my second mother (as she sometimes so nicely calls me as her oldest daughter) Jana Bimča Starková, who not only introduced me to her millions, but also was extremely supportive and has always been here to listen no matter what.

I would like to express my deepest gratitude to all my friends outside the lab, who have been helping me to overcome all the down periods of my doctoral studies. Special thanks belong to my life-gained sisters Dianka Pávová, Luci Seidlová and Zuzi Korábová, who have always believed in me and were here for me anytime I asked. Our retreatment weekends were always an energy boost for me so I deeply hope we will manage to keep going to these weekends until the retirement age and further. My deepest gratitude also belongs to Petra Fousová, a soul mate and a flat mate in one person, who's never ending support and always-to-be-here-for-me attitude made a great deal in getting to the point of submitting my thesis. Nobody outside our friendship understands and I would as well not understand if I was not part of it. After more than 10 years of our friendship, I still cannot believe how lucky I was to have met her.

Na závěr bych chtěla poděkovat svým rodičům, sestřám a babičce za veškerou lásku a podporu, kterou mi poskytují. Moc děkuji za vytvoření silného rodinného zázemí, které mi usnadnilo úspěšné dokončení vysokoškolský studií. V dnešním světě není takové zázemí vůbec samozřejmostí, a proto si ho velmi považuji.

TABLE OF CONTENTS

| | |
|---|-----------|
| ABBREVIATIONS | 10 |
| 1. INTRODUCTION | 12 |
| 1.1. DISCOVERY OF GLUTAMATE CARBOXYPEPTIDASE II (GCPII)..... | 12 |
| 1.2. HUMAN AND MOUSE GCPII: FROM DNA TO PROTEIN..... | 13 |
| 1.2.1. <i>GCPII-encoding genes and mRNA</i> | 13 |
| 1.2.2. <i>GCPII protein</i> | 13 |
| 1.3. GCPII ENZYMOLOGY | 16 |
| 1.4. EXPRESSION PROFILE OF HUMAN AND MOUSE GCPII | 18 |
| 1.4.1. <i>Expression profile on the mRNA level</i> | 18 |
| 1.4.2. <i>Expression profile on the protein level</i> | 18 |
| 1.4.2.1. Expression in healthy tissues | 19 |
| 1.4.2.2. Expression in pathological conditions | 22 |
| 1.5. GCPII IN PHYSIOLOGICAL AND PATHOLOGICAL CONDITIONS | 23 |
| 1.5.1. <i>GCPII function in the brain</i> | 23 |
| 1.5.2. <i>GCPII function in the small intestine</i> | 25 |
| 1.5.3. <i>Proposed functions of GCPII</i> | 27 |
| 1.6. GCPII-DEFICIENT MICE | 28 |
| 1.6.1. <i>Common gene disruption techniques for generation of knockout mice</i> | 29 |
| 1.6.2. <i>Folh1 gene disruption</i> | 33 |
| 1.7. GCPII PARALOGUES..... | 34 |
| 1.7.1. <i>Glutamate carboxypeptidase III (GCPIII) in humans and mice</i> | 35 |
| 1.8. GCPII AS A PHARMACEUTICAL TARGET..... | 37 |
| 1.8.1. <i>GCPII as target for neurological diseases</i> | 38 |
| 1.8.2. <i>GCPII as target for cancer diagnosis and therapy</i> | 38 |
| 2. AIMS AND OBJECTIVES | 41 |
| 3. MATERIALS AND METHODS | 43 |
| 3.1. MATERIALS | 43 |
| 3.1.1. <i>Chemicals and solutions</i> | 43 |
| 3.1.2. <i>Instruments and devices</i> | 45 |
| 3.1.3. <i>Other material</i> | 46 |
| 3.1.3.1. Antibodies | 46 |
| 3.1.3.2. Enzymes..... | 47 |
| 3.1.3.3. Cell cultures | 47 |
| 3.1.3.4. Primers | 47 |
| 3.1.3.5. Vectors | 48 |
| 3.1.3.6. Chromatography columns and recyclable filters | 49 |
| 3.1.3.7. Consumables | 49 |
| 3.1.4. <i>Software</i> | 50 |
| 3.2. METHODS..... | 50 |
| 3.2.1. <i>Preparation of GCPII mutant mice</i> | 50 |
| 3.2.1.1. Phenol-chloroform extraction of chromosomal DNA | 50 |
| 3.2.1.2. Analysis of TALEN-mediated mutations | 51 |
| 3.2.1.3. Establishment of GCPII mutant mouse colonies and colony management | 52 |
| 3.2.1.4. GCPII-mutant mice genotyping..... | 52 |

| | |
|---|------------|
| 3.2.2. Preparation of membrane-bound protein variants of mouse GCPII | 53 |
| 3.2.2.1. Cloning of vectors encoding membrane-bound protein variants of mGCPII | 53 |
| 3.2.2.2. Expression of membrane-bound protein variants of mGCPII using HEK293 cells | 55 |
| 3.2.2.3. Analysis of the protein yield of membrane-bound mGCPII variants | 56 |
| 3.2.3. Preparation and characterization of extracellular parts of protein variants of mouse GCPII ... | 57 |
| 3.2.3.1. Cloning of vectors encoding extracellular parts of protein variants of mGCPII | 57 |
| 3.2.3.2. Expression of extracellular parts of protein variants of mGCPII using <i>Drosophila</i> S2 cells | 58 |
| 3.2.3.3. Purification of extracellular parts of protein variants of mGCPII | 59 |
| 3.2.3.4. Sodium dodecyl sulphate-polyacrylamide gel electrophoresis (SDS-PAGE) | 60 |
| 3.2.3.5. Size-exclusion chromatography | 61 |
| 3.2.3.6. Thermofluor assay | 62 |
| 3.2.4. Preparation of mouse tissue lysates | 62 |
| 3.2.4.1. Collection of mouse tissues | 62 |
| 3.2.4.2. Preparation of kidney and brain lysates | 62 |
| 3.2.4.3. Preparation of urogenital tissue lysates | 63 |
| 3.2.5. Determination of protein concentration | 64 |
| 3.2.5.1. NanoDrop measurement of protein concentration | 64 |
| 3.2.5.2. Bradford protein assay | 64 |
| 3.2.6. Western blot analysis | 65 |
| 3.2.7. NAAG-hydrolysing activity assay | 67 |
| 3.2.7.1. Reaction setup for determination of kinetic parameters of NAAG-hydrolysing reaction | 67 |
| 3.2.7.2. Reaction setup for analysis of enzyme activity of membrane-bound protein variants of mGCPII ... | 68 |
| 3.2.7.3. Reaction setup for analysis of NAAG hydrolysis in mouse tissue lysates | 68 |
| 3.2.7.4. Analysis of NAAG conversion during NAAG-hydrolysing reaction | 69 |
| 3.2.8. Mouse phenotyping | 70 |
| 3.2.8.1. Gross anatomy | 70 |
| 3.2.8.2. Histopathology and immunohistochemistry | 70 |
| 3.2.8.3. Metabolomic analysis of mouse urine | 71 |
| 3.2.9. Statistical analysis | 73 |
| 4. RESULTS | 74 |
| 4.1. GENERATION OF GCPII-MUTANT MICE | 74 |
| 4.1.1. TALEN-mediated disruption of <i>Folh1</i> gene | 74 |
| 4.1.2. GCPII-mutant mouse colony management | 76 |
| 4.2. CHARACTERIZATION OF MOUSE GCPII AND ITS MUTANT VARIANTS | 78 |
| 4.2.1. Kinetic characterization of recombinant mouse GCPII | 78 |
| 4.2.2. NAAG-hydrolysing activity of membrane-bound mutant variants of mGCPII | 79 |
| 4.2.3. Expression and purification of extracellular parts of mGCPII mutant variants | 82 |
| 4.2.4. Biochemical properties of <i>rm-GCPIIΔel3</i> | 84 |
| 4.3. CHARACTERIZATION OF GCPII-MUTANT MICE | 87 |
| 4.3.1. Investigation of expression of mGCPII protein variants in GCPII-mutant mice | 87 |
| 4.3.2. Characterization of GCPII-deficient mice | 89 |
| 4.4. INVESTIGATION OF REPRODUCTIVE TISSUE PHENOTYPE OF GCPII-DEFICIENT MICE | 91 |
| 4.5. INVESTIGATION OF POTENTIAL GCPII INVOLVEMENT IN RENAL FUNCTION | 95 |
| 4.5.1. Mouse urine collection | 95 |
| 4.5.2. Targeted metabolomics of mouse urine | 96 |
| 4.5.3. Histopathological examination of kidneys from aged mice | 99 |
| 4.6. MY CONTRIBUTION TO THE PROJECT | 100 |
| 5. DISCUSSION | 102 |
| 6. CONCLUSIONS | 111 |
| 7. LIST OF PUBLICATIONS | 113 |

| | |
|----------------------------|------------|
| 8. REFERENCES | 115 |
| APPENDICES | 137 |
| APPENDIX 1..... | 138 |
| APPENDIX 2..... | 155 |
| APPENDIX 3..... | 169 |

ABBREVIATIONS

| | |
|--------------------------|---|
| APS | ammonium persulfate |
| BCG | β -citryl-L-glutamate |
| BSA | bovine serum albumin |
| BTP | BIS-TRIS propane |
| C12E8 | octaethylene glycol monododecyl ether |
| CCD | charge-coupled device |
| CRISPR | Clustered Regularly Interspaced Short Palindromic Repeats |
| cv | column volumes |
| Da | daltons |
| DNA | deoxyribonucleic acid |
| dNTPs | deoxyribonucleotide triphosphates |
| dpm | disintegrations per minute |
| DSB | double-strand break |
| <i>E.coli</i> | <i>Escherichia coli</i> |
| EDTA | ethylenediaminetetraacetic acid |
| EF | elution fraction |
| ELISA | enzyme-linked immunosorbent assay |
| ESCs | embryonic stem cells |
| EST | expressed sequence tag |
| FDA | US Food and Drug Administration |
| FBS | fetal bovine serum |
| FolGlu _n | poly-gamma-glutamylated folates |
| Folh1 | folate hydrolase |
| <i>FOLH1</i> | folate hydrolase 1 gene encoding human GCPII |
| <i>Folh1</i> | folate hydrolase 1 gene encoding mouse GCPII |
| Folh1 ^{+/+} | mouse homozygous for <i>Folh1</i> |
| Folh1 ^{+/-} | mouse carrying <i>Folh1</i> as well as disrupted <i>Folh1</i> |
| Folh1 ^{-/-} | mouse homozygous for disrupted <i>Folh1</i> |
| Folh1 ^{mut/mut} | mouse homozygous for mutant <i>Folh1</i> |
| G-a-M | goat anti-mouse |
| GCPII | glutamate carboxypeptidase II |
| GCPIII | glutamate carboxypeptidase III |
| HDR | homology-directed repair |
| H&E | haematoxylin and eosin |
| hGCPII | human GCPII |
| hGCPIII | human GCPIII |
| HPLC-MS/MS | high-performance liquid chromatography-tandem mass spectrometry |
| HRP | horseradish peroxidase |
| IBD | inflammatory bowel disease |

| | |
|-----------|--|
| IF | insoluble fraction |
| IMPC | International Mouse Phenotyping Consortium |
| INDEL | insertion or deletion |
| IMG CAS | Institute of Molecular Genetics of the Czech Academy of Sciences |
| IOCB CAS | Institute of Organic Chemistry and Biochemistry of the Czech Academy of Sciences |
| LB | Luria-Bertani broth |
| MMAE | monomethylauristatin E |
| mGCPII | mouse GCPII |
| mGCPIII | mouse GCPIII |
| mGluR3s | type 3 metabotropic glutamate receptors |
| mCRPC | metastatic castration-resistant prostate cancer |
| mRNA | messenger RNA |
| NAAG | N-acetyl-L-aspartyl-L-glutamate |
| NAALADase | N-acetylated alpha-linked acidic dipeptidase |
| NCBI | National Center of Biotechnology Information |
| NMDARs | N-methyl-D-aspartate receptors |
| NHEJ | non-homologous end joining |
| PAGE | polyacrylamide gel electrophoresis |
| PBS | phosphate buffered saline |
| PCR | polymerase chain reaction |
| PDB | Protein Data Bank |
| PET | positron emission tomography |
| PSA | prostate specific antigen |
| PSMA | prostate specific membrane antigen |
| rh-GCPII | recombinant hGCPII, extracellular part of hGCPII |
| rm-GCPII | recombinant mGCPII, extracellular part of mGCPII |
| RNA | ribonucleic acid |
| SDS | sodium dodecyl sulfate |
| SF | soluble fraction |
| SPECT | single-photon emission computed tomography |
| TALEN | Transcription Activator-Like Effector Nuclease |
| TAE | tris-acetate-EDTA |
| TBE | tris-borate-EDTA |
| TBI | traumatic brain injury |
| TBS | tris buffered saline |
| TEMED | tetramethylethylenediamine |
| Tris | tris(hydroxymethyl)aminomethane |
| WF | washing fraction |
| WT | wild type |

1. INTRODUCTION

1.1. Discovery of glutamate carboxypeptidase II (GCPII)

The first research reports regarding glutamate carboxypeptidase II (GCPII) were published in late 1980s. Back then, three distinct designations for GCPII – N-acetylated alpha-linked acidic dipeptidase (NAALADase), prostate specific membrane antigen (PSMA) and folate hydrolase (Folh1) – were invented since the scientists from three unrelated research fields – neurology, urology and dietology – worked on this protein independently.

Indeed, in two reports from 1986 and 1987, Robinson and colleagues showed identification of a membrane-bound enzyme able to hydrolyse a peptide neurotransmitter N-acetyl-L-aspartyl-L-glutamate (NAAG) and entitled it NAALADase (Robinson *et al.* 1986; Robinson *et al.* 1987). In a completely different report from 1986, Chandler and colleagues isolated folate hydrolase from jejunal brush-border and demonstrated that this enzyme is involved in folate absorption (Chandler *et al.* 1986). Around the same time, Horoszewicz and colleagues developed a monoclonal antibody 7E11 that strongly interacted with human prostatic cells (Horoszewicz *et al.* 1987). The antigen recognized by this antibody was identified several years later and denoted as PSMA (Pinto *et al.* 1996).

Interestingly, it took almost a decade for the scientists from the three fields to realize that NAALADase, PSMA and folate hydrolyse are in fact a single enzyme entity. First, PSMA was shown to be capable of folate hydrolysis (Pinto *et al.* 1996) as well as NAAG hydrolysis (Carter *et al.* 1996). A computational prediction (Rawlings and Barrett 1997) followed by a series of experimental studies from the laboratory of Joseph T. Coyle then demonstrated that the three proteins possess identical sequences and enzyme properties (Luthi-Carter *et al.* 1998b; Luthi-Carter *et al.* 1998a; Luthi-Carter *et al.* 1998c; Halsted *et al.* 1998). A united name – glutamate carboxypeptidase II – for all three original designations was thus introduced. Although this name was also approved by International Union of Biochemistry and Molecular Biology and should be thus used preferentially, one of the original names – PSMA – still prevails in the literature.

1.2. Human and mouse GCPII: from DNA to protein

1.2.1. GCPII-encoding genes and mRNA

Human GCPII is encoded by a gene designated as *FOLH1*, which is localized on 11th chromosome at a position 11p11-p12 (O'Keefe *et al.* 1998; Rinkerschaeffer *et al.* 1995; Maraj *et al.* 1998). *FOLH1* spans 62035 base pairs and originally consists of 19 exons and 18 introns (O'Keefe *et al.* 1998). Nevertheless, at least six alternative splicing variants have been identified including four variants with alternatively spliced exon 1 – PSM' (Su *et al.* 1995), PSM-C, PSM-D (O'Keefe *et al.* 2001; Schmittgen *et al.* 2003), PSM-E (Cao *et al.* 2007) – and two variants with specific exon deletions – PSMA Δ 6 and PSMA Δ 18 (Williams and Kole 2006). Moreover, number of other alternative splice variants could to be found in public databases (<http://www.ncbi.nlm.nih.gov>; <http://www.ensembl.org>).

Mouse GCPII is encoded by a gene designated as *Folh1*, which is localized on 7th chromosome at a position 7D1-D2 (Bacich *et al.* 2001). Public databases indicate that *Folh1* spans around 57000 base pairs and its intron/exon structure is similar to human orthologue (<http://www.ncbi.nlm.nih.gov>; <http://www.ensembl.org>). Even though no alternative splicing of mouse mRNA have been reported to date, several splice variants are deposited in public databases (<http://www.ncbi.nlm.nih.gov>; <http://www.ensembl.org>).

1.2.2. GCPII protein

GCPII is type II transmembrane glycoprotein consisting of a short intracellular domain, a single membrane-spanning domain and a large extracellular domain (Rawlings and Barrett 1997; Bacich *et al.* 2001). Human GCPII (hGCPII) contains 750 amino acids (Israeli *et al.* 1993) and shares 86% sequence identity and 91% sequence similarity with mouse GPCII (mGCPII) that contains 752 amino acids (Bacich *et al.* 2001; Knedlik *et al.* 2017). An alignment of primary structures of both orthologues is depicted in Figure 1 (p. 14).

human GCPII (1) MWNLLHETDSAVATARPRWLCAGALVLAG-GFFLLIGFLFGWFIKSSNEA
 mouse GCPII (1) MWNALQDRDSAQEVLRHRQRWLRVGTLVLALVTGTFLLIGFLFGWFIKPSNEA

human GCPII (50) T-NITPKHNMKAFLDELKAENIKKFLY-NFTQIPHLAGTEQNFQLAKQIQS
 mouse GCPII (51) TGNVSHSGMKKEFLHELKAENIKKFLY-NFTRTPHLAGTQNNFELAKQIHD

human GCPII (99) QWKEFGLDSV-ELAHYDVLLSYPN-KTHPNYISIIINEDGNEIF-N-TSLFEP
 mouse GCPII (101) QWKEFGLDLV-ELSHYDVLLSYPN-KTHPNYISIIINEDGNEIFK-TSLSEQPP

human GCPII (149) PGYENVSDIVPPFSAFSPQGMPEGDLVYVNYARTEDFFKLERDMKINCSG
 mouse GCPII (151) PGYENISDVVPPYSAFSPQGTPEGDLVYVNYARTEDFFKLEREMKISCSG

human GCPII (199) KIVIARYGKVFVRGNKVKNAQLAGAKGVILYSDPADYFAPGVKSYPDGWNL
 mouse GCPII (201) KIVIARYGKVFVRGNMVKNAQLAGAKGMILYSDPADYFVPAVKSYPDGWNL

human GCPII (249) PGGGVQRGNITLNLNGAGDPLTPGYPANEYAYRRGIAEAVGLPSIPVHPIG
 mouse GCPII (251) PGGGVQRGNVITLNLNGAGDPLTPGYPANEHAYRHELTNAVGLPSIPVHPIG

human GCPII (299) YYDAQKLLKMGGSAPPDSSWRGSLKVPYNVGGPFTGNFSTQKVKMHIHS
 mouse GCPII (301) YDDAQKLLKMGGSAPPDSSWKGGLKVPYNVGGPFTGNFSTQKVKMHIHS

human GCPII (349) TNEVTRIYNVIGTLRGAVEPDRYVILGGHRDSWVFGGIDPQSGAAVVHEI
 mouse GCPII (351) YTKVTRIYNVIGTLKGALEPDRYVILGGHRDAWVFGGIDPQSGAAVVHEI

human GCPII (399) VRSFGTLKKEGWRPRRTILFASWDAEEFGLLGSTEWAEENSRLQERGVA
 mouse GCPII (401) VRSFGTLKKGRRPRRTILFASWDAEEFGLLGSTEWAEHSRLQERGVA

human GCPII (449) YINADSSIEGNYTLRVDCTPLMYSLVHNLTKELKSPDEGFEGKSLYESWT
 mouse GCPII (451) YINADSSIEGNYTLRVDCTPLMYSLVYHNLTKELQSPDEGFEGKSLYDSWK

human GCPII (499) KKSPSPEFSGMPRISKLGSGNDFEVFFQRLGIASGRARYTKNWETNKFSG
 mouse GCPII (501) EKSPSPEFSGMPRISKLGSGNDFEVFFQRLGIASGRARYTKNWKTNKVSS

human GCPII (549) YPLYHSVYETYELVEKFYDPMFKYHLLTVAQVRGGMVFEANLSIVLPFDCR
 mouse GCPII (551) YPLYHSVYETYELVVKFYDPTFKYHLLTVAQVRGAMVFEANLSIVLPFDCR

human GCPII (599) DYAVVLRKYADKIYSISMKHPQEMKTYSVSFDLSLFSAVK-NFTETIASKFSE
 mouse GCPII (601) SYAVALKKYADTIY-NISMKHPQEMKAYMISFDLSLFSAVN-NFTDVAASKFNQ

human GCPII (649) RLQDFDKSNPIVLRMMNDQLMFLERAFIDPLGLPDRPFYRHVIYAPSSHN
 mouse GCPII (651) RLQELDKSNPIILLRIMNDQLMYLERAFIDPLGLPGRPFYRHIYIYAPSSHN

human GCPII (699) KYAGESFPGIYDALFDIESKVDPSKAWGEVKRQIYVAAFTVQAAAETLSE
 mouse GCPII (701) KYAGESFPGIYDALFDISSKVNASKAWNEVKRQISLATFTVQAAAETLRE

human GCPII (749) VA
 mouse GCPII (751) VA

Figure 1: Sequence alignment of human and mouse full-length GCPII proteins. Identical amino acid residues are highlighted in light blue, similar residues in pink and non-similar residues in white. Black rectangle defines predicted GCPII transmembrane domain; dashed red rectangle marks epitope of the antibody GCP2-04 (Barinka *et al.* 2004a; Tykvar *et al.* 2014). Black rings mark potential N-glycosylation sites. The residues participating on substrate recognition, hydrolysis and product binding are designated as stars. Red stars: residues forming the S1 pocket (Barinka *et al.* 2008); blue stars: zinc ligands (Speno *et al.* 1999; Mesters *et al.* 2006); black star: catalytic base (Klusak *et al.* 2009); green stars: residues defining the S1' pocket (Barinka *et al.* 2007). The figure was adapted from (Knedlik *et al.* 2017).

Both proteins contain 10 potential N-linked glycosylation sites from which at least some are glycosylated. Indeed, while the molecular weight of GCPII was predicted from the amino acid sequence to be around 84 kDa, the molecular weight of GCPII determined experimentally is around 100 kDa (Israeli *et al.* 1994; Bacich *et al.* 2001). In addition, high sequence identity of both proteins ensures that some monoclonal antibodies produced as tools for hGCPII detection could be also used in mGCPII research (Tykvar *et al.* 2014). Especially, the epitope of the antibody GCP2-04 is highly conserved (see Figure 1, p. 14) (Barinka *et al.* 2004a; Tykvar *et al.* 2014).

Tertiary structure of extracellular portion of GCPII was resolved by protein crystallography for hGCPII (see Figure 2) (Davis *et al.* 2005; Mesters *et al.* 2006) but not yet for mGCPII. Nevertheless, due to the high sequence similarity, it can be expected that mGCPII 3D structure closely resembles the 3D structure of hGCPII.

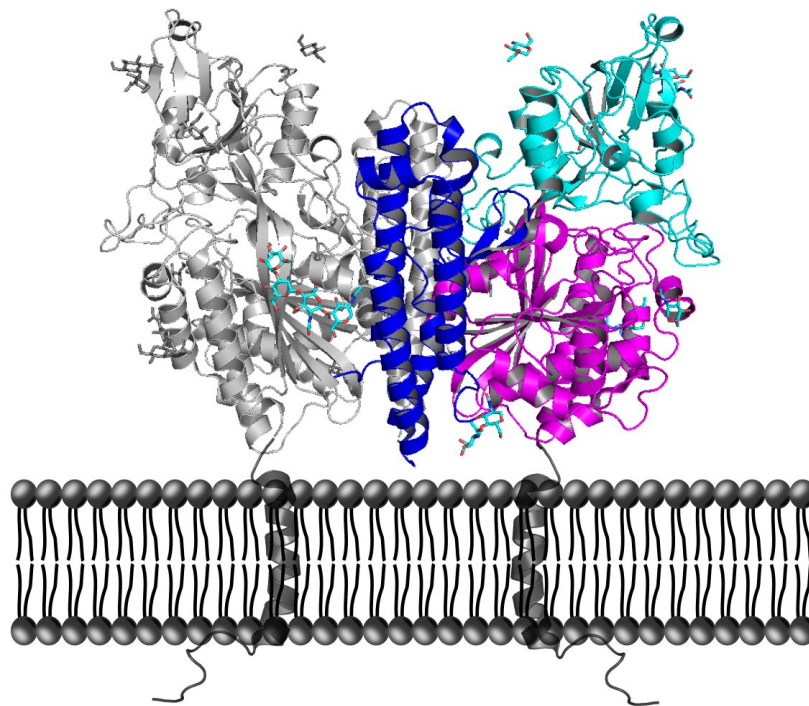


Figure 2: 3D structure of human GCPII. Crystal structure of extracellular part of human GCPII homodimer in cartoon representation (PDB identification code 2PVW) tethered to plasmatic membrane. One monomer is displayed in light grey; in the other monomer, individual domains are shown by distinct colours: the protease-like domain in pink, the apical domain in cyan, and the C-terminal domain (i.e. dimerization domain) in blue. The structure was created using PyMol (DeLano 2004). Illustrative display of transmembrane and intracellular part of GCPII is coloured dark grey.

The extracellular part of human GCPII (amino acids 44-750) consists of three domains – the protease-like domain (amino acids 59-116 and 352-590), the apical domain (amino acids 117-351) and the C-terminal or the dimerization domain (amino acids 591 - 750) (see Figure 2, p. 15) (Davis *et al.* 2005; Mesters *et al.* 2006; Barinka *et al.* 2012). Through the dimerization domain, the extracellular part of GCPII folds to a homodimer, which displays a pronounced overall fold similarity to the transferrin receptor (Mesters *et al.* 2006; Lawrence *et al.* 1999).

1.3. GCPII enzymology

As the name suggests, GCPII (EC 3.4.17.21) is a peptidase that hydrolyses its substrates at C-terminal glutamate. According to MEROPS database, GCPII belongs to a metallopeptidase subfamily M28B (Rawlings *et al.* 2016) since it requires 2 co-catalytic zinc cations for its activity (Speno *et al.* 1999). Moreover, GCPII needs to be post-translationally N-glycosylated (see Chapter 1.2., p. 13) in order to be capable of proteolysis (Ghosh and Heston 2003; Barinka *et al.* 2004b).

The active sites as well as S1 and S1' specificity pockets in the human and mouse GCPII are conserved (see Figure 1, p. 14); the structural studies performed on hGCPII should thus also apply to mGCPII. Four residues responsible for substrate binding into S1 pocket of hGCPII – Arg463, Asn519, Arg534 and Arg536 – were identified (Barinka *et al.* 2008). The S1 pocket seems to be relatively specific since the P1 position within the substrate needs to be occupied by negatively charged residue in order to ensure efficient hydrolysis (Hlouchova *et al.* 2012a).

The active site itself harbours catalytic Glu424 (in hGCPII, Glu426 in mGCPII) and 2 zinc atoms (Speno *et al.* 1999; Mesters *et al.* 2006). The catalytic Glu424 is a general base in the catalytic mechanism (Speno *et al.* 1999); it has been shown that a specific mutation E424A leads to complete loss of GCPII enzymatic activity (Klusak *et al.* 2009). The zinc atoms are coordinated by five residues – His377, Asp387, Glu425, Asp453 and His553 – which specific mutations result in severely reduced enzymatic activity (Speno *et al.* 1999).

Due to the conservation of the active site and the specific pockets, hGCPII and mGCPII possess similar substrate profiles. Indeed, both orthologues have been shown to process most of the N-acetylated dipeptides in a dipeptide library Ac-X-Glu-OH, where X is any proteinogenic amino acid (Barinka *et al.* 2002; Tykvart *et al.* 2015; Knedlik *et al.* 2017). With regard to the physiologically relevant substrates, both hGCPII and mGCPII hydrolyse *N*-acetyl-L-aspartyl-L-glutamate (NAAG) and poly- γ -glutamylated folates (FolGlu_n) (for more information on the physiological function see Chapter 1.5., p. 23) (Robinson *et al.* 1987; Halsted 1991; Bacich *et al.* 2001). While cleavage of NAAG yields *N*-acetyl-L-aspartate and L-glutamate, successive hydrolysis of FolGlu_n eventually results in release of folate and several free L-glutamates (see Figure 3) (Robinson *et al.* 1987; Bacich *et al.* 2001; Navratil *et al.* 2014).

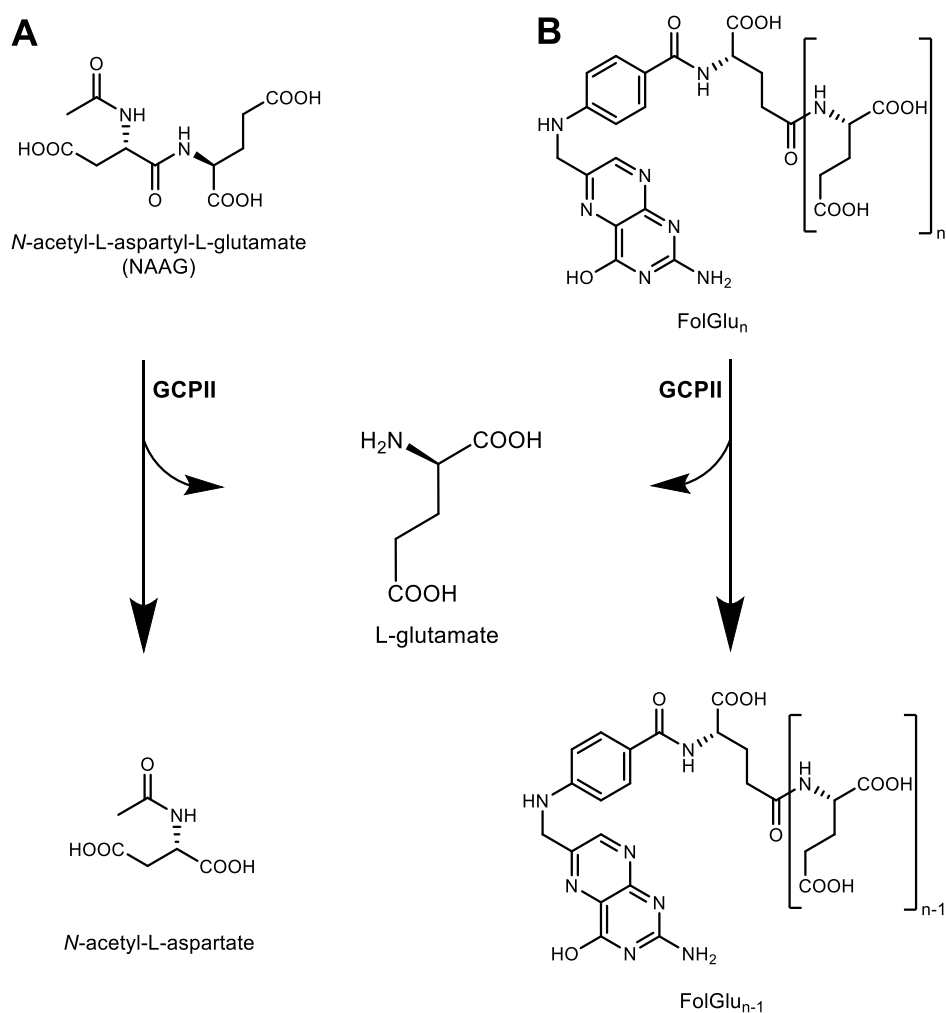


Figure 3: GCPII-catalysing hydrolysis of naturally occurring substrates. **A:** Catalysis of *N*-acetyl-L-aspartyl-L-glutamate (NAAG) cleavage. **B:** Catalysis of poly- γ -glutamylated folates (FolGlu_n) hydrolysis.

1.4. Expression profile of human and mouse GCPII

1.4.1. Expression profile on the mRNA level

GCPII mRNA profile was mainly studied by RT-PCR which showed predominant expression in the human prostate. In other tissues such as brain, kidney, small intestine, colon, liver, spleen, pancreas, testis, ovary and heart, the mRNA was also detected but in more than one order of magnitude lower amount than in the prostate (Israeli *et al.* 1994; Pangalos *et al.* 1999; Renneberg *et al.* 1999; Gala *et al.* 2000; Cunha *et al.* 2006).

In contrast with humans, almost no GCPII mRNA expression was observed in the mouse prostate (Bacich *et al.* 2001; Knedlik *et al.* 2017). Nevertheless, it is important to note that the anatomy of mammalian prostate is rather complex. Mouse prostate consists of four separate lobes differing in anatomy as well as histology (Oliveira *et al.* 2016), which the authors did not seem to take into consideration. The highest amount of mRNA was detected in the mouse kidney followed by the testis, brain, eyes, lungs, spleen, ovary, uterus and salivary gland (Bacich *et al.* 2001; Collard *et al.* 2011; Knedlik *et al.* 2017).

It is possible that GCPII mRNA is also expressed in other human and mouse tissues since not all tissues have been examined. On the other hand, it cannot be excluded that some of the published data were only false positive results. It is thus not surprising that the EST profiles available for both human and mouse in the UniGene database (<https://www.ncbi.nlm.nih.gov/unigene>) only partially correspond to the published data.

1.4.2. Expression profile on the protein level

Since the development of the first antibody 7E11 (Horoszewicz *et al.* 1987), expression profile of GCPII protein in both the physiological and pathophysiological conditions has been thoroughly investigated. However, the data are inconsistent, which is most probably caused by two main reasons. First, individual studies utilised different detection methods ranging from Western blotting, ELISA and immunohistochemistry to *in vivo* imaging (Barinka *et al.* 2012). The generated data may thus considerably differ due to variable detection limits of each method. Second, distinct antibodies have been

used but most of them were poorly characterized, which could have led to improper exploitation of the antibodies and thus generation of false positive/negative results.

From these reasons, the most commonly used antibodies against GCPII were recently thoroughly characterized and their performances in different detection methods were compared directly (Tykvart *et al.* 2014). The authors of this report then suggested guidelines on how to use the antibodies in a proper and the most efficient way. To decrease the data inconsistency, it will be desirable if this study would get into the general awareness of researchers working in the GCPII field.

In comparison to numerous of antibodies being produced against hGCPII, not many antibodies intended for mGCPII research are available. Due to the high sequence identity of both orthologues (see Chapter 1.2.2., p. 13), some of the antibodies against hGCPII could be used for detection of mGCPII (Tykvart *et al.* 2014). Nevertheless, the data collected for mGCPII expression profile has been mainly generated using NAAG-hydrolysing assay.

1.4.2.1. Expression in healthy tissues

Despite the data inconsistency, a consensus has been reached on GCPII expression within human body in the prostate, nervous system, small intestine and kidney (Barinka *et al.* 2012). These tissues were further examined using either human or rat histological samples to determine the exact localization of GCPII. It was found that GCPII is expressed in the acinar epithelium within the prostate (Rovenska *et al.* 2008; Kinoshita *et al.* 2006; Silver *et al.* 1997), astrocytes and Schwann cells within the nervous system (Berger *et al.* 1995; Berger *et al.* 1999; Sacha *et al.* 2007; Carozzi *et al.* 2008), duodenal mucosa within the small intestine (Kinoshita *et al.* 2006; Silver *et al.* 1997) and proximal tubules within the kidney (Dumas *et al.* 1999; Rovenska *et al.* 2008; Kinoshita *et al.* 2006; Silver *et al.* 1997).

Several studies also showed that GCPII expression profile within the human body is much broader and is thus not restricted only to the prostate, nervous system, small intestine and kidney. It should be noted though that the level of GCPII in other than the mentioned tissues is much lower. The list of tested tissues together with the number of studies investigating individual tissues is summarized in Table 1 (p. 20).

Table 1: Expression profile of GCPII protein in humans and mice. The numbers indicate the amount of reports showing GCPII expression in particular tissue out of all the reports investigating the particular tissue.

| TISSUE | humans | mice | REFERENCE |
|-----------------|--------|------|--|
| adrenal gland | 1/5 | 1/1 | (Horoszewicz <i>et al.</i> 1987), (Lopes <i>et al.</i> 1990), (Silver <i>et al.</i> 1997), (Chang <i>et al.</i> 1999b), (Kinoshita <i>et al.</i> 2006), (Knedlik <i>et al.</i> 2017) |
| blood | 4/5 | --- | (Rochon <i>et al.</i> 1994), (Troyer <i>et al.</i> 1995), (Beckett <i>et al.</i> 1999), (Xiao <i>et al.</i> 2001), (Knedlik <i>et al.</i> 2014) |
| brain | 5/10 | 2/2 | (Horoszewicz <i>et al.</i> 1987), (Lopes <i>et al.</i> 1990), (Troyer <i>et al.</i> 1995), (Silver <i>et al.</i> 1997), (Zhang <i>et al.</i> 1998), (Chang <i>et al.</i> 1999b), (Bacich <i>et al.</i> 2001), (Kinoshita <i>et al.</i> 2006), (Mhaweck-Fauceglia <i>et al.</i> 2007), (Sacha <i>et al.</i> 2007), (Rovenska <i>et al.</i> 2008), (Knedlik <i>et al.</i> 2017) |
| breast | 4/9 | --- | (Horoszewicz <i>et al.</i> 1987), (Troyer <i>et al.</i> 1995), (Silver <i>et al.</i> 1997), (Zhang <i>et al.</i> 1998), (Chang <i>et al.</i> 1999b), (Sokoloff <i>et al.</i> 2000), (Kinoshita <i>et al.</i> 2006), (Mhaweck-Fauceglia <i>et al.</i> 2007), (Rovenska <i>et al.</i> 2008) |
| colon | 3/10 | --- | (Horoszewicz <i>et al.</i> 1987), (Lopes <i>et al.</i> 1990), (Troyer <i>et al.</i> 1995), (Silver <i>et al.</i> 1997), (Zhang <i>et al.</i> 1998), (Chang <i>et al.</i> 1999b), (Sokoloff <i>et al.</i> 2000), (Kinoshita <i>et al.</i> 2006), (Mhaweck-Fauceglia <i>et al.</i> 2007), (Rovenska <i>et al.</i> 2008) |
| esophagus | 1/2 | --- | (Chang <i>et al.</i> 1999b), (Kinoshita <i>et al.</i> 2006) |
| gall bladder | 0/1 | --- | (Mhaweck-Fauceglia <i>et al.</i> 2007) |
| heart | 2/5 | 0/2 | (Horoszewicz <i>et al.</i> 1987), (Lopes <i>et al.</i> 1990), (Troyer <i>et al.</i> 1995), (Bacich <i>et al.</i> 2001), (Mhaweck-Fauceglia <i>et al.</i> 2007), (Rovenska <i>et al.</i> 2008), (Knedlik <i>et al.</i> 2017) |
| kidney | 9/11 | 2/2 | (Horoszewicz <i>et al.</i> 1987), (Lopes <i>et al.</i> 1990), (Silver <i>et al.</i> 1997), (Liu <i>et al.</i> 1997), (Zhang <i>et al.</i> 1998), (Chang <i>et al.</i> 1999b), (Dumas <i>et al.</i> 1999), (Sokoloff <i>et al.</i> 2000), (Bacich <i>et al.</i> 2001), (Kinoshita <i>et al.</i> 2006), (Mhaweck-Fauceglia <i>et al.</i> 2007), (Rovenska <i>et al.</i> 2008), (Knedlik <i>et al.</i> 2017) |
| liver | 2/9 | 0/2 | (Horoszewicz <i>et al.</i> 1987), (Lopes <i>et al.</i> 1990), (Troyer <i>et al.</i> 1995), (Silver <i>et al.</i> 1997), (Zhang <i>et al.</i> 1998), (Chang <i>et al.</i> 1999b), (Sokoloff <i>et al.</i> 2000), (Bacich <i>et al.</i> 2001), (Kinoshita <i>et al.</i> 2006), (Rovenska <i>et al.</i> 2008), (Knedlik <i>et al.</i> 2017) |
| lung | 1/8 | 0/1 | (Horoszewicz <i>et al.</i> 1987), (Lopes <i>et al.</i> 1990), (Troyer <i>et al.</i> 1995), (Zhang <i>et al.</i> 1998), (Chang <i>et al.</i> 1999b), (Kinoshita <i>et al.</i> 2006), (Mhaweck-Fauceglia <i>et al.</i> 2007), (Rovenska <i>et al.</i> 2008), (Knedlik <i>et al.</i> 2017) |
| lymph node | 0/5 | --- | (Horoszewicz <i>et al.</i> 1987), (Lopes <i>et al.</i> 1990), (Silver <i>et al.</i> 1997), (Zhang <i>et al.</i> 1998), (Mhaweck-Fauceglia <i>et al.</i> 2007) |
| ovary | 3/8 | 0/1 | (Horoszewicz <i>et al.</i> 1987), (Troyer <i>et al.</i> 1995), (Zhang <i>et al.</i> 1998), (Chang <i>et al.</i> 1999b), (Sokoloff <i>et al.</i> 2000), (Kinoshita <i>et al.</i> 2006), (Mhaweck-Fauceglia <i>et al.</i> 2007), (Rovenska <i>et al.</i> 2008), (Knedlik <i>et al.</i> 2017) |
| pancreas | 1/6 | 0/1 | (Horoszewicz <i>et al.</i> 1987), (Lopes <i>et al.</i> 1990), (Silver <i>et al.</i> 1997), (Chang <i>et al.</i> 1999b), (Mhaweck-Fauceglia <i>et al.</i> 2007), (Rovenska <i>et al.</i> 2008), (Knedlik <i>et al.</i> 2017) |
| prostate | 13/13 | 0/2 | (Horoszewicz <i>et al.</i> 1987), (Lopes <i>et al.</i> 1990), (Troyer <i>et al.</i> 1995), (Wright <i>et al.</i> 1995), (Silver <i>et al.</i> 1997), (Liu <i>et al.</i> 1997), (Zhang <i>et al.</i> 1998), (Chang <i>et al.</i> 1999b), (Sokoloff <i>et al.</i> 2000), (Bacich <i>et al.</i> 2001), (Kinoshita <i>et al.</i> 2006), (Mhaweck-Fauceglia <i>et al.</i> 2007), (Rovenska <i>et al.</i> 2008), (Wolf <i>et al.</i> 2010), (Knedlik <i>et al.</i> 2017) |
| salivary gland | 2/3 | 2/2 | (Troyer <i>et al.</i> 1995), (Bacich <i>et al.</i> 2001), (Mhaweck-Fauceglia <i>et al.</i> 2007), (Wolf <i>et al.</i> 2010), (Knedlik <i>et al.</i> 2017) |
| skeletal muscle | 1/7 | 0/1 | (Horoszewicz <i>et al.</i> 1987), (Lopes <i>et al.</i> 1990), (Troyer <i>et al.</i> 1995), (Silver <i>et al.</i> 1997), (Zhang <i>et al.</i> 1998), (Chang <i>et al.</i> 1999b), (Rovenska <i>et al.</i> 2008), (Knedlik <i>et al.</i> 2017) |

| TISSUE | humans | mice | REFERENCE |
|------------------|--------|------|---|
| seminal fluid | 2/2 | --- | (Troyer <i>et al.</i> 1995), (Sokoloff <i>et al.</i> 2000) |
| seminal vesicles | 0/2 | --- | (Bostwick <i>et al.</i> 1998), (Kinoshita <i>et al.</i> 2006) |
| skin | 1/7 | --- | (Horszewicz <i>et al.</i> 1987), (Lopes <i>et al.</i> 1990), (Silver <i>et al.</i> 1997), (Chang <i>et al.</i> 1999b), (Sokoloff <i>et al.</i> 2000), (Mhaweck-Fauceglia <i>et al.</i> 2007), (Rovenska <i>et al.</i> 2008) |
| small intestine | 8/11 | 0/1 | (Horszewicz <i>et al.</i> 1987), (Lopes <i>et al.</i> 1990), (Troyer <i>et al.</i> 1995), (Silver <i>et al.</i> 1997), (Liu <i>et al.</i> 1997), (Chang <i>et al.</i> 1999b), (Sokoloff <i>et al.</i> 2000), (Kinoshita <i>et al.</i> 2006), (Mhaweck-Fauceglia <i>et al.</i> 2007), (Rovenska <i>et al.</i> 2008), (Wolf <i>et al.</i> 2010), (Knedlik <i>et al.</i> 2017) |
| spleen | 1/4 | 1/1 | (Horszewicz <i>et al.</i> 1987), (Lopes <i>et al.</i> 1990), (Mhaweck-Fauceglia <i>et al.</i> 2007), (Rovenska <i>et al.</i> 2008), (Knedlik <i>et al.</i> 2017) |
| stomach | 1/7 | --- | (Horszewicz <i>et al.</i> 1987), (Lopes <i>et al.</i> 1990), (Silver <i>et al.</i> 1997), (Zhang <i>et al.</i> 1998), (Chang <i>et al.</i> 1999b), (Kinoshita <i>et al.</i> 2006), (Mhaweck-Fauceglia <i>et al.</i> 2007) |
| testis | 2/7 | 0/2 | (Horszewicz <i>et al.</i> 1987), (Lopes <i>et al.</i> 1990), (Silver <i>et al.</i> 1997), (Zhang <i>et al.</i> 1998), (Chang <i>et al.</i> 1999b), (Bacich <i>et al.</i> 2001), (Mhaweck-Fauceglia <i>et al.</i> 2007), (Rovenska <i>et al.</i> 2008), (Knedlik <i>et al.</i> 2017) |
| thyroid gland | 0/5 | --- | (Horszewicz <i>et al.</i> 1987), (Lopes <i>et al.</i> 1990), (Silver <i>et al.</i> 1997), (Chang <i>et al.</i> 1999b), (Mhaweck-Fauceglia <i>et al.</i> 2007) |
| urinary bladder | 3/6 | --- | (Horszewicz <i>et al.</i> 1987), (Silver <i>et al.</i> 1997), (Chang <i>et al.</i> 1999b), (Kinoshita <i>et al.</i> 2006), (Mhaweck-Fauceglia <i>et al.</i> 2007), (Rovenska <i>et al.</i> 2008) |
| urothelium | 2/4 | --- | (Horszewicz <i>et al.</i> 1987), (Bostwick <i>et al.</i> 1998), (Gala <i>et al.</i> 2000), (Kinoshita <i>et al.</i> 2006) |
| uterus | 2/4 | --- | (Horszewicz <i>et al.</i> 1987), (Zhang <i>et al.</i> 1998), (Mhaweck-Fauceglia <i>et al.</i> 2007), (Rovenska <i>et al.</i> 2008) |

In agreement with mRNA expression profile, the distribution of hGCPII and mGCPII proteins slightly differs. While the prostate is considered as a tissue with the one of the highest GCPII expression level within humans (Sokoloff *et al.* 2000), mouse prostate does not contain almost any GCPII protein (Bacich *et al.* 2001; Knedlik *et al.* 2017). Nevertheless, similarly to mRNA experiments, the mouse prostate lobe utilized for the analysis of GCPII protein level was not specified. It cannot be thus excluded that the GCPII is expressed in some of the mouse prostate lobes. The mouse tissue with the highest amount of expressed GCPII is the kidney followed by the brain (Bacich *et al.* 2001; Knedlik *et al.* 2017). In contrast, almost no GCPII was detected in the small intestine. The comparison of the GCPII expression within humans and mice is summarized in Table 1 (p. 20).

1.4.2.2. Expression in pathological conditions

As the alternative name ‘prostate-specific membrane antigen’ indicates, it has been consecutively shown that GCPII is overexpressed in the prostate cancer cells (Horoszewicz *et al.* 1987; Lopes *et al.* 1990; Troyer *et al.* 1995; Wright *et al.* 1995; Liu *et al.* 1997; Silver *et al.* 1997; Bostwick *et al.* 1998; Chang *et al.* 1999b; Sokoloff *et al.* 2000; Kinoshita *et al.* 2006; Mhaweche-Fauceglia *et al.* 2007; Perner *et al.* 2007; Minner *et al.* 2011; Chaux *et al.* 2013). GCPII is thus considered as one of the prostate cancer markers and several reports pointed out that the amount of GCPII increases with increasing prostate cancer grade (Bostwick *et al.* 1998; Perner *et al.* 2007; Minner *et al.* 2011). Moreover, considerable level of GCPII is also present in different prostate cancer metastases (Horoszewicz *et al.* 1987; Wright *et al.* 1995; Silver *et al.* 1997; Chang *et al.* 2001; Perner *et al.* 2007).

In addition to the prostate cancer, expression of GCPII has been also observed in numerous other carcinomas such as bladder carcinoma, breast carcinoma, colorectal adenocarcinoma, non-small cell lung carcinoma, glioma, clear cell renal cell carcinoma, thyroid carcinomas among others (Liu *et al.* 1997; Silver *et al.* 1997; Chang *et al.* 1999b; Dumas *et al.* 1999; Gala *et al.* 2000; Sokoloff *et al.* 2000; Kinoshita *et al.* 2006; Baccala *et al.* 2007; Mhaweche-Fauceglia *et al.* 2007; Lane *et al.* 2008; Haffner *et al.* 2009; Samplaski *et al.* 2011; Zeng *et al.* 2012; Nomura *et al.* 2014; Abdel-Hadi *et al.* 2014; Ren *et al.* 2014; Wernicke *et al.* 2014; Wang *et al.* 2015; Crowley *et al.* 2016; Salas Fragomeni *et al.* 2017; Kasoha *et al.* 2017; Schmidt *et al.* 2017; Heitkotter *et al.* 2017; Bychkov *et al.* 2017; Moore *et al.* 2017; Klein Nulent *et al.* 2017; Spatz *et al.* 2018; Tolkach *et al.* 2018; Heitkotter *et al.* 2018; Matsuda *et al.* 2018). Most of these carcinomas express GCPII in tumour-associated neovasculature (Liu *et al.* 1997; Silver *et al.* 1997; Chang *et al.* 1999a; Chang *et al.* 1999b; Dumas *et al.* 1999; Haffner *et al.* 2009), which is in contrast with the prostate cancer, where GCPII is mainly localized on the tumour cells (Wright *et al.* 1995; Silver *et al.* 1997; Bostwick *et al.* 1998; Perner *et al.* 2007; Minner *et al.* 2011).

Except of different types of cancer, GCPII seems to be also overexpressed in inflammatory bowel disease (IBD). Indeed, it has been shown that *FOLH1* gene is upregulated in IBD (Noble *et al.* 2010; Zhang *et al.* 2012; Ben-Shachar *et al.* 2013) and in one of the cases, immunohistochemistry was performed to further confirm GCPII

expression on the protein level (Zhang *et al.* 2012). Recently, 2.8 to 40-fold increase of GCPII enzymatic activity was reported in the affected intestinal mucosa of IBD patients when compared to normal colon from healthy volunteers (Rais *et al.* 2016). Taking these findings together, GCPII may serve as a biomarker for IBD.

1.5. GCPII in physiological and pathological conditions

In spite of the fact that GCPII is expressed in numerous healthy as well as malignant tissues (see Chapter 1.4., p. 18), its biological role has been only established in the brain and small intestine. The GCPII functions in both tissues correspond with its two enzymatic activities (see Chapter 1.3., p. 16) and are thus distinct. While in the brain, GCPII fulfils a neuromodulatory role (see Chapter 1.5.1., p. 23), in the small intestine, it is involved in folate metabolism (see Chapter 1.5.2., p. 25). In addition, GCPII has been suggested to play several distinct (though also contradictory) roles in healthy prostate and different carcinomas but not enough convincing data has been gathered for any hypothesis to be widely accepted by scientific community (see Chapter 1.5.3., p. 27). Interestingly, the function of GCPII in the kidney remains completely elusive.

1.5.1. GCPII function in the brain

GCPII fulfils the neuromodulatory role through cleavage and thus deactivation of NAAG, which is the most abundant peptide neurotransmitter in the mammalian brain (Neale *et al.* 2000). NAAG has been suggested to bind to two distinct types of receptors during the synaptic transmission – N-methyl-d-aspartate receptors (NMDARs) and type 3 metabotropic glutamate receptors (mGluR3s) (Wroblewska *et al.* 1993; Westbrook *et al.* 1986). Since the physiological relevance of NAAG action through NMDARs has been repeatedly questioned in the literature (Neale *et al.* 2011), it will not be discussed here further. On the other hand, the neuromodulatory function of NAAG executed through mGluR3s seems to be generally accepted (Khacho *et al.* 2016; Neale *et al.* 2011). The basic mechanism of the synaptic transmission is depicted in Figure 4 (p. 24).

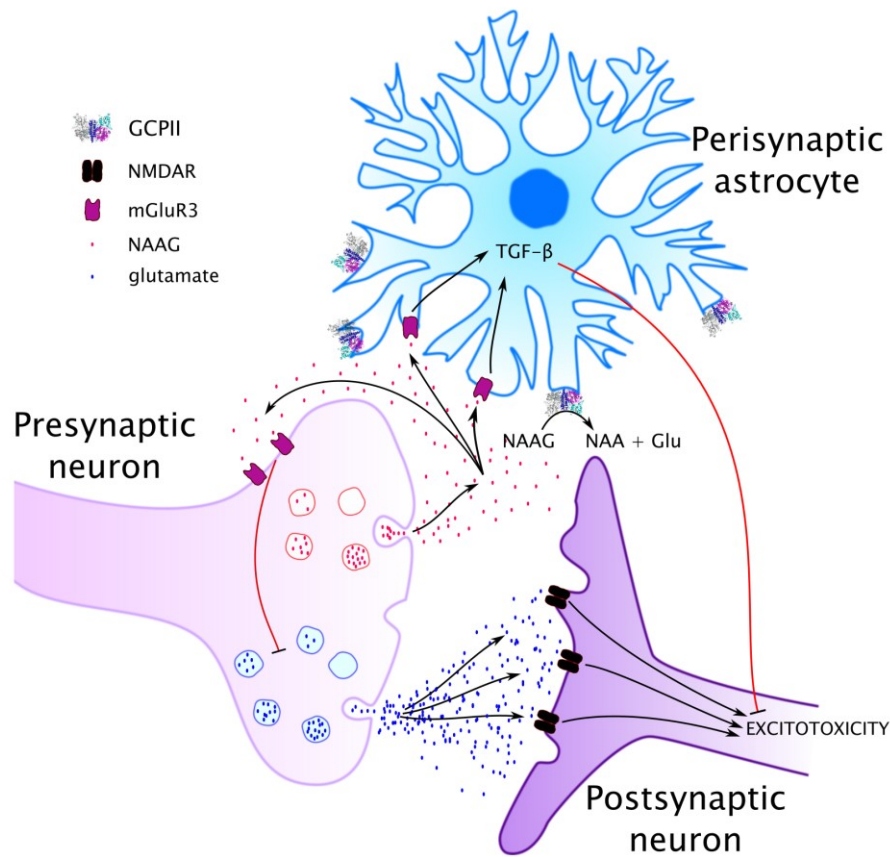


Figure 4: Involvement of NAAG and GCPII in neuromodulation. During the synaptic transmission, NAAG is released together with excitatory neurotransmitter (such as glutamate) from the presynaptic neuron (Neale *et al.* 2011). Subsequently, glutamate triggers the postsynaptic neuron stimulation through binding into NMDARs, while NAAG activates mGluR3s situated on presynaptic neurons and perisynaptic astrocytes (Wroblewska *et al.* 1997; Wroblewska *et al.* 1998; Wroblewska *et al.* 2006). Activation of presynaptic mGluR3 leads to inhibition of additional release of neurotransmitters from the presynaptic neuron (Zhao *et al.* 2001; Zhong *et al.* 2006; Sanabria *et al.* 2004; Romei *et al.* 2013); stimulation of mGluR3 on astrocytes triggers signalling pathway resulting in the secretion of neuroprotective factors such as TGF- β (Thomas *et al.* 2001; Bruno *et al.* 1998; Ruocco *et al.* 1999). Both these actions help to prevent excitotoxicity. In contrast, GCPII located on astrocytes hydrolyses NAAG into N-acetyl-L-aspartyl (NAA) and glutamate (Glu) and thus discontinues the neuroprotective actions. The figure was adapted from (Knedlik 2017).

During the synaptic transmission, postsynaptic nerve may be overstimulated by excessive level of excitatory neurotransmitter, such as glutamate. This can lead to neurotoxicity and subsequent severe pathological effects (Doble 1999). To avoid such pathological conditions, a neuroprotective agent, such as NAAG, is released from the presynaptic neuron together with the primary neurotransmitter. The stimulation of the

postsynaptic neuron is then downregulated by a combination of neuroprotective actions resulting from mGluR3s activation (Khacho *et al.* 2016; Neale *et al.* 2011). Since GCPII serves as NAAG deactivator, it is not surprising that substantial amount of effort has been made to find a selective GCPII inhibitor that could be possibly used in a treatment of neurological disorders (see Chapter 1.8., p. 37).

1.5.2. GCPII function in the small intestine

GCPII participates in the folate metabolism through facilitation of their absorption. The natural folates are usually present in a diet as folylpoly-gamma-glutamates (Zhao *et al.* 2009; McNulty and Pentieva 2010; Miller 2013). However, the proton-coupled folate transporter responsible for folate absorption from the intestinal lumen is highly specific for monoglutamylated folates (Qiu *et al.* 2006; Qiu *et al.* 2007). The polyglutamylated folates need to be thus first hydrolysed on intestinal brush-border by GCPII (Halsted 1991). The GCPII action in the folate absorption is thus crucial. The process of folate absorption and transport within the human body is depicted in Figure 5 (p. 26).

Interestingly, in the rat intestine, polyglutamylated folates are not hydrolysed by GCPII but by γ -glutamylhydrolase (Shafizadeh and Halsted 2007). Since GCPII seems not to be present in the mouse intestine (see Chapter 1.4.2.1., p. 19), it is likely that the folate absorption in mice is facilitated similarly as in rats.

Once absorbed into the portal circulation, most of the folates is taken up by the liver, where it is appropriately metabolized and then either retained or distributed throughout the body (Shane 2010). The major circulating form of folate is 5-methyl-tetrahydrofolate (5-MTHF) (Damaraju *et al.* 2008). After the cellular uptake, 5-MTHF is metabolized to its polyglutamylated forms, which ensures retention of folate pools within the cell (Balinska *et al.* 1982). In the cells, folates participate in the one-carbon metabolism such as methionine synthesis from homocysteine, synthesis of purine basis or synthesis of thymidine (Stover 2010).

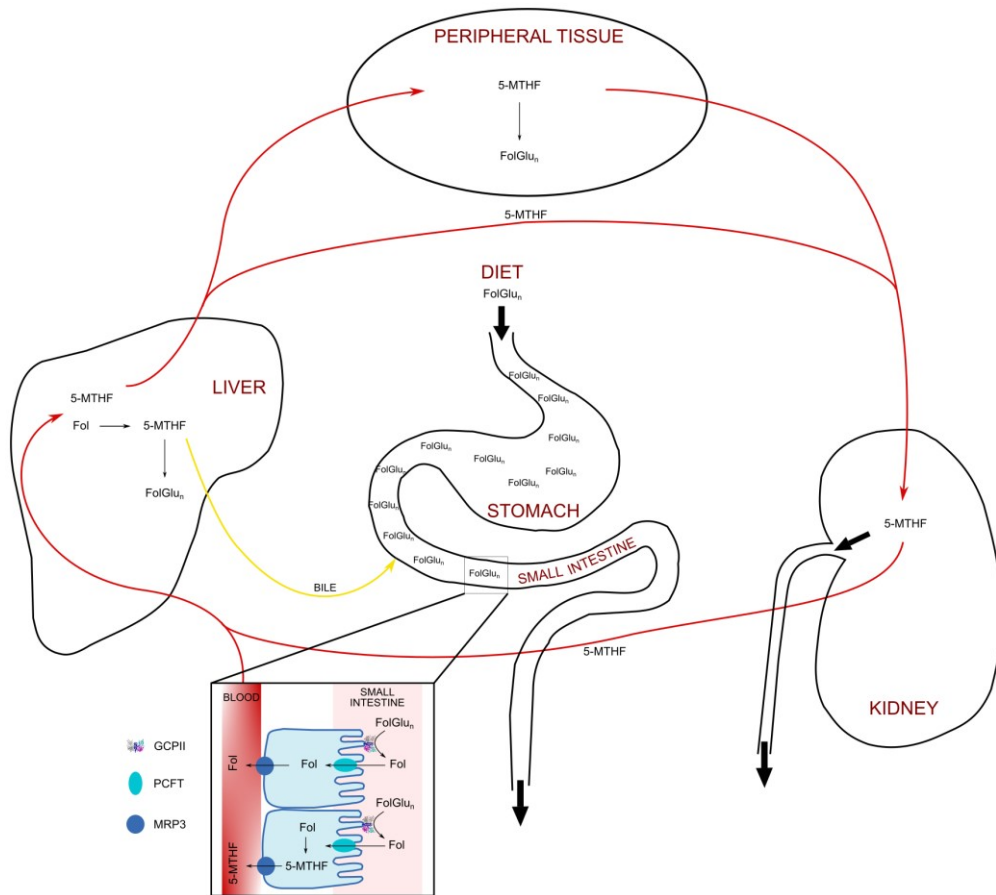


Figure 5: Folate absorption and transport within human body. Foliates occurring in a diet as folylpolyglutamates (FolGlu_n) are first hydrolysed on the brush-border membrane of small intestine by GCP II (Halsted 1991). Monoglutamylated folates (Fol) are then taken up by the intestinal cells through proton-coupled folate transporter (PCFT) and either released unmodified into the portal circulation through multidrug resistant protein 3 (MRP3) or transformed into 5-methyl-tetrahydrofolate (5-MTHF), which can be then also released into the blood through MRP3 (Patanwala *et al.* 2014). After the absorption, most of the folate is taken up by the liver, where it is transformed to 5-MTHF and either polyglutamylated, which ensures retention within the cells, or released to the blood or bile (Shane 2010). Through the blood, 5-MTHF is transported to peripheral tissue, where it is also transformed to polyglutamylated form in which executes a desired function. The folate homeostasis is maintained by glomerular filtration and tubular reabsorption in the kidney (Damaraju *et al.* 2008). The figure was adapted from (Patanwala *et al.* 2014) and (Halsted *et al.* 2010).

Due to the involvement of GCP II in the folate absorption, number of reports dealing with a possible influence of *FOLH1* gene polymorphisms on folate metabolism emerged (Devlin *et al.* 2000; Lievers *et al.* 2002; Vargas-Martinez *et al.* 2002; Morin *et al.* 2003; Afman *et al.* 2003; Melse-Boonstra *et al.* 2004; Chen *et al.* 2004; Devlin *et al.* 2006; Halsted *et al.* 2007; DeVos *et al.* 2008; Eklof *et al.* 2008; Guo *et al.* 2013; Roffman *et al.* 2013; Cummings *et al.* 2017). Nevertheless, the published data are rather

conflicting and further research is thus desirable. Two naturally occurring polymorphisms have been reported to date – rs61886492 (also known as C1561T) and rs202676 (also known as T484C).

rs61886492 polymorphism has been associated with increased serum folate levels (Halsted *et al.* 2007; Lievers *et al.* 2002; Afman *et al.* 2003; DeVos *et al.* 2008; Melse-Boonstra *et al.* 2004; Eklof *et al.* 2008). Two of the reports also demonstrated decreased serum homocysteine levels in association with rs61886492 (Eklof *et al.* 2008; Halsted *et al.* 2007), but others failed to confirm this phenomenon (Lievers *et al.* 2002; Afman *et al.* 2003; DeVos *et al.* 2008; Melse-Boonstra *et al.* 2004). Moreover, number of studies did not observe any effect of rs61886492 on serum folate or homocysteine (Vargas-Martinez *et al.* 2002; Morin *et al.* 2003; Chen *et al.* 2004; Devlin *et al.* 2006). The expression of *FOLH1* gene with rs61886492 polymorphism results in a protein product with a mutation H475Y (Devlin *et al.* 2000). This mutation has been shown not to alter GCPII activity towards polyglutamylated folates (Navratil *et al.* 2014). If this polymorphism is indeed associated with altered serum folate levels, the mechanism of action most probably does not involve proteolytic activity of the mutated enzyme and remains to be determined.

rs202676 polymorphism has been studied to much lesser extent but the recent reports have shown that it correlates with lower red blood cells folate levels (Roffman *et al.* 2013; Guo *et al.* 2013; Cummings *et al.* 2017). Interestingly, the expression of *FOLH1* gene with this missense mutation leads to a protein product with a mutation Y75H that has been predicted by structural modelling to alter both the secondary and tertiary structure of GCPII (Guo *et al.* 2013). Consequently, this mutation could affect the binding of polyglutamylated folates into the GCPII (Guo *et al.* 2013) and the folate absorption could be thus possibly impaired.

1.5.3. Proposed functions of GCPII

As mentioned previously, the function of GCPII in other tissues than the brain and small intestine is unclear. It is still debated whether additional physiological substrate of GCPII could exist or whether GCPII could also serve as a receptor for yet unknown extracellular ligand. Indeed, since GCPII possesses structural similarity to transferrin

receptor (see Chapter 1.2.2., p. 13) and is able to internalize upon ligand binding (Liu *et al.* 1998; Rajasekaran *et al.* 2003), the receptor hypothesis is suggestive. One report has even proposed that GCPII might itself be capable of folate uptake into the cell (Yao *et al.* 2010). However, no follow-up research has been carried out in this matter since.

In case of the GCPII role in the prostate cancer cells and tumour-associated neovasculature (see Chapter 1.4.2.2., p. 22), the literature is not unified. Some reports associate GCPII function with carcinogenesis and tumour progression (Yao *et al.* 2008; Yao *et al.* 2010). This hypothesis is strengthened by the fact that GCPII has been repeatedly detected in prostate cancer metastases (see Chapter 1.4.2.2., p. 22). On the contrary, others show that GCPII rather suppresses cancer invasiveness (Ghosh *et al.* 2005). A detailed current status of knowledge on how GCPII could be involved in malignant processes is beyond the scope of this thesis but has been recently reviewed elsewhere (Evans *et al.* 2016).

1.6. GCPII-deficient mice

In order to study the physiological function of GCPII in more detail, inactivation of *Folh1* gene in mouse seems to be an ideal direction. Indeed, since the enzymatic properties and expression profiles of mGCPII and hGCPII are similar (see Chapter 1.3., p. 16 and 1.4.2.1., p. 19), mice may well approximate humans. Several research groups attempted to produce GCPII deficient mice but the results were rather controversial. Some reports showed that inactivation of *Folh1* gene leads to generation of viable GCPII deficient mice with no obvious phenotype (Bacich *et al.* 2002; Gao *et al.* 2015). In contrast, others demonstrated that GCPII deficiency is embryonically lethal (Tsai *et al.* 2003; Han *et al.* 2009).

It remains unclear why such striking differences in outcomes of GCPII deficient mice preparation have been observed. In all cases, an embryonic stem cells (ESCs) manipulation was chosen for the gene disruption (see Chapter 1.6.1., p. 29). The methodologies thus mainly differed in the design of the targeting construct (see Chapter 1.6.2., p. 33).

1.6.1. Common gene disruption techniques for generation of knockout mice

A traditional technique for generation of knockout mice – ESCs manipulation – was first utilized in late 1980s (Joyner *et al.* 1989; Zijlstra *et al.* 1989; Schwartzberg *et al.* 1989). Since then, large number of publications has used this technique to describe functions of genes in living mice. The generation of gene disruption by ESCs manipulation is based on homology recombination. In a general setting, ESCs are first cultivated from mouse blastocysts and subsequently transfected by targeting vector (construct) (Anastassiadis *et al.* 2013). The vector contains a disruption within the targeting gene and long homology arms for the specific recombination (see Figure 6). The disruption design varies but usually one or more exons of targeting gene are replaced by a combination of a selectable marker resistance (such as PGK-Neo for selection in a presence of neomycine) and reporter gene (such as LacZ) (Mountford *et al.* 1994).

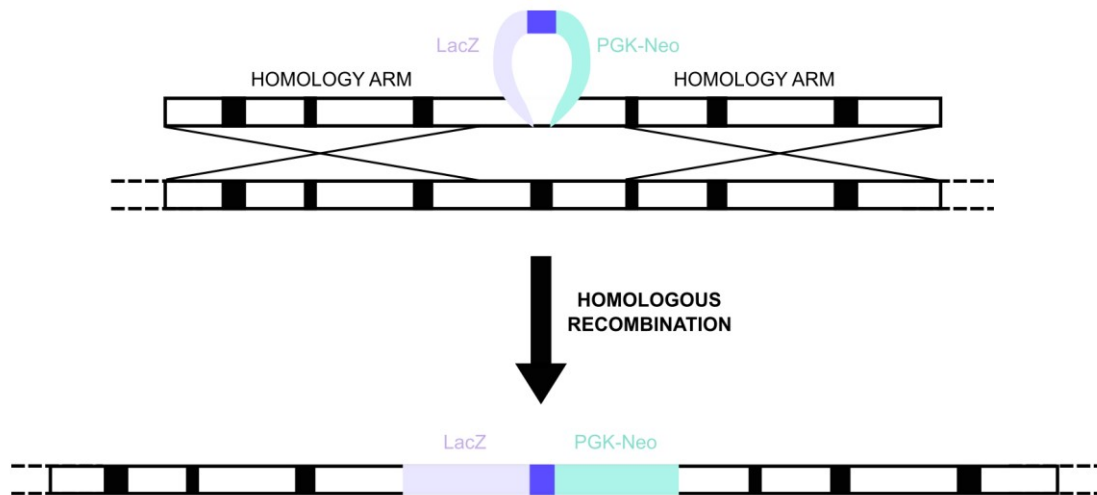


Figure 6: Gene disruption in mouse embryonic stem cells (ESCs). Targeting vector for gene disruption contains long homology arms as well as replacement of a part of the targeting gene by selectable marker resistance (such as neomycine – Neo) and reporter gene (such as LacZ). The homology recombination of targeting vector and the targeted gene in the ESCs may then result in generation of a specific gene disruption.

Once the targeting vector is transfected into the ESCs, homologous recombination between the construct and the targeted gene may occur. The ESCs containing the construct within the genome may be then selected by culturing in media supplemented by the selectable marker. Finally, ESCs with desired gene disruption are injected into recipient blastocysts that are subsequently implanted into recipient pseudo-pregnant foster mother. From the progeny, a mouse with desired gene disruption may be selected to establish knockout mouse colony (Capecchi 2005).

Despite its widespread usage, ESCs manipulation possesses several drawbacks. First, ESC lines were traditionally derived from 129 mouse strain, which is not ideal background for phenotyping (Seong *et al.* 2004). Even though ESC lines from C57 mouse strain are also available (Ledermann and Burki 1991), the ESCs with 129 genetic background display much more favourable properties for manipulation (Limaye *et al.* 2009). The knockout mice have been thus routinely prepared using 129 genetic background but they needed to be backcrossed to C57 strain, which displays much better properties for phenotyping studies (Seong *et al.* 2004; Bouabe and Okkenhaug 2013). This process is not only time-consuming and costly but also does not lead to generation of knockout mice on pure genetic background, which may influence the phenotyping results.

Second, retention of selectable marker cassette within the targeted loci may result in unexpected phenotypes of knockout mice. Indeed, it has been repeatedly demonstrated that the selectable marker cassette strongly influences expression of neighbouring genes (Olson *et al.* 1996; Pham *et al.* 1996). Such striking drawback has been overcome by removal of the selectable marker cassette from the targeted loci by site-specific recombination. This is enabled by the cassette being flanked by site-specific recombination target sites (such as loxP or FRT) (Anastassiadis *et al.* 2013). Nevertheless, number of knockout mice routinely used for experiments does not contain these sites, thus the removal of the selectable marker cassette is not possible.

Finally, ESCs manipulation is labour- and time-consuming process since it consists of many steps that may take as long as several months. From these reasons, alternative ways of gene disruption in mice have emerged. These mainly include gene targeting by engineering (programmable) nucleases such as Zinc-Finger Nucleases, Transcription Activator-Like Effector Nucleases (TALENs) and CRISPR/Cas9 (for 'Clustered Regularly Interspaced Short Palindromic Repeats' in a combination with Cas9

endonuclease) (Pauwels *et al.* 2014). In addition to time saving, these technologies enable production of knockout mice on a pure genetic background and do not require selectable marker. A detailed description of gene targeting using programmable nucleases is beyond the scope of this thesis. Here, only a basic principle with focus on TALENs will be introduced.

The engineering nucleases comprise two basic domains – sequence-specific DNA-binding domain and sequence-nonspecific DNA-cleaving domain (Gaj *et al.* 2013). TALEN design is depicted in Figure 7 as an example. DNA-binding domain in TALENs is composed of highly conserved protein repeats that are customisable for essentially any sequence. As the DNA-cleaving domain, *FokI* nuclease is usually utilized (Joung and Sander 2013). To generate mouse with specific gene ablation, mRNA encoding particular TALENs is injected into the recipient blastocysts where TALENs are produced using host translation apparatus (Sung *et al.* 2013). Once assembled, TALENs may cleave within a desired DNA sequence generating double-strand breaks (DSB) (see Figure 7).

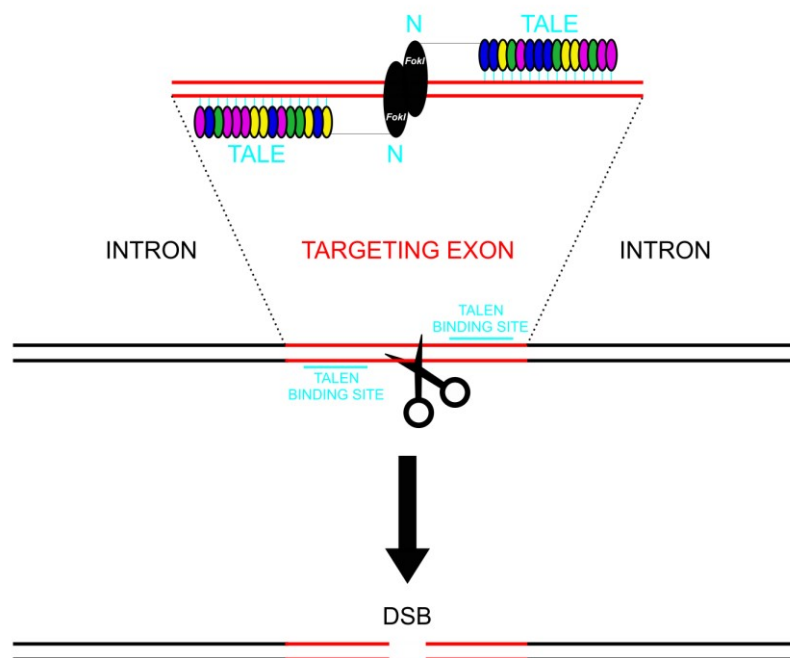


Figure 7: TALEN design and action. TALENs bind and cleave the desired DNA sequence as dimers. Each monomer of a TALEN compromise DNA binding domain (TALE from Transcription Activator-Like Effector), which consists of a combination of protein repeats that specifically recognize particular nucleobases, and DNA-cleaving domain (N from Nuclease) responsible for generation of DNA double-strand breaks (DSBs). DNA-cleaving domain is usually represented by one monomer of *FokI* nuclease, which needs to dimerize in order to execute the DNA cleavage (Pauwels *et al.* 2014).

The nuclease-induced DSBs stimulate DNA repair mechanisms – non-homologous end joining (NHEJ) or homology directed repair (see Figure 8) (Gaj *et al.* 2013). NHEJ frequently introduces variable length insertions or deletions within the targeted gene, which may result in a generation of frame-shift mutations (Pauwels *et al.* 2014). The protein products of such disrupted gene may either be produced as truncated versions or not be produced at all. In contrast, HDR may occur when a donor DNA is provided and thus this DNA repair mechanism leads to customized gene alteration (Pauwels *et al.* 2014).

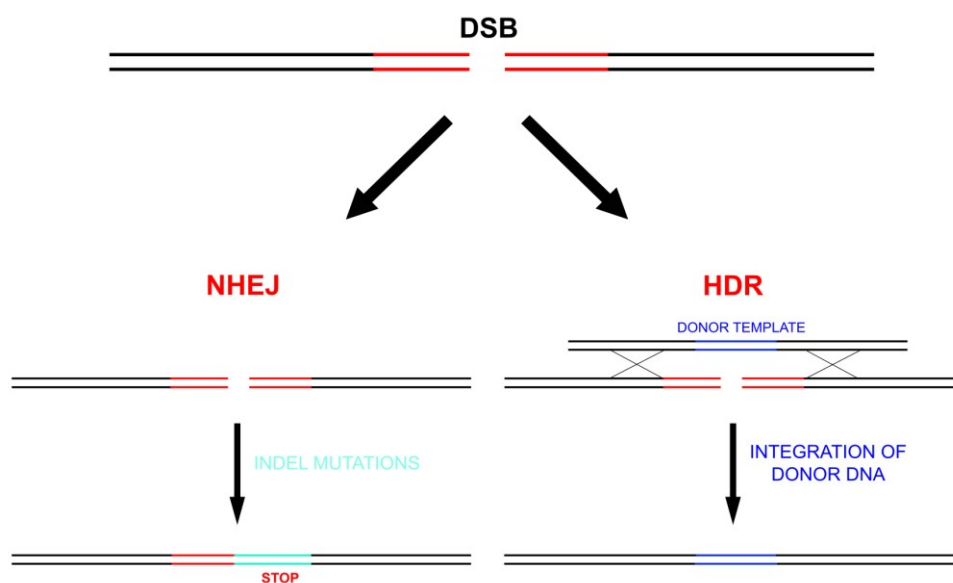


Figure 8: Nuclease-mediated gene modifications. Once nuclease-induced DSB occurs in the cell, DNA repair mechanisms are stimulated. These include non-homologous end joining (NHEJ) and homology-directed repair (HDR). NHEJ generates insertions or deletions (INDEL mutations) through which a premature stop codon may be introduced into the targeted gene. Homology-directed repair can only occur when donor template DNA is provided. It may result in introduction of precise nucleotide insertions or substitutions (Joung and Sander 2013; Gaj *et al.* 2013; Pauwels *et al.* 2014).

The rest of the process of knockout mice preparation by programmable nucleases is similar to that by ESCs manipulation. Nuclease-modified blastocysts are implanted into the recipient pseudo-pregnant foster mother and the resulting progeny is screened for the presence of nuclease-mediated gene alterations (Sung *et al.* 2013). Founder mice with desired mutations may be then selected to establish a knockout mouse colony.

1.6.2. *Folh1* gene disruption

The first GCPII-deficient mice were reported in 2002 by Bacich and colleagues (Bacich *et al.* 2002). These mice were prepared by manipulation of ESCs of 129^{sv} genetic background with subsequent injection, implantation and backcrossing to C57 strain. The targeting construct lacked intron-exon boundary sequences of exons 1 and 2 of the *Folh1* gene and contained several in-frame stop codons between exon 1 and 2. As a selectable marker resistance, PGK-Neo was used. Unfortunately, the site-specific recombination target sites, which would flank the neomycine cassette, were not introduced; the removal of the cassette is thus not possible.

GCPII-deficient mice produced by Bacich and colleagues displayed dramatically decreased NAAG-hydrolysing activity in the brain and kidney as compared with wild type (WT) littermates. Interestingly, the NAAG and glutamate levels in the brains of GCPII-deficient mice were not significantly impaired. It was thus suggested that deletion of *Folh1* gene might lead to induction of expression of other genes such as Naalad2 gene that encodes mGCPIII (see Chapter 1.7, p. 34).

Following study performed by Bzdega and co-workers questioned this hypothesis since the authors did not observe increase of GCPIII mRNA in the brains of GCPII-deficient mice when compared to their WT counterparts (Bzdega *et al.* 2004). Nevertheless, experiments confirming this observation on protein level need to be performed before this hypothesis will be definitely disproved. It cannot be also excluded that the low level of NAAG-hydrolysing activity detected in GCPII-deficient mice is sufficient for complementing the main GCPII-related functions. When performing phenotypic examination of GCPII WT vs. deficient mice, no significant differences in standard neurological behaviour were observed. However, it was shown that GCPII-deficient mice are protected from peripheral neuropathies and traumatic brain injury (TBI) (Bacich *et al.* 2005).

In 2003, another report regarding preparation of GCPII-deficient mice was published (Tsai *et al.* 2003). Surprisingly, in this work, the research group of Joseph T. Coyle showed that manipulation of ESCs cells by deletion of exons 9 and 10 of *Folh1* gene leads to embryonic lethality. The reason for deletion of exons 9 and 10 rather than exons at the beginning of *Folh1* gene lied in the effort to disrupt the active site of GCPII. Indeed, these exons encode zinc ligand domain, which is essential for enzyme activity

(see Chapter 1.3., p. 16). Similar to Bacich and colleagues, the research group of Joseph T. Coyle performed the ESCs manipulation on 129sv background followed by injection and implantation to C57 strain.

Moreover, the neomycine cassette was not removed from the genome. It was thus hypothesized that the selectable marker retention could be connected with the embryonic lethality. Nevertheless, the same research group subsequently attempted to reproduce the work of Bacich and co-workers by deletion of exons 1 and 2 of *Folh1* gene in ESCs from 129sv mice, and, in this case, flanked the neomycine cassette by loxP sites. Neither simulation of the successful design nor removal of neomycine cassette resulted in generation of viable GCPII-deficient mice (Han *et al.* 2009).

In 2015, independent research group described production of GCPII-deficient mice by deletion of exon 3 to 5 of *Folh1* gene in ESCs of 129sv background followed by injection and implantation to C57 strain (Gao *et al.* 2015). The neomycine cassette was also not flanked by the site-specific recombination target sites; its removal is thus impossible. In agreement with the report of Bacich and co-workers, Gao and colleagues observed dramatic decrease of NAAG-hydrolysing activity in the GCPII-deficient mouse brains when compared with their WT counterparts. Moreover, GCPII-deficient mice of Gao and co-workers showed similar phenotypic characteristics as these of Bacich and colleagues. Indeed, in comparison with WT mice, GCPII-deficient mice did not display overt behavioural alterations but were less susceptible to TBI and their long-term behavioural outcomes after the TBI were improved (Gao *et al.* 2015).

1.7. GCPII paralogues

Several different GCPII paralogues could be found in the human proteome. In general, all paralogues possess structural similarity with GCPII but their functions are not known (Hlouchova *et al.* 2012b). The closest GCPII paralogue is PSMA-like (PSMAL; 98% sequence identity) followed by glutamate carboxypeptidase III (GCPIII; 68% sequence identity), N-acetylated α -linked Acidic Dipeptidase-like (37% sequence identity) and N-acetylated α -linked Acidic Dipeptidase-like 2 (20% sequence identity) (Hlouchova *et al.* 2012b). Despite the high sequence identity of GCPII and PSMAL,

While hGCPIII has been tested against all three substrates (Hlouchova *et al.* 2007; Navratil *et al.* 2016), the enzymological data for mGCPIII are only available for NAAG and BCG (Collard *et al.* 2011). Nevertheless, due to the high sequence identity of mGCPIII with hGCPIII, it can be expected that mGCPIII is also capable of FolGlu_n hydrolysis.

Since GCPII and GCPIII possess similar substrate specificity, it is not surprising that several studies comparing their catalytic performance have emerged (Bzdega *et al.* 2004; Hlouchova *et al.* 2007; Navratil *et al.* 2016; Collard *et al.* 2011). The main difference between both enzymes seems to be their response to a presence of metal ions during hydrolysing reactions. Indeed, while both hGCPII and mGCPII are rather metal-insensitive, hGCPIII and mGCPIII can be stimulated or inhibited by addition of divalent metal ions (Collard *et al.* 2011; Navratil *et al.* 2016). In the absence of divalent metal ions, GCPII has been shown to be two orders of magnitude more efficient towards both NAAG and FolGlu_n than GCPIII. The activity assays could be thus exploited for specific detection of GCPII in the tissue lysates or body fluids, especially in cases when hGCPII needs to be quantified (Knedlik *et al.* 2014) or generally in mGCPII research, where not many efficient antibodies for immunological techniques are available.

The behaviour of GCPIII in the hydrolysing reaction depends on the combination of the substrate being hydrolysed and metal ion being present. When hydrolysing NAAG, both hGCPIII and mGCPIII are stimulated by addition of Mn²⁺ or Zn²⁺ and slightly inhibited by addition of Ca²⁺ (Collard *et al.* 2011; Navratil *et al.* 2016). In case of FolGlu_n, only FolGlu₁ hydrolysis by hGCPIII was tested and showed activation in the presence of all three investigating metal ions (Mn²⁺, Zn²⁺ and Ca²⁺) (Navratil *et al.* 2016). In contrast, when hydrolysing BCG, both hGCPIII and mGCPIII are stimulated by addition of Mn²⁺ or Ca²⁺ and slightly inhibited by addition of Zn²⁺ (Collard *et al.* 2011; Navratil *et al.* 2016).

The localization of GCPIII protein in humans and mice has not been studied in detail since not many research tools are available. Nevertheless, it is widely accepted that both hGCPIII and mGCPIII are mainly expressed in the testis (Collard *et al.* 2011; Navratil *et al.* 2016), where high level of BCG is also present (Miyake *et al.* 1982). In addition, using BCG-hydrolysing assay, reasonable amount of GCPIII was detected in the human prostate, brain, kidney and small intestine (Navratil *et al.* 2016) as well as in the mouse kidney, lungs, uterus and bladder (Collard *et al.* 2011). Nevertheless, the tested

sets of human and mouse tissues were not complete and the number of biological replicates was not sufficient. Further research is thus necessary to reach the final consensus of what is the expression profile of GCPIII within the body.

The physiological function of GCPIII remains to be still revealed. Since GCPIII possesses similar substrate specificities as GCPII and, in addition, GCPII deficient mice display residual NAAG-hydrolysing activity, it has been proposed that GCPIII may serve as a complementary enzyme to GCPII (Bacich *et al.* 2002). Nevertheless, in the testis, the expression level of GCPIII is more than one order of magnitude higher than that of GCPII (Navratil *et al.* 2016). It is thus possible that GCPIII plays also other roles within the body. These may be connected with BCG metabolism. However, the function of BCG is also unclear. It was proposed that BCG may participate in the brain development (Miyake *et al.* 1978; Miyake and Kakimoto 1981), spermatogenesis (Miyake *et al.* 1982) and physiologically important chelation of iron and copper, which leads to inhibition of xanthine oxidase, activation of aconitase or scavenging of reactive oxygen species (Hamada-Kanazawa *et al.* 2010; Narahara *et al.* 2010; Hamada-Kanazawa *et al.* 2011). Nevertheless, BCG has been only studied by one research group and further research is thus necessary.

1.8. GCPII as a pharmaceutical target

Considering its overexpression in cancer (see Chapter 1.4.2.2., p. 22) and neuromodulatory function in the brain (see Chapter 1.5.1., p. 23), it is not surprising that GCPII represents a promising pharmaceutical target. Recently, GCPII has been also proposed as a pharmaceutical target for IBD (Rais *et al.* 2016; Date *et al.* 2017). In the prostate cancer as well as all cancers containing GCPII-expressing neovasculature, GCPII may be used as a molecular address for targeted delivery of diagnostic and therapeutic substances (Evans *et al.* 2016; Wustemann *et al.* 2018; Salas Fragomeni *et al.* 2018). In contrast, in neurological disorders, GCPII may serve as a target for specific inhibition of NAAG-hydrolysing activity leading to alleviation of excitotoxicity (Evans *et al.* 2016). Similarly, with yet unknown mechanism, GCPII inhibitors seem to decrease severity of IBD (Rais *et al.* 2016; Date *et al.* 2017). A detailed description of diagnostic

and therapeutic potential of GCPII is beyond the scope of this thesis but has been recently reviewed elsewhere (Evans *et al.* 2016; Wustemann *et al.* 2018). Here, only a brief overview of state-of-the-art focusing on substances already tested in clinical settings will be presented.

1.8.1. GCPII as target for neurological diseases

As already mentioned, the therapeutic potential of GCPII inhibition in neurological diseases is based on the blocking of NAAG degradation. Consequently, NAAG as the neuroprotective agent help to attenuate symptoms of pathological conditions. Studies performed on rats and mice have shown a positive impact of GCPII inhibition on ischemic-hypoxic and traumatic brain injury (Slusher *et al.* 1999; Tortella *et al.* 2000; Zhong *et al.* 2005; Feng *et al.* 2012), inflammatory and neuropathic pain (Yamamoto *et al.* 2001; Yamamoto *et al.* 2004; Carpenter *et al.* 2003), amyotrophic lateral sclerosis (Ghadge *et al.* 2003), schizophrenia (Olszewski *et al.* 2004; Olszewski *et al.* 2012), multiple sclerosis (Rahn *et al.* 2012) and autoimmune encephalomyelitis (Ha *et al.* 2016).

Even though rats and mice are ideal animal models for development of GCPII-related treatment of neuropathies since both GCPII orthologues well approximate the human enzyme (Rovenska *et al.* 2008; Knedlik *et al.* 2017), none of the GCPII inhibitors has made it to a clinical practice to date. Indeed, most of the compounds are polar and their ability to cross blood-brain barrier is thus limited (Zhong *et al.* 2014). To improve pharmacokinetic profiles of GCPII inhibitors, prodrugs of current compounds or completely novel scaffolds with higher lipophilicity need to be tested.

1.8.2. GCPII as target for cancer diagnosis and therapy

Cancer imaging and therapy has become the most studied field in GCPII research. To deliver imaging or therapeutic substance into the GCPII-expressing malignancy, antibody-based or small ligand-based targeting is most frequently used. For cancer imaging, the targeting substance is mainly combined with a radionuclide and utilized in emission tomography (usually PET or SPECT). In contrast, the spectrum of targeting

cargos for cancer therapy is much broader including radionuclides and variety of cytotoxic (mainly antimitotic) molecules.

The only imaging agent approved by the US Food and Drug Administration (FDA) for diagnosis of prostate cancer is monoclonal antibody 7E11 labelled by ^{111}In (Kahn *et al.* 1994; Haseman *et al.* 1996), which targets intramembrane part of GCPII and its detection capabilities *in vivo* are thus limited to dead or necrotic cells (Wustemann *et al.* 2018). From this reason, monoclonal antibodies binding to extracellular part of GCPII have been developed and some of them already tested in clinical trials (Bander *et al.* 2003). Nevertheless, antibodies usually possess great half-life resulting in slow clearance from the body and prolonged exposure of the patient. Small molecule-based targeting has thus simultaneously emerged. To date, number of distinct GCPII inhibitors has been labelled with variety of radioisotopes including ^{68}Ga , $^{99\text{m}}\text{Tc}$, ^{18}F and ^{64}Cu (Wustemann *et al.* 2018). Several of the prepared GCPII radioligands such as ^{68}Ga -PSMA-11, $^{99\text{m}}\text{Tc}$ -MIP-1404 or ^{18}F -DCFPyL have already been investigating in preclinical and clinical studies (Psimadas *et al.* 2018; Wustemann *et al.* 2018).

The first antibody conjugate tested in clinical trials for treatment of prostate cancer was 7E11 antibody radiolabelled with ^{90}Y . However, its efficacy was extremely low and the patients exhibited high hematologic toxicity (Deb *et al.* 1996; Kahn *et al.* 1999). In contrast, the second-generation antibody J591 labelled with ^{177}Lu demonstrated excellent targeting in patients suffering from metastatic castration-resistant prostate cancer (mCRPC). Moreover, serum level of PSA, which is a marker routinely used for prostate cancer monitoring (Adhyam and Gupta 2012), displayed a dose-dependent decline in some patients after administration of the ^{177}Lu -J591 antibody (Bander *et al.* 2005; Tagawa *et al.* 2013; Tagawa *et al.* 2010). Apart from radiolabelled antibodies, antibodies conjugated to antimitotic drugs mertansine (DM1) and monomethyl auristatin E (MMAE) have already entered clinical trials. While the antibody-DM1 conjugate exhibited neurotoxicity and limited activity in mCRPC patients (Milowsky *et al.* 2016), the antibody-MMAE conjugate displayed low toxicity and PSA decline of more than 50% in one of three mCRPC patients (the complete results of the Phase 2 trial can be accessed at <https://clinicaltrials.gov/ct2/show/record/NCT02020135>).

Despite promising clinical testing, therapeutic antibodies targeting GCPII display dose-limiting myelosuppression (Psimadas *et al.* 2018). Development of therapeutic small ligands of GCPII has been thus also on the rise. Especially, a molecule labelled

with ^{177}Lu designated as ^{177}Lu -PSMA-617 has been showing promising results of clinical trials in terms of its safety and efficacy (Kratochwil *et al.* 2016; Baum *et al.* 2016; Rahbar *et al.* 2017). Indeed, the PSA decline exceeding 50% occurred in one of two mCRPC patients (Brauer *et al.* 2017; Rahbar *et al.* 2017). In addition, small selective GCPII inhibitors conjugated with antimetabolic drugs docetaxel and tubulysin have entered first phases of clinical trials for treatment of nonsmall-cell lung cancer and recurrent mCRPC, respectively (Srinivasarao and Low 2017).

Finally, GCPII-based immunotherapy of prostate cancer has been increasingly investigated. Even though only a few studies have been performed in a clinical setting, several different therapies have been suggested. These include therapies based on dendritic cells (Meng *et al.* 2016; Xi *et al.* 2015), GCPII-CD3 diabodies and F_{ab} conjugates (Baum *et al.* 2013; Patterson *et al.* 2017), T-cells bearing a chimeric antigen receptor (Santoro *et al.* 2015; Serganova *et al.* 2017; Junghans *et al.* 2016; Zhang *et al.* 2018).

2. AIMS AND OBJECTIVES

The efforts to inactivate *Folh1* gene in mice by manipulation of the embryonal stem cells have led to rather conflicting results ranging from embryonal lethality to production of viable GCPII-deficient mice with no obvious phenotype. One of the aims of this study was thus to resolve this discrepancy by utilisation of an alternative way for *Folh1* gene inactivation.

The reason why some of the GCPII-deficient mice are viable could relate to residual NAAG-hydrolysing activity detected in these mice. In contrast, the embryonic lethality of other GCPII-deficient mice could be a result of a complete inactivation of *Folh1* gene. The aim was thus to specifically disrupt *Folh1* gene within a sequence encoding active site of GCPII. This would avoid not only potential production of partially active GCPII from alternatively spliced mRNA but also embryonic lethality. We hypothesized that if GCPII fulfils both the receptor and the enzyme functions within the body, GCPII-mutant mice expressing inactive mutant variant of GCPII could be possibly viable.

Finally, even though GCPII has been thoroughly studied for more than three decades, its biological function outside brain and small intestine is still not fully understood. Even in the case of GCPII-deficient mice, researchers mainly focused on its involvement in nervous system. If GCPII-deficient or GCPII-mutant mice were viable, the aim of this study would be to explore the physiological function of GCPII in urogenital system.

To meet the aims, following objectives were set:

1. Perform TALEN-mediated *Folh1* gene disruption in mice within a sequence encoding active site of GCPII
2. Analyse TALEN-mediated mutations and select founder mice carrying both the frame-shift mutations and deletions potentially resulting in only small deletion within the active site of GCPII

3. Establish mutant mouse colonies and develop reliable genotyping protocol
4. Characterize recombinant mouse GCPII in terms of its kinetic properties in NAAG hydrolysis reaction
5. Prepare and characterize recombinant mutant variants of GCPII that would potentially be expressed in GCPII-mutant mice
6. Characterize GCPII-mutant and GCPII-deficient mice
7. Investigate the impact of GCPII disruption on reproductive tissue and renal function by careful examination of GCPII-mutant and GCPII-deficient mice

3. MATERIALS AND METHODS

3.1. Materials

3.1.1. Chemicals and solutions

| | |
|--|----------------------------------|
| acetic acid | Penta (Prague, Czechia) |
| N-acetyl-L-aspartyl-L-glutamic acid | Sigma-Aldrich (St. Louis, USA) |
| acrylamide..... | Sigma-Aldrich (St. Louis, USA) |
| agarose | Serva (Heidelberg, Germany) |
| Albumin standard (2 mg/ml)..... | Thermo Scientific (Waltham, USA) |
| All Blue Prestained Protein Standards for SDS-PAGE | Bio-Rad (Hercules, USA) |
| ammonium persulfate | Serva (Heidelberg, Germany) |
| ampicillin | Sigma-Aldrich (St. Louis, USA) |
| D-biotin..... | GeneTiCA (Prague, Czechia) |
| BIS-TRIS propane | Sigma-Aldrich (St. Louis, USA) |
| blasticidin..... | Invitrogen (Carlsbad, USA) |
| boric acid..... | USB (Cleveland, USA) |
| bromphenol blue | Sigma-Aldrich (St. Louis, USA) |
| Casein Buffer 20X-4X Concentrate..... | SDT (Baesweiler, Germany) |
| chloroform | Sigma-Aldrich (St. Louis, USA) |
| Complete Mini, EDTA free, Protease inhibitor cocktail tablets..... | Roche (Basel, Switzerland) |
| copper(II) sulfate..... | Lachema (Brno, Czechia) |
| Creatinine Standard..... | Dialab (Wiener Neudorf, Austria) |
| dimethylformamide..... | Sigma-Aldrich (St. Louis, USA) |
| dimethyl sulfoxide | Sigma-Aldrich (St. Louis, USA) |
| DNA ladders 100 bp and 1 kbp | Qiagen (Hilden, Germany) |
| dNTP mix..... | Serva (Heidelberg, Germany) |
| ethanol..... | Penta (Prague, Czechia) |
| ethylenediaminetetraacetic acid (EDTA)..... | Sigma-Aldrich (St. Louis, USA) |
| fetal bovine serum (FBS)..... | Gibco (Carlsbad, USA) |
| formaldehyde | Penta (Prague, Czechia) |
| Formalin solution, neutral buffered, 10%..... | Sigma-Aldrich (St. Louis, USA) |
| formic acid | Penta (Prague, Czechia) |
| GelRed Nucleic Acid Gel Stain | Biotinum (Fremont, USA) |
| L-glutamine..... | Sigma-Aldrich (St. Louis, USA) |
| glycerol | Penta (Prague, Czechia) |
| glycine..... | Duchefa (Haarlem, Netherlands) |
| hydrochloric acid | Penta (Prague, Czechia) |
| hydrogen peroxide | Sigma-Aldrich (St. Louis, USA) |
| hygromycin B | Invitrogen (Carlsbad, USA) |

| | |
|---|--------------------------------------|
| Igepal CA-630..... | Sigma-Aldrich (St. Louis, USA) |
| IMDM medium..... | Gibco (Carlsbad, USA) |
| 4-iodophenol..... | Thermo Scientific (Waltham, USA) |
| isopropanol..... | Penta (Prague, Czechia) |
| LB agar..... | Sigma-Aldrich (St. Louis, USA) |
| LB medium..... | Sigma-Aldrich (St. Louis, USA) |
| LC-MS Grade water..... | Fisher Chemicals (Loughborough, UK) |
| luminol..... | Sigma-Aldrich (St. Louis, USA) |
| 2-mercaptoethanol..... | Sigma-Aldrich (St. Louis, USA) |
| methanol..... | Penta (Prague, Czechia) |
| N,N'-metylen-bis(acrylamide)..... | USB (Cleveland, USA) |
| MilliQ deionized water..... | Millipore (Billerica, USA) |
| Narkamon 50 mg/ml..... | Bioveta (Ivanovice na Hane, Czechia) |
| Octaethylene Glycol Monododecyl Ether (C12E8)..... | Affymetrix (Santa Clara, USA) |
| opti-MEM medium..... | Gibco (Carlsbad, USA) |
| Phenol solution equilibrated with Tris HCl, pH 8.0..... | Sigma-Aldrich (St. Louis, USA) |
| polyethylenimine..... | Sigma-Aldrich (St. Louis, USA) |
| potassium chloride..... | Sigma-Aldrich (St. Louis, USA) |
| potassium hydroxide..... | Penta (Prague, Czechia) |
| potassium phosphate dibasic..... | Sigma-Aldrich (St. Louis, USA) |
| PPP Master Mix..... | Top-Bio (Vestec, Czechia) |
| Protein Assay Dye Reagent Concentrate..... | Bio-Rad (Hercules, USA) |
| Rometar 20 mg/ml..... | Bioveta (Ivanovice na Hané, Czechia) |
| Rotiszint ECO Plus scintillation cocktail..... | Carl Roth (Karlsruhe, Germany) |
| SF900II medium..... | Gibco (Carlsbad, USA) |
| silver nitrate..... | Lachema (Brno, Czechia) |
| sodium acetate trihydrate..... | Penta (Prague, Czechia) |
| sodium carbonate..... | Penta (Prague, Czechia) |
| sodium chloride..... | Lachema (Brno, Czechia) |
| sodium dodecyl sulfate..... | Sigma-Aldrich (St. Louis, USA) |
| sodium hydroxide..... | Penta (Prague, Czechia) |
| sodium phosphate dibasic..... | Sigma-Aldrich (St. Louis, USA) |
| sodium thiosulfate pentahydrate..... | Penta (Prague, Czechia) |
| sucrose..... | Sigma-Aldrich (St. Louis, USA) |
| SuperSignal West Femto..... | Thermo Scientific (Waltham, USA) |
| SYPRO® Orange Protein Gel Stain..... | Sigma-Aldrich (St. Louis, USA) |
| TEMED (tetramethylethyldiamine)..... | Fluka (Buchs, Switzerland) |
| Tris (tris(hydroxymethyl)aminomethane)..... | USB (Cleveland, USA) |
| Trypan Blue..... | Sigma-Aldrich (St. Louis, USA) |
| Tween 20..... | USB (Cleveland, USA) |
| urea..... | Sigma-Aldrich (St. Louis, USA) |
| X-gal..... | Thermo Scientific (Waltham, USA) |
| Zoletil..... | Virbac (Prague, Czechia) |

3.1.2. Instruments and devices

| | |
|--------------------------|---|
| autoclave: | MLS-3020U, Sanyo (Osaka, Japan) |
| centrifuges: | Biofuge Pico, Heraeus Instruments (Hanau, Germany) Beckman Allegra X-15R, Beckman Coulter (Brea, USA) Centrifuge 5415R, Eppendorf (Hamburg, Germany) Fresco 21 Centrifuge, Thermo Scientific (Waltham, USA) Megafuge 2.0R, Heraeus Instruments (Hanau, Germany) Sorvall Evolution RC, Thermo Scientific (Waltham, USA) |
| chromatography: | ÄKTApurifier 10, GE Healthcare (Chicago, USA) |
| electrophoresis systems: | B1A Gel Electrophoresis, Thermo Scientific (Waltham, USA) B3 Gel Electrophoresis, Thermo Scientific (Waltham, USA) Vertical Electrophoresis Sigma-Aldrich (St. Louis, USA) |
| filtration system: | LabScale™ TFF system, Millipore (Billerica, USA) |
| homogenizer: | TissueLyser II, Qiagen (Hilden, Germany) |
| imaging systems: | LAS-3000 CCD Camera, Fujifilm (Tokyo, Japan) Odyssey CLx Infrared Imaging System, LI-COR Biosciences (Lincoln, USA) UV lamp UVT-20 SML, Herolab (Wiesloch, Germany) |
| incubators: | CO ₂ incubator MCO-17AI, Sanyo (Osaka, Japan) CO ₂ incubator MCO-19AIC, Sanyo (Osaka, Japan) Innova44, New Brunswick Scientific (Enfield, USA) IPP400, Memmert (Schwabach, Germany) |
| laboratory scales: | EK-400H, A&D Company, (Tokyo, Japan) PLS 4000-2, KERN & Sohn GmpH (Postfach, Germany) XA 116/X, Radwag (Sumperk, Czechia) |
| shakers: | KS 260 basic, IKA (Staufen im Breisgau, Germany) Sky Line DRS-12, Elmi (Calabasas, USA) |
| PCR Thermocycler | TGradient, Biometra (Göttingen, Germany) TRIO 48, Biometra (Göttingen, Germany) LightCycler®480 II, Roche (Basel, Switzerland) |
| pH-meter: | pH 50, XS instruments (Carpi, Italy) |

| | |
|-------------------------|--|
| pipettes: | C200-12, CappAero 12-Channel Pipette, CAPP (Nordhausen, Germany) |
| | Pipetman L (2 μ l, 10 μ l, 20 μ l, 200 μ l, 1 ml), Gilson (Middleton, USA) |
| | Pipetman Neo Multichannel (12 channels, 2 – 20 μ l), Gilson (Middleton, USA) |
| | 12-channel pipette 20 - 200 μ l C200-12 (Capp) |
| | REPETMAN Electronic Pipette, Gilson (Middleton, USA) |
| scanner: | CanoScan 8400F, Canon (Tokyo, Japan) |
| scintillation counter: | Tri-Carb Liquid Scintillation Counter, PerkinElmer (Waltham, USA) |
| sonication bath: | S 30 Elmasonic, Elma (Singen, Germany) |
| spectrophotometers: | Infinite® M1000 PRO, Tecan (Männedorf, Switzerland) |
| | NanoDrop ND-1000, Thermo Scientific (Waltham, USA) |
| thermostats: | mixing block MB-102, Bioer (Hangzhou, China) |
| | water bath, Grant (Shepreth, United Kingdom) |
| vortexes: | LTM2, Vývojové dílny ČSAV (Prague, Czechia) |
| | MX-S, Dragonlab (Beijing, China) |
| Western blot apparatus: | Mini Trans-Blot® Cell, Bio-Rad (Hercules, USA) |

3.1.3. Other material

3.1.3.1. Antibodies

| | |
|---|--|
| GCP2-04 | Exbio (Prague, Czechia) |
| GCP2-02 | (Barinka <i>et al.</i> 2004a) |
| Mouse Monoclonal Anti- β -Actin antibody, clone AC-15 |Sigma-Aldrich (St. Louis, USA) |
| YPSMA..... | Anogen (Toronto, Canada) |
| Neutravidin-HRP (1mg/ml) | Thermo Scientific (Waltham, USA) |
| IRDye 680 RD Goat anti-Mouse antibody | LI-COR Biosciences (Lincoln, USA) |
| Goat anti-Mouse IgG (H+L) Secondary Antibody, HRP (0.8 mg/ml) | Thermo Scientific (Waltham, USA) |
| Histofine Simple Stain™ MAX PO (MULTI) | Nichirei Biosciences (Tokyo, Japan) |

3.1.3.2. Enzymes

Benzonase Nuclease Novagen (Madison, USA)
 Restriction enzymes BstZ17I, DpnI, XhoI New England BioLabs (Ipswich, USA)
 Pfu DNA Polymerase..... New England BioLabs (Ipswich, USA)
 Phusion High-Fidelity DNA Polymerase New England BioLabs (Ipswich, USA)
 proteinase K..... New England BioLabs (Ipswich, USA)

3.1.3.3. Cell cultures

E. coli Top10 cells Invitrogen (Carlsbad, USA)
Drosophila Schneider's S2 cells..... Invitrogen (Carlsbad, USA)
 HEK 293 cells..... ATTC (Manassas, USA)

3.1.3.4. Primers

All primers were purchased from Sigma-Aldrich. Primers 1-4 were used for genotyping (see Chapter 3.2.1.2., p. 51 and 3.2.1.4., p. 52), primers 5-16 for mutagenesis (see Chapter 3.2.2.1., p. 53) and primers 17-22 for sequencing (see Chapter 3.2.1.2., p. 51, 3.2.2.1., p. 53 and 3.2.3.1., p. 57).

| # | DESIGNATION | SEQUENCE |
|----|------------------|--|
| 1 | Folh1-F | 5'-GGGCTATGCATTTTTCAGGA-3' |
| 2 | Folh1-R | 5'-GCAGCAAGTGCCTTAACCAG-3' |
| 3 | F-mGCPII_genotyp | 5'-ATTTTGTGGCAAGCTGG-3' |
| 4 | R-mGCPII_genotyp | 5'-CACTCAGTAGAACCAAGAAGG-3' |
| 5 | F-mGCPIIdel3 | 5'-TGCAAGCTGGGATGCAGAAGTTGGCCTTCTTGGTTCTACT-3' |
| 6 | R-mGCPIIdel3 | 5'-AGTAGAACCAAGAAGGCCAATTCTGCATCCCAGCTTGCA-3' |
| 7 | F-mGCPIIdel4 | 5'-TGCAAGCTGGGATGCAGATGTGGCCTTCTTGGTTCTACTG-3' |
| 8 | R-mGCPIIdel4 | 5'-CAGTAGAACCAAGAAGGCCACATCTGCATCCCAGCTTGCA-3' |
| 9 | F-mGCPIIdel6 | 5'-TGCAAGCTGGGATGCAGAAGGCCTTCTTGGTTCTACTG-3' |
| 10 | R-mGCPIIdel6 | 5'-CAGTAGAACCAAGAAGGCCTTCTGCATCCCAGCTTGCA-3' |
| 11 | F-mGCPIIdel9 | 5'-TTTGTGGCAAGCTGGGATGAAGGCCTTCTTGGTTCTACT-3' |
| 12 | R-mGCPIIdel9 | 5'-AGTAGAACCAAGAAGGCCTTCATCCCAGCTTGCAAACAAA-3' |
| 13 | F-mGCPIIdel12 | 5'-TTTGTGGCAAGCTGGGATGGCCTTCTTGGTTCTACTGAG-3' |
| 14 | R-mGCPIIdel12 | 5'-CTCAGTAGAACCAAGAAGGCCATCCCAGCTTGCAAACAAA-3' |
| 15 | F-mGCPIIdel17 | 5'-CAATTTTGTGGCAAGCTGGCCTTCTTGGTTCTACTGAGT-3' |
| 16 | R-mGCPIIdel17 | 5'-ACTCAGTAGAACCAAGAAGGCCAGCTTGCAAACAAAATTG-3' |
| 17 | M13 Reverse | 5'-CAGGAAACAGCTATGAC-3' |
| 18 | FseqpTRETight | 5'-AGGCGTATCACGAGGCCCTTTCGT-3' |
| 19 | RseqpTRETight | 5'-TATTACCGCTTTGAGTGAGCTGA-3' |
| 20 | RMin1-forward | 5'-GCACGAAGTGAAGACTTCTTTAACTGGAACGGG-3' |
| 21 | RMin3-reverse | 5'-CATAGACACTGTGATAGAGAGGATAGCTGC-3' |
| 22 | BGH-reverse | 5'-TAGAAGGCACAGTCGAGG-3' |

3.1.3.5. Vectors

- pCoBlast Invitrogen (Carlsbad, USA)
 pCR™II-TOPO® Invitrogen (Carlsbad, USA)
 pTreTight-mGCPII (Knedlik 2008)

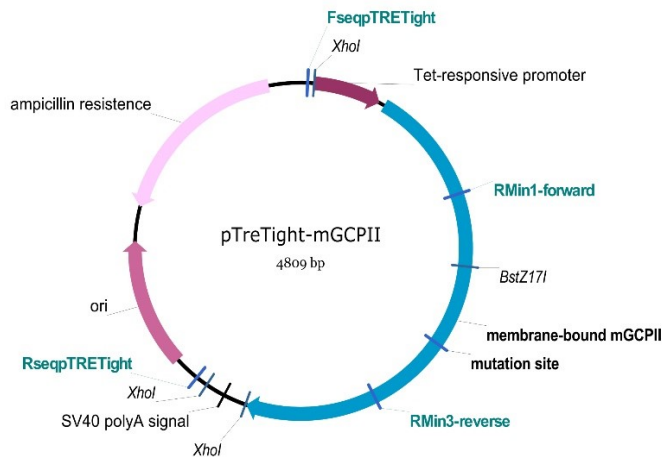


Figure 10: Vector map of pTreTight-mGCPII encoding membrane-bound mGCPII in mammalian cells. The approximate site where the deletions were introduced in order to generate vectors encoding membrane-bound mGCPII mutant variants is designated as ‘mutation site’ (for more information see Chapter 3.2.2.1., p. 53). Restriction sites for *BstZ171* and *XhoI* to clone the mutated part into the pMT/BiP/Avi_rm-GCPII are shown. Sequencing primers are designated teal.

- pMT/BiP/Avi_rm-GCPII (Knedlik *et al.* 2017)

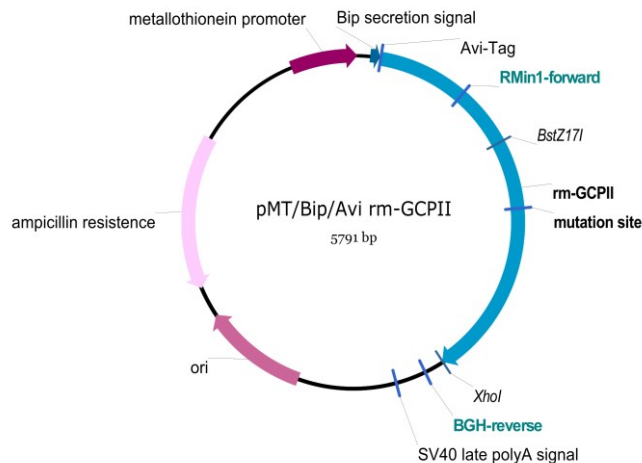


Figure 11: Vector map of pMT/BiP/Avi_rm-GCPII encoding extracellular part of mGCPII in insect cells (rm-GCPII). The protein construct rm-GCPII consists of extracellular part of mGCPII and Avi-Tag that is specifically biotinylated during the protein expression. The expression is induced by addition of Cu^{2+} cations that bind to the metallothionein (MT) promoter (for more information see Chapter 3.2.3.2., p. 58). The ‘Bip secretion signal’ ensures that the expressed protein is secreted into the conditioned media of the cells. Restriction sites for *BstZ171* and *XhoI* to clone the mutated part from pTreTight-mGCPII mutant variants into the pMT/BiP/Avi_rm-GCPII in order to generate vectors encoding rm-GCPII mutant variants are shown (for more information see Chapter 3.2.3.1., p. 57). Sequencing primers are designated teal.

3.1.3.6. Chromatography columns and recyclable filters

| | |
|--------------------------------------|------------------------------|
| AG1-X resin..... | Bio-Rad (Hercules, USA) |
| HiLoad™ Superdex™ 200 10/300 GL..... | GE-Healthcare (Chicago, USA) |
| Pellicon XL Biomax50 cassette..... | Millipore (Billerica, USA) |
| Streptavidin Mutein Matrix™..... | Roche (Basel, Switzerland) |

3.1.3.7. Consumables

| | |
|---|-----------------------------------|
| Amicon® Ultra 0.5 mL..... | Millipore (Billerica, USA) |
| Amicon® Ultra 15 mL..... | Millipore (Billerica, USA) |
| Cell Culture plates 35mm, 100mm..... | Biotech (Prague, Czechia) |
| Calcium Phosphate Transfection Kit..... | Invitrogen (Carlsbad, USA) |
| Creatinine enzymatic kit..... | Dialab (Wiener Neudorf, Austria) |
| disposable 5ml gravity-flow columns..... | Thermo Scientific (Waltham, USA) |
| disposable pipettes 5 ml, 10 ml, 25 ml..... | Baria (Prague, Czechia) |
| Gilson pipette tips 10 µl, 200 µl, 300 µl, 1000 µl..... | SIPOCH (Prague, Czechia) |
| LightCycler® 480 Multiwell Plate 96..... | Roche (Basel, Switzerland) |
| LightCycler® 480 Sealing Foil..... | Roche (Basel, Switzerland) |
| Micro-tubes 1.5 ml, 2 ml..... | Sarstedt (Prague, Czechia) |
| Microcon-10kDa Centrifugal Filter..... | Millipore (Billerica, USA) |
| Microtitration 96-well plate, F-bottom..... | P-lab (Prague, Czechia) |
| Microtitration 96-well plate, U-bottom..... | P-lab (Prague, Czechia) |
| Mouse Direct PCR Kit..... | Bimake (Houston, USA) |
| nitrocellulose membrane..... | Bio-Rad (Hercules, USA) |
| NUNC Maxisorb 96 well plate..... | Trigon Plus (Cestlice, Czechia) |
| Pasteur pipettes..... | P-lab (Prague, Czechia) |
| PCR tubes..... | Shoeller Pharma (Prague, Czechia) |
| PCR strips..... | Biogen (Prague, Czechia) |
| Petri dishes 90mm..... | GAMA (Ceske Budejovice, Czechia) |
| Pipette filter tips 10 µl, 200 µl, 1000 µl..... | SIPOCH (Prague, Czechia) |
| QIAquick Gel Extraction Kit..... | Qiagen (Hilden, Germany) |
| Repet-tips 0.5 ml, 5 ml, 12.5 ml..... | Gilson (Middleton, USA) |
| Sorensen pipette tips 10 µl, 200 µl, 1000 µl..... | MUF-Pro (Prague, Czechia) |
| TOPO® TA Cloning® Kit..... | Invitrogen (Carlsbad, USA) |
| tubes 15 ml, 50 ml..... | Sarstedt (Prague, Czechia) |
| Whatman filter paper, Grade 470..... | GE-Healthcare (Chicago, USA) |
| Zyppy™ Plasmid Miniprep Kit..... | Zymo Research (Irvine, USA) |

3.1.4. Software

| | |
|------------------------|--|
| ChemDraw 13 | PerkinElmer (Waltham) |
| Gimp 2.10.4 | The GIMP Development Team |
| GraFit 5 | Erithacus Software Ltd (Horley Surrey, United Kingdom) |
| Inkscape | The Inkscape Development Team |
| Microsoft Office | Microsoft Corporation (Redmond, USA) |
| Vector NTI 11 | Invitrogen (Carlsbad, USA) |

3.2. Methods

3.2.1. Preparation of GCPII mutant mice

All animal procedures were performed in accordance with European directive 2010/63/EU, ethically reviewed and approved by the Czech Central Commission for Animal Welfare. All mice were housed under standard pathogen-free conditions. GCPII deficient mice were prepared by Transcription Activator-Like Effector Nuclease (TALEN)-mediated genome editing, which was performed by Dr. Petr Kasparek at IMG CAS. More information on the preparation of F0 generation could be found in (Vorlova *et al.* 2018).

3.2.1.1. Phenol-chloroform extraction of chromosomal DNA

Chromosomal DNA was isolated from tail biopsies of newborn pups, which were performed by trained technician in the Animal Facility of IMG CAS. First, tail was incubated in 1 ml of lysis buffer containing 100 mM Tris-HCl, 200 mM NaCl, 5 mM EDTA, 0.2% SDS and 250 µg/ml Proteinase K overnight at 55 °C. Second, phenol solution equilibrated with 10 mM Tris HCl, pH 8.0 (Sigma-Aldrich) was mixed with chloroform in a ratio of 1:1 and phenol/chloroform extraction was performed by addition of 750 µl of phenol/chloroform into the tail digest solution. After 15 seconds of shaking, solution was centrifuged at 16000 g for 3 minutes and the upper aqueous phase was transferred into a new tube. The phenol/chloroform extraction was repeated once, aqueous phase was subsequently transferred into a new tube and mixed thoroughly with 100 µl of 3 M sodium acetate, pH 6.0 and 1 ml of 100% ethanol (Penta). The solution

with precipitated DNA was centrifuged at 16000 g for 5 minutes followed by aspiration of the supernatant and washing of the pellet by 750 µl of 75% ethanol. Finally, the solution was centrifuged at 16000 g for 5 minutes, the supernatant aspirated and the pellet dried out for 1-2h before being dissolved in 100 µl of deionized water.

3.2.1.2. Analysis of TALEN-mediated mutations

Chromosomal DNA isolated from tail biopsies was used as a template for PCR to generate fragments of around 500 bp (546 bp for wild type allele) that were ligated into pCRII-TOPO vector and analysed for the presence of TALEN-mediated mutations using Sanger sequencing. PCR reactions of total volume of 20 µl consisted of 10-50 ng of chromosomal DNA, 1µM primers – Folh1-F and Folh1-R (for more information see Chapter 3.1.3.4., p. 47) – and PPP Master Mix (Top-Bio) that contains Taq DNA polymerase, dNTPs and optimized reaction buffer. The reactions were run in PCR Thermocycler (Biometra) using initialization for 3 minutes at 95 °C followed by 33 cycles of denaturation for 30 seconds at 95 °C, annealing for 30 seconds at 63 °C and elongation for 40 seconds at 72 °C. Final elongation was performed for 5 minutes at 72 °C. PCR products were separated by horizontal agarose electrophoresis at 120V for 40 minutes using 1% agarose (Serva) in TAE buffer (40 mM Tris-acetate, pH 8.4, 1 mM EDTA) containing GelRed 10000X (Biotinum) and visualized by UV lamp (Herolab). Fragments of around 500 bp were isolated from the gel using QIAquick Gel Extraction Kit (Qiagen) according to manufacturer's instructions.

Isolated DNA fragments were ligated into pCRII-TOPO vector using TOPO TA Cloning Kit (Invitrogen) according to manufacturer's instructions. As the competent cells, *E. coli* strain Top10 (Invitrogen) was used. Next day, at least 6 white colonies from each agar plate were taken and cultured with LB medium containing 50 µg/ml ampicillin overnight at 37 °C. The subsequent isolation of amplified plasmids was performed using Zyppy™ Plasmid Miniprep Kit (Zymo Research) according to manufacturer's instructions. Plasmid DNA purity and concentration was assessed by spectrophotometry using NanoDrop (Thermo Scientific) and the resulting plasmids were sequenced by GATC Biotech (Konstanz, Germany) using M13 Reverse primer (for more information see Chapter 3.1.3.4., p. 47). DNA sequences were analysed using Vector NTI software (Invitrogen).

3.2.1.3. Establishment of GCPII mutant mouse colonies and colony management

Three founder mice carrying in total 5 deletions – 3 bp (del3), 4 bp (del4), 6 bp (del6), 12 bp (del12) and 17 bp (del17) – within exon 11 of *Folh1* gene were bred with C57Bl/6NCrl wild type (WT) mouse to produce F1 generation. To avoid genetic drift, all colonies were bred in a breeding scheme heterozygous mutant × wild type. For each generation, C57Bl/6NCrl WT mice were supplemented from the Animal Facility of IMG CAS. Homozygous mutants and their heterozygous mutant and WT littermates were produced by crossbreeding of heterozygous mutants of at least F2 generation.

3.2.1.4. GCPII-mutant mice genotyping

Tail biopsies of 3-weeks old pups were taken by trained technician in the Animal Facility of IMG CAS. Chromosomal DNA was isolated from tail biopsies using Mouse Direct PCR Kit (Bimake) according to manufacturer's instructions with slight modifications. The mouse tail was incubated with 50 µl of Buffer L and 1 µl of Protease Plus (both supplemented in the Mouse Direct PCR Kit) for 30 minutes at 55°C followed by incubation for 5 minutes at 95 °C.

The tissue lysate was subsequently used as a template for nested PCR consisting of 2 successive rounds of PCR. In the first round, *Folh1*-F and *Folh1*-R primers were used to amplify fragment of around 540 bp (546 bp for WT allele, 543 bp for del3 allele, 542 bp for del4 allele, 540 bp for del6 allele, 534 bp for del12 allele and 529 bp for del17 allele). PCR reactions of total volume of 20 µl consisted of 1 µl template, 0.25 µM primers and M-PCR OPTI mix (supplemented in the Mouse Direct PCR Kit) that contains Taq DNA polymerase, dNTPs and optimized reaction buffer. The reactions were run in PCR Thermocycler (Biometra) using initialization for 3 minutes at 95 °C followed by 33 cycles of denaturation for 30 seconds at 95 °C, annealing for 30 seconds at 57 °C and elongation for 40 seconds at 72 °C. Final elongation was performed for 5 minutes at 72 °C. PCR reactions from the first round of nested PCR were subsequently diluted 200-fold by deionized water and served as templates for second round of nested PCR.

In the second round, PCR reactions of total volume of 20 µl consisted of 1 µl diluted template, 0.25 µM primers – F-mGCPII_genotyp and R-mGCPII_genotyp (for more information see Chapter 3.1.3.4., p. 47) – and PPP Master Mix (Top-Bio) that

contains Taq DNA polymerase, dNTPs and optimized reaction buffer. The reactions were run in PCR Thermocycler (Biometra) using initialization for 3 minutes at 95 °C followed by 33 cycles of denaturation for 30 seconds at 95 °C, annealing for 30 seconds at 58 °C and elongation for 30 seconds at 72 °C. Final elongation was performed for 1 minute at 72 °C.

PCR products of the second round of nested PCR were analysed by DNA polyacrylamide gel electrophoresis (DNA-PAGE). The gel consisted of TBE buffer (89 mM Tris-borate, pH 8.3, 2 mM EDTA), 16% (v/v) acrylamide mixture (acrylamide with N,N'-bisacrylamide in a ratio of 19:1), 0.1% (w/v) ammonium persulfate (APS) and 0.01% (v/v) TEMED. 5 µl of the reaction mixture from the second round of nested PCR were loaded into the polyacrylamide gel and PCR products were separated in vertical electrophoresis apparatus (Sigma-Aldrich) filled by the TBE running buffer at 160V for 90 minutes. To analyse the amplified fragments of specific length (56 bp for WT allele, 53 bp for del3 allele, 52 bp for del4 allele, 50 bp for del6 allele, 44 bp for del12 allele, 39 bp for del17 allele), the polyacrylamide gel was incubated in 10000× diluted GelRed (Biotium) in TBE buffer for 30 minutes and visualized by UV lamp (Herolab).

3.2.2. Preparation of membrane-bound protein variants of mouse

GCPII

3.2.2.1. Cloning of vectors encoding membrane-bound protein variants of

mGCPII

All vectors encoding membrane-bound mutant variants (del3, del4, del6, del12 and del17) were prepared by site-directed mutagenesis. As a starting vector, pTreTight-mGCPII plasmid (see Chapter 3.1.3.5., p. 48), which encodes full-length mGCPII protein was used. This vector was previously prepared by colleagues in our laboratory.

Plasmids pTreTight-mGCPIIdel3, pTreTight-mGCPIIdel4 and pTreTight-mGCPIIdel6 were prepared from pTreTight-mGCPII using Phusion High-Fidelity DNA Polymerase (New England BioLabs) according to manufacturer's instructions with slight modifications. PCR reactions of total volume of 40 µl consisted

of 20 ng of template vector, 0.75 μ M primers (for more information see Chapter 3.1.3.4., p. 47), Phusion HF buffer (New England BioLabs), 250 μ M dNTPs and 0.6 U of Phusion High-Fidelity DNA Polymerase. The reactions were run in PCR Thermocycler (Biometra) using initialization for 1 minute at 98 °C followed by 20 cycles of denaturation for 15 seconds at 98 °C, annealing for 45 seconds at 40 °C and elongation for 4 minutes at 72 °C. Final elongation was performed for 10 minutes at 72 °C.

Plasmids pTreTight-mGCPII~~12~~ and pTreTight-mGCPII~~17~~ were prepared by site-directed mutagenesis using Pfu DNA polymerase (New England BioLabs). First, an intermediate step of site-directed mutagenesis producing the plasmid pTreTight-mGCPII~~9~~ from the plasmid pTreTight-mGCPII~~6~~ was performed. The plasmid pTreTight-mGCPII~~9~~ then served as a template for preparation of the plasmid pTreTight-mGCPII~~12~~. Finally, the plasmid pTreTight-mGCPII~~12~~ was used as a template for preparation of the pTreTight-mGCPII~~17~~. PCR reactions of total volume of 50 μ l consisted of 50 ng of template vector, 1 μ M primers (for more information see Chapter 3.1.3.4., p. 47), reaction buffer (New England BioLabs), 250 μ M dNTPs and 2.5 U of Pfu DNA polymerase. The reactions were run in PCR Thermocycler (Biometra) using initialization for 30 seconds at 95 °C followed by 18 cycles of denaturation for 30 seconds at 95 °C, annealing for 1 minute at 55 °C and elongation for 5 minutes at 68 °C.

After the site-directed mutagenesis, 20 U of DpnI (New England BioLabs) was added into each PCR reaction mixture and the reactions were incubated for 1 hour at 37 °C. Uncleaved plasmids were subsequently purified using QIAquick Gel Extraction Kit (Qiagen) according to manufacturer's instructions and transformed into the *E. coli* Top10 competent cells (Invitrogen) according to the manufacturer's instruction. The success of mutagenesis was monitored by colony PCR. At least 5 colonies from each agar plate were taken and each of the colonies was suspended in 10 μ l of deionized water. 3 μ l of this bacterial mixture were used as a template for PCR reaction that was performed the same way as the second round of nested PCR within the GCPII-mutant mice genotyping (see Chapter 3.2.1.4., p. 54). Additionally, 2 μ l of the bacterial mixture was transformed onto the new agar plate containing ampicillin and let grow overnight at 37 °C.

Based on the result of colony PCR, a bacterial colony from each mutagenesis was chosen and cultured with LB medium containing 50 μ g/ml ampicillin overnight at 37 °C.

The subsequent isolation of amplified plasmids was performed using Zyppy™ Plasmid Miniprep Kit (Zymo Research) according to manufacturer's instructions. Plasmid DNA purity and concentration was assessed by spectrophotometry using NanoDrop (Thermo Scientific) and the resulting plasmids were sequenced by GATC Biotech (Konstanz, Germany) using several different primers – FseqpTRETight, RseqpTRETight, RMin1-forward and RMin3-reverse (for more information see Chapter 3.1.3.4., p. 47). DNA sequences were analysed using Vector NTI software (Invitrogen).

3.2.2.2. Expression of membrane-bound protein variants of mGCPII using

HEK293 cells

Membrane-bound protein variants of mGCPII were expressed after transient transfection of pTreTight- vectors (mGCPII, mGCPII~~13~~, mGCPII~~14~~, mGCPII~~16~~, mGCPII~~12~~ and mGCPII~~17~~; see Chapter 3.2.2.1., p. 53) into the cell line HEK293offA2. This cell line contains Tet-Off expression system and was derived from HEK293 cells (human embryonic kidney cell line) by stable transfection of a plasmid pTet-Off-Advanced (Clontech). The preparation of HEK293offA2 was performed previously by Dr. Pavel Šácha and Jana Starková in our laboratory.

HEK293offA2 cells were cultured in 100 mm plates filled by 10 ml IMDM complete medium (IMDM (Gibco) supplemented by 10% FBS (Gibco) and 40 mM L-glutamine) until reaching a confluence of 60-70%. The transfection mixture of total volume of 830 µl consisted of opti-MEM medium (Gibco), 21 µg of plasmid DNA and 10% (v/v) polyethylenimine (Sigma-Aldrich). After 15 minutes incubation at room temperature, the transfection mixture was carefully added into and gently mixed with the IMDM complete medium in the plates with HEK293offA2 cells. The cells were incubated at 37 °C and 5% CO₂ for 3 days before being harvested by suspending in the IMDM complete medium followed by centrifugation for 5 minutes at 500 g. Finally, the cells were washed twice by PBS and stored lysed by cell lysis buffer (see Chapter 3.2.2.3., p. 56).

3.2.2.3. Analysis of the protein yield of membrane-bound mGCPII variants

HEK293offA2 cells with expressed membrane-bound mGCPII variants were lysed by cell lysis buffer, which consisted of 50 mM Tris-HCl, pH 7.4, 100 mM NaCl, 1× cOmplete protease inhibitor cocktail (Roche) and 1% C12E8 detergent (Affymetrix). Cells harvested from one 100 mm plate were suspended in 450 µl of cell lysis buffer, sonicated three times for 1 minute in a cold-water bath and incubated on ice for 45 minutes. Subsequently, the cell suspension was sonicated for 1 minute in a cold-water bath and centrifuged for 20 minutes at 600 g, 4 °C. The protein concentration was measured in the supernatant using Bradford protein assay (see Chapter 3.2.5.2., p. 64) and the approximate level of expression of all membrane-bound mGCPII variants was assessed by Western blotting (see Chapter 3.2.6., p. 65).

To measure the exact amount of membrane-bound mGCPII variants in the cell lysates, denatured ELISA was performed. For this purpose, standard (rm-GCPII, see Chapter 3.2.3., p. 57) as well as cell lysate solutions were first denatured. Standard was diluted by cell lysis buffer containing 1% SDS to a final concentration of 50 ng/µl and heated by temperature gradient 0.2 °C/s to 70 °C followed by rapid cooling to 20 °C. The denatured solution was then diluted by ELISA sample buffer, which consisted of 50 mM Tris-HCl, pH 7.4, 100 mM NaCl, 0.2% Tween-20 and 0.08% SDS, to generate standard solutions of concentrations of 100, 75, 50, 37.5, 25, 10, 5, 2.5, 1.25 and 0.63 pg/µl. Cell lysates of total protein amount of 30 µg approximately were mixed with 10% SDS to reach a final concentration of SDS of 1%. Subsequently, the mixtures were heated by temperature gradient 0.2 °C/s to 70 °C, rapidly cooled down to 20 °C and diluted 20×, 40×, 80× and 160× by ELISA sample buffer.

ELISA was performed in a 96-well plate format and all procedures were carried out at room temperature. All incubations and washes were carried out on an orbital shaker at 100 RPM and 500 RPM, respectively. The NUNC Maxisorb 96-well plate was coated with 500 ng of capturing antibody GCP-04 (Exbio) diluted in 100 mM borate, pH 9.5, per well for 75 minutes. The wells were subsequently washed three times by TBS (50 mM Tris-HCl, pH 7.6, 137 mM NaCl, 2.7 mM KCl) and blocked for 4 hours by 250 µl of Casein Buffer 20X-4X Concentrate (SDT) diluted 10× in TBS. After washing for three times by 250 µl of TBS containing 0.05% Tween-20, 100 µl of denatured standard solutions or denatured cell lysates were added to pre-coated wells and incubated for 1 hour. The wells were then washed three times with TBS containing

0.05% Tween-20, and incubated for 35 minutes with 50 ng of biotinylated antibody GCP-02 (Barinka *et al.* 2004a) diluted in the ELISA sample buffer. After next washing step, all wells were incubated for 30 minutes with 50 ng of neutravidin-HRP (Pierce) diluted in TBS containing 0.1% Tween-20. Subsequently, plates were washed five times with TBS containing 0.05% Tween-20 and 175 μ l of chemiluminescent substrate solution (100 mM Tris-HCl, pH 8.0, 2.5 mM luminol (Sigma-Aldrich), 2 mM 4-iodophenol (Thermo Scientific) and 0.018% hydrogen peroxide (Sigma-Aldrich)) were added to each well. The chemiluminescence was measured for 500 ms using an Infinite® M1000 PRO (Tecan).

3.2.3. Preparation and characterization of extracellular parts of protein variants of mouse GCPII

3.2.3.1. Cloning of vectors encoding extracellular parts of protein variants of mGCPII

The plasmid pMT/BiP/Avi_rm-GCPII (see Chapter 3.1.3.5., p. 48) encoding extracellular part of mGCPII wild type (WT) was generated previously in our laboratory (Knedlik *et al.* 2017). All mutant variants (del3, del4, del6, del12 and del17) were prepared by Lenka Simonova, who performed restriction enzyme digestion of corresponding pTreTight- vectors and pMT/BiP/Avi_rm-GCPII using enzymes BstZ17I and XhoI (New England BioLabs) followed by ligation of the fragment from pTreTight- vector into the cleaved pMT/BiP/Avi_rm-GCPII.

The reaction mixture consisted of 1 μ g of plasmid DNA, CutSmart buffer supplemented with the enzymes, 20 U of XhoI and 20 U of BstZ17I. After the incubation for 1 hour at 37 °C, the samples were mixed with DNA loading buffer (40% sucrose, 0.25% bromphenol blue) and the restriction enzyme digestion products were separated by horizontal agarose electrophoresis (1% agarose in TAE buffer containing GelRed 10000X, 120V, 40 minutes).

The fragments from pTreTight- vectors of around 1400 bp and the linearized pMT/BiP/Avi_rm-GCPII of around 3400 bp were isolated from the gel using QIAquick Gel Extraction Kit (Qiagen) according to manufacturer's instructions. The ligation of the

fragments into the linearized vector was carried out by T4 DNA ligase (New England BioLabs) according to manufacturer's instructions. As the competent cells, *E. coli* strain Top10 (Invitrogen) was used. Next day, a colony from each agar plate was taken and cultured with LB medium containing 50 µg/ml ampicillin overnight at 37 °C.

The subsequent isolation of amplified plasmids pMT/BiP/Avi_rm-GCPII~~3~~, pMT/BiP/Avi_rm-GCPII~~4~~, pMT/BiP/Avi_rm-GCPII~~6~~, pMT/BiP/Avi_rm-GCPII~~12~~ and pMT/BiP/Avi_rm-GCPII~~17~~ was performed using Zyppy™ Plasmid Miniprep Kit (Zymo Research) according to manufacturer's instructions. Plasmid DNA purity and concentration was assessed by spectrophotometry using NanoDrop (Thermo Scientific) and the resulting plasmids were sequenced by GATC Biotech (Konstanz, Germany) using Rmin1-forward and BGH-reverse primers (for more information see Chapter 3.1.3.4., p. 47). DNA sequences were analysed using Vector NTI software (Invitrogen).

3.2.3.2. Expression of extracellular parts of protein variants of mGCPII using

***Drosophila* S2 cells**

The extracellular parts of wild type and mutant variants of mouse GCPII (rm-GCPII, rm-GCPII~~3~~, rm-GCPII~~4~~, rm-GCPII~~6~~, rm-GCPII~~12~~ and rm-GCPII~~17~~) were expressed in a similar fashion as previously described in (Knedlik *et al.* 2017). The stably transfected cultures of *Drosophila* S2 cells expressing these recombinant proteins were prepared by Jana Starkova. For the stable transfection, *Drosophila* S2 (BiP-BirA-KDEL) cells previously prepared in our laboratory were utilized. These cells were generated by stable co-transfection of *Drosophila* S2 cells by pMT/BiP/BirA/KDEL (Tykvar *et al.* 2012) and pCoHygro (Invitrogen) to generate hygromycin-resistant cell cultures that express biotin-protein ligase (*BirA*) within endoplasmic reticulum.

Drosophila S2 (BiP-BirA-KDEL) cells were grown in a 35 mm plate in SF900II complete medium (SF900II (Gibco) supplemented by 10% FBS (Gibco)) at 25 °C until reaching a density of 2×10^6 cells per ml. The co-transfection of the cells by pMT/BiP/Avi_rm-GCPII- vectors and pCoBlast (Invitrogen) was subsequently performed using the Calcium Phosphate Transfection Kit (Invitrogen) according to manufacturer's instruction. Cells containing transfected vectors were selected using

cultivation of the transfectants at 25 °C in the SF900II complete medium containing blasticidin (Invitrogen) and hygromycin B (Invitrogen).

To investigate the ability of the stably transfected cultures to express rm-GCP II WT and mutant variants, the cells were cultured at 25 °C in a 35-mm plate in SF900II medium (Gibco) and the protein expression was induced by CuSO₄ as described in (Knedlik *et al.* 2017). The presence of the rm-GCP II WT and mutant variants in the conditioned media was analysed by Western blotting (see Chapter 3.2.6., p. 65). The cell cultures expressing the highest amounts of the recombinant proteins were used for large-scale expression. Large-scale expression was carried out in a similar fashion as previously described for recombinant human GCP II (rh-GCP II) (Barinka *et al.* 2002). Briefly, stably transfected cell cultures were cultured in SF900II medium (Gibco) in a spinner flask at 25 °C until reaching a density of 8×10⁶ cells per ml in 500-1000 ml cell suspension. The recombinant protein expression was induced by 1 mM CuSO₄ followed by procedures identical to those described in (Barinka *et al.* 2002). The cells were harvested after 8 days from induction by centrifugation at 500 g for 10 minutes. The supernatants were then centrifuged at 4000 g for 30 minutes, analysed for expression yield of rm-GCP II WT and mutant variants using Western blotting (see Chapter 3.2.6., p. 65) and stored at -80 °C until further use.

3.2.3.3. Purification of extracellular parts of protein variants of mGCP II

The supernatants from recombinant protein expressions (see Chapter 3.2.3.2., p. 58) containing biotinylated rm-GCP II and its mutant variants were thawed, centrifuged for 30 minutes at 5250 g, 4 °C and concentrated 10× using LabScale™ TFF system (Millipore) with a Pellicon XL Biomax50 cassette (Millipore). The recombinant proteins were subsequently purified from the concentrated S2 cell media using Streptavidin Mutein Matrix (Roche) according to previously published protocol (Tykvart *et al.* 2012) with minor modifications. Briefly, two rounds of purification were performed; each round consisted of incubation of equilibrated conditioned medium (i.e. flow-through fraction from the first round in case of the second round) with Streptavidin Mutein Matrix overnight at 4 °C, two washing steps and five elution steps. The first washing step was performed by 2 column volumes (cv) of washing buffer (100 mM Tris-HCl, pH 7.2, 150 mM NaCl), while the second washing step was performed by 25cv of washing

buffer. All elution steps were performed by 1 cv of elution buffer (100 mM Tris-HCl, pH 7.2, 150 mM NaCl, 2 mM D-biotin).

Following the purification, the fractions containing the highest amount of the recombinant proteins were poured and their buffers were changed to 10 mM Tris-HCl, pH 7.4, 100 mM NaCl using Amicon Ultra centrifugal filters (Millipore) according to manufacturer's instructions. Finally, the protein concentration in the solutions was determined by spectrophotometry using NanoDrop (Thermo Scientific) (see Chapter 3.2.5.1., p. 64) and the solutions were concentrated using Amicon Ultra centrifugal filters (Millipore) to reach a minimum protein concentration of 1 mg/ml.

3.2.3.4. Sodium dodecyl sulphate-polyacrylamide gel electrophoresis (SDS-PAGE)

To monitor the purification, discontinuous SDS-PAGE followed by silver staining of the polyacrylamide gel was performed. All gels consisted of 11% resolving gel and 5% stacking gel. All samples for the SDS-PAGE were mixed with SDS-PAGE loading buffer (350 mM Tris, pH 6.8, 30% glycerol, 10% SDS, 4% 2-mercaptoethanol, 0.01% bromphenol blue) in a ratio of 5:1 and boiled for 10 minutes. The samples for the SDS-PAGE were collected from all purification steps. While in most cases 10 µl of the purification fraction were analysed, in case of the first elution fraction, 1 µl was usually sufficient. To compare purification outcomes of different protein variants using SDS-PAGE followed by silver staining, 250 ng of total protein were loaded into the polyacrylamide gel.

The mixture for 11% resolving gel consisted of 375 mM Tris-HCl (pH 8.8), 11% (v/v) acrylamide mixture (acrylamide with N,N'-bisacrylamide in the ratio 35.7:1), 0.1% (w/v) SDS, 0.1% (w/v) ammonium persulfate (APS) and 0.01% (v/v) TEMED. The mixture for 5% stacking gel consisted of 250 mM Tris-HCl (pH 6.8), 5% (v/v) acrylamide mixture (acrylamide with N,N'-bisacrylamide in a ratio 35.7:1), 0.1% (w/v) SDS, 0.1% (w/v) ammonium persulfate (APS) and 0.02% (v/v) TEMED. SDS-PAGE was run in the vertical electrophoresis apparatus (Sigma-Aldrich) filled by SDS running buffer (25 mM Tris- glycine, pH 8.8, 0.1% SDS) at a constant voltage of 150 V until the bromphenol blue dye reached the bottom of the gel.

The separated proteins were visualized by silver staining. First, the gel was fixed by fixation buffer (12% (v/v) acetic acid, 50% (v/v) methanol, 0.02% (v/v) formaldehyde) for 20 minutes and washed three times by 50% (v/v) methanol for 5 minutes. Exposure, impregnation and development were always followed by washing for three times using distilled water. The exposure was performed by 0.02% (w/v) sodium thiosulfate pentahydrate for 1 minute and the impregnation by 0.2% (w/v) silver nitrate and 0.02% (v/v) formaldehyde for 15 minutes. The gel was subsequently developed by 566 mM sodium carbonate, 16 μ M sodium thiosulfate pentahydrate and 0.02% (v/v) formaldehyde until the protein bands were clearly visible. The gel was additionally incubated in 12% (v/v) acetic acid and 50% (v/v) methanol for 10 minutes and scanned on the scanner (Canon).

3.2.3.5. Size-exclusion chromatography

Size-exclusion chromatography was performed with recombinant proteins rm-GCP_{II} and rm-GCP_{II}del₃ using ÄKTApurifier 10 (GE Healthcare) with a column HiLoad™ Superdex™ 200 10/300 GL (GE-Healthcare). As a mobile phase, buffer consisting of 10 mM Tris-HCl, pH 7.4 and 150 mM NaCl was used. At least 0.5 mg of the recombinant protein (200 μ l of 2.5 mg/ml rm-GCP_{II}, 350 μ l of 1.6 mg/ml rm-GCP_{II}del₃) purified by Streptavidin Mutein (see Chapter 3.2.3.3., p. 59) was injected into the injection valve by an injection loop of 500 μ l. Separation was performed in a flow rate of 0.5 ml/min followed by fractionation by 0.5 ml.

The fractions containing proteins were analysed by SDS-PAGE followed by silver staining in a similar fashion as described in Chapter 3.2.3.4 (p. 60). The sample volume for preparation of SDS-PAGE samples was 5 μ l. Following the size-exclusion chromatography, the fractions containing the highest amount of the recombinant proteins were poured and their buffers were changed to 25 mM BIS-TRIS propane (BTP)/HCl, pH 7.4, 150 mM NaCl using Amicon Ultra centrifugal filters (Millipore) according to manufacturer's instructions. Finally, the protein concentration in the solutions was determined by spectrophotometry using NanoDrop (Thermo Scientific) (see Chapter 3.2.5.1., p. 64) and the solutions were concentrated using Amicon Ultra centrifugal filters (Millipore) to reach a minimum protein concentration of 0.8 mg/ml.

3.2.3.6. Thermofluor assay

To assess thermal stability of rm-GCPII and rm-GCPII^{del3}, Thermofluor assay using protocol similar to that described previously by others (Ericsson 2006) was performed. Thermofluor assay was carried out in a 96-well plate format (LightCycler® 480 Multiwell Plate 96, Roche) with total volume of a tested mixture being 25 µl. The tested mixture consisted of 625× diluted Sypro Orange (Sigma-Aldrich) and 1.5 µg of a recombinant protein diluted in a buffer containing 25 mM BTP/HCl, pH 7.4 and 150 mM NaCl. Thermofluor assay was performed in LightCycler®480 II (Roche) with a temperature range between 20 °C and 95 °C in an increment of 0.01 °C/s. 50 acquisitions were taken per °C. The protein melting temperatures were subsequently analysed using the LightCycler®480 II software (Roche).

3.2.4. Preparation of mouse tissue lysates

3.2.4.1. Collection of mouse tissues

Mice were sacrificed using intraperitoneal injection of anesthetics followed by cervical dislocation. As the anesthetics, a mixture of either ketamine (Narkamon, 125mg/kg) and xylazine (Rometar, 20mg/kg) or tiletamine (Zoletil, 125mg/kg), zolazepam (Zoletil, 125mg/kg) and xylazine (Rometar, 10mg/kg) was used. All dissections were carried out in a maximum of 60 minutes after mice death. Most of the urogenital organs were dissected by MUDr. František Sedlák. Tissues were frozen using dry ice immediately after the collection and stored at -80 °C until processed further.

3.2.4.2. Preparation of kidney and brain lysates

For the tissue lysate preparation, whole male kidney and whole one of the two identical hemispheres of the male brain were taken. All procedures were performed on ice. The tissues were weighted and 3 µl of cold tissue lysis buffer (50 mM Tris-HCl, pH 7.4, 100 mM NaCl, 1× Roche cOmplete protease inhibitor cocktail) were added per 1 mg of the tissue. The homogenization was performed using TissueLyser II (Qiagen) according to manufacturer's instructions. The tissues were first homogenized at 30 Hz and 4 °C for 3 minutes. 120 µl of the tissue homogenate were then taken and mixed with

180 μ l of cold tissue lysis buffer. Usually, the mixture was then additionally homogenized by TissueLyser II at 30 Hz and 4 °C for 3 minutes. The second homogenisation step was not included in the first stages of tissue lysate preparations though, which led to incomplete solubilisation of mGCPII (see Chapter 4.3.1., p. 87).

Prepared homogenates of 300 μ l were mixed with 300 μ l of cold lysis buffer supplemented by 2% Igepal CA-630 (Sigma-Aldrich). The samples were sonicated in a water bath four times for 1 minute at 0 °C and subsequently centrifuged at 16000 g and 4 °C for 30 minutes. While the supernatants (i.e. soluble fractions of tissue lysates) were stored at -80 °C until used further, the pellets (i.e. insoluble fractions of tissue lysates) were processed straight after.

First, the pellets were washed twice by 500 μ l of PBS (12 mM phosphate, pH 7.4, 137 mM NaCl, 2.7 mM KCl) and incubated with 1.3 U of Benzonase Nuclease (Novagen) diluted in PBS. Next, the pellets were suspended in 120 μ l of pellet sample buffer (60 mM Tris, pH 6.8, 15% glycerol, 1% SDS, 4 M urea, 4% 2-mercaptoethanol, 0.01% bromphenol blue) and boiled until completely dissolved. Finally, the samples were mixed thoroughly and stored at -20 °C until further use.

3.2.4.3. Preparation of urogenital tissue lysates

For the male urogenital tissue lysate preparation, whole organs of the urogenital system were taken. The organs included testicle, epididymis, spermatic cord, kidney, ureter, urinary bladder, urethra, seminal vesicle, anterior prostate, dorsal prostate, lateral prostate, ventral prostate, bulbourethral gland and preputial gland. All procedures were performed on ice. The tissues were weighted and 3 μ l of cold tissue lysis buffer (50 mM Tris-HCl, pH 7.4, 100 mM NaCl, 1 \times Roche cOmplete protease inhibitor cocktail) were added per 1 mg of the tissue. The homogenization was performed using TissueLyser II (Qiagen) according to manufacturer's instructions at 30Hz and 4 °C for 5 minutes.

Prepared homogenates were mixed with appropriate amount of cold lysis buffer supplemented by 5% Igepal CA-630 (Sigma-Aldrich) to reach a final detergent concentration of 1%. The mixtures were sonicated in a water bath four times for 1 minute at 0 °C. Finally, the samples were centrifuged at 16000 g and 4 °C for 30 minutes and the supernatants were stored at -80 °C until used further.

3.2.5. Determination of protein concentration

3.2.5.1. NanoDrop measurement of protein concentration

NanoDrop (Thermo Scientific) was used to determine the concentration of purified proteins (see Chapter 3.2.3.3., p. 59 and 3.2.3.5., p. 61). The application module ‘Protein A280’, which measures protein concentration using spectrophotometry at 280 nm, was chosen and the measurement was performed according to manufacturer’s instructions with Sample Type being set to 1 Abs = 1 mg/mL. The final concentration of rm-GCPII WT and mutant variants was then calculated using equation, which takes the extinction coefficient of the proteins into an account:

$$c_{rm-GCPII} = c_{measured} \cdot 0.75$$

3.2.5.2. Bradford protein assay

To determine the protein concentration in the cell lysates (see Chapter 3.2.2.3., p. 56) and tissue lysates (see Chapter 3.2.4., p. 62), Bradford protein assay (Bradford 1976) in a 96-well plate format was utilized. A calibration curve consisted of 10 concentrations of Albumin standard (2 mg/ml, Thermo Scientific) diluted in PBS, the total amount of standard per well ranged from 0.25 µg to 4 µg. The lysates were diluted appropriately to ensure the resulting absorbance being approximately in the middle of the calibration curve.

The samples for protein concentration measurement were prepared by pipetting of 20 µl of diluted standard/lysate into the well of 96-well transparent plate with flat bottom (P-lab) followed by addition of 180 µl of Protein Assay Dye diluted 4.5× in deionized water. The solutions were mixed thoroughly with a multichannel pipette and incubated 5 minutes at room temperature. The absorbance was measured at 595 nm using an Infinite microplate reader (Tecan) and the protein concentrations were subsequently calculated in Microsoft Excel.

3.2.6. Western blot analysis

A combination of SDS-PAGE and wet electroblotting was used for Western blot analysis. Western blotting was utilized to approximate the level of expression of membrane-bound mGCPII variants (see Chapter 3.2.2.3., p. 56), to monitor preparation of the extracellular parts of mGCPII variants (see Chapter 3.2.3., p. 57) and to analyse mouse tissue lysates (see Chapter 3.2.4.2., p. 62). The SDS-PAGE procedure was almost identical to that described in Chapter 3.2.3.4. (p. 60), only the amount of samples loaded into the polyacrylamide gel differed in dependence on the application (see below). The electroblotting was performed onto nitrocellulose membrane in the Mini Trans-Blot® Cell (Bio-Rad) filled by electroblotting buffer (12.5 mM Tris-glycine, pH 8.3, 10% (v/v) methanol) at a constant voltage of 100 V for 1 hour. Membranes were then blocked with casein solution (Casein Buffer 20X-4X Concentrate (SDT) diluted 20× in PBS) for at least 1 hour at room temperature. The subsequent antibody incubations differed in dependence on the application (see below).

When using Western blot analysis to approximate the level of expression of membrane-bound mGCPII variants (see Chapter 3.2.2.3., p. 56), 50 µg of total protein was loaded into the gel. After the casein blocking step, the membrane was incubated for 1 hour at room temperature with 1 µg of GCPII-04 antibody (Exbio) diluted in casein solution. Subsequently, the membrane was washed three times with PBS containing 0.05% Tween-20 and incubated with goat anti-mouse (G-a-M) antibody conjugated with horseradish peroxidase (HRP) diluted 1:25000 in casein solution for 1 hour at room temperature. The second washing step (three times in PBS containing 0.05% Tween-20) was then performed and the membrane was developed using chemiluminescence (see below).

In case of monitoring the preparation of the extracellular parts of mGCPII variants (see Chapter 3.2.3., p. 57), three different Western blot analysis were performed. First, 15 µl of conditioned media were analysed to investigate the ability of stably transfected cell cultures (see Chapter 3.2.3.2., p. 58) to express rm-GCPII WT and mutant variants. Second, after the large-scale expression (see Chapter 3.2.3.2., p. 58), 15 µl of conditioned media were analysed to estimate the expression yield of rm-GCPII WT and mutant variants. Third, 20 ng of rm-GCPII variant approximately (as estimated from the silver stained polyacrylamide gel, see Chapter 3.2.3.4., p. 60) was loaded into the gel in order to compare purification outcomes of rm-GCPII WT and mutant variants. After the casein

blocking step, the membranes were incubated for 2 hours at 4 °C with 2 µg of neutravidin-HRP (Pierce) diluted in casein solution. Subsequently, the membranes were washed four times with PBS containing 0.05% Tween-20 and developed using chemiluminescence (see below).

When using Western blotting to analyse mouse tissue lysates (see Chapter 3.2.4.2., p. 62), an amount of supernatant corresponding to 100 µg of total protein or 20 µl of processed pellet were loaded into the gel. After the casein blocking step, the membranes were incubated overnight at 4 °C with antibody mixture diluted in casein solution. The antibody mixture contained antibody against mGCPII and antibody against β-actin, which served as a loading control. For the detection of mGCPII, antibody GCP-04 (Exbio) labelled by HRP (GCPII-04-HRP) diluted 1:250 in casein solution was used. GCPII-04-HRP was prepared by MUDr. František Sedlák, who conjugated GCPII-04 with HRP at pH 9.4 using EZ-Link™ Plus Activated Peroxidase Kit (Thermo Scientific) according to manufacturer's instructions. For detection of β-actin, Mouse Monoclonal Anti-β-Actin antibody, clone AC-15 (Sigma-Aldrich) in dilutions of 1:5000 (for the kidney and seminal vesicle lysates) and 1:200000 (for the brain lysates) in casein solution was used. Next day, membranes were washed four times with PBS containing 0.05% Tween-20 and incubated for 1 hour at room temperature with IRDye 680 RD Goat anti-Mouse antibody (LI-COR Biosciences) diluted 1:15000 in casein solution. The second washing step (three times in PBS containing 0.05% Tween-20) was then performed and the membranes were developed using both chemiluminescence (to visualize mGCPII, see below) and fluorescence (to visualize β-actin, see below).

Finally, the membranes dedicated for chemiluminescence capturing were incubated with 500 µl of SuperSignal West Femto chemiluminescent substrate (Thermo Scientific) and developed using either LAS-3000 CCD Camera (Fujifilm) or ChemiDoc-It 600 Imaging System (UVP). The membranes dedicated for fluorescence capturing were developed straight after the second washing step using 700 nm channel in Odyssey CLx Infrared Imaging System (LI-COR Biosciences).

3.2.7. NAAG-hydrolysing activity assay

NAAG-hydrolysing activity assay was performed to compare kinetic parameters of NAAG-hydrolysing reaction catalysed by rm-GCPII and rh-GCPII (see Chapter 3.2.7.1.), to analyse enzyme activity of membrane-bound protein variants of mGCPII (see Chapter 3.2.7.2., p. 68), to characterize GCPII-deficient mice (see Chapter 3.2.7.3., p. 68) and to investigate the amount of GCPII present in chosen mouse tissues (see Chapter 3.2.7.3., p. 68). NAAG radiolabelled by tritium on the terminal glutamate (^3H -NAAG) was used as a substrate for all enzyme reactions. The procedure was performed as previously described (Knedlik *et al.* 2014) with minor modifications.

3.2.7.1. Reaction setup for determination of kinetic parameters of NAAG-hydrolysing reaction

Recombinant biotinylated proteins rm-GCPII and rh-GCPII for determination of kinetic parameters of NAAG-hydrolysing reaction were prepared previously in our laboratory (Knedlik *et al.* 2017; Tykvart *et al.* 2012). The protein concentration was determined by Ing. Radko Souček at IOCB CAS, who performed quantitative amino acid analysis (Biochrom) following the manufacturer's protocol.

Reactions were carried out in a 96-well plate format (Microtitration 96-well plate with U-bottom, P-lab) at 37 °C in a reaction buffer containing 25 mM BTP-HCl, pH 7.4, 150 mM NaCl and 0.001% C12E8. The total volume of a reaction was 100 μl . The total concentration of NAAG (i.e. a mixture of NAAG (Sigma-Aldrich) and ^3H -NAAG (prepared by Dr. Tomas Elbert at IOCB Prague)) in the reaction ranged from 20 nM to 40 μM . The concentration of ^3H -NAAG in the reaction was 5 nM for all NAAG concentration points lower than 5 μM and 10 nM for all NAAG concentration points between 5 μM and 40 μM . The concentration of the enzyme was set accordingly to ensure NAAG conversion being lower than 25%. The reactions were started by addition of the substrate and stopped after 20 minutes by addition of a stopping buffer (see Chapter 3.2.7.4., p. 69). Subsequent analyses of NAAG conversion together with K_M and k_{cat} determination are described in Chapter 3.2.7.4 (p. 69). The data are presented as the mean of three independent measurements \pm standard deviation; one measurement consisted of 12 different NAAG concentrations.

3.2.7.2. Reaction setup for analysis of enzyme activity of membrane-bound protein variants of mGCPII

Reactions were carried out at 37 °C in a reaction mixture consisting of 35 µl of reaction buffer (TBS supplemented by 0.1% Tween-20) and 55 µl of the cell lysate diluted appropriately in the cell lysis buffer (see Chapter 3.2.2.2., p. 55). The amount of the cell lysate per reaction corresponded to 5 ng of membrane-bound protein variant of mGCPII as determined by ELISA (see Chapter 3.2.2.3., p. 56). As a positive control, a lysate from HEK293offA2 cells stably transfected by pTreTight-mGCPII vector (see Chapter 3.1.3.5., p. 48) was used. This cell line was prepared previously in our laboratory by Jana Starková. As a negative control, a lysate from non-transfected HEK293offA2 cells was used and its amount was set to a total amount of proteins to be the highest from the tested lysates.

The total volume of the reaction mixture containing the reaction buffer and the lysate was 90 µl. Reactions were started by addition of 10 µl of 1 µM NAAG (containing 50 nM ³H-NAAG) and stopped after 60 minutes by a stopping buffer (see Chapter 3.2.7.4., p. 69). Subsequent analysis of NAAG conversion is described in Chapter 3.2.7.4. (p. 69). The reactions were performed in triplicates and the data are presented as the mean of technical replicates ± standard deviation.

3.2.7.3. Reaction setup for analysis of NAAG hydrolysis in mouse tissue lysates

Reactions were carried out at 37 °C in a reaction mixture consisting of 70 µl of reaction buffer (20 mM Tris-HCl, pH 7.4, 150 mM NaCl, 0.1% Tween-20) and 20 µl of the tissue lysate diluted appropriately in the tissue lysis buffer (see Chapter 3.2.4., p. 62). The total amount of the proteins was 100 µg for the characterization of GCPII-deficient mice using kidney and brain lysates (see Chapter 3.2.4.2., p. 62) and 30 µg for estimation of the amount of GCPII present in chosen mouse tissues (see Chapter 3.2.4.3., p. 63). For a precise determination of GCPII amount in the epididymis and spermatic cord, the total amounts of proteins were set to 0.3 µg and 20 µg, respectively. In each sample set, a calibration curve of rm-GCPII (10 pg, 25 pg, 50 pg, 100 pg, 125 pg and 250 pg of rm-GCPII per reaction) was included.

Reactions were started by addition of 10 μl of 1 μM NAAG (containing 50 nM ^3H -NAAG) into the reaction mixture and stopped after 17 hours (i.e. after overnight incubation) or 6 hours using stopping buffer (see Chapter 3.2.7.4., p. 69). Subsequent analysis of NAAG conversion is described in Chapter 3.2.7.4. (p. 69). The reactions were performed in duplicates or triplicates. The data from radioactive assay are presented as the mean of biological replicates \pm standard deviation.

3.2.7.4. Analysis of NAAG conversion during NAAG-hydrolysing reaction

The reactions were stopped by 100 μl of ice-cold stopping buffer (200 mM KH_2PO_4 , 2 mM 2-mercaptoethanol, pH 7.4). The released glutamate was separated from the unreacted NAAG using ion exchange chromatography following slightly modified protocol described previously (Robinson 1987). Briefly, ion exchange mini-columns were prepared using glass Pasteur capillary pipettes and AG1-X resin (Bio-Rad) (2 ml of 50% slurry) that was pre-washed by degassed deionized water. 200 μl reactions were subsequently applied and the free glutamate was eluted by 2.5 ml of 1 M formic acid. The eluate containing radioactive glutamate was mixed with 6 ml of the Rotiszint ECO Plus scintillation cocktail (Roth) and the radioactivity was quantified by liquid scintillation using a Tri-Carb Liquid Scintillation Counter (Perkin-Elmer). The NAAG conversion was calculated using following equation:

$$\text{NAAG conversion [\%]} = \frac{\text{dpm}_{\text{sample}} - \text{dpm}_{\text{blank}}}{\text{dpm}_{\text{total}} - \text{dpm}_{\text{blank}}} \cdot 100$$

where *blank* is a reaction, in which NAAG was incubated using the same reaction conditions as in case of the *sample*, only the enzyme was not added, and *total* is a reaction, where a recombinant enzyme was added in a great excess to ensure complete cleavage of NAAG. NAAG conversions then served either as outcomes of the analysis itself or as starting values for further analysis.

To determine GCPII amount in the mouse epididymis and spermatic cord, NAAG conversions in the tissues were compared with the NAAG conversion of rm-GCPII calibration curve (see Chapter 3.2.7.3., p. 68). To determine K_M and k_{cat} values

(see Chapter 3.2.7.1., p. 67), the amount of glutamate released was first calculated from NAAG conversion and the reaction rate was subsequently calculated using equation:

$$v = \frac{c_{glutamate}}{c_{enzyme} \cdot t}$$

K_M and k_{cat} values were then determined using GraFit program, version 5 (Erithacus Software Limited) (Leatherbarrow 2001), where the dependence of the reaction rate on the concentration of the substrate was fitted into the Michaelis-Menten equation by non-linear regression.

3.2.8. Mouse phenotyping

3.2.8.1. Gross anatomy

Mice were sacrificed using intraperitoneal injection of a mixture of ketamine (Narkamon, 125mg/kg) and xylazine (Rometar, 20mg/kg) followed by cervical dislocation. A midline skin incision extending from the lower jaw to the caudal abdomen was then usually performed and the main organs were examined for possible abnormalities. Subsequently, the seminal vesicles were localized and their images were taken together with a length scale. Using the length scale as an internal standard, seminal vesicle area was measured by ImageJ software (Rueden *et al.* 2017).

3.2.8.2. Histopathology and immunohistochemistry

Following gross anatomy examination, selected mouse tissues including kidney and most tissues from urogenital system were collected. Most of the urogenital organs were dissected by MUDr. František Sedlák. All dissections were performed in a maximum of 60 minutes after mice death. Tissues were immersed in 10% neutral buffered formalin (Sigma-Aldrich) immediately after the collection and stored at 4 °C before processed further. Human epididymis slices were obtained from prof. MUDr. Josef Zámečník, Ph.D. from Motol University Hospital.

The mouse kidneys and seminal vesicles were examined by MUDr. Tomáš Olejář, Ph.D. at First Faculty of Medicine using standard histopathological procedures. Briefly, tissues were taken out of the buffered formalin and transversely sectioned. Subsequently, the sections were dehydrated using graded ethanol, immersed in xylene and embedded in paraffin. Slices of depth of 5 μm were then prepared and stained, haematoxylin and eosin (H&E) and thoroughly examined.

Immunohistochemistry (IHC) was performed to localize mGCPII within the male mouse urogenital system and to explore possible expression of hGCPII in human epididymis. IHC was mainly performed by MUDr. František Sedlák and the protocol is described in (Vorlova *et al.* 2018) in detail. To detect GCPII in different parts of male mouse urogenital system, antibodies GCP-04 (Exbio) and GCP-02 (Barinka *et al.* 2004a) were used. To detect GCPII in the human epididymis, antibodies GCP-04 (Exbio), GCP-02 (Barinka *et al.* 2004a) and YPSMA-1 (Anogen) were used. As the secondary antibody, Histofine Simple Stain™ MAX PO (MULTI) (Nichirei Biosciences) was utilized.

3.2.8.3. Metabolomic analysis of mouse urine

The mouse urine samples had been collected straight before mice were anesthetized (see Chapter 3.2.4.1., p. 62 and 3.2.8.1., p. 70). The mice were taken out of the cage and let urinate on the sterile plastic foil. The urine was then aspirated by automatic pipette, frozen on a dry ice and stored at -80 °C until being analysed for creatinine concentration.

The creatinine concentration was determined in all urine samples in order to normalize them for metabolomic analysis (see below). The urines were thawed on ice and centrifuged for 10 minutes at 16000 g and 4 °C. A small volume (2 μl - 5 μl) of each urine sample was then analysed using Creatinine enzymatic kit (Dialab), which is based on a series of coupled reactions where creatinine serves as a starting substrate and a dye as end product. The amount of the produced dye measured spectrophotometrically is proportional to the amount of creatinine in the tested sample. The protocol recommended by the manufacturer was modified for measurement in 96-well format.

A calibration curve consisted of 12 concentrations of Creatinine standard (177 μM , Dialab) diluted in normal saline (154 mM NaCl), the total amount of standard per well

ranged from 177 pmol to 2655 pmol. The urine samples were diluted 30× in normal saline. In case the creatinine concentration determined was not within the calibration curve, the measurement was repeated with appropriate amount of urine sample. Three different control samples were included in each measurement in order to monitor the quality control.

15 µl of diluted urine sample/control sample/standard were pipetted into the 96-well transparent plate with flat bottom (P-lab), mixed with 150 µl of Reagent 1 (Creatinine enzymatic kit, Dialab) using a multichannel pipette and incubated 5 minutes at 37 °C. The absorbance was measured at 550 nm using an Infinite microplate reader (Tecan) in a 9-reads-per-well mode. 50 µl of Reagent 2 (Creatinine enzymatic kit, Dialab) were subsequently added and the reactions were mixed thoroughly by a multichannel pipette. After additional incubation for 5 minutes at 37 °C, the absorbance was measured at 550 nm using an Infinite microplate reader (Tecan) in a 9-reads-per-well mode. The creatinine concentration was calculated using Microsoft Excel.

All urine samples containing sufficient amount of creatinine for metabolomic analysis were diluted by cold LC-MS Grade water (Thermo Scientific) to reach a final concentration of creatinine of 700 µM. Such diluted samples were then transferred to Microcon-10kDa centrifugal filters (Millipore) and centrifuged at 14000 g and 4 °C until the flow-through fractions reached required volumes. Aliquots of 2 µl of each flow through fraction were then poured to generate a pooled sample for quality control of metabolomic analysis. Finally, all flow through urine samples and the pooled sample were frozen in liquid nitrogen and stored at -80 °C until further use.

Additional sample preparation and the targeted metabolomic analysis using high-performance liquid chromatography coupled to tandem mass spectrometry (HPLC-MS/MS) was performed by Dr. David Friedecky and colleagues at Institute of Molecular and Translational Medicine (IMTM) at Faculty of Medicine and Dentistry of Palacky University in Olomouc. The amount of sample injected per run corresponded approximately to 500 pmol of creatinine. The methodology was identical to that described by the colleagues from IMTM for targeted metabolomics of rat cerebrospinal fluid and plasma in (Karlikova *et al.* 2017).

3.2.9. Statistical analysis

Statistical analysis of mouse seminal vesicle enlargements was performed by Dr. Marek Maly at National Institute of Public Health using statistical software Stata, release 9.2 (Stata Corp LP, College Station, TX). More information could be found in (Vorlova *et al.* 2018).

Statistical analysis of metabolomics data was performed by Dr. David Friedecky and colleagues at IMTM using the R programme (version 3.1.2). A statistical evaluation and data treatment performed by the colleagues at IMTM was previously described for metabolomic analysis of rat cerebrospinal fluid and plasma in (Karlikova *et al.* 2017).

4. RESULTS

4.1. Generation of GCPII-mutant mice

4.1.1. TALEN-mediated disruption of *Folh1* gene

In order to generate GCPII-mutant mice, *Folh1* gene disruption using targeted endonucleases was performed. Dr. Petr Kaspárek from IMG CAS designed TALENs that targeted exon 11 of *Folh1* gene within the sequence encoding active site of mGCPII (specifically, the sequence encoding zinc-coordinating Glu427 and the catalytic base Glu426, see Figure 12) and performed two independent microinjections into mouse zygotes (for more information see (Vorlova *et al.* 2018)). This resulted in production of F0 generation consisting of 65 transgenic mice in C57BL/6NCrl genetic background. These were analysed for a presence of TALEN-mediated mutations (see Chapter 3.2.1.2., p. 51).

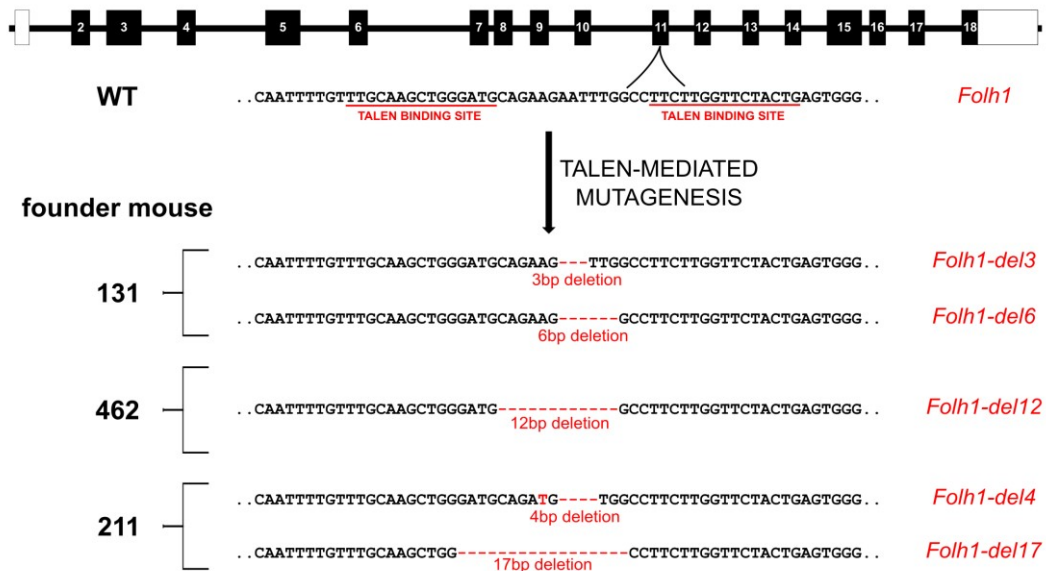


Figure 12: TALEN-mediated *Folh1* gene disruption performed by Dr. Petr Kaspárek at IMG CAS. TALEN activity followed by non-homologous end joining generated several different mutations within exon 11 of *Folh1* gene. Three transgenic mice (designated as 131, 462 and 211) in C57BL/6NCrl genetic background were then selected as founders for establishing the GCPII-mutant mouse colonies. The *Folh1* gene and *Folh1*-mutant gene sequences were generated and analysed using Vector NTI.

Three distinct founder mice were then selected for establishing GCPII-mutant mouse colonies – a mouse designated as 131 that carried deletions of 3 bp (del3) and 6 bp (del6) within exon 11 of *Folh1* gene, a mouse 462 with deletion of 12 bp (del12) and a mouse 211 with deletions of 4 bp (del4) and 17 bp (del17) (see Figure 12 , p. 74).

The potential protein products of the *Folh1*-mutant gene expression are summarized in Figure 13. An expression of *Folh1-del3*, *Folh1-del6* and *Folh1-del12* would lead to production of full-length mGCPII with 1, 2 or 4, respectively, amino acid deletions within the active site of mGCPII (mGCPIIdel3, mGCPIIdel6 and mGCPIIdel12). While mGCPIIdel3 and mGCPIIdel6 lack one from the two active site glutamates, mGCPIIdel12 lacks both of them. The mouse colonies carrying these mutations could thus potentially express inactive variants of mGCPII. Nevertheless, following experiments showed that not only the biochemical properties of recombinantly prepared mGCPIIdel3, mGCPIIdel6 and mGCPIIdel12 dramatically differ from those of mGCPII wild type (WT) protein (see Chapter 4.2.3., p. 82 and 4.2.4., p. 84), but also these variants were not detected in the GCPII-mutant mouse tissues (see Chapter 4.3.1., p. 87).

| GENE | POTENTIAL PROTEIN PRODUCT | LABEL | AA | MW [Da] |
|--------------------|--|-------------|-----|---------|
| <i>Folh1</i> | ..VRSFGLKKGRRRPRRTILFASWDAAEEFLLGSTEWAEEHSRLLQERGVAYINADSSIE.. | mGCPII | 752 | 84567 |
| <i>Folh1-del3</i> | ..VRSFGLKKGRRRPRRTILFASWDAAEV--GLLGSTEWAEEHSRLLQERGVAYINADSSIE.. | mGCPIIdel3 | 751 | 84390 |
| <i>Folh1-del6</i> | ..VRSFGLKKGRRRPRRTILFASWDAE--GLLGSTEWAEEHSRLLQERGVAYINADSSIE.. | mGCPIIdel6 | 750 | 84291 |
| <i>Folh1-del12</i> | ..VRSFGLKKGRRRPRRTILFASWD---GLLGSTEWAEEHSRLLQERGVAYINADSSIE.. | mGCPIIdel12 | 748 | 84090 |
| <i>Folh1-del4</i> | ..VRSFGLKKGRRRPRRTILFASWDADVAFLVLLSGQRNIQDSYKSEVWLILMLLP---- | mGCPIIdel4 | 456 | 50780 |
| <i>Folh1-del17</i> | ..VRSFGLKKGRRRPRRTILFASWPSWFI----- | mGCPIIdel17 | 428 | 47717 |

Figure 13: Protein product of *Folh1* gene expression compared to potential protein products of *Folh1*-mutant gene expression. Protein sequences were generated and analysed using Vector NTI.

The genes *Folh1-del4* and *Folh1-del17* contain frameshift sequences and their potential expression would thus result in shorten protein products (456 and 428, respectively, instead of 752 amino acids). However, no such protein product was detected in GCPII-del4 and GCPII-del17 mutant mice (see Chapter 4.3.1., p. 87 and 4.3.2., p. 89).

4.1.2. GCPII-mutant mouse colony management

F1 generations of all five GCPII-mutant mouse colonies were produced by breeding of F0 transgenic mice 131, 462 and 211 with C57BL/6NCrl wild type mice. To monitor the genotypes of newborns, a robust genotyping method based on nested PCR was established (see Figure 14). This method consists of two successive PCRs. In the first round, a fragment of around 540 bp is amplified (the exact length of the fragment depends on the *Folh1* gene variant). The second round of nested PCR then uses the fragment from the first round as a template to produce small fragments of defined lengths that are analysed by DNA-PAGE (see Figure 15, p. 77).

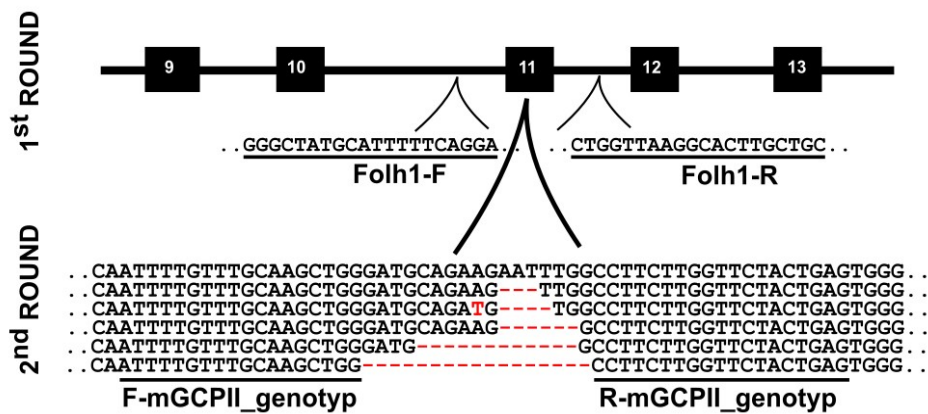


Figure 14: Schematic representation of GCPII-mutant mice genotyping procedure based on nested PCR. The first round of nested PCR uses chromosomal DNA as a template together with Folh1-F and Folh1-R primers to amplify fragments of around 540 bp. The second round uses the fragment amplified in the first round as a template together with primers F-mGCPII_genotyp and R- mGCPII_genotyp to generate fragments of a specific length depending on genotype.

F1 generation of all GCPII-mutant variants bred normally and did not show any obvious phenotype. Similarly, heterozygous mice of F2 and all following generations carrying *Folh1-del3*, *Folh1-del4* or *Folh1-del17* did not show any reproductive or phenotypic abnormalities. The mouse colonies carrying *Folh1-del3*, *Folh1-del4* or *Folh1-del17* were maintained using heterozygote × wild type breeding scheme. The mice homozygous for *Folh1-del3*, *Folh1-del4* or *Folh1-del17* were generated by intercrossing

of heterozygous mice of at least F2 generation. Neither embryonic lethality nor any obvious phenotypes of mice homozygous for *Folh1-del3*, *Folh1-del4* or *Folh1-del17* were observed. Subsequent intercrossing of the homozygous mice was also in correspondence with usual breeding performance of C57BL/6NCrl mice.

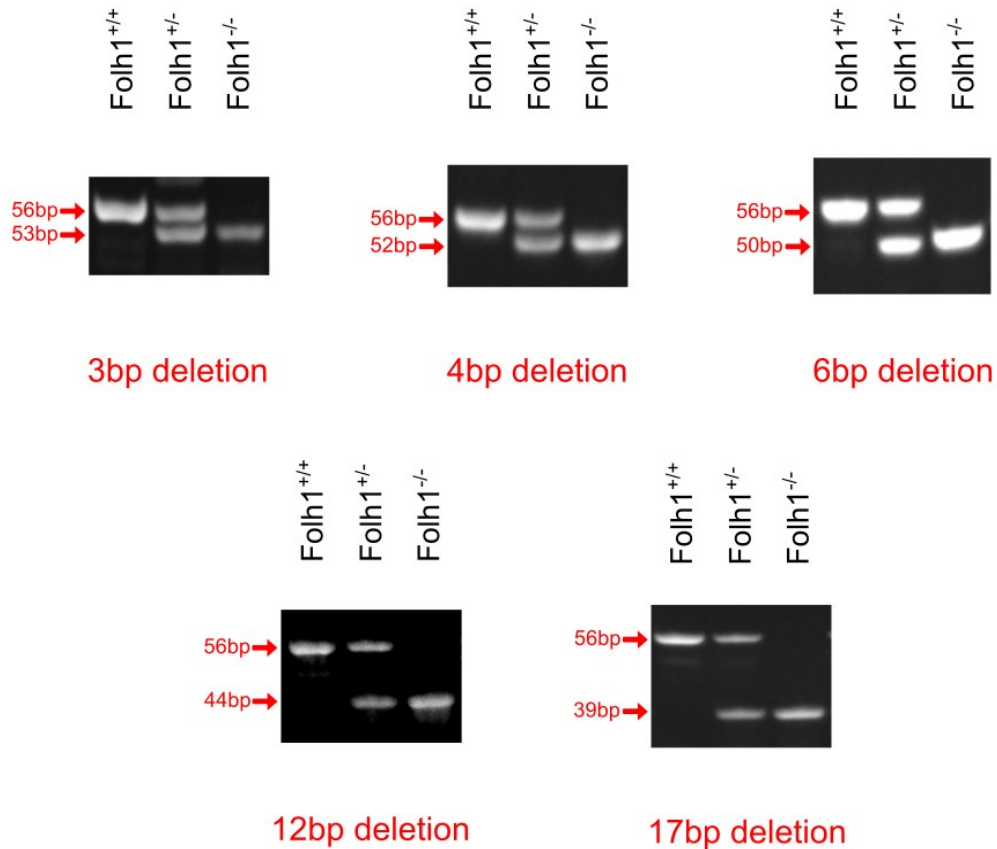


Figure 15: Analysis of fragments from second round of nested PCR. The PCR products were separated by DNA-PAGE followed by gel staining using GelRed (see Chapter 3.2.1.4., p. 52). The specific lengths of fragments for each genotype variant are stated. *Folh1*^{+/+} indicates WT mice, *Folh1*^{+/-} indicates heterozygous mice and *Folh1*^{-/-} indicate mice homozygous for a specific *Folh1*-mutant gene variant.

In agreement with other GCPII-mutant variants, the heterozygous mice of F2 generation carrying *Folh1-del6* or *Folh1-del12* did not show any obvious phenotype. These colonies were not expanded much further; a reproduction performance was thus not studied in detail. Nevertheless, no reproductive abnormalities were observed in a small cohort of *Folh1-del6* homozygous mice. In addition, mice homozygous for *Folh1-del6* or *Folh1-del12* did not show any obvious phenotype.

4.2. Characterization of mouse GCPII and its mutant variants

4.2.1. Kinetic characterization of recombinant mouse GCPII

Kinetic parameters of recombinant mouse GCPII (i.e. extracellular part of mGCPII) were published in (Knedlik *et al.* 2017) (see Appendix 1), where a direct comparison of rm-GCPII and its human counterpart was performed. Here, only kinetic properties of both enzymes when catalysing NAAG hydrolysis are summarized. The recombinant enzymes of high purity were prepared previously in our laboratory (Knedlik *et al.* 2017; Tykvart *et al.* 2012) by recombinant expression in insect cells. The amount of the enzyme was optimized for each NAAG concentration to ensure that the substrate conversion is below 25% and the kinetic measurements are thus performed within the initial reaction velocity. The Michaelis-Menten kinetics for NAAG hydrolysis catalysed by rm-GCPII and rh-GCPII is depicted in Figure 16.

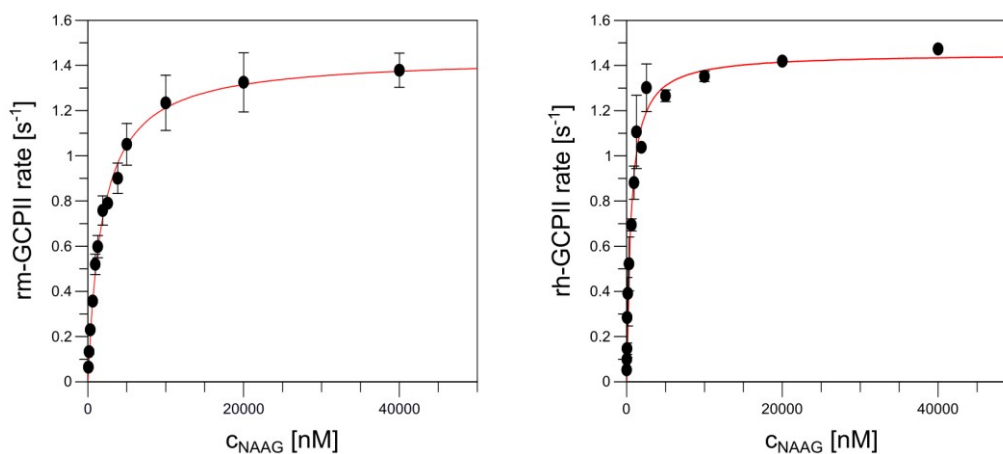


Figure 16: Michaelis-Menten kinetics of recombinant mouse GCPII (rm-GCPII) and recombinant human GCPII (rh-GCPII) for NAAG-hydrolysing reaction. The reactions were carried out in a reaction buffer containing 25 mM BTP-HCl, pH 7.4, 150 mM NaCl and 0.001% C12E8 for 20 minutes at 37 °C. The amount of the enzyme was set accordingly to ensure substrate conversion being below 25%. The error bars represent standard deviation of at least two independent measurements. The data were modelled using non-linear regression function in GraFit 5.0.4 (Leatherbarrow 2001).

The kinetic parameters were calculated using GraFit 5.0.4 (Leatherbarrow 2001) and are summarized in Table 2. It was determined that the catalytic efficiency of recombinant mouse GCPII is lower than that of its human counterpart. Indeed, even though the turnover numbers are very similar, the K_M value of rm-GCPII is almost four times higher than that of rh-GCPII (see Table 2).

Table 2: Kinetic parameters of recombinant mouse GCPII (rm-GCPII) and recombinant human GCPII (rh-GCPII) for NAAG-hydrolysing reaction. The calculations were performed in GraFit 5.0.4 (Erithacus Software Limited) (Leatherbarrow 2001).

| Enzyme | K_M [nM] | k_{cat} [s^{-1}] | k_{cat}/K_M [$\times 10^7 s^{-1} M$] |
|----------|----------------|------------------------|--|
| rm-GCPII | 1900 \pm 100 | 1.44 \pm 0.02 | 0.077 \pm 0.001 |
| rh-GCPII | 550 \pm 60 | 1.45 \pm 0.04 | 0.265 \pm 0.007 |

4.2.2. NAAG-hydrolysing activity of membrane-bound mutant variants of mGCPII

To investigate whether the potential protein products of the *Folh1*-mutant gene expression (see Figure 13, p. 75) lose the ability to hydrolyse NAAG, the membrane-bound recombinant mutant variants of mGCPII were tested. For this purpose, pTreTight plasmids intended for transient transfection of HEK293 cells were first prepared using site directed mutagenesis (see Chapter 3.2.2.1., p. 53). The pTreTight-mGCPII vector (see Chapter 3.1.3.5., p. 48) served as a template and the deletions identical to those identified in the founder mice (see Figure 12, p. 74) were gradually introduced.

The mutagenesis was performed in several steps (see Table 3, p. 80) since an attempt to delete more than 6 bp within one site-directed mutagenesis reaction was repeatedly unsuccessful. Moreover, straight preparation of a vector with 12 bp deletion from a vector with 6 bp also failed. The intermediate step of 9 bp deletion needed to be thus included. The sequences of all vectors were verified by Sanger sequencing (see Chapter 3.2.2.1., p. 53).

Table 3: Summary of site-directed mutagenesis performed to prepare vectors encoding membrane-bound mutant variants of mGCPII. The vectors utilized for subsequent transient transfection of HEK293 cells are highlighted in bold. More information about primers could be found in Chapter 3.1.3.4. (p. 47).

| Step | Template | Primers | Product |
|------|-----------------------|--------------------------------|------------------------------|
| 1 | pTreTight-mGCPII | F-mGCPIIdel3 R-mGCPIIdel3 | pTreTight-mGCPIIdel3 |
| | | F-mGCPIIdel4 R-mGCPIIdel4 | pTreTight-mGCPIIdel4 |
| | | F-mGCPIIdel6 R-mGCPIIdel6 | pTreTight-mGCPIIdel6 |
| 2 | pTreTight-mGCPIIdel6 | F-mGCPIIdel9 R-mGCPIIdel9 | pTreTight-mGCPIIdel9 |
| 3 | pTreTight-mGCPIIdel9 | F-mGCPIIdel12 R-mGCPIIdel12 | pTreTight-mGCPIIdel12 |
| 4 | pTreTight-mGCPIIdel12 | F-mGCPIIdel17 R-mGCPIIdel17 | pTreTight-mGCPIIdel17 |

All membrane-bound protein variants of mGCPII together with membrane-bound mGCPII WT (i.e. mGCPII full-length protein) were expressed using transient transfection of HEK293A2off cells by corresponding pTreTight vectors (for more details see Chapter 3.2.2.2., p. 55). HEK293A2off cells not transfected by any vector served as a negative control. As a positive control, HEK293A2off cells stably transfected by pTreTight-mGCPII (previously prepared in our laboratory, see Chapter 3.2.7.2., p. 68) cultured in the same conditions as the cells intended for transient transfection, were utilized.

The Western blot analysis of HEK293A2off cell lysates performed 3 days after the transfection revealed that all membrane-bound mutant variants of mGCPII were expressed (see Figure 17, panel A, p. 81; for predicted molecular weight of each mutant variant Figure 13, p. 75). The expression yield determined by ELISA (see Chapter 3.2.2.3., p. 56) was similar for all proteins produced transiently and ranged from 40 pg to 200 pg of mGCPII variant per 1 µg total protein. In contrast, the expression yield of mGCPII WT produced in stably transfected cells was more than one order of magnitude higher (around 2.5 ng of full-length mGCPII per 1 µg total protein).

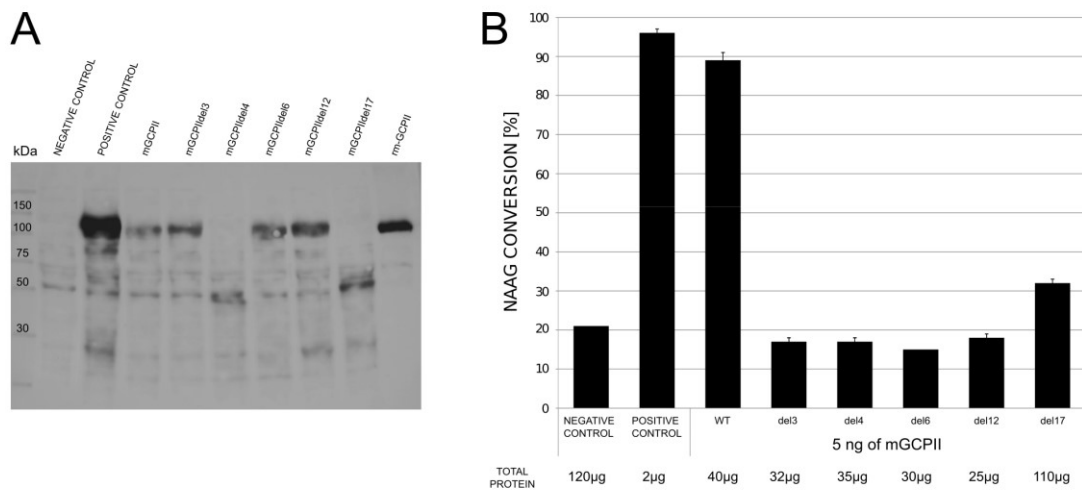


Figure 17: Expression and NAAG hydrolysis analysis of membrane-bound mGCPII and its mutant variants. **A:** Western blot analysis of lysates of HEK293A2off cells that were transiently transfected by pTreTight vectors encoding membrane-bound mGCPII variants compared to positive and negative control. The positive control indicates lysate of HEK293A2off cells stably transfected by pTreTight-mGCPII vector. The negative control indicates lysate of HEK293A2off cells that were not transfected by any vector. 50 µg of total protein from each cell lysate was analysed. rm-GCPII indicates purified extracellular part of mouse GCPII, which served as a standard (10 ng were loaded). To detect mGCPII, antibody GCPII-04 (Exbio) was used since its epitope is located between amino acids 94E and 111V (Tykvar *et al.* 2014). **B:** NAAG hydrolysis activity in lysates of HEK293A2off cells that were transiently transfected by pTreTight vectors encoding membrane-bound mGCPII variants compared to positive and negative control. The amount of lysate corresponding to 5 ng of membrane-bound mGCPII variant was tested. The amount of negative control was set to a total amount of proteins to be the highest from the tested lysates. The reactions were incubated for 1 hour at 37 °C in TBS supplemented by 0.1% Tween-20. The error bars represent standard deviations of technical triplicates.

Based on the ELISA results, an amount of each cell lysate corresponding to 5 ng of mGCPII variant was incubated for 1 hour with NAAG (see Figure 17, panel B). While the NAAG conversion in the cell lysate containing transiently expressed membrane-bound mGCPII WT was as high as that in the lysate of stably transfected cells (i.e. around 90%), the NAAG-hydrolysing activity was dramatically decreased in all cell lysates containing membrane-bound mGCPII mutant variants. The NAAG conversion in these lysates varied between 15% and 32%, which was comparable to 21% NAAG conversion in the negative control.

4.2.3. Expression and purification of extracellular parts of mGCPII mutant variants

To investigate whether except of the enzyme activity, the properties of mGCPII mutant variants possessing a small deletion within the active site (mGCPIIdel3, mGCPIIdel6 and mGCPIIdel12; see Figure 13, p. 75) are the same as those of mGCPII WT, recombinant extracellular parts of mGCPII mutant variants were prepared. At the same time, an attempt to express rm-GCPIIdel4 and rm-GCPIIdel17 was made.

First, pMT/Bip/Avi_rm-GCPIIdel3/4/6/12/17 plasmids containing deletions identical to those identified in founder mice (see Figure 12, p. 74) were cloned from pMT/Bip/Avi_rm-GCPII (see Chapter 3.1.3.5., p. 48) and pTreTight-mGCPIIdel3/4/6/12/17 (see Chapter 3.2.2.1., p. 53) cleaved by suitable restriction endonucleases (see Chapter 3.2.3.1., p. 57). Subsequently, Jana Starkova used the prepared plasmids to stably transfect *Drosophila* S2 cells. The cell cultures expressing the highest amount of each rm-GCPII variant were selected for large-scale expression and the level of the expression was analysed using Western blotting (see Figure 18, for more information on the methodology see Chapter 3.2.3.2., p. 58 and 3.2.6., p. 65).

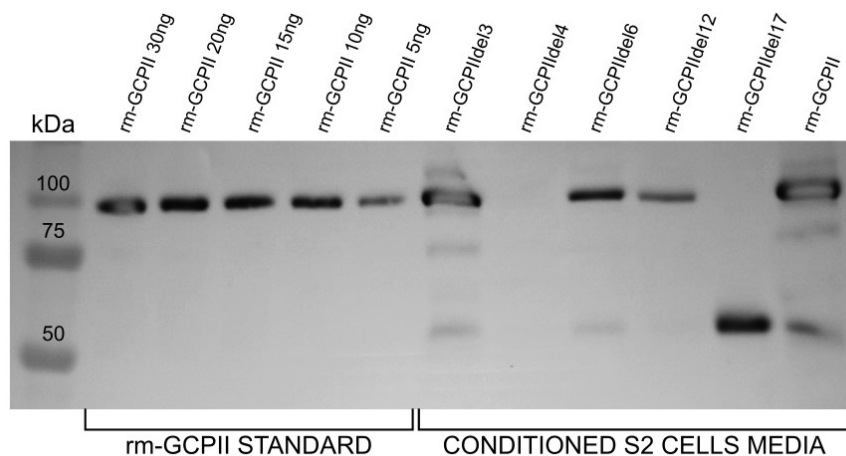


Figure 18: Western blot analysis of conditioned media of S2 cells stably transfected by plasmids encoding extracellular part of mGCPII (rm-GCPII) and its mutant variants. rm-GCPII STANDARD indicates purified extracellular part of mouse GCPII. 15 μ l of conditioned media from each stably transfected S2 cell culture was analysed. To detect rm-GCPII and its mutant variants, neutravidin-HRP was used. The neutravidin is capable of binding to biotinylated Avi-Tag, which is a part of the recombinant proteins expressed by S2 cells stably transfected by pMT/Bip/Avi vectors (see Figure 11, p. 48).

While expression yield of rm-GCPII~~13~~ was as high as that of rm-GCPII WT (more than 2 ng per 1 μ l conditioned media when compared to calibration range of purified rm-GCPII; see Figure 18, p. 82), the expression yield of rm-GCPII~~16~~ and rm-GCPII~~12~~ was much lower (around 0.5 ng per 1 μ l conditioned media). Interestingly, preparation of stably transfected S2 cell culture expressing rm-GCPII~~14~~ was not fruitful since no signal around 50kDa was detected in their conditioned media. The expression yield of rm-GCPII~~17~~ was estimated to 1.5 ng per 1 μ l conditioned media.

Next, rm-GCPII WT, rm-GCPII~~13~~, rm-GCPII~~16~~ and rm-GCPII~~12~~ were purified from conditioned media using Streptavidin Mutein Matrix (Roche) with purification steps being monitored by SDS-PAGE (see Chapter 3.2.3.3., p. 59 and 3.2.3.4., p. 60). When purifying mutant variants of rm-GCPII, the purification was much less efficient than in case of rm-GCPII WT (data not shown). In comparison to rm-GCPII, the portion of the mutant proteins that stayed in the conditioned media after incubation with the Streptavidin Mutein Matrix was much higher. Moreover, the mutant proteins were present in the washing fractions to much higher extent than rm-GCPII WT.

Finally, selected elution fractions from each purification were combined and concentrated to a suitable volume. Since the amount of rm-GCPII~~16~~ and rm-GCPII~~12~~ in the elution fractions was extremely low (see below), the second washing fractions from the both purification steps of these proteins were also combined and concentrated. Surprisingly, while concentrating all mutant variants of rm-GCPII, pronounced precipitation occurred. Nevertheless, the protein concentration was still measurable in all concentrates.

The purification outcomes are depicted in Figure 19 (p. 84). The highest purity was reached in case of rm-GCPII WT (more than 90%) followed by rm-GCPII~~13~~ (around 70%). The purity of rm-GCPII~~16~~ and rm-GCPII~~12~~ was quite low (see Figure 19, panel A, p. 84). The purification yields were estimated from the gel stained by silver to 3 mg per 1 l of conditioned media (3 mg/L) for rm-GCPII WT, 0.5 mg/L for rm-GCPII~~13~~ and 50 μ g/L for rm-GCPII~~12~~. The purification yield of rm-GCPII~~16~~ was not measurable.

All rm-GCPII variants were also analysed using Western blotting to detect potential degradation process during purification (see Figure 19, panel B, p. 84). Almost no degradation products were observed in the combined and concentrated elution

fractions of rm-GCPII and rm-GCPIIdel3. In contrast, rm-GCPIIdel6 was completely degraded in the combined and concentrated elution fractions and only a small amount of a full-length rm-GCPIIdel6 was detected in the combined and concentrated washing fractions. Rm-GCPIIdel12 was degraded to a lesser extent than rm-GCPIIdel6 but the degradation process was still much more pronounced than in case of rm-GCPII and rm-GCPIIdel3.

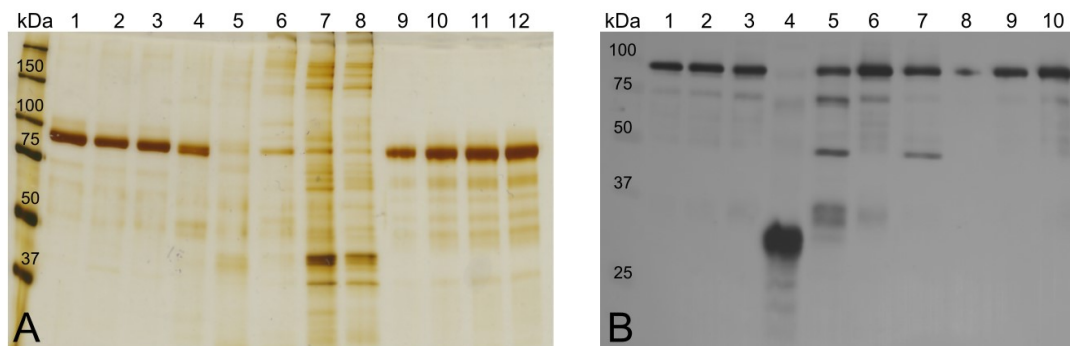


Figure 19: Comparison of purification outcomes of rm-GCPII and its mutant variants.

A: Analysis of purity of rm-GCPII and its mutant variants using SDS-PAGE followed by silver staining. 250 ng of total protein (as determined by NanoDrop) were analysed. 1 – rm-GCPII WT, combined elution fractions (EF) 1-5 from 1st purification round (1EF1-1EF5); 2 – rm-GCPII WT, EF1-EF3 from 2nd purification round (2EF1-2EF3); 3 – rm-GCPII WT, 2EF4+2EF5; 4 – rm-GCPIIdel3, 1EF2; 5 – rm-GCPIIdel6, 1EF1-1EF5+2EF1-2EF3; 6 – rm-GCPIIdel6, combined 2nd washing fractions (WF2) from both purification rounds (1WF2+2WF2); 7 – rm-GCPIIdel12, 1EF1-1EF4+2EF2; 8 – rm-GCPIIdel12, 1WF1+2WF2; 9 – 12 – calibration range of rm-GCPII WT purified previously (100 ng, 200 ng, 250 ng and 300 ng). **B:** Western blot analysis of potential degradations of rm-GCPII and its mutant variants during purification. 20 ng of rm-GCPII variant (as estimated from gel stained by silver, see panel A) was analysed. Neutravidin-HRP was used to detect rm-GCPII variants. 1 – rm-GCPII WT, 1EF1-1EF5; 2 – rm-GCPII WT, 2EF1-2EF3); 3 – rm-GCPIIdel3, 1EF2; 4 – rm-GCPIIdel6, 1EF1-1EF5+2EF1-2EF3; 5 – rm-GCPIIdel6, 1WF1+2WF2; 6 – rm-GCPIIdel12, 1EF1-1EF4+2EF2; 7 – rm-GCPIIdel12, 1WF1+2WF2; 8 – 10 – calibration range of rm-GCPII WT purified previously (2 ng, 10 ng and 20 ng).

4.2.4. Biochemical properties of rm-GCPIIdel3

Since the recombinant proteins rm-GCPIIdel6 and rm-GCPIIdel12 displayed significantly different properties than rm-GCPII WT even during expression and purification (see Chapter 4.2.3., p. 82), they were not studied further. In contrast, the biochemical properties of rm-GCPIIdel3 were additionally investigated using size-exclusion chromatography and Thermofluor assay. For this purpose, elution

fractions from both purification rounds of rm-GCPII Δ el3 were combined with the second washing fractions from both purification rounds, subjected to buffer exchange and concentrated (see Chapter 3.2.3.5., p. 61).

Both, the rm-GCPII Δ el3 mixture containing around 0.6 mg of total protein and the purified rm-GCPII WT prepared previously in our laboratory, were first analysed by size-exclusion chromatography (see Figure 20). Surprisingly, the chromatogram of rm-GCPII Δ el3 differed dramatically from that of rm-GCPII WT. While the elution volume of the main peak was 12 ml when analysing rm-GCPII WT, the elution volume of the main peak in case of rm-GCPII Δ el3 was shifted to 13 ml.

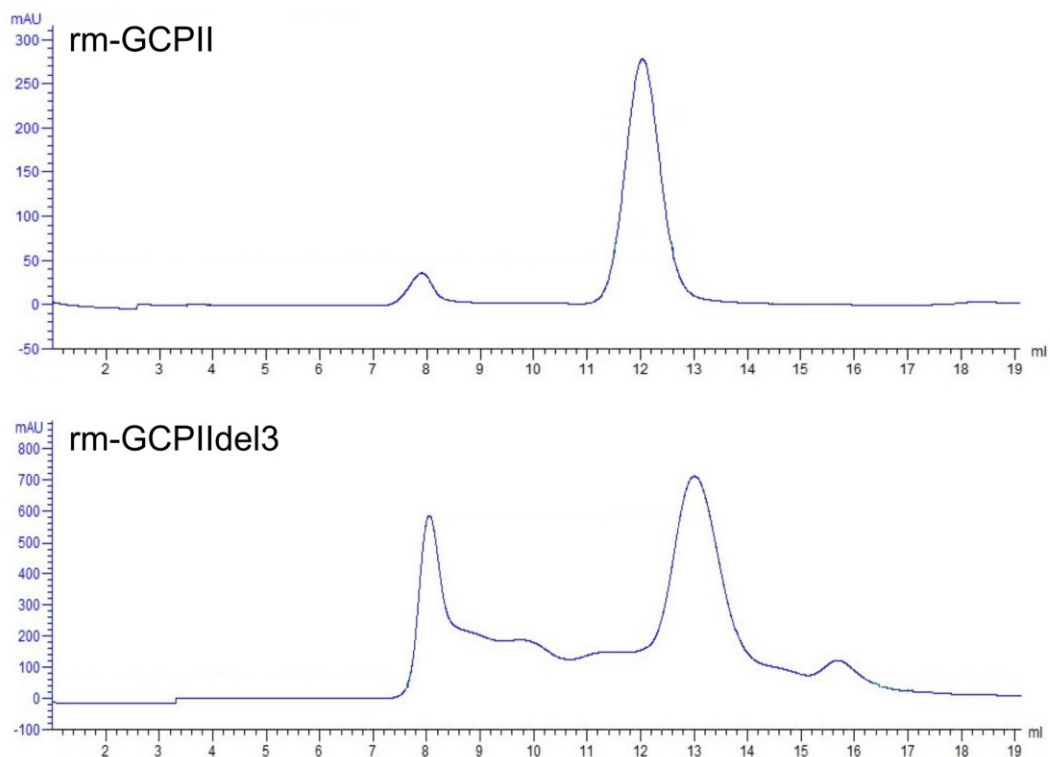


Figure 20: Comparison of chromatograms from size-exclusion chromatography performed with rm-GCPII and rm-GCPII Δ el3. The size-exclusion chromatography was carried out on a column HiLoad™ Superdex™ 200 10/300 GL (GE-Healthcare) in a buffer consisting of 10mM Tris-HCl, pH 7.4 and 150mM NaCl at a flow rate of 0.5 ml per minute. Approximately 0.4 mg of rm-GCPII (purified previously in our laboratory) and 0.6 mg of total protein in rm-GCPII Δ el3 solution (pooled fraction of 1EF1-1EF3, 2EF1, 2EF2, 1WF2 and 2WF2) were loaded.

Moreover, in contrast to minimum number of additional peaks in chromatogram of rm-GCPII WT, large portion of aggregate-like peaks was observed in the chromatogram of rm-GCPIIdel3. To explore whether these protein forms originate from rm-GCPIIdel3, selected size-exclusion chromatography fractions were analysed by SDS-PAGE. Indeed, after the denaturation, most of the protein forms displayed identical molecular weight of around 90 kDa (data not shown).

The thermal stability of native rm-GCPII WT and rm-GCPIIdel3 was then compared using ThermoFluor assay (see Figure 21). For this purpose, aggregate-free fractions from size-exclusion chromatography were combined, subjected to buffer exchange and concentrated. Following thermal stability analysis then revealed that the melting curves of both recombinant proteins significantly differ. While the melting temperature for rm-GCPII WT was around 75 °C, the melting temperature of rm-GCPIIdel3 was slightly below 50 °C.

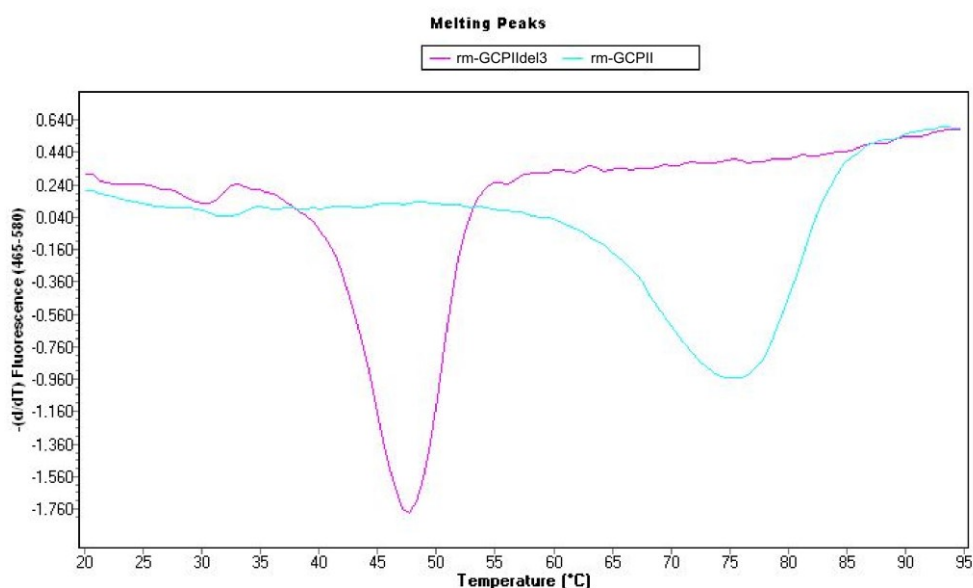


Figure 21: Comparison of thermal stabilities of rm-GCPII and rm-GCPIIdel3. The melting curves were measured by ThermoFluor assay using 1.5 µg of a protein diluted in a buffer consisting of 25 mM BTP-HCl, pH 7.4, 150 mM NaCl. The data were analysed in LightCycler®480 II software (Roche).

4.3. Characterization of GCPII-mutant mice

4.3.1. Investigation of expression of mGCPII protein variants in GCPII-mutant mice

Tissue lysates from all GCPII-mutant mouse colonies were subjected to Western blot analysis in order to examine whether the GCPII mutant proteins are solely or at least partially expressed in GCPII-expressing tissues. For this purpose, kidneys and brains of mutant mice of distinct ages were analysed (see Figure 22, p. 87 and Figure 23, p. 88).

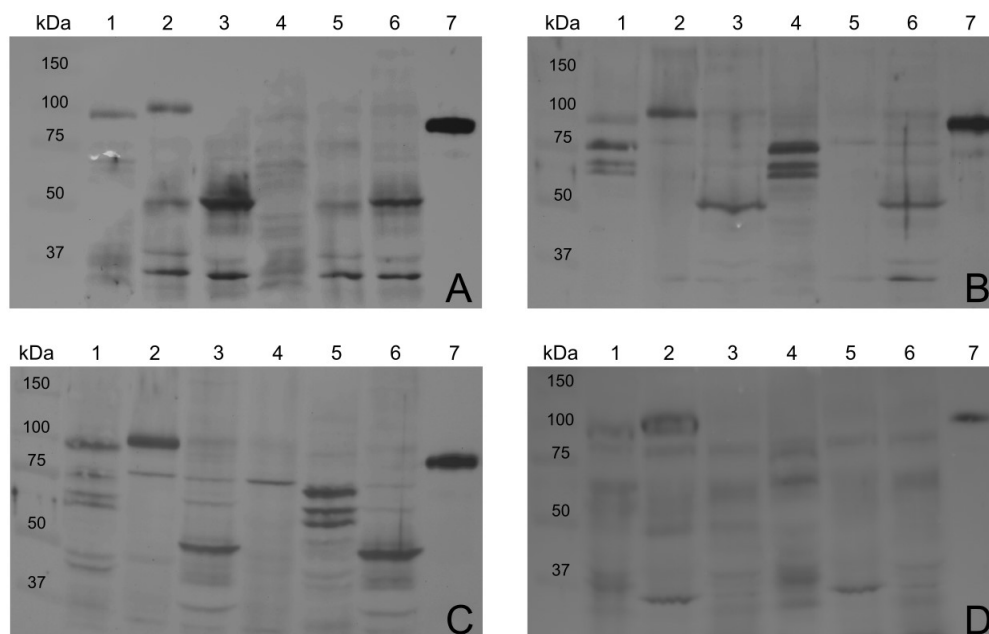


Figure 22: Western blot analysis of tissue lysates from mutant mice carrying *Folh1-del3*, *Folh1-del6* and *Folh1-del12*. In all cases, purified rm-GCPII served as mGCPII standard and antibody GCPII-04 (Exbio) was used since it is able to detect not only mGCPII WT but also its mutant variants. **A,B:** Analysis of soluble fractions of lysates from mutant mice carrying *Folh1-del6* (A) (9 weeks old) and *Folh1-del12* (B) (11-12 weeks old). 100µg of total protein were analysed. 1 – brain lysate from mouse homozygous for WT variant of *Folh1* (*Folh1*^{+/+} mouse); 2 – kidney lysate from *Folh1*^{+/+} mouse; 3 – colon lysate from *Folh1*^{+/+} mouse; 4 – brain lysate from mouse homozygous for mutant variant of *Folh1* (*Folh1*^{mut/mut} mouse); 5 – kidney lysate from *Folh1*^{mut/mut} mouse; 6 – colon lysate from *Folh1*^{mut/mut} mouse; 7 – 5ng of rm-GCPII. **C:** Analysis of soluble fractions of lysates from mutant mice carrying *Folh1-del3* (27 weeks old). 100µg of total protein were analysed. 1 – brain lysate from *Folh1*^{+/+} mouse; 2 – kidney lysate from *Folh1*^{+/+} mouse; 3 – colon lysate from *Folh1*^{+/+} mouse; 4 – kidney lysate from *Folh1*^{mut/mut} mouse; 5 – brain lysate from *Folh1*^{mut/mut} mouse; 6 – colon lysate from *Folh1*^{mut/mut} mouse; 7 – 5ng of rm-GCPII. **D:** Analysis of insoluble fractions (IF) of lysates from mutant mice carrying *Folh1-del3* (27 weeks old). 20 µl of insoluble fraction mixtures (see Chapter 3.2.4.2., p. 62) were analysed. 1 – IF of brain lysate from *Folh1*^{+/+} mouse; 2 – IF of kidney lysate from *Folh1*^{+/+} mouse; 3 – IF of colon lysate from *Folh1*^{+/+} mouse; 4 – IF of brain lysate from *Folh1*^{mut/mut} mouse; 5 – IF of kidney lysate from *Folh1*^{mut/mut} mouse; 6 – IF of colon lysate from *Folh1*^{mut/mut} mouse; 7 – 2ng of rm-GCPII.

First, mutant mice homozygous for *Folh1-del3*, *Folh1-del6* and *Folh1-del12* (together with mice homozygous for *Folh1-del4* and *Folh1-del17* collectively referred as $Folh1^{mut/mut}$ mice) were compared with their WT littermates (referred as $Folh1^{+/+}$ mice) (see Figure 22, p. 87). While a signal corresponding to full-length mGCPII was detected in the brain and kidney lysates of $Folh1^{+/+}$ mice, no such signal was observed in any lysate from $Folh1^{mut/mut}$ mice. Moreover, no mGCPII mutant protein variant was visible in the insoluble fractions of lysates from $Folh1^{mut/mut}$ mice (data shown only for mouse colony carrying *Folh1-del3*). Interestingly, a significant portion of mGCPII protein was detected in the insoluble fractions of $Folh1^{+/+}$ mice. Additional homogenisation step was thus included into the tissue lysis protocol (see Chapter 3.2.4.2., p. 62).

Next, mouse colonies carrying *Folh1-del4* and *Folh1-del17* were examined (see Figure 23). The comparison of soluble and insoluble fractions of lysates from $Folh1^{+/+}$ mice revealed that the tissue lysis performed according to optimized protocol leads to solubilisation of vast majority of mGCPII. When analysing mice homozygous for *Folh1-del4* and *Folh1-del17*, neither mGCPII full-length protein nor any truncated form of GCPII were detected in the brain or kidney lysates. Similarly as other GCPII-mutant mice, no signal corresponding to full-length or truncated form of mGCPII was observed in insoluble fractions of tissue lysates from $Folh1^{mut/mut}$ mice carrying *Folh1-del4* or *Folh1-del17*.

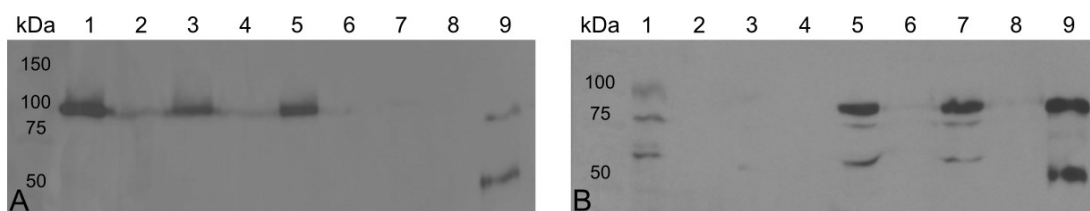


Figure 23: Western blot analysis of soluble and insoluble fractions of tissue lysates from mutant mice carrying *Folh1-del4* and *Folh1-del17*. An amount of soluble fractions corresponding to 100 μ g of total protein and 20 μ l of insoluble fraction mixtures (see Chapter 3.2.4.2., p. 62) were analysed. Purified rm-GCPII and rm-GCPIIdel17 served as mGCPII standards. Antibody GCPII-04 (Exbio) was used since it is able to detect not only mGCPII WT but also its mutant variants. **A:** Analysis of kidney lysates from 70 weeks old mutant mice carrying *Folh1-del4*. 1,3,5 – soluble fraction of tissue lysate (SF) from mice homozygous for WT variant of *Folh1* ($Folh1^{+/+}$ mice); 2,4,6 – insoluble fraction of tissue lysate (IF) from $Folh1^{+/+}$ mice; 7 – SF from mouse carrying mutant variant of *Folh1* on both alleles ($Folh1^{mut/mut}$ mouse); 8 – IF from $Folh1^{mut/mut}$ mouse; 9 – mixture of 5 ng of rm-GCPII and 5 ng rm-GCPIIdel17. **B:** Analysis of brain lysates from 8 weeks old mutant mice carrying *Folh1-del17*. 1,3 – SF from $Folh1^{mut/mut}$ mice; 2,4 – IF from $Folh1^{mut/mut}$ mice; 5,7 – SF from $Folh1^{+/+}$ mice; 6,8 – IF from $Folh1^{+/+}$ mice; 9 – mixture of 5 ng of rm-GCPII and 5 ng rm-GCPIIdel17.

4.3.2. Characterization of GCPII-deficient mice

Since no GCPII mutant protein variant was detected in any of the GCPII-mutant mice (see Chapter 4.3.1., p. 87), GCPII-mutant mice will be hereafter referred as GCPII-deficient or *Folh1*^{-/-}. To characterize GCPII-deficient mice thoroughly, brain and kidney lysates from 6 *Folh1*^{+/+} mice, 3 *Folh1*^{+/-} mice and 6 *Folh1*^{-/-} mice were analysed using Western blotting and NAAG hydrolysis assay.

Representative Western blot analysis is depicted in Figure 24. To demonstrate that the loaded amount of total protein was identical in all cases, a detection of β -actin as a loading control was included. To demonstrate that antibody GCPII-04 is able to recognize truncated forms of mGCPII, not only rm-GCPII WT but also rm-GCPII Δ 17 served as the protein standards (see Chapter 4.2.3., p. 82). It was confirmed that no band corresponding to full-length or any truncated variant of mGCPII could be detected in lysates from *Folh1*^{-/-} mice. Interestingly, the signal around 100kDa corresponding to mGCPII full-length protein displayed lower intensity in case of *Folh1*^{+/-} mice than in case of *Folh1*^{+/+} mice. Nevertheless, no truncated variant of mGCPII was observed in the lysates from *Folh1*^{+/-} mice.

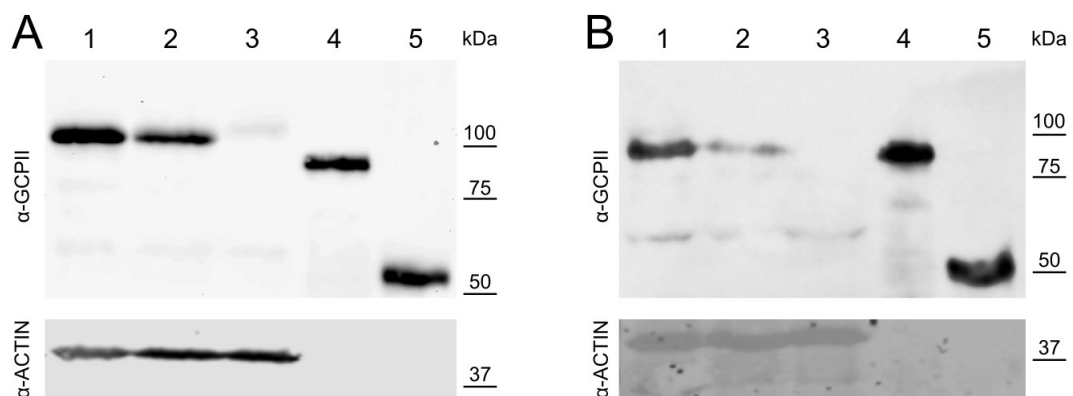


Figure 24: Characterization of GCPII-deficient mice using Western blot analysis of kidney (A) and brain (B) lysates. Male mice of age around 8 weeks carrying *Folh1-del17* (see Chapter 4.1.) were used. 100 μ g of total protein were analysed. To detect mGCPII, antibody GCPII-04 (Exbio) was used – here designated as α -GCPII. To detect β -actin, Monoclonal Anti- β -Actin antibody, clone AC-15 (Sigma-Aldrich) was used – here designated as α -ACTIN. Purified rm-GCPII and rm-GCPII Δ 17 served as mGCPII standards. 1 – *Folh1*^{+/+} mouse; 2 – *Folh1*^{+/-} mouse; 3 – *Folh1*^{-/-} mouse; 4 – 5ng of rm-GCPII; 5 – 5ng of rm-GCPII Δ 17.

Finally, NAAG hydrolysis analysis was performed in order to confirm that GCPII-deficient mice are indeed devoid of specific GCPII activity (see Figure 25). While overnight incubation of the brain and kidney lysates from *Folh1*^{+/+} mice with NAAG led to almost complete hydrolysis of the substrate (NAAG conversion higher than 80%), NAAG conversion in the lysates from *Folh1*^{-/-} mice did not exceed 6%. In correspondence with Western blotting observations, NAAG hydrolysis activity was decreased in lysates from *Folh1*^{+/-} mice as compared to lysates from *Folh1*^{+/+} mice.

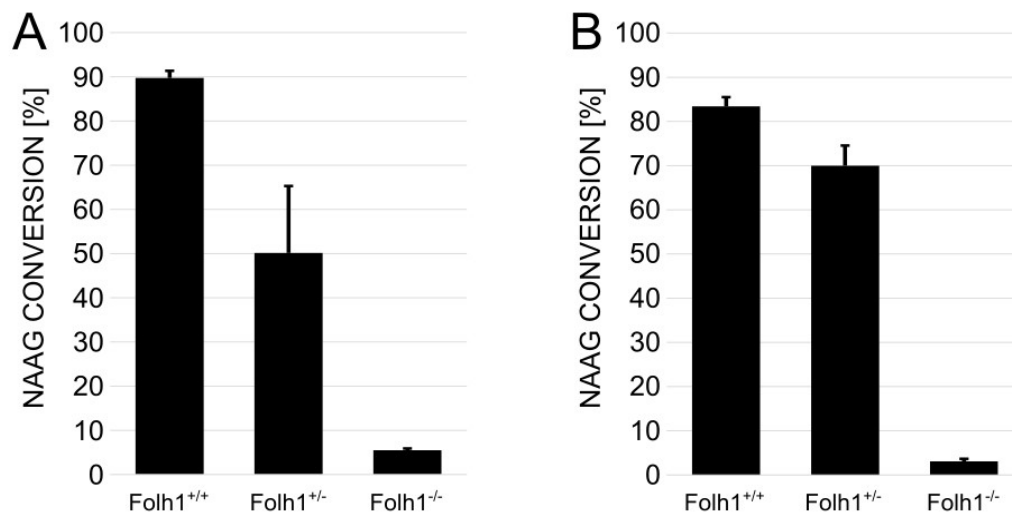


Figure 25: Characterization of GCPII-deficient mice using NAAG hydrolysis analysis of kidney (A) and brain (B) lysates. Male mice of age around 8 weeks carrying *Folh1-del17* (see Chapter 4.1., p. 74) were used. 100µg of total protein were analysed. Tissue lysates were incubated in 50mM Tris-HCl, 0.1% Tween, pH 7.4 with 100nM NAAG overnight at 37 °C. Error bars represent standard deviation of 6 biological replicates (for *Folh1*^{+/+} and *Folh1*^{-/-} mice) and 3 biological replicates (for *Folh1*^{+/-} mice).

4.4. Investigation of reproductive tissue phenotype of GCPII-deficient mice

The reproductive tissue phenotype was described in (Vorlova *et al.* 2018) in detail (see Appendix 2). Here, only the main results will be summarized. The mouse colonies carrying *Folh1-del3*, *Folh1-del4* and *Folh1-del17* were utilized in this study. We found that aged GCPII-deficient mice possess higher propensity for seminal vesicles enlargement than possess their WT counterparts. A typical gross anatomy of seminal vesicles of aged *Folh1^{+/+}* mice and some *Folh1^{-/-}* mice is depicted in Figure 26.

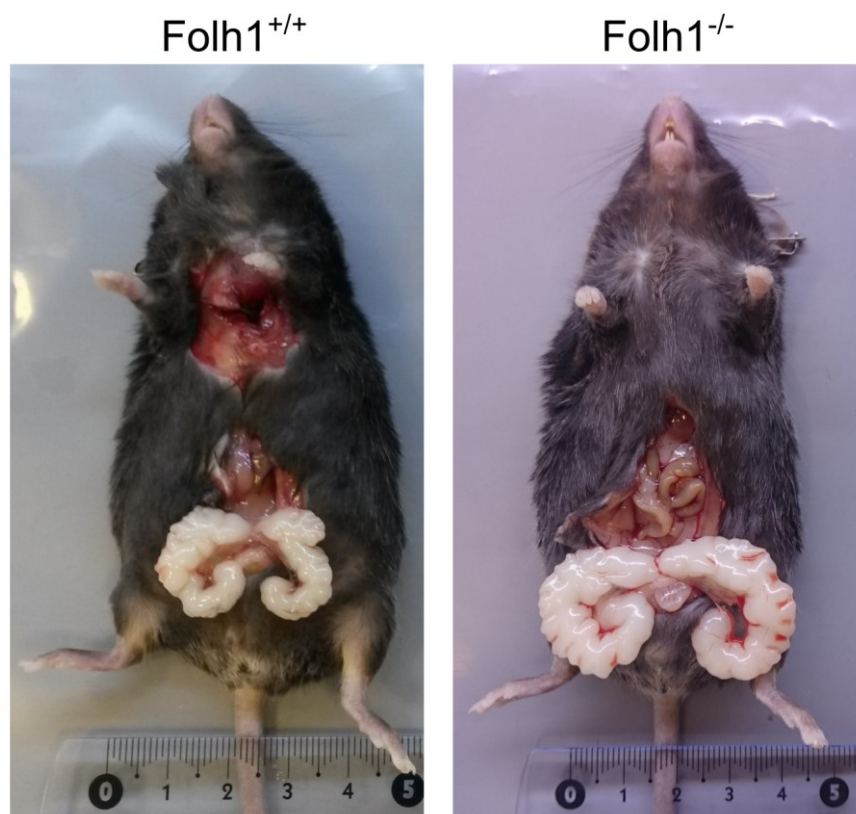


Figure 26: Typical gross anatomy of seminal vesicles of aged *Folh1^{+/+}* mice and some *Folh1^{-/-}* mice.

We further explored this phenomenon using cohorts of 20 *Folh1*^{+/+} mice, 26 *Folh1*^{+/-} mice and 9 *Folh1*^{-/-} mice with average age of 70.4 – 70.5 weeks (see Figure 27, panel A). We showed that the overall difference in seminal vesicle area among these three cohorts is highly statistically significant ($p < 0.002$) and not only difference between *Folh1*^{+/+} and *Folh1*^{-/-} mice, but also difference between *Folh1*^{+/+} and *Folh1*^{+/-} mice is statistically significant ($p < 0.001$ and $p = 0.028$, respectively). Moreover, we analysed the level of GCPII in kidney lysates of mice of all three genotypes (*Folh1*^{+/+}, *Folh1*^{+/-} and *Folh1*^{-/-}) and found that the level of GCPII in *Folh1*^{+/-} kidneys is about a half of the level in *Folh1*^{+/+} mice as determined by NAAG-hydrolysing activity (see Figure 27, panel B) and Western blotting (see Appendix 2, Figure 5).

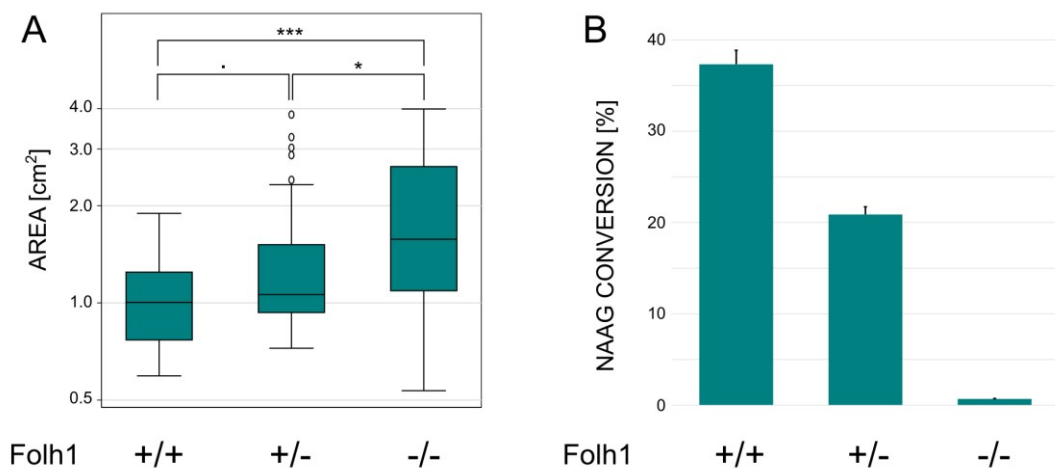


Figure 27: Statistical analysis of enlarged seminal vesicles and NAAG-hydrolysing activity in kidney lysates of aged mice of distinct genotypes. **A:** Comparison of seminal vesicle areas among *Folh1*^{+/+}, *Folh1*^{+/-} and *Folh1*^{-/-} mice. *** indicates $p < 0.001$, * indicates $p = 0.028$ and · indicates $p = 0.052$. Seminal vesicle areas were measured by MUDr. Frantisek Sedlak using ImageJ software (Rueden *et al.* 2017). Statistical analysis was performed by Dr. Marek Maly at National Institute of Public Health. **B:** Comparison of NAAG-hydrolysing activity (see Chapter 3.2.7., p. 67) in kidney lysates of *Folh1*^{+/+}, *Folh1*^{+/-} and *Folh1*^{-/-} mice. NAAG-hydrolysing analysis was carried out in 0.5 µg total protein. Tissue lysates were incubated in 50 mM Tris-HCl, 0.1% Tween, pH 7.4, with 100 nM NAAG at 37 °C for 6 hours. Error bars represent standard deviation of 2 (for -/-) or 3 (for +/+ and +/-) biological replicates. The figure was adapted from (Vorlova *et al.* 2018).

Next, we set out to investigate the possible source of the seminal vesicle enlargement. We examined urogenital system of WT mice using NAAG-hydrolysing activity assay (see Chapter 3.2.7., p. 67) and found that the NAAG conversion in seminal vesicles and most surrounding urogenital tissues including all four prostate lobes corresponds to less than 2.5 pg of GCPII per 1 μ g of total protein (considering that GCPII is the only enzyme capable of NAAG cleavage, see Figure 28). Except of kidney (which served as a positive control), only epididymis and spermatic cord exhibited NAAG conversion at least 50% when 30 μ g total protein was measured overnight.

The epididymis and spermatic cord were thus examined for accurate determination of GCPII level. Using tissues from *Folh1*^{-/-} mice as negative controls, we found out that spermatic cord contains only around 2.3 pg of GCPII per 1 μ g total protein (see Appendix 2, Figure 6). Nevertheless, the level of GCPII in the mouse epididymis was as high as its level in the mouse kidney (see Table 4, p. 94).

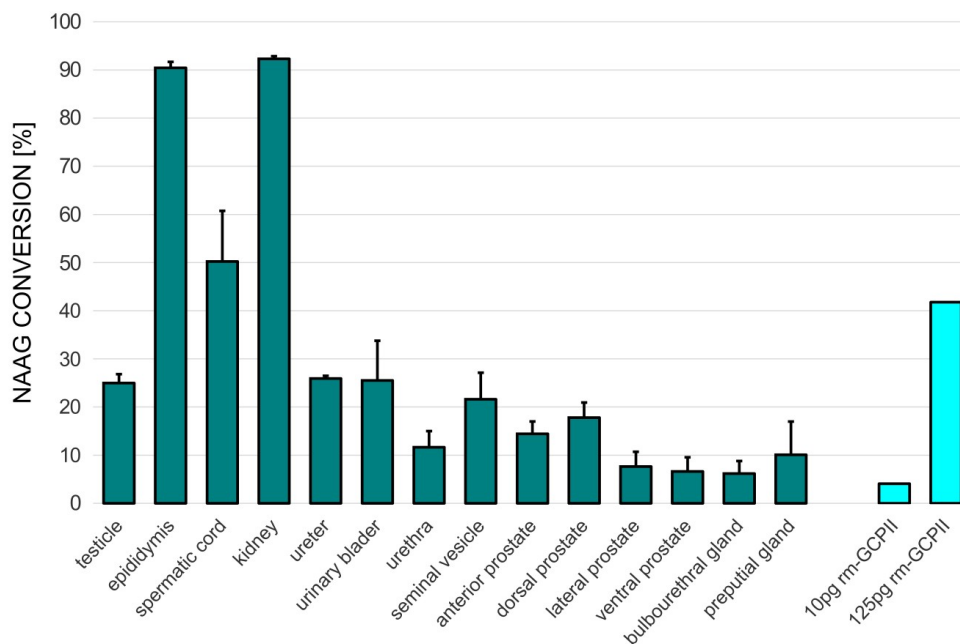


Figure 28: NAAG-hydrolysing activity in the male mouse urogenital system. Tissue lysates were incubated in 50 mM Tris-HCl, 0.1% Tween, pH 7.4, with 100 nM NAAG overnight at 37 °C. NAAG conversion in reactions with 30 μ g total protein per tissue lysate (designated as teal) was compared to NAAG conversion in reactions with 10 pg and 125 pg of recombinant mouse GCPII (rm-GCPII, designated as light blue). Error bars of NAAG conversions in tissue lysates represent standard deviations of biological replicates (from 3 to 5 mice of at least 2 of 3 different ages: 8 weeks, 17 weeks and 30 weeks). The dependence of NAAG conversion on the rm-GCPII amount from 10 pg to 125 pg was linear (only the extreme points of calibration curve are shown). Error bars of NAAG conversions by rm-GCPII represent standard deviations of 6 independent measurements. The figure was adapted from (Vorlova *et al.* 2018).

Table 4: Calculated amount of GCPII in the mouse epididymis as compared with previously published GCPII levels in the mouse kidney and brain (Knedlik *et al.* 2017). The calculation was performed by comparison of NAAG conversion in 0.3 µg of total protein in mouse epididymis with rm-GCPII calibration curve.

| mouse tissue | mGCPII [ng/mg] |
|--------------|----------------|
| epididymis | 182 ± 12 |
| kidney* | 100 – 250 |
| brain* | 2.5 – 10 |

We thus decided to examine whether GCPII is also present in the human epididymis. Indeed, using immunochemistry with three different antibodies against GCPII, we showed that GCPII-positive cells could be detected in all parts of human epididymis (see Figure 29 as well as Appendix 2, Figure 8).

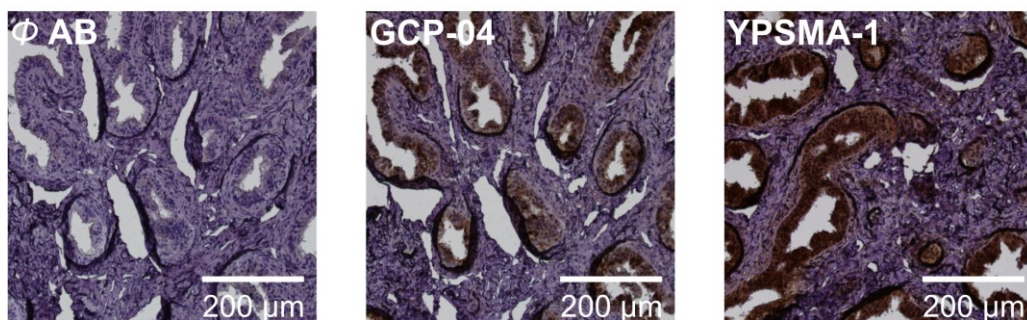


Figure 29: Representative immunohistochemical staining of human epididymis. Formalin-fixed paraffin-embedded human epididymis tissue sections were incubated with the antibodies against GCPII at a concentration of 10 µg/ml to detect GCPII-positive cells. Here, examples of staining using antibodies GCP-04 (Exbio) and YPSMA-1 (Anogen) are shown. As a negative control (designated as Φ AB), immunohistochemistry using only secondary antibody Histofine Simple Stain™ MAX PO (MULTI) (Nichirei Biosciences Inc.) was performed. The tissue sections were provided by prof. Josef Zamecnik from Motol University Hospital. The immunochemistry was performed by MUDr. Frantisek Sedlak. The figure was adapted from (Vorlova *et al.* 2018).

4.5. Investigation of potential GCPII involvement in renal function

4.5.1. Mouse urine collection

The urine samples were collected from total number of 129 mice of distinct genotypes (*Folh1*^{+/+} and *Folh1*^{-/-}), sex (males and females) and ages (young: – 8-12 weeks – and aged – 63-81 weeks). The mouse colonies carrying *Folh1-del3*, *Folh1-del4* and *Folh1-del17* were utilized in this study. The volume of the collected urine ranged from 2 μ l to 500 μ l. The concentration of creatinine measured in all collected samples varied between 450 μ M and 7 mM but did not correlate with the volume of the collected urine. Moreover, no dependency of the creatinine level on the genotype, sex or age was observed.

The urine samples of sufficient volume and creatinine concentration (to reach the minimum creatinine amount of 30 nmol required for further sample processing and metabolomic analysis) were then selected for dilution and filtration (for more information see Chapter 3.2.8.3., p. 71). A total number of 116 samples were sent for metabolomic analysis, including 2 samples with creatinine concentration slightly below 700 μ M (640 μ M and 690 μ M, respectively). The numbers of samples per each study group are summarized in Table 5. The creatinine concentration in the pooled sample (i.e. a mixture of 2 μ l aliquots from each sample) was 670 μ M.

Table 5: Summary of the processed mouse urine samples sent to metabolomic analysis performed by Dr. David Friedecky and colleagues at IMTM.

| | SEX | GENOTYPE | AVERAGE AGE | NUMBER OF SAMPLES |
|------------|--------|-----------------------------|----------------|-------------------|
| YOUNG MICE | female | <i>Folh1</i> ^{+/+} | 9.2 \pm 1.3 | 12 |
| | | <i>Folh1</i> ^{-/-} | 8.6 \pm 0.4 | 9 |
| | male | <i>Folh1</i> ^{+/+} | 9.1 \pm 1.3 | 9 |
| | | <i>Folh1</i> ^{-/-} | 8.4 \pm 0.1 | 7 |
| AGED MICE | female | <i>Folh1</i> ^{+/+} | 70.5 \pm 0.7 | 20 |
| | | <i>Folh1</i> ^{-/-} | 70.6 \pm 0.6 | 19 |
| | male | <i>Folh1</i> ^{+/+} | 73.2 \pm 4.6 | 26 |
| | | <i>Folh1</i> ^{-/-} | 72.3 \pm 4.7 | 14 |

4.5.2. Targeted metabolomics of mouse urine

Using targeted metabolomics, 193 metabolites were detected in the mouse urines (for the complete list of metabolites and their abbreviations see Appendix 3). Multivariate cluster analysis revealed that metabolomics profiles were age and sex specific rather than genotype specific (see Figure 30). Within the age-dependent clustering, more than 40 discriminating metabolites were found including N-acetylasparatate, glutarate, betaine, isoleucine, trigonelline, citrate, succinate, choline, proline and hydroxyproline. Within the sex-dependent clustering, more than 30 metabolites were detected including lactate, 2-hydroxyisobutyrate, hydroxybutyrate, 3-aminoisobutyrate and 4-aminobutanoate.

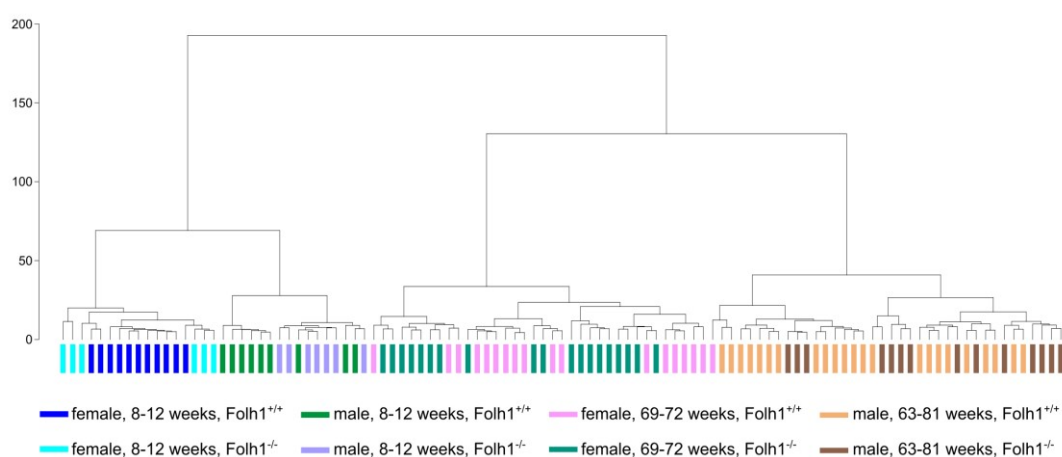


Figure 30: Cluster analysis of targeted metabolomics data obtained by HPLC-MS/MS analysis of mouse urines. The HPLC-MS/MS and subsequent statistical analysis of metabolomics data were performed by Dr. David Friedecky and colleagues at IMTM.

To investigate further possible differences in metabolite profiles of urines from Folh1^{+/+} and Folh1^{-/-} mice, multivariate statistics using OPLS-DA analysis was performed (see Figure 31, p. 97). Interestingly, no folate-related metabolite, including different forms of folate as well as homocysteine, was discriminating between both genotypes. Nevertheless, only monoglutamylated forms of folate were tested since the detection of polyglutamylated forms was not successful. Even though the OPLS-DA

S-plot did not show typical S-shape, 12 metabolites were selected for additional evaluation by supervised univariate analysis using box plot displays (see Figure 32, p. 98).

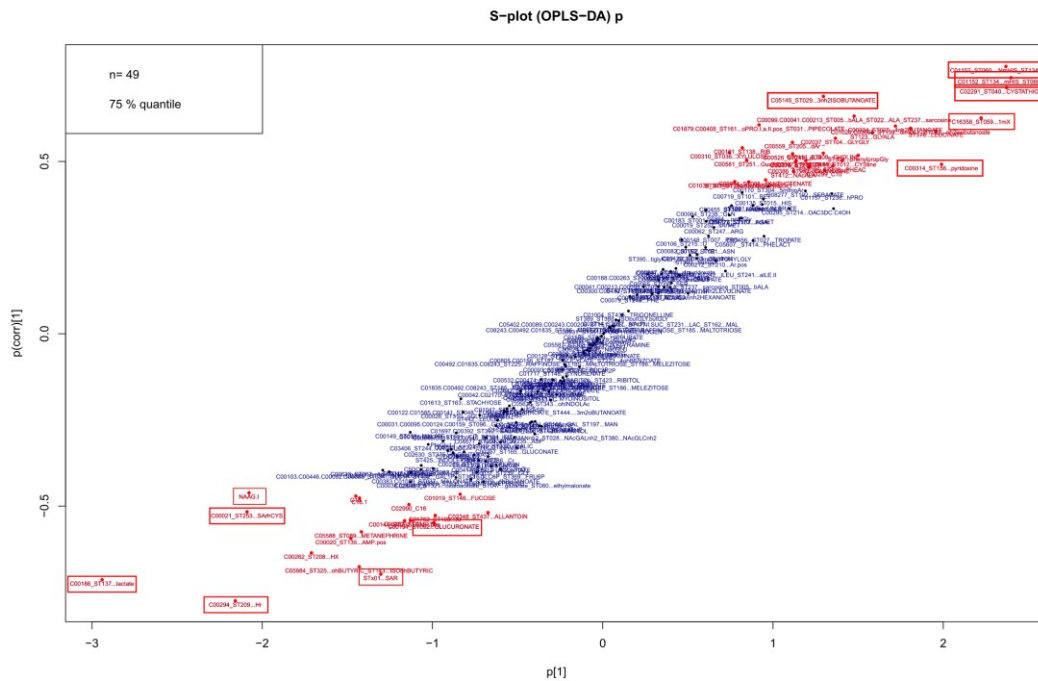


Figure 31: S-plot build for targeted metabolomic analysis of urine samples from Folh1^{+/+} and Folh1^{-/-} mice. p[1] represents covariance (a magnitude of the model component scores) and p(corr)[1] represents correlation (a reliability of the model component scores). The metabolites selected for univariate analysis using box plots are marked by red rectangles. The statistical analysis of metabolomics data was performed by Dr. David Friedecky and colleagues at IMTM.

When comparing Folh1^{+/+} and Folh1^{-/-} mice, 11 out of the 12 selected metabolites displayed p-values below 0.05, among those 6 metabolites displayed p-values lower than 0.01. Nevertheless, by application of Bonferroni correction, the alpha level decreased to 2.59×10^{-4} ($0.05/\text{number of detected metabolites} = 0.05/193$). Therefore, only 3 metabolites (inosine, succinyladenosine and NAAG) could be considered as metabolites significantly discriminating Folh1^{+/+} and Folh1^{-/-} mice. The most significant difference was shown for NAAG since its increased level in Folh1^{-/-} mouse as compared to Folh1^{+/+} mice displayed p-value of 9.28×10^{-18} .

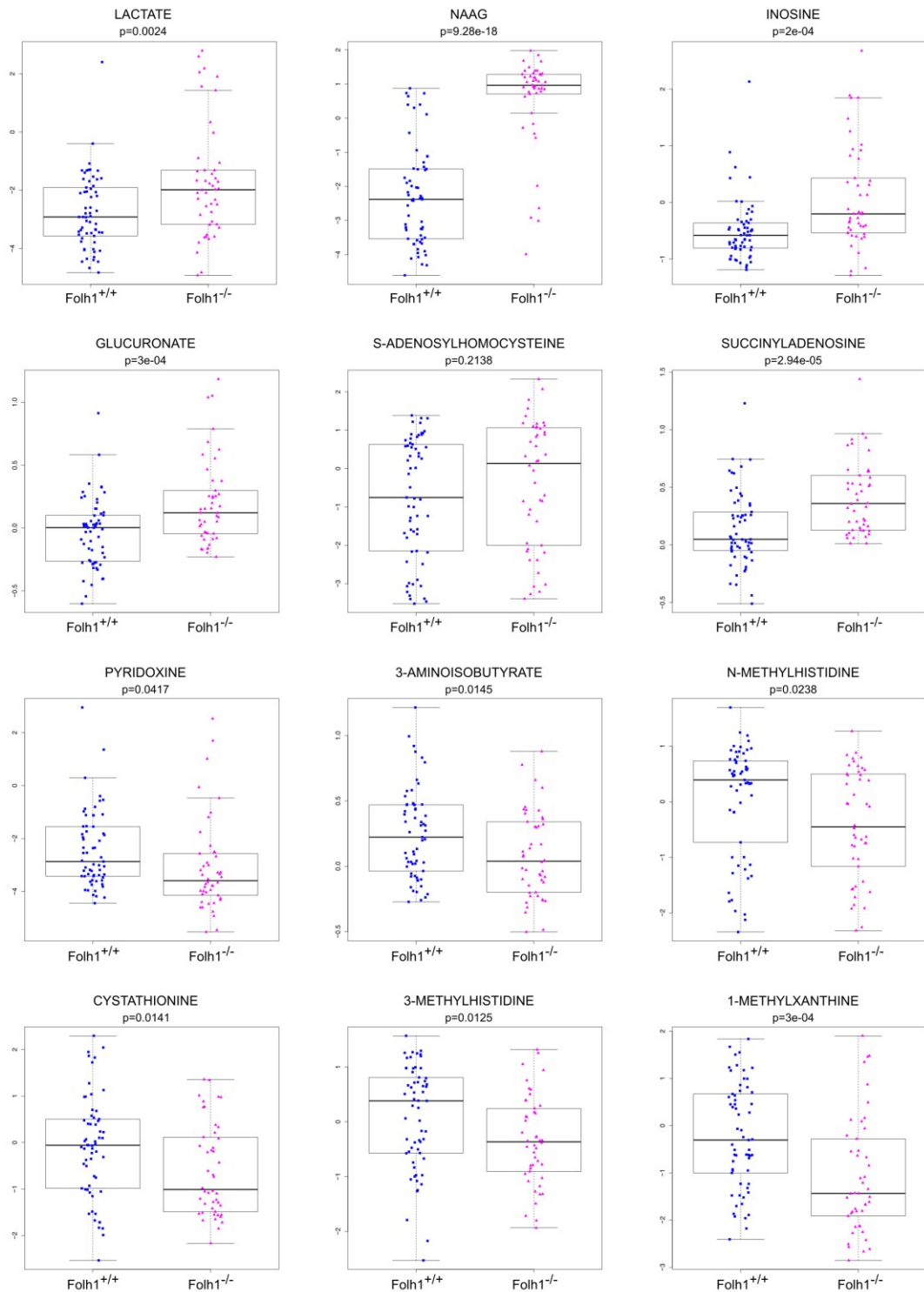


Figure 32: Box plot displays of selected metabolites detected in mouse urine samples. The statistical analysis of metabolomics data was performed by Dr. David Friedecky and colleagues at IMTM.

4.5.3. Histopathological examination of kidneys from aged mice

Mouse kidneys were investigated for possible abnormalities by MUDr. Tomas Olejar, Ph.D. at First Faculty of Medicine using histology followed by H&E staining. No histopathological changes were observed in the kidneys of young mice (data not shown). The histological examination of kidneys of old mice is depicted in Figure 33.

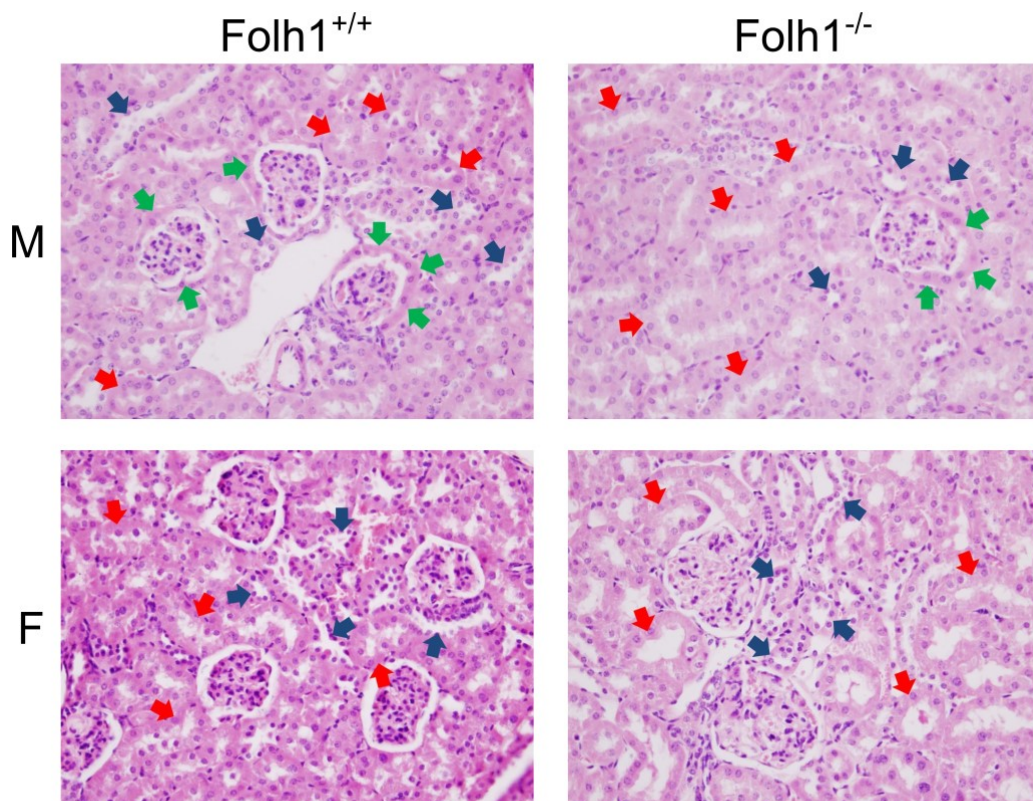


Figure 33: Representative histopathological examination of kidney cross sections of 70 weeks old mice. The kidneys were fixed by formalin, embedded in paraffin, sectioned and stained with haematoxylin and eosin. The red arrows indicate proximal tubules, the blue arrows indicate distal tubules and the green arrows indicate tubularization of Bowman's capsule. The histopathology was performed by MUDr. Tomas Olejar, Ph.D. at First Faculty of Medicine.

No significant differences in proximal and distal tubules between Folh1^{+/+} and Folh1^{-/-} mice were observed. The tubules showed typical cuboidal epithelium with no dilatation, the histology of collecting ducts as well as interstitium was also normal.

Most glomeruli possessed normal structure, atrophy or focal glomerulosclerosis were observed occasionally. Nevertheless, normally squamous layer of Bowman's capsule was frequently transformed into a columnar epithelium similar to epithelium of proximal tubules. This tubularization phenomenon was found in the male kidneys more often than in the female kidneys but was not genotype-specific.

4.6. My contribution to the project

The data presented in this thesis were generated by several members of our laboratory as well as external collaborators. Here, my contributions to the dissertation project results are summarized.

1. Majority of chromosomal DNA isolations and analyses of TALEN-mediated mutations
2. Selection of the founder mice and mouse colony management
3. Development of genotyping protocol
4. Execution of a routine genotype analysis in cooperation with Ing. Karolina Sramkova
5. Kinetic characterization of rm-GCPII
6. Preparation and characterisation of mutant variants of membrane-bound mGCPII
7. Purification of majority of recombinant proteins
8. Investigation of physical properties of rm-GCPII^{del3}
9. Dissection of vast majority of the mice
10. Optimisation of mouse tissue lysis protocol, Western blotting protocol and NAAG hydrolysis assay protocol
11. Design of all the experiments related to mouse tissue lysis, Western blotting and NAAG hydrolysis assay
12. Execution of the experiments related to mouse tissue lysis, Western blotting and NAAG hydrolysis assay in cooperation with Ing. Karolina Sramkova
13. Contribution to optimisation of immunohistochemistry protocol

14. Mouse urine collection and optimisation of a protocol for determination of creatinine concentration
15. Design of most of the experimental procedures for preparation of the urine samples for metabolomic analysis
16. Execution of the experimental procedures for preparation of the urine samples for metabolomic analysis in cooperation with MUDr. Frantisek Sedlak and Ing. Karolina Sramkova
17. Design of most experiments and analysis of the data
18. Preparation of drafts of all manuscripts describing the results obtained during this research project

5. DISCUSSION

Despite extensive research for more than 30 years, the physiological role of GCPII has not been fully determined. The attempts to generate GCPII-deficient mice in order to decipher GCPII function have led to conflicting results ranging from embryonic lethality (Tsai *et al.* 2003; Han *et al.* 2009) to production of GCPII-deficient mice with no obvious phenotype (Bacich *et al.* 2002; Gao *et al.* 2015). This dissertation project thus aimed to dissect the discrepancy using gene disruption technique different from ESCs manipulation, which had been utilized in all previous studies.

To study GCPII function, mouse model seems to be a suitable approach. Indeed, our direct comparison of recombinant human and mouse GCPII revealed that not only the sequences (see Figure 1, p. 14), but also the enzymatic properties of both orthologues are similar (Knedlik *et al.* 2017). They possess comparable substrate specificities and inhibition profiles; only the catalytic efficiency of mGCPII towards physiological substrates appears to be lower than that of hGCPII. Moreover, while the catalytic efficiency for NAAG differs only about four times (see Table 2, p. 79), the catalytic efficiency for FolGlu_n is more pronounced (more than one order of magnitude) (Knedlik *et al.* 2017).

FolGlu_n-hydrolysing activity of GCPII has a defined function only in the human small intestine, where it is involved in folate absorption (Halsted 1991). In the mouse small intestine, this process is probably facilitated by a different enzyme (see Chapter 1.5.2., p. 25) since mGCPII level in this tissue is extremely low (Knedlik *et al.* 2017). It is thus uncertain, if the FolGlu_n-hydrolysing activity of GCPII is crucial in the mouse body. Except of the small intestine, the level of GCPII expression also differs in the prostate (see Chapter 1.4.2.1., p. 19). Indeed, while the prostate is one of the tissues with the highest GCPII expression in humans (Sokoloff *et al.* 2000), the amount of GCPII in the mouse prostate seems to be negligible. The absence of GCPII in the mouse prostate was published previously (Bacich *et al.* 2001; Knedlik *et al.* 2017), though the exact prostate lobe used for the experiments has not been specified. Since mouse prostate consists of four lobes that differ in anatomy and histology (Oliveira *et al.* 2016), we examined all four lobes separately but did not observe a pronounced GCPII expression in any of them (see Figure 28, p. 93). In contrast to the small intestine and prostate,

the level of GCPII expression in the brain and kidney seems to be very similar for both orthologues (Knedlik 2010). The mouse model can be thus used for revealing the function of GCPII in the nervous and urogenital system.

For the attempt to inactivate *Folh1* gene in mouse, we used one of the modern gene disruption technique – TALEN technology (Cermak *et al.* 2011; Miller *et al.* 2011; Bogdanove and Voytas 2011). Recently, simpler-to-design CRISPR/Cas9 technology (Jinek *et al.* 2012) is being most frequently used for mouse genome modifications. However, at the start of this dissertation project, CRISPR/Cas9 technology was not available. Moreover, off-target activity seems to be a more significant problem for CRISPR/Cas9 than for TALENs (Boettcher and McManus 2015).

When inactivating *Folh1* gene by TALENs, we intended to disrupt the active site of mGCPII. This strategy was selected to avoid two main obstacles that were not addressed in previous reports. First, several publications detected novel alternative splice variants in the knockout mice and showed that these variants may rescue severe phenotype of completely inactivated gene (Gros-Louis *et al.* 2008; Kraemer *et al.* 2015). We hypothesized that the viable GCPII-deficient mice published by Bacich and colleagues could contain alternatively spliced variants that enabled partial preservation of GCPII activity (Bacich *et al.* 2002). This was strengthened by the facts that the authors saw residual NAAG-hydrolysing activity in the brains of GCPII-deficient mice and that the attempt of Tsai and colleagues to generate GCPII-deficient mice, in which the disruption of the mGCPII active site was performed, led to embryonic lethality (Tsai *et al.* 2003).

Second, for the purpose of disrupting the active site of GCPII, Tsai and colleagues replaced exons 9 and 10 of *Folh1* gene encoding zinc ligands by PGK-Neo (Tsai *et al.* 2003). Therefore, the authors did not only disable GCPII activity, but also GCPII 3D structure. In case GCPII fulfils both the enzyme and the receptor functions (see Chapter 1.5.3., p. 27), disrupting both functions at the same time could lead to embryonic lethality. We thus hypothesized that together with greater disruptions leading to complete inactivation of *Folh1* gene, TALEN technology may also generate small deletions within the active site of mGCPII. These small modifications could possibly only disable mGCPII activity but not its structure and the potential receptor function would be thus preserved.

From two independent attempts to generate mice with TALEN-mediated indel mutations of *Folh1* gene, we selected three founder mice that altogether contained 2 frame-shift deletions (*Folh1-del4* and *Folh1-del17*) and 3 small deletions within the mGCPII active site (*Folh1-del3*, *Folh1-del6* and *Folh1-del12*) (see Figure 12, p. 74 and Figure 13, p. 75). To establish all five mutant mouse colonies, we bred the founder mice with C57BL/6NCrl wild type mice and monitored the resulting genotypes by developed genotyping method, which is based on nested PCR (see Figure 14, p. 76 and Figure 15, p. 77).

During the breeding process, we attempted to prepare recombinant variants of the potential products of *Folh1* mutant gene expression. This was performed from two main reasons. First, we wanted to ensure that all the potential protein products lack GCPII-related activity. For this purpose, we transiently expressed membrane-bound mutant variants of mGCPII in HEK293A2off cells and subsequently compared the capability of the cell lysates to hydrolyse NAAG (see Chapter 4.2.2., p. 79). The NAAG-hydrolysing activity of all lysates containing mutant variants was comparable to that of the negative control (see Figure 17, p. 81). We thus concluded that if the products of *Folh1* mutant genes would be expressed in the GCPII-mutant mice, there active sites are definitely disrupted.

Second, we wanted to investigate, whether the small deletions within the active site of mGCPII do not impair mGCPII 3D structure. For this purpose, we attempted to express and purify extracellular parts of mGCPIIdel3, mGCPIIdel6 and mGCPIIdel12. Only rm-GCPIIdel3 that possesses a single amino acid deletion and a single amino acid mutation within the active site of mGCPII (see Figure 13, p. 75) displayed comparable expression performance as mGCPII WT (see Figure 18, p. 82). The expression yield of rm-GCPIIdel6 and rm-GCPIIdel12 was at least five times lower. Moreover, the purification process of all three mutant rm-GCPII variants was much less efficient than that of rm-GCPII WT. Indeed, the mutant variants of rm-GCPII were incapable of strong interaction with Streptavidin Mutein Matrix, which led to higher proportion of the rm-GCPII mutant variant staying in the flow-through fraction and present in the washing fractions. Not surprisingly, the purity and purification yield of rm-GCPIIdel6 and rm-GCPIIdel12 was extremely low (see Figure 19, p. 84). Moreover, rm-GCPIIdel6 was highly instable since it degraded during the protein concentration. We thus deduced that

the mGCPII mutant variants with more than one amino acid deletion within the active site lose the physical properties of mGCPII WT and did not investigate them further.

Even though the expression yield of rm-GCPII~~3~~ was also decreased when compared to the expression yield of rm-GCPII WT, the difference was not dramatic (see Chapter 4.2.3., p. 82). We thus decided to compare the physical properties of rm-GCPII~~3~~ and rm-GCPII WT using two independent methods (see Chapter 4.2.4., p. 84). Surprisingly, both size-exclusion chromatography (see Figure 20, p. 85) and ThermoFluor assay (see Figure 21, p. 86) showed that while rm-GCPII WT behaves as a dimer, which is the natural form of GCPII in the solution (Mesters *et al.* 2006), rm-GCPII~~3~~ displays rather monomeric structure surrounded by great amount of aggregates. These results suggest that even a single amino acid deletion within the active site of mGCPII leads to dramatic changes in the protein structure. Therefore, we concluded that even if the mutant variants of mGCPII with one, two or four amino acid deletions within the active site would be expressed in corresponding GCPII-mutant mice, these mice could not be utilized for investigation of possible GCPII receptor function.

By heterozygous mating of all five established GCPII-mutant mouse colonies, we were able to obtain offsprings with typical Mendelian inheritance. We did not observe embryonic lethality of mice homozygous for *Folh1* mutant gene. We thus set out to investigate whether the mutant variants of GCPII are expressed in the GCPII-mutant mice. We performed Western blot analysis of two distinct tissues that normally express the highest level of GCPII in mice – brain and kidney. The signal corresponding to GCPII was not observed in either the soluble fractions or the insoluble fractions of tissue lysates from GCPII-mutant mice (see Figure 22, p. 87 and Figure 23, p. 88). In these mutant mice, GCPII is either expressed and immediately degraded or not expressed at all. The mutant mice bearing any of the *Folh1* mutant variant could be thus considered as GCPII-deficient mice.

To thoroughly characterize GCPII-deficient mice (also referred as *Folh*^{-/-}), we utilized two independent methods – Western blotting and NAAG-hydrolysing activity assay – to analyse brain and kidney lysates from the number of 8 weeks old mice that was sufficient for statistical significance. Western blot analysis did not detect GCPII full-length protein or GCPII truncated variant, which could possibly be a product of expression of *Folh1-del4* and *Folh1-del17* gene, in any lysate from GCPII-deficient mice (see Figure 24, p. 89). Moreover, NAAG-hydrolysing activity was dramatically

decreased in all lysates from GCPII-deficient mice (see Figure 25, p. 90). Based on these reasons, we are confident that our attempt to inactivate *Folh1* gene in mice through GCPII active site disruption led to generation of viable GCPII-deficient mice.

We thus confirmed the results of the original publication of Bacich and colleagues (Bacich *et al.* 2002) and disproved that GCPII deficiency is embryonically lethal as was repeatedly reported by the research group of Joseph T. Coyle (Tsai *et al.* 2003; Han *et al.* 2009). Moreover, during the time when this dissertation project has been in the process, another publication reporting viable GCPII-deficient mice emerged (Gao *et al.* 2015). Recently, International Mouse Phenotyping Consortium (IMPC) also released information about preparation of viable GCPII-deficient mice (Koscielny *et al.* 2014). It remains unclear why any strategy of Coyle's research group for inactivation of *Folh1* gene did not result in production of live GCPII-deficient mice. However, thanks to the work of four independent laboratories (us including), it seems to be evident that disruption of GCPII encoding gene does not lead to embryonic lethality of the mice.

Interestingly, when comparing tissue lysates from GCPII WT mice (also referred as *Folh*^{+/+}) and mice bearing both *Folh1* and *Folh1*-mutant alleles (also referred as *Folh*^{+/-}), the intensity of Western blot signal of GCPII differed. Indeed, we observed that the amount of GCPII in lysates from *Folh*^{+/-} heterozygous mice was about a half the amount of GCPII in lysates from *Folh*^{+/+} mice (see Figure 24, p. 89). This observation was further confirmed by NAAG-hydrolysing activity assay, which displayed NAAG conversion in the lysates from *Folh*^{+/-} mice being around a half the NAAG conversion in the lysates from *Folh*^{+/+} mice (see Figure 25, p. 90). Such observation is in accordance with the reports published previously (Bacich *et al.* 2002; Gao *et al.* 2015). In contrast, while residual NAAG-hydrolysing activity in the brains of our GCPII-deficient mice seems to be negligible since the NAAG conversion in saturation did not exceed 4% of the values obtained for WT mice (see Figure 25, p. 90), others showed NAAG conversion in GCPII-deficient mice within the linear range of reaction velocity ranging from 6% to 18% of the values obtained for WT mice (Bacich *et al.* 2002; Gao *et al.* 2015). Since none of the viable mice produced by others was generated by disruption of active site, it cannot be excluded that these mice indeed contain the alternatively spliced variants that partially preserve GCPII activity.

On top of the fact that *Folh1* gene disruption using TALENs is much more convenient and rapid than ESCs manipulation, TALEN technology also enabled us to

directly manipulate mouse zygotes of C57 genetic background, which was also the intended background of the GCPII-deficient mouse colony. Thus, potential phenotypic variations, which could be caused by mixed genetic backgrounds (Yoshiki and Moriwaki 2006), were eliminated. From the other laboratories that produced GCPII-deficient mice, only IMPC generated the mice on a pure genetic background (Koscielny *et al.* 2014). In contrast, the mice of Bacich and colleagues and Gao and colleagues were prepared by manipulation of ESCs of 129sv background with subsequent backcrossing to C57 background (Bacich *et al.* 2002; Gao *et al.* 2015).

Since TALEN technology does not require selectable marker, our GCPII-deficient mice do not contain PGK-Neo cassette, which could influence expression of neighbouring genes within the locus and subsequently cause unexpected phenotypes of knockout mice (Olson *et al.* 1996; Pham *et al.* 1996). Out of three laboratories with established GCPII-deficient mouse colonies, only IMPC removed PGK-Neo cassette using Cre-Lox system before investigating the GCPII-deficient mice further (Koscielny *et al.* 2014). Other two GCPII-deficient colonies do not probably contain any LoxP sites and the PGK-Neo cassette removal is thus impossible (Bacich *et al.* 2002; Gao *et al.* 2015). These mice have been repeatedly utilized for wide range of different experiments (Rais *et al.* 2016; Caromile *et al.* 2017; Cao *et al.* 2016) but it cannot be excluded that the results of the experiments were influenced by the presence of PGK-Neo.

In agreement with other studies (Bacich *et al.* 2002; Koscielny *et al.* 2014; Gao *et al.* 2015), our GCPII-deficient mice did not show any reproductive or overt phenotypic abnormalities. Since the publications focusing on GCPII-deficient mice phenotype have mainly investigated the nervous system (Bacich *et al.* 2005; Gao *et al.* 2015; Cao *et al.* 2016), we decided to explore the impact of *Folh1* gene inactivation on the mouse urogenital system. We first performed gross anatomy of a small group of both the young and the aged GCPII-deficient mice. While no obvious abnormalities were observed in young mice, aged GCPII-deficient mice displayed bilaterally enlarged seminal vesicles with higher frequency than their WT counterparts (see Figure 26, p. 91). By investigation the statistically sufficient number of mice aged between 69 to 72 weeks, we concluded that GCPII-deficient mice indeed possess higher propensity for seminal vesicle enlargement (Figure 27, p. 92). Interestingly, this phenotype was not observed only in *Folh1*^{-/-} mice but to a lesser extent also in *Folh1*^{+/-} mice. Therefore, it is possible that the enlargement of seminal vesicle is somehow connected with GCPII activity since not only

the young *Folh1*^{+/-} mice but also the aged *Folh1*^{+/-} mice display decreased expression level of GCPII when compared to *Folh1*^{+/+} mice (see Figure 27, p. 92).

The seminal vesicle dilation in our GCPII-deficient mice seemed to originate solely from accumulation of luminal fluid (Vorlova *et al.* 2018). This phenotype of C57 mice has been previously reported as one of the signs of aging (Finch and Girgis 1974; Pettan-Brewer and Treuting 2011). Nevertheless, the mice, which showed enlargement of seminal vesicles caused by accumulation of luminal fluid, were at least 24 months old (Finch and Girgis 1974), i.e. much older than the mice investigated in our study. Enlarged seminal vesicles were also reported in aged C57 mice with lower age limit of 16 months (Pettan-Brewer and Treuting 2011). However, in this case, the seminal vesicle dilation was a result of either an infection or a presence of abdominal tumour, neither of which we saw during our histopathological examination (Vorlova *et al.* 2018).

In order to research the possible source of seminal vesicle dilation in GCPII-deficient mice, we investigated the expression level of GCPII in the seminal vesicles and most surrounding tissues of WT mice using NAAG-hydrolysing activity assay (see Figure 28, p. 93). Surprisingly, GCPII seemed to be only present in the epididymis and spermatic cord since no other urogenital tissue displayed a pronounced NAAG conversion. Nevertheless, it cannot be excluded that GCPII is present in the seminal vesicles in an amount sufficient for execution of a specific function. Indeed, 60-75% of the seminal vesicle mass is represented by the seminal fluid (Finch and Girgis 1974) and thus only around 35-40% of the seminal vesicle mass remains for the cells. Since protein concentration in the seminal fluid can be as high as 86 mg/ml (Dyck *et al.* 1999), the amount of GCPII expressed in the seminal vesicle cells can be dramatically underestimated. Similarly, male urogenital tissues such as urethra comprise different types of cells (Ruberte Jose 2017). In case GCPII is present in only one cell type, the amount GCPII may be physiologically relevant.

Although the NAAG-hydrolysing activity assay was performed using the reaction conditions highly specific for GCPII (Navratil *et al.* 2016), enzymes such as GCPIII, which could be possibly also present in the studied tissue, may influence the outcome of the analysis. It has been shown that GCPIII is expressed in considerable amounts in the mouse testis, kidney and bladder (Collard *et al.* 2011). No other tissues of male urogenital system have been explored though. To exclude a potential participation of other enzymes including GCPIII, we investigated NAAG-hydrolysing activity of the spermatic cord and

epididymis (as the only tissues displaying pronounced NAAG conversion) from both WT and GCPII-deficient mice (Vorlova *et al.* 2018). As a result, apart from kidneys (Knedlik *et al.* 2017), only epididymis may be additionally considered as a GCPII-expressing tissue in mice. Interestingly, the epididymis appears to express one of the highest levels of GCPII within the mouse body (see Table 4, p. 94).

To put our findings into the context of human physiology, we investigated a potential presence of GCPII in the human epididymis using immunochemistry (see Figure 29, p. 94). Based on the results, we concluded that not only GCPII mRNA (Renneberg *et al.* 1999), but also GCPII protein is expressed in the human epididymis. In humans, ejaculatory duct obstruction is rather uncommon but has been indicated as one of the causes of male infertility (Fisch *et al.* 2006). It may be only speculated whether the absence of GCPII in the epididymis is somehow associated with increased occurrence of enlarged seminal vesicles. The reason why the inactivation of *Folh1* gene leads to seminal vesicles dilation in aged GCPII-deficient mice thus remains enigmatic and further research is desirable.

Surprisingly, the function of GCPII in the kidney has not been studied yet, though this tissue expresses one of the highest levels of GCPII in both the humans and mice (Rovenska *et al.* 2008; Bacich *et al.* 2001; Knedlik *et al.* 2017). We hypothesized that inactivation of *Folh1* gene in mice could somehow impair the kidney function and would thus point out to the possible role of GCPII in this tissue. To investigate this assumption, we performed histopathological examination of the kidney and metabolomic analysis of mouse urine samples.

Neither kidneys of young GCPII-deficient mice nor kidneys of aged GCPII-deficient mice displayed any histological abnormalities (see Figure 33, p. 99). Moreover, from 193 tested metabolites present in mouse urine, only 3 metabolites discriminated between *Folh1*^{+/+} and *Folh1*^{-/-} mice (see Figure 32, p. 98). This would suggest that the function of GCPII in the kidney is not crucial. Such conclusion would be particularly profitable for small-ligand based targeting of anti-cancer drug since the GCPII inhibition in the kidney would probably not cause much harm. A nephrotoxicity caused by kidney intake of anti-cancer drug could be then avoided by serial co-medication of one of the potent GCPII inhibitor such as PMPA (Kratochwil *et al.* 2015).

From the three metabolites that were shown to significantly discriminate *Folh1*^{+/+} and *Folh1*^{-/-} mice, NAAG is particularly interesting. It has been shown that NAAG level in the brains of GCPII-deficient mice does not significantly differ from that of GCPII WT mice (Bacich *et al.* 2002). Therefore, it seems that GCPII-deficient mice control the amount of NAAG by its increased excretion. Even though the portion of metabolites discriminating the genotypes was low, it cannot be excluded that GCPII disruption does not lead to metabolic changes. Number of metabolites, such as polyglutamylated folates or different types of lipophilic molecules, was not included in the screen at all. In addition, the two other metabolites discriminating *Folh1*^{+/+} and *Folh1*^{-/-} mice – inosine and succinyladenosine – have not been yet studied in terms of why their levels are sensitive to the presence of GCPII. Further investigation is thus needed before coming to a conclusion of the necessity of GCPII in the kidney.

It remains unclear, why none of the generated GCPII-deficient mice shows any pronounced phenotype. It is possible that the lack of the strong phenotype is connected with inappropriate experimental settings. Indeed, in case GCPII-deficient mice need to be first challenged before the phenotype would be obvious, the standard housing conditions would not reveal it. In addition, as already suggested by others (Bacich *et al.* 2002), other proteins, such as GCPIII, could at least partially compensate the GCPII action. As a follow-up of this dissertation project, it would be thus interesting to attempt preparation of mice that would be not only GCPII-deficient, but also GCPIII-deficient.

6. CONCLUSIONS

1. TALENs were utilized to disrupt *Folh1* gene in mice within a sequence encoding active site of GCPII.
2. All 65 transgenic mice of F0 generation were analysed for TALEN-mediated mutations. Three founder mice carrying altogether two frame-shift deletions (*Folh1-del4* and *Folh1-del17*) and three small in-frame deletions (*Folh1-del3*, *Folh1-del6* and *Folh1-del12*) within the active site of GCPII were used to establish GCPII-mutant mouse colonies.
3. For facile monitoring of mouse breeding, reliable genotyping protocol based on nested PCR was developed.
4. Recombinant mouse and human GCPII were compared in terms of their kinetic properties for NAAG-hydrolysing reaction. The catalytic efficiency of rm-GCPII was more than 3 times lower than that of rh-GCPII, the difference mainly resulted from distinct K_M values.
5. Mutant variants of full-length mGCPII, which could be potentially expressed in GCPII-mutant mice as a result of gene manipulation, were prepared using transient transfection of mammalian cells. It was confirmed that none of the mutant variants possesses NAAG-hydrolysing activity.
6. Recombinant extracellular parts of all GCPII mutant variants were expressed and variants rm-GCPIIdel3, rm-GCPIIdel6 and rm-GCPIIdel12 were purified. The characterization of their physical properties revealed that none of the variants is capable of folding into the natural dimeric form.
7. GCPII-mutant mice were characterize in terms of the expression of the potential GCPII mutant variants using Western blotting. Since none of the variants was detected in the brains or kidneys of GCPII-mutant mice, these mice may be

considered as GCPII-deficient mice. NAAG-hydrolysing activity in the brain and kidney lysates from GCPII-deficient mice was almost completely abolished.

8. GCPII-deficient mice were viable, bred normally and did not show any obvious phenotype.
9. Closer examination of urogenital system revealed increased propensity to seminal vesicle enlargement in aged GCPII-deficient mice as compared with their WT counterparts. The source of this phenotype is to be determined since in WT mouse urogenital system, GCPII seems to be present in substantial levels only in the epididymis and kidney. Nevertheless, this finding is relevant to human physiology since GCPII was also detected in the human epididymis.
10. No pronounced phenotype was seen in the kidneys of aged GCPII-deficient mice as investigated by histopathology and metabolomic analysis of urine. This observation could be beneficial in cancer treatment using drugs conjugated to small ligand targeting GCPII in tumours. Since the inhibition of GCPII in the kidney would probably not cause much harm, patients could obtain GCPII inhibitor as a co-medication to avoid nephrotoxicity caused by anti-cancer drug.

7. LIST OF PUBLICATIONS

Publications related to dissertation project

a) Research articles

1. **Vorlová B.**, Sedlák F., Kašpárek P., Šrámková K., Malý M., Zámečník J., Šácha P., Konvalinka J.: A novel PSMA/GCPII-deficient mouse model shows enlarged seminal vesicles upon aging. *Prostate*, 2018; In press, doi: 10.1002/pros.23717. **IF=3.347**
2. Knedlík T., **Vorlová B.**, Navrátil V., Tykvart J., Sedlák F., Vaculín Š., Franěk M., Šácha P., Konvalinka J.: Mouse glutamate carboxypeptidase II (GCPII) has a similar enzyme activity and inhibition profile but a different tissue distribution to human GCPII. *FEBS Open Bio*, 2017; 7(9): 1362-78. **IF=1.782**

b) Review articles

Vorlová B., Knedlík T., Tykvart J., Konvalinka J.: GCPII and its close homolog GCPIII: from a neuropeptidase to a cancer marker and beyond. Invited review to *Front Biosci (Landmark Ed)*, 2018; Submitted. **IF=2.349**

c) Meeting abstracts

1. **Vorlová B.**, Kašpárek P., Šácha P., Sedláček R., Konvalinka J.: Generation and basic characterization of glutamate carboxypeptidase II knock-out mice. *Transgenic Res*, 2016; 25(2): 267
2. **Vorlová B.**, Kašpárek P., Šácha P., Sedláček R., Konvalinka J.: Revealing novel functions of glutamate carboxypeptidase II using knock-out mice. *FEBS J*, 2017; 284: 358
3. **Vorlová B.**, Sedlák F., Kašpárek P., Sedláček R., Šácha P., Konvalinka J.: Revealing novel functions of glutamate carboxypeptidase ii, a diagnostic and therapeutic target in neuropathologies and prostate cancer. *Mol Biol Cell*, 2017; 28

Other publications

1. **Vorlová B.**, Nachtigallová D., Jirásková-Vaničková J., Ajani H., Jansa P., Rezáč J., Fanfrlík J., Otyepka M., Hobza P., Konvalinka J., Lepšík M.: Malonate-based inhibitors of mammalian serine racemase: kinetic characterization and structure-based computational study. *Eur J Med Chem*, 2015; 89:189-97. **IF=4.816**
2. Jirásková-Vaničková J., Ettrich R., **Vorlová B.**, Hoffman H.E., Lepšík M., Jansa P., Konvalinka J.: Inhibition of human serine racemase, an emerging target for medicinal chemistry. *Current Drug Targets*, 2011; 12(7): 1037-55. **IF=3.112**

8. REFERENCES

- Abdel-Hadi, M., Ismail, Y., and Younis, L. (2014). 'Prostate-specific membrane antigen (PSMA) immunoexpression in the neovasculature of colorectal carcinoma in Egyptian patients', *Pathol Res Pract*, **210**(11): 759-63.
- Adhyam, M., and Gupta, A. K. (2012). 'A Review on the Clinical Utility of PSA in Cancer Prostate', *Indian J Surg Oncol*, **3**(2): 120-9.
- Afman, L. A., Trijbels, F. J. M., and Blom, H. J. (2003). 'The H475Y polymorphism in the glutamate carboxypeptidase II gene increases plasma folate without affecting the risk for neural tube defects in humans', *Journal of Nutrition*, **133**(1): 75-77.
- Anastassiadis, K., Schnutgen, F., von Melchner, H., and Stewart, A. F. (2013). 'Gene targeting and site-specific recombination in mouse ES cells', *Methods Enzymol*, **533**:133-55.
- Baccala, A., Sercia, L., Li, J., Heston, W., and Zhou, M. (2007). 'Expression of prostate-specific membrane antigen in tumor-associated neovasculature of renal neoplasms', *Urology*, **70**(2): 385-90.
- Bacich, D. J., Pinto, J. T., Tong, W. P., and Heston, W. D. (2001). 'Cloning, expression, genomic localization, and enzymatic activities of the mouse homolog of prostate-specific membrane antigen/NAALADase/folate hydrolase', *Mamm Genome*, **12**(2): 117-23.
- Bacich, D. J., Ramadan, E., O'Keefe, D. S., Bukhari, N., Wegorzewska, I., Ojeifo, O., Olszewski, R., Wrenn, C. C., Bzdega, T., Wroblewska, B., Heston, W. D. W., and Neale, J. H. (2002). 'Deletion of the glutamate carboxypeptidase II gene in mice reveals a second enzyme activity that hydrolyzes N-acetylaspartylglutamate', *Journal of Neurochemistry*, **83**(1): 20-29.
- Bacich, D. J., Wozniak, K. M., Lu, X. C. M., O'Keefe, D. S., Callizot, N., Heston, W. D. W., and Slusher, B. S. (2005). 'Mice lacking glutamate carboxypeptidase II are protected from peripheral neuropathy and ischemic brain injury', *Journal of Neurochemistry*, **95**(2): 314-23.
- Balinska, M., Nimec, Z., and Galivan, J. (1982). 'Characteristics of methotrexate polyglutamate formation in cultured hepatic cells', *Arch Biochem Biophys*, **216**(2): 466-76.
- Bander, N. H., Trabulsi, E. J., Kostakoglu, L., Yao, D., Vallabhajosula, S., Smith-Jones, P., Joyce, M. A., Milowsky, M., Nanus, D. M., and Goldsmith, S. J. (2003). 'Targeting metastatic prostate cancer with radiolabeled monoclonal antibody J591 to the extracellular domain of prostate specific membrane antigen', *J Urol*, **170**(5): 1717-21.
- Bander, N. H., Milowsky, M. I., Nanus, D. M., Kostakoglu, L., Vallabhajosula, S., and Goldsmith, S. J. (2005). 'Phase I trial of 177lutetium-labeled J591, a monoclonal antibody to prostate-specific membrane antigen, in patients with androgen-independent prostate cancer', *Journal of Clinical Oncology*, **23**(21): 4591-601.

- Barinka, C., Rinnova, M., Sacha, P., Rojas, C., Majer, P., Slusher, B. S., and Konvalinka, J. (2002). 'Substrate specificity, inhibition and enzymological analysis of recombinant human glutamate carboxypeptidase II', *J Neurochem*, **80**(3): 477-87.
- Barinka, C., Mlcochova, P., Sacha, P., Hilgert, I., Majer, P., Slusher, B. S., Horejsi, V., and Konvalinka, J. (2004a). 'Amino acids at the N- and C-termini of human glutamate carboxypeptidase II are required for enzymatic activity and proper folding', *European Journal of Biochemistry*, **271**(13): 2782-90.
- Barinka, C., Sacha, P., Sklenar, J., Man, P., Bezouska, K., Slusher, B. S., and Konvalinka, J. (2004b). 'Identification of the N-glycosylation sites on glutamate carboxypeptidase II necessary for proteolytic activity', *Protein Sci*, **13**(6): 1627-35.
- Barinka, C., Rovenska, M., Mlcochova, P., Hlouchova, K., Plechanovova, A., Majer, P., Tsukamoto, T., Slusher, B. S., Konvalinka, J., and Lubkowski, J. (2007). 'Structural insight into the pharmacophore pocket of human glutamate carboxypeptidase II', *Journal of Medicinal Chemistry*, **50**(14): 3267-73.
- Barinka, C., Hlouchova, K., Rovenska, M., Majer, P., Dauter, M., Hin, N., Ko, Y. S., Tsukamoto, T., Slusher, B. S., Konvalinka, J., and Lubkowski, J. (2008). 'Structural basis of interactions between human glutamate carboxypeptidase II and its substrate analogs', *Journal of Molecular Biology*, **376**(5): 1438-50.
- Barinka, C., Rojas, C., Slusher, B., and Pomper, M. (2012). 'Glutamate Carboxypeptidase II in Diagnosis and Treatment of Neurologic Disorders and Prostate Cancer', *Current Medicinal Chemistry*, **19**(6): 856-70.
- Baum, R. P., Kulkarni, H. R., Schuchardt, C., Singh, A., Wirtz, M., Wiessalla, S., Schottelius, M., Mueller, D., Klette, I., and Wester, H. J. (2016). '177Lu-Labeled Prostate-Specific Membrane Antigen Radioligand Therapy of Metastatic Castration-Resistant Prostate Cancer: Safety and Efficacy', *J Nucl Med*, **57**(7): 1006-13.
- Baum, V., Buhler, P., Gierschner, D., Herchenbach, D., Fiala, G. J., Schamel, W. W., Wolf, P., and Elsasser-Beile, U. (2013). 'Antitumor activities of PSMAxCD3 diabodies by redirected T-cell lysis of prostate cancer cells', *Immunotherapy*, **5**(1): 27-38.
- Beckett, M. L., Cazares, L. H., Vlahou, A., Schellhammer, P. F., and Wright, G. L., Jr. (1999). 'Prostate-specific membrane antigen levels in sera from healthy men and patients with benign prostate hyperplasia or prostate cancer', *Clin Cancer Res*, **5**(12): 4034-40.
- Ben-Shachar, S., Yanai, H., Baram, L., Elad, H., Meirovithz, E., Ofer, A., Brazowski, E., Tulchinsky, H., Pasmanik-Chor, M., and Dotan, I. (2013). 'Gene expression profiles of ileal inflammatory bowel disease correlate with disease phenotype and advance understanding of its immunopathogenesis', *Inflamm Bowel Dis*, **19**(12): 2509-21.
- Berger, U. V., Carter, R. E., McKee, M., and Coyle, J. T. (1995). 'N-acetylated alpha-linked acidic dipeptidase is expressed by non-myelinating Schwann cells in the peripheral nervous system', *J Neurocytol*, **24**(2): 99-109.

- Berger, U. V., Luthi-Carter, R., Passani, L. A., Elkabes, S., Black, I., Konradi, C., and Coyle, J. T. (1999). 'Glutamate carboxypeptidase II is expressed by astrocytes in the adult rat nervous system', *Journal of Comparative Neurology*, **415**(1): 52-64.
- Boettcher, M., and McManus, M. T. (2015). 'Choosing the Right Tool for the Job: RNAi, TALEN, or CRISPR', *Mol Cell*, **58**(4): 575-85.
- Bogdanove, A. J., and Voytas, D. F. (2011). 'TAL effectors: customizable proteins for DNA targeting', *Science*, **333**(6051): 1843-6.
- Bostwick, D. G., Pacelli, A., Blute, M., Roche, P., and Murphy, G. P. (1998). 'Prostate specific membrane antigen expression in prostatic intraepithelial neoplasia and adenocarcinoma: a study of 184 cases', *Cancer*, **82**(11): 2256-61.
- Bouabe, H., and Okkenhaug, K. (2013). 'Gene targeting in mice: a review', *Methods Mol Biol*, **1064**:315-36.
- Bradford, M. M. (1976). 'A rapid and sensitive method for the quantitation of microgram quantities of protein utilizing the principle of protein-dye binding', *Anal Biochem*, **72**:48-54.
- Brauer, A., Grubert, L. S., Roll, W., Schrader, A. J., Schafers, M., Bogemann, M., and Rahbar, K. (2017). '177Lu-PSMA-617 radioligand therapy and outcome in patients with metastasized castration-resistant prostate cancer', *Eur J Nucl Med Mol Imaging*, **44**(10): 1663-70.
- Bruno, V., Battaglia, G., Casabona, G., Copani, A., Caciagli, F., and Nicoletti, F. (1998). 'Neuroprotection by glial metabotropic glutamate receptors is mediated by transforming growth factor-beta', *Journal of Neuroscience*, **18**(23): 9594-600.
- Bychkov, A., Vutrapongwatana, U., Tepmongkol, S., and Keelawat, S. (2017). 'PSMA expression by microvasculature of thyroid tumors - Potential implications for PSMA theranostics', *Sci Rep*, **7**(1): 5202.
- Bzdega, T., Crowe, S. L., Ramadan, E. R., Sciarretta, K. H., Olszewski, R. T., Ojeifo, O. A., Rafalski, V. A., Wroblewska, B., and Neale, J. H. (2004). 'The cloning and characterization of a second brain enzyme with NAAG peptidase activity', *Journal of Neurochemistry*, **89**(3): 627-35.
- Cao, K. Y., Mao, X. P., Wang, D. H., Xu, L., Yuan, G. Q., Dai, S. Q., Zheng, B. J., and Qiu, S. P. (2007). 'High expression of PSM-E correlated with tumor grade in prostate cancer: a new alternatively spliced variant of prostate-specific membrane antigen', *Prostate*, **67**(16): 1791-800.
- Cao, Y., Gao, Y., Xu, S., Bao, J., Lin, Y., Luo, X., Wang, Y., Luo, Q., Jiang, J., Neale, J. H., and Zhong, C. (2016). 'Glutamate carboxypeptidase II gene knockout attenuates oxidative stress and cortical apoptosis after traumatic brain injury', *BMC Neurosci*, **17**:15.
- Capecchi, M. R. (2005). 'Gene targeting in mice: functional analysis of the mammalian genome for the twenty-first century', *Nat Rev Genet*, **6**(6): 507-12.

- Caromile, L. A., Dortche, K., Rahman, M. M., Grant, C. L., Stoddard, C., Ferrer, F. A., and Shapiro, L. H. (2017). 'PSMA redirects cell survival signaling from the MAPK to the PI3K-AKT pathways to promote the progression of prostate cancer', *Sci Signal*, **10**(470): eaag3326.
- Carozzi, V. A., Canta, A., Oggioni, N., Ceresa, C., Marmioli, P., Konvalinka, J., Zoia, C., Bossi, M., Ferrarese, C., Tredici, G., and Cavaletti, G. (2008). 'Expression and distribution of 'high affinity' glutamate transporters GLT1, GLAST, EAAC1 and of GCP II in the rat peripheral nervous system', *J Anat*, **213**(5): 539-46.
- Carpenter, K. J., Sen, S., Matthews, E. A., Flatters, S. L., Wozniak, K. M., Slusher, B. S., and Dickenson, A. H. (2003). 'Effects of GCP-II inhibition on responses of dorsal horn neurones after inflammation and neuropathy: an electrophysiological study in the rat', *Neuropeptides*, **37**(5): 298-306.
- Carter, R. E., Feldman, A. R., and Coyle, J. T. (1996). 'Prostate-specific membrane antigen is a hydrolase with substrate and pharmacologic characteristics of a neuropeptidase', *Proceedings of the National Academy of Sciences of the United States of America*, **93**(2): 749-53.
- Cermak, T., Doyle, E. L., Christian, M., Wang, L., Zhang, Y., Schmidt, C., Baller, J. A., Somia, N. V., Bogdanove, A. J., and Voytas, D. F. (2011). 'Efficient design and assembly of custom TALEN and other TAL effector-based constructs for DNA targeting', *Nucleic Acids Res*, **39**(12): e82.
- Chandler, C. J., Wang, T. T. Y., and Halsted, C. H. (1986). 'Pteroylpolyglutamate Hydrolase from Human Jejunal Brush-Borders - Purification and Characterization', *Journal of Biological Chemistry*, **261**(2): 928-33.
- Chang, S. S., O'Keefe, D. S., Bacich, D. J., Reuter, V. E., Heston, W. D. W., and Gaudin, P. B. (1999a). 'Prostate-specific membrane antigen is produced in tumor-associated neovasculature', *Clinical Cancer Research*, **5**(10): 2674-81.
- Chang, S. S., Reuter, V. E., Heston, W. D., Bander, N. H., Grauer, L. S., and Gaudin, P. B. (1999b). 'Five different anti-prostate-specific membrane antigen (PSMA) antibodies confirm PSMA expression in tumor-associated neovasculature', *Cancer Res*, **59**(13): 3192-8.
- Chang, S. S., Reuter, V. E., Heston, W. D., and Gaudin, P. B. (2001). 'Comparison of anti-prostate-specific membrane antigen antibodies and other immunomarkers in metastatic prostate carcinoma', *Urology*, **57**(6): 1179-83.
- Chaux, A., Eifler, J., Karram, S., Al-Hussain, T., Faraj, S., Pomper, M., Rodriguez, R., and Netto, G. J. (2013). 'Focal positive prostate-specific membrane antigen (PSMA) expression in ganglionic tissues associated with prostate neurovascular bundle: implications for novel intraoperative PSMA-based fluorescent imaging techniques', *Urol Oncol*, **31**(5): 572-5.
- Chen, J., Kyte, C., Valcin, M., Chan, W., Wetmur, J. G., Selhub, J., Hunter, D. J., and Ma, J. (2004). 'Polymorphisms in the one-carbon metabolic pathway, plasma folate levels and colorectal cancer in a prospective study', *Int J Cancer*, **110**(4): 617-20.

- Collard, F., Vertommen, D., Constantinescu, S., Buts, L., and Van Schaftingen, E. (2011). 'Molecular Identification of beta-Citrylglutamate Hydrolase as Glutamate Carboxypeptidase 3', *Journal of Biological Chemistry*, **286**(44): 38220-30.
- Crowley, M. J., Scognamiglio, T., Liu, Y. F., Kleiman, D. A., Beninato, T., Aronova, A., Liu, H., Jhanwar, Y. S., Molina, A., Tagawa, S. T., Bander, N. H., Zarnegar, R., Elemento, O., and Fahey, T. J., 3rd. (2016). 'Prostate-Specific Membrane Antigen Is a Potential Antiangiogenic Target in Adrenocortical Carcinoma', *J Clin Endocrinol Metab*, **101**(3): 981-7.
- Cummings, D., Dowling, K. F., Silverstein, N. J., Tanner, A. S., Eryilmaz, H., Smoller, J. W., and Roffman, J. L. (2017). 'A Cross-Sectional Study of Dietary and Genetic Predictors of Blood Folate Levels in Healthy Young Adults', *Nutrients*, **9**(9).
- Cunha, A. C., Weigle, B., Kiessling, A., Bachmann, M., and Rieber, E. P. (2006). 'Tissue-specificity of prostate specific antigens: Comparative analysis of transcript levels in prostate and non-prostatic tissues', *Cancer Letters*, **236**(2): 229-38.
- Damaraju, V. L., Cass, C. E., and Sawyer, M. B. (2008). 'Renal conservation of folates role of folate transport proteins', *Vitam Horm*, **79**185-202.
- Date, A. A., Rais, R., Babu, T., Ortiz, J., Kanvinde, P., Thomas, A. G., Zimmermann, S. C., Gadiano, A. J., Halpert, G., Slusher, B. S., and Ensign, L. M. (2017). 'Local enema treatment to inhibit FOLH1/GCPII as a novel therapy for inflammatory bowel disease', *J Control Release*.
- Davis, M. I., Bennett, M. J., Thomas, L. M., and Bjorkman, P. J. (2005). 'Crystal structure of prostate-specific membrane antigen, a tumor marker and peptidase', *Proceedings of the National Academy of Sciences of the United States of America*, **102**(17): 5981-86.
- Deb, N., Goris, M., Trisler, K., Fowler, S., Saal, J., Ning, S., Becker, M., Marquez, C., and Knox, S. (1996). 'Treatment of hormone-refractory prostate cancer with 90Y-CYT-356 monoclonal antibody', *Clin Cancer Res*, **2**(8): 1289-97.
- DeLano, W. L. (2004). 'Use of PYMOL as a communications tool for molecular science.', *Abstracts of Papers of the American Chemical Society*, **228**U313-U14.
- Devlin, A. M., Ling, E. H., Peerson, J. M., Fernando, S., Clarke, R., Smith, A. D., and Halsted, C. H. (2000). 'Glutamate carboxypeptidase II: a polymorphism associated with lower levels of serum folate and hyperhomocysteinemia', *Human Molecular Genetics*, **9**(19): 2837-44.
- Devlin, A. M., Clarke, R., Birks, J., Evans, J. G., and Halsted, C. H. (2006). 'Interactions among polymorphisms in folate-metabolizing genes and serum total homocysteine concentrations in a healthy elderly population', *Am J Clin Nutr*, **83**(3): 708-13.
- DeVos, L., Chanson, A., Liu, Z. H., Ciappio, E. D., Parnell, L. D., Mason, J. B., Tucker, K. L., and Crott, J. W. (2008). 'Associations between single nucleotide polymorphisms in folate uptake and metabolizing genes with blood folate, homocysteine, and DNA uracil concentrations', *American Journal of Clinical Nutrition*, **88**(4): 1149-58.

- Doble, A. (1999). 'The role of excitotoxicity in neurodegenerative disease: implications for therapy', *Pharmacol Ther*, **81**(3): 163-221.
- Dumas, F., Gala, J. L., Berteau, P., Brasseur, F., Eschwege, P., Paradis, V., Lacour, B., Philippe, M., and Loric, S. (1999). 'Molecular expression of PSMA mRNA and protein in primary renal tumors', *Int J Cancer*, **80**(6): 799-803.
- Dyck, M. K., Gagne, D., Ouellet, M., Senechal, J. F., Belanger, E., Lacroix, D., Sirard, M. A., and Pothier, F. (1999). 'Seminal vesicle production and secretion of growth hormone into seminal fluid', *Nat Biotechnol*, **17**(11): 1087-90.
- Eklof, V., Van Guelpen, B., Hultdin, J., Johansson, I., Hallmans, G., and Palmqvist, R. (2008). 'The reduced folate carrier (RFC1) 80G > A and folate hydrolase 1 (FOLH1) 1561C > T polymorphisms and the risk of colorectal cancer: a nested case-referent study', *Scand J Clin Lab Invest*, **68**(5): 393-401.
- Evans, J. C., Malhotra, M., Cryan, J. F., and O'Driscoll, C. M. (2016). 'The therapeutic and diagnostic potential of the prostate specific membrane antigen/glutamate carboxypeptidase II (PSMA/GCPII) in cancer and neurological disease', *Br J Pharmacol*, **173**(21): 3041-79.
- Feng, J. F., Gurkoff, G. G., Van, K. C., Song, M., Lowe, D. A., Zhou, J., and Lyeth, B. G. (2012). 'NAAG peptidase inhibitor reduces cellular damage in a model of TBI with secondary hypoxia', *Brain Research*, **1469**: 144-52.
- Finch, C. E., and Girgis, F. G. (1974). 'Enlarged seminal vesicles of senescent C57BL-6J mice', *J Gerontol*, **29**(2): 134-8.
- Fisch, H., Lambert, S. M., and Goluboff, E. T. (2006). 'Management of ejaculatory duct obstruction: etiology, diagnosis, and treatment', *World J Urol*, **24**(6): 604-10.
- Gaj, T., Gersbach, C. A., and Barbas, C. F., 3rd. (2013). 'ZFN, TALEN, and CRISPR/Cas-based methods for genome engineering', *Trends Biotechnol*, **31**(7): 397-405.
- Gala, J. L., Loric, S., Guiot, Y., Denmeade, S. R., Gady, A., Brasseur, F., Heusterspreute, M., Eschwege, P., De Nayer, P., Van Cangh, P., and Tombal, B. (2000). 'Expression of prostate-specific membrane antigen in transitional cell carcinoma of the bladder: prognostic value?', *Clin Cancer Res*, **6**(10): 4049-54.
- Gao, Y., Xu, S., Cui, Z., Zhang, M., Lin, Y., Cai, L., Wang, Z., Luo, X., Zheng, Y., Wang, Y., Luo, Q., Jiang, J., Neale, J. H., and Zhong, C. (2015). 'Mice lacking glutamate carboxypeptidase II develop normally, but are less susceptible to traumatic brain injury', *J Neurochem*, **134**(2): 340-53.
- Ghadge, G. D., Slusher, B. S., Bodner, A., Canto, M. D., Wozniak, K., Thomas, A. G., Rojas, C., Tsukamoto, T., Majer, P., Miller, R. J., Monti, A. L., and Roos, R. P. (2003). 'Glutamate carboxypeptidase II inhibition protects motor neurons from death in familial amyotrophic lateral sclerosis models', *Proc Natl Acad Sci U S A*, **100**(16): 9554-9.

Ghosh, A., and Heston, W. D. (2003). 'Effect of carbohydrate moieties on the folate hydrolysis activity of the prostate specific membrane antigen', *Prostate*, **57**(2): 140-51.

Ghosh, A., Wang, X., Klein, E., and Heston, W. D. (2005). 'Novel role of prostate-specific membrane antigen in suppressing prostate cancer invasiveness', *Cancer Res*, **65**(3): 727-31.

Gros-Louis, F., Kriz, J., Kabashi, E., McDearmid, J., Millicamps, S., Urushitani, M., Lin, L., Dion, P., Zhu, Q., Drapeau, P., Julien, J. P., and Rouleau, G. A. (2008). 'Als2 mRNA splicing variants detected in KO mice rescue severe motor dysfunction phenotype in Als2 knock-down zebrafish', *Hum Mol Genet*, **17**(17): 2691-702.

Guo, J., Xie, H., Wang, J., Zhao, H., Wang, F., Liu, C., Wang, L., Lu, X., Bao, Y., Zou, J., Wang, G., Niu, B., and Zhang, T. (2013). 'The maternal folate hydrolase gene polymorphism is associated with neural tube defects in a high-risk Chinese population', *Genes Nutr*, **8**(2): 191-7.

Ha, D., Bing, S. J., Ahn, G., Kim, J., Cho, J., Kim, A., Herath, K. H., Yu, H. S., Jo, S. A., Cho, I. H., and Jee, Y. (2016). 'Blocking glutamate carboxypeptidase II inhibits glutamate excitotoxicity and regulates immune responses in experimental autoimmune encephalomyelitis', *FEBS J*, **283**(18): 3438-56.

Haffner, M. C., Kronberger, I. E., Ross, J. S., Sheehan, C. E., Zitt, M., Muhlmann, G., Ofner, D., Zelger, B., Ensinger, C., Yang, X. J., Geley, S., Margreiter, R., and Bander, N. H. (2009). 'Prostate-specific membrane antigen expression in the neovasculature of gastric and colorectal cancers', *Hum Pathol*, **40**(12): 1754-61.

Halsted, C. H. (1991). 'Jejunal brush-border folate hydrolase. A novel enzyme', *West J Med*, **155**(6): 605-9.

Halsted, C. H., Ling, E. H., Luthi-Carter, R., Villanueva, J. A., Gardner, J. M., and Coyle, J. T. (1998). 'Folypoly-gamma-glutamate carboxypeptidase from pig jejunum - Molecular characterization and relation to glutamate carboxypeptidase II', *Journal of Biological Chemistry*, **273**(32): 20417-24.

Halsted, C. H., Wong, D. H., Peerson, J. M., Warden, C. H., Refsum, H., Smith, A. D., Nygard, O. K., Ueland, P. M., Vollset, S. E., and Tell, G. S. (2007). 'Relations of glutamate carboxypeptidase II (GCPII) polymorphisms to folate and homocysteine concentrations and to scores of cognition, anxiety, and depression in a homogeneous Norwegian population: the Hordaland Homocysteine Study', *Am J Clin Nutr*, **86**(2): 514-21.

Halsted, C.H. , Medici, V., and Esfandiari, F. (2010). 'Influence of Alcohol on Folate Status and Methionine Metabolism in Relation to Alcoholic Liver Disease.' in L. B. Bailey (ed.) *Folate in health and disease*. Taylor & Francis Group: Boca Raton, US (p. 429-48).

Hamada-Kanazawa, M., Kouda, M., Odani, A., Matsuyama, K., Kanazawa, K., Hasegawa, T., Narahara, M., and Miyake, M. (2010). 'beta-Citryl-L-glutamate Is an Endogenous Iron Chelator That Occurs Naturally in the Developing Brain', *Biological & Pharmaceutical Bulletin*, **33**(5): 729-37.

- Hamada-Kanazawa, M., Narahara, M., Takano, M., Min, K. S., Tanaka, K., and Miyake, M. (2011). 'beta-Citryl-L-glutamate Acts as an Iron Carrier to Activate Aconitase Activity', *Biological & Pharmaceutical Bulletin*, **34**(9): 1455-64.
- Han, L., Picker, J. D., Schaevitz, L. R., Tsai, G., Feng, J., Jiang, Z., Chu, H. C., Basu, A. C., Berger-Sweeney, J., and Coyle, J. T. (2009). 'Phenotypic characterization of mice heterozygous for a null mutation of glutamate carboxypeptidase II', *Synapse*, **63**(8): 625-35.
- Haseman, M. K., Reed, N. L., and Rosenthal, S. A. (1996). 'Monoclonal antibody imaging of occult prostate cancer in patients with elevated prostate-specific antigen. Positron emission tomography and biopsy correlation', *Clin Nucl Med*, **21**(9): 704-13.
- Heitkotter, B., Trautmann, M., Grunewald, I., Bogemann, M., Rahbar, K., Gevensleben, H., Wardelmann, E., Hartmann, W., Steinestel, K., and Huss, S. (2017). 'Expression of PSMA in tumor neovasculature of high grade sarcomas including synovial sarcoma, rhabdomyosarcoma, undifferentiated sarcoma and MPNST', *Oncotarget*, **8**(3): 4268-76.
- Heitkotter, B., Steinestel, K., Trautmann, M., Grunewald, I., Barth, P., Gevensleben, H., Bogemann, M., Wardelmann, E., Hartmann, W., Rahbar, K., and Huss, S. (2018). 'Neovascular PSMA expression is a common feature in malignant neoplasms of the thyroid', *Oncotarget*, **9**(11): 9867-74.
- Hlouchova, K., Barinka, C., Klusak, V., Sacha, P., Mlcochova, P., Majer, P., Rulisek, L., and Konvalinka, J. (2007). 'Biochemical characterization of human glutamate carboxypeptidase III', *Journal of Neurochemistry*, **101**(3): 682-96.
- Hlouchova, K., Barinka, C., Konvalinka, J., and Lubkowski, J. (2009). 'Structural insight into the evolutionary and pharmacologic homology of glutamate carboxypeptidases II and III', *Febs Journal*, **276**(16): 4448-62.
- Hlouchova, K., Barinka, C., and Konvalinka, J. (2012a). 'Glutamate carboxypeptidase II as a therapeutic target.' in B. M. Dunn (ed.) *Proteinases as Drug Targets*. Royal Society of Chemistry Publishing: Cambridge, UK (p. 63–95).
- Hlouchova, K., Navratil, V., Tykvar, J., Sacha, P., and Konvalinka, J. (2012b). 'GCPII Variants, Paralogs and Orthologs', *Current Medicinal Chemistry*, **19**(9): 1316-22.
- Horoszewicz, J. S., Kawinski, E., and Murphy, G. P. (1987). 'Monoclonal antibodies to a new antigenic marker in epithelial prostatic cells and serum of prostatic cancer patients', *Anticancer Res*, **7**(5B): 927-35.
- Israeli, R. S., Powell, C. T., Fair, W. R., and Heston, W. D. (1993). 'Molecular cloning of a complementary DNA encoding a prostate-specific membrane antigen', *Cancer Res*, **53**(2): 227-30.
- Israeli, R. S., Powell, C. T., Corr, J. G., Fair, W. R., and Heston, W. D. W. (1994). 'Expression of the Prostate-Specific Membrane Antigen', *Cancer Research*, **54**(7): 1807-11.

- Jinek, M., Chylinski, K., Fonfara, I., Hauer, M., Doudna, J. A., and Charpentier, E. (2012). 'A programmable dual-RNA-guided DNA endonuclease in adaptive bacterial immunity', *Science*, **337**(6096): 816-21.
- Joung, J. K., and Sander, J. D. (2013). 'TALENs: a widely applicable technology for targeted genome editing', *Nat Rev Mol Cell Biol*, **14**(1): 49-55.
- Joyner, A. L., Skarnes, W. C., and Rossant, J. (1989). 'Production of a mutation in mouse En-2 gene by homologous recombination in embryonic stem cells', *Nature*, **338**(6211): 153-6.
- Junghans, R. P., Ma, Q., Rathore, R., Gomes, E. M., Bais, A. J., Lo, A. S., Abedi, M., Davies, R. A., Cabral, H. J., Al-Homsi, A. S., and Cohen, S. I. (2016). 'Phase I Trial of Anti-PSMA Designer CAR-T Cells in Prostate Cancer: Possible Role for Interacting Interleukin 2-T Cell Pharmacodynamics as a Determinant of Clinical Response', *Prostate*, **76**(14): 1257-70.
- Kahn, D., Williams, R. D., Seldin, D. W., Libertino, J. A., Hirschhorn, M., Dreicer, R., Weiner, G. J., Bushnell, D., and Gulfo, J. (1994). 'Radioimmunoscinigraphy with 111indium labeled CYT-356 for the detection of occult prostate cancer recurrence', *J Urol*, **152**(5 Pt 1): 1490-5.
- Kahn, D., Austin, J. C., Maguire, R. T., Miller, S. J., Gerstbrein, J., and Williams, R. D. (1999). 'A phase II study of [90Y] yttrium-capromab pendetide in the treatment of men with prostate cancer recurrence following radical prostatectomy', *Cancer Biother Radiopharm*, **14**(2): 99-111.
- Karlikova, R., Micova, K., Najdekr, L., Gardlo, A., Adam, T., Majerova, P., Friedecky, D., and Kovac, A. (2017). 'Metabolic status of CSF distinguishes rats with tauopathy from controls', *Alzheimers Res Ther*, **9**(1): 78.
- Kasoha, M., Unger, C., Solomayer, E. F., Bohle, R. M., Zaharia, C., Khreich, F., Wagenpfeil, S., and Juhasz-Boss, I. (2017). 'Prostate-specific membrane antigen (PSMA) expression in breast cancer and its metastases', *Clin Exp Metastasis*, **34**(8): 479-90.
- Khacho, P., Wang, B., and Bergeron, R. (2016). 'The Good and Bad Sides of NAAG', *Adv Pharmacol*, **76**311-49.
- Kinoshita, Y., Kuratsukuri, K., Landas, S., Imaida, K., Rovito, P. M., Wang, C. Y., and Haas, G. P. (2006). 'Expression of prostate-specific membrane antigen in normal and malignant human tissues', *World Journal of Surgery*, **30**(4): 628-36.
- Klein Nulent, T. J. W., van Es, R. J. J., Krijger, G. C., de Bree, R., Willems, S. M., and de Keizer, B. (2017). 'Prostate-specific membrane antigen PET imaging and immunohistochemistry in adenoid cystic carcinoma-a preliminary analysis', *Eur J Nucl Med Mol Imaging*, **44**(10): 1614-21.
- Klusak, V., Barinka, C., Plechanovova, A., Mlcochova, P., Konvalinka, J., Rulisek, L., and Lubkowski, J. (2009). 'Reaction mechanism of glutamate carboxypeptidase II revealed by mutagenesis, X-ray crystallography, and computational methods', *Biochemistry*, **48**(19): 4126-38.

Knedlik, T. (2008). 'Myší glutamátcarboxypeptidasa II: klonování, exprese a aktivita', Bachelor Thesis, Department of Biochemistry, Faculty of Science, Charles University in Prague.

Knedlik, T. (2010). 'Klonování, exprese a biochemická charakterizace myší glutamátcarboxypeptidasy II', Diploma Thesis, Department of Biochemistry, Faculty of Science, Charles University in Prague.

Knedlik, T., Navratil, V., Vik, V., Pacik, D., Sacha, P., and Konvalinka, J. (2014). 'Detection and quantitation of glutamate carboxypeptidase II in human blood', *Prostate*, **74**(7): 768-80.

Knedlik, T. (2017). 'Glutamate Carboxypeptidase II as a Drug Target and a Molecular Address for Cancer Treatment', Dissertation Thesis, Department of Biochemistry, Faculty of Science, Charles University in Prague.

Knedlik, T., Vorlova, B., Navratil, V., Tykvar, J., Sedlak, F., Vaculin, S., Franek, M., Sacha, P., and Konvalinka, J. (2017). 'Mouse glutamate carboxypeptidase II (GCPII) has a similar enzyme activity and inhibition profile but a different tissue distribution to human GCPII', *FEBS Open Bio*, **7**(9): 1362-78.

Koscielny, G., Yaikhom, G., Iyer, V., Meehan, T. F., Morgan, H., Atienza-Herrero, J., Blake, A., Chen, C. K., Easty, R., Di Fenza, A., Fiegel, T., Griffiths, M., Horne, A., Karp, N. A., Kurbatova, N., Mason, J. C., Matthews, P., Oakley, D. J., Qazi, A., Regnart, J., Retha, A., Santos, L. A., Sneddon, D. J., Warren, J., Westerberg, H., Wilson, R. J., Melvin, D. G., Smedley, D., Brown, S. D., Flicek, P., Skarnes, W. C., Mallon, A. M., and Parkinson, H. (2014). 'The International Mouse Phenotyping Consortium Web Portal, a unified point of access for knockout mice and related phenotyping data', *Nucleic Acids Res*, **42**(Release 7.0): D802-9.

Kraemer, N., Issa-Jahns, L., Neubert, G., Ravindran, E., Mani, S., Ninnemann, O., and Kaindl, A. M. (2015). 'Novel Alternative Splice Variants of Mouse Cdk5rap2', *PLoS One*, **10**(8): e0136684.

Kratochwil, C., Giesel, F. L., Leotta, K., Eder, M., Hoppe-Tich, T., Youssoufian, H., Kopka, K., Babich, J. W., and Haberkorn, U. (2015). 'PMPA for nephroprotection in PSMA-targeted radionuclide therapy of prostate cancer', *J Nucl Med*, **56**(2): 293-8.

Kratochwil, C., Giesel, F. L., Stefanova, M., Benesova, M., Bronzel, M., Afshar-Oromieh, A., Mier, W., Eder, M., Kopka, K., and Haberkorn, U. (2016). 'PSMA-Targeted Radionuclide Therapy of Metastatic Castration-Resistant Prostate Cancer with ¹⁷⁷Lu-Labeled PSMA-617', *J Nucl Med*, **57**(8): 1170-6.

Lambert, L. A., and Mitchell, S. L. (2007). 'Molecular evolution of the transferrin receptor/glutamate carboxypeptidase II family', *J Mol Evol*, **64**(1): 113-28.

Lane, Z., Hansel, D. E., and Epstein, J. I. (2008). 'Immunohistochemical expression of prostatic antigens in adenocarcinoma and villous adenoma of the urinary bladder', *Am J Surg Pathol*, **32**(9): 1322-6.

Lawrence, C. M., Ray, S., Babyonyshev, M., Galluser, R., Borhani, D. W., and Harrison, S. C. (1999). 'Crystal structure of the ectodomain of human transferrin receptor', *Science*, **286**(5440): 779-82.

Leatherbarrow, R.J. 2001. *GraFit Version 5* (Erithacus Software Ltd.: Horley, U.K.).

Ledermann, B., and Burki, K. (1991). 'Establishment of a germ-line competent C57BL/6 embryonic stem cell line', *Exp Cell Res*, **197**(2): 254-8.

Lievers, K. J. A., Kluijtmans, L. A. J., Boers, G. H. J., Verhoef, P., den Heijer, M., Trijbels, F. J. M., and Blom, H. J. (2002). 'Influence of a glutamate carboxypeptidase II (GCPII) polymorphism (1561C -> T) on plasma homocysteine, folate and vitamin B-12 levels and its relationship to cardiovascular disease risk', *Atherosclerosis*, **164**(2): 269-73.

Limaye, A., Hall, B., and Kulkarni, A. B. (2009). 'Manipulation of mouse embryonic stem cells for knockout mouse production', *Curr Protoc Cell Biol*, **Chapter 19**Unit 19 13 19 13 1-24.

Liu, H., Moy, P., Kim, S., Xia, Y., Rajasekaran, A., Navarro, V., Knudsen, B., and Bander, N. H. (1997). 'Monoclonal antibodies to the extracellular domain of prostate-specific membrane antigen also react with tumor vascular endothelium', *Cancer Res*, **57**(17): 3629-34.

Liu, H., Rajasekaran, A. K., Moy, P., Xia, Y., Kim, S., Navarro, V., Rahmati, R., and Bander, N. H. (1998). 'Constitutive and antibody-induced internalization of prostate-specific membrane antigen', *Cancer Res*, **58**(18): 4055-60.

Lopes, A. D., Davis, W. L., Rosenstraus, M. J., Uveges, A. J., and Gilman, S. C. (1990). 'Immunohistochemical and pharmacokinetic characterization of the site-specific immunoconjugate CYT-356 derived from antiprostata monoclonal antibody 7E11-C5', *Cancer Res*, **50**(19): 6423-9.

Luthi-Carter, R., Barczak, A. K., Speno, H., and Coyle, J. T. (1998a). 'Molecular characterization of human brain N-acetylated alpha-linked acidic dipeptidase (NAALADase)', *J Pharmacol Exp Ther*, **286**(2): 1020-5.

Luthi-Carter, R., Barczak, A. K., Speno, H., and Coyle, J. T. (1998b). 'Hydrolysis of the neuropeptide N-acetylaspartylglutamate (NAAG) by cloned human glutamate carboxypeptidase II', *Brain Res*, **795**(1-2): 341-8.

Luthi-Carter, R., Berger, U. V., Barczak, A. K., Enna, M., and Coyle, J. T. (1998c). 'Isolation and expression of a rat brain cDNA encoding glutamate carboxypeptidase II', *Proc Natl Acad Sci U S A*, **95**(6): 3215-20.

Maraj, B. H., Leek, J. P., Karayi, M., Ali, M., Lench, N. J., and Markham, A. F. (1998). 'Detailed genetic mapping around a putative prostate-specific membrane antigen locus on human chromosome 11p11.2', *Cytogenet Cell Genet*, **81**(1): 3-9.

Matsuda, M., Ishikawa, E., Yamamoto, T., Hatano, K., Joraku, A., Iizumi, Y., Masuda, Y., Nishiyama, H., and Matsumura, A. (2018). 'Potential use of prostate specific

membrane antigen (PSMA) for detecting the tumor neovasculature of brain tumors by PET imaging with (89)Zr-Df-IAB2M anti-PSMA minibody', *J Neurooncol*, **138**(3): 581-89.

McNulty, Helene, and Pentieva, Kristina. (2010). 'Folate Bioavailability.' in L. B. Bailey (ed.) *Folate in health and disease* Taylor & Francis Group: Boca Raton, US (p. 25-48).

Melse-Boonstra, A., Lievers, K. J. A., Blom, H. J., and Verhoef, P. (2004). 'Bioavailability of polyglutamyl folic acid relative to that of monoglutamyl folic acid in subjects with different genotypes of the glutamate carboxypeptidase II gene', *American Journal of Clinical Nutrition*, **80**(3): 700-04.

Meng, F. D., Wang, S., Jiang, Y. H., and Sui, C. G. (2016). 'Antitumor effect of dendritic cells transfected with prostate-specific membrane antigen recombinant adenovirus on prostate cancer: An in vitro study', *Mol Med Rep*, **13**(3): 2124-34.

Mesters, J. R., Barinka, C., Li, W. X., Tsukamoto, T., Majer, P., Slusher, B. S., Konvalinka, J., and Hilgenfeld, R. (2006). 'Structure of glutamate carboxypeptidase II, a drug target in neuronal damage and prostate cancer', *Embo J*, **25**(6): 1375-84.

Mhaweck-Fauceglia, P., Zhang, S., Terracciano, L., Sauter, G., Chadhuri, A., Herrmann, F. R., and Penetrante, R. (2007). 'Prostate-specific membrane antigen (PSMA) protein expression in normal and neoplastic tissues and its sensitivity and specificity in prostate adenocarcinoma: an immunohistochemical study using multiple tumour tissue microarray technique', *Histopathology*, **50**(4): 472-83.

Miller, J. C., Tan, S., Qiao, G., Barlow, K. A., Wang, J., Xia, D. F., Meng, X., Paschon, D. E., Leung, E., Hinkley, S. J., Dulay, G. P., Hua, K. L., Ankoudinova, I., Cost, G. J., Urnov, F. D., Zhang, H. S., Holmes, M. C., Zhang, L., Gregory, P. D., and Rebar, E. J. (2011). 'A TALE nuclease architecture for efficient genome editing', *Nat Biotechnol*, **29**(2): 143-8.

Miller, J. W. (2013). 'Folic Acid.' in B Caballero (ed.) *Encyclopedia of Human Nutrition*. Academic Press: Waltham, MA (p. 262-69).

Milowsky, M. I., Galsky, M. D., Morris, M. J., Crona, D. J., George, D. J., Dreicer, R., Tse, K., Petruck, J., Webb, I. J., Bander, N. H., Nanus, D. M., and Scher, H. I. (2016). 'Phase 1/2 multiple ascending dose trial of the prostate-specific membrane antigen-targeted antibody drug conjugate MLN2704 in metastatic castration-resistant prostate cancer', *Urol Oncol*, **34**(12): 530 e15-30 e21.

Minner, S., Wittmer, C., Graefen, M., Salomon, G., Steuber, T., Haese, A., Huland, H., Bokemeyer, C., Yekebas, E., Dierlamm, J., Balabanov, S., Kilic, E., Wilczak, W., Simon, R., Sauter, G., and Schlomm, T. (2011). 'High level PSMA expression is associated with early PSA recurrence in surgically treated prostate cancer', *Prostate*, **71**(3): 281-8.

Miyake, M., Kakimoto, Y., and Sorimachi, M. (1978). 'Isolation and Identification of Beta-Citryl-L-Glutamic Acid from Newborn Rat-Brain', *Biochimica Et Biophysica Acta*, **544**(3): 656-66.

- Miyake, M., and Kakimoto, Y. (1981). 'Developmental-Changes of N-Acetyl-L-Aspartic Acid, N-Acetyl-Alpha-Aspartylglutamic Acid and Beta-Citryl-L-Glutamic Acid in Different Brain-Regions and Spinal Cords of Rat and Guinea Pig', *Journal of Neurochemistry*, **37**(4): 1064-67.
- Miyake, M., Kume, S., and Kakimoto, Y. (1982). 'Correlation of the level of beta-citryl-L-glutamic acid with spermatogenesis in rat testes', *Biochimica Et Biophysica Acta*, **719**(3): 495-500.
- Moore, M., Panjwani, S., Mathew, R., Crowley, M., Liu, Y. F., Aronova, A., Finnerty, B., Zarnegar, R., Fahey, T. J., 3rd, and Scognamiglio, T. (2017). 'Well-Differentiated Thyroid Cancer Neovasculature Expresses Prostate-Specific Membrane Antigen-a Possible Novel Therapeutic Target', *Endocr Pathol*, **28**(4): 339-44.
- Morin, I., Devlin, A. M., Leclerc, D., Sabbaghian, N., Halsted, C. H., Finnell, R., and Rozen, R. (2003). 'Evaluation of genetic variants in the reduced folate carrier and in glutamate carboxypeptidase II for spina bifida risk', *Molecular Genetics and Metabolism*, **79**(3): 197-200.
- Mountford, P., Zevnik, B., Duwel, A., Nichols, J., Li, M., Dani, C., Robertson, M., Chambers, I., and Smith, A. (1994). 'Dicistronic targeting constructs: reporters and modifiers of mammalian gene expression', *Proc Natl Acad Sci U S A*, **91**(10): 4303-7.
- Narahara, M., Hamada-Kanazawa, M., Kouda, M., Odani, A., and Miyake, M. (2010). 'Superoxide Scavenging and Xanthine Oxidase Inhibiting Activities of Copper S-Citryl-L-glutamate Complex', *Biological & Pharmaceutical Bulletin*, **33**(12): 1938-43.
- Navratil, M., Ptacek, J., Sacha, P., Starkova, J., Lubkowski, J., Barinka, C., and Konvalinka, J. (2014). 'Structural and biochemical characterization of the folyl-poly-gamma-l-glutamate hydrolyzing activity of human glutamate carboxypeptidase II', *FEBS J.*
- Navratil, M., Tykvart, J., Schimer, J., Pachel, P., Navratil, V., Rokob, T. A., Hlouchova, K., Rulisek, L., and Konvalinka, J. (2016). 'Comparison of human glutamate carboxypeptidases II and III reveals their divergent substrate specificities', *FEBS J.*, **283**(13): 2528-45.
- Neale, J. H., Bzdega, T., and Wroblewska, B. (2000). 'N-acetylaspartylglutamate: The most abundant peptide neurotransmitter in the mammalian central nervous system', *Journal of Neurochemistry*, **75**(2): 443-52.
- Neale, J. H., Olszewski, R. T., Zuo, D. Y., Janczura, K. J., Profaci, C. P., Lavin, K. M., Madore, J. C., and Bzdega, T. (2011). 'Advances in understanding the peptide neurotransmitter NAAG and appearance of a new member of the NAAG neuropeptide family', *Journal of Neurochemistry*, **118**(4): 490-98.
- Noble, C. L., Abbas, A. R., Lees, C. W., Cornelius, J., Toy, K., Modrusan, Z., Clark, H. F., Arnott, I. D., Penman, I. D., Satsangi, J., and Diehl, L. (2010). 'Characterization of intestinal gene expression profiles in Crohn's disease by genome-wide microarray analysis', *Inflamm Bowel Dis*, **16**(10): 1717-28.

- Nomura, N., Pastorino, S., Jiang, P., Lambert, G., Crawford, J. R., Gymnopoulos, M., Piccioni, D., Juarez, T., Pingle, S. C., Makale, M., and Kesari, S. (2014). 'Prostate specific membrane antigen (PSMA) expression in primary gliomas and breast cancer brain metastases', *Cancer Cell Int*, **14**(1): 26.
- O'Keefe, D. S., Su, S. L., Bacich, D. J., Horiguchi, Y., Luo, Y., Powell, C. T., Zandvliet, D., Russell, P. J., Molloy, P. L., Nowak, N. J., Shows, T. B., Mullins, C., Vonder Haar, R. A., Fair, W. R., and Heston, W. D. W. (1998). 'Mapping, genomic organization and promoter analysis of the human prostate-specific membrane antigen gene', *Biochimica Et Biophysica Acta-Gene Structure and Expression*, **1443**(1-2): 113-27.
- O'Keefe, D. S., Bacich, D. J., and Heston, W. D. W. (2004). 'Comparative analysis of prostate-specific membrane antigen (PSMA) versus a prostate-specific membrane antigen-like gene', *Prostate*, **58**(2): 200-10.
- O'Keefe, D., Bacich, D., and Heston, W.W. (2001). 'Prostate Specific Membrane Antigen.' in L.K. Chung, W. Isaacs and J. Simons (eds.), *Prostate Cancer: biology, genetics and the new therapeutics*. Humana Press: Totowa, NJ (p. 307-26).
- Oliveira, D. S., Dzinic, S., Bonfil, A. I., Saliganan, A. D., Sheng, S., and Bonfil, R. D. (2016). 'The mouse prostate: a basic anatomical and histological guideline', *Bosn J Basic Med Sci*, **16**(1): 8-13.
- Olson, E. N., Arnold, H. H., Rigby, P. W., and Wold, B. J. (1996). 'Know your neighbors: three phenotypes in null mutants of the myogenic bHLH gene MRF4', *Cell*, **85**(1): 1-4.
- Olszewski, R. T., Bukhari, N., Zhou, J., Kozikowski, A. P., Wroblewski, J. T., Shamimi-Noori, S., Wroblewska, B., Bzdega, T., Vicini, S., Barton, F. B., and Neale, J. H. (2004). 'NAAG peptidase inhibition reduces locomotor activity and some stereotypes in the PCP model of schizophrenia via group II mGluR', *Journal of Neurochemistry*, **89**(4): 876-85.
- Olszewski, R. T., Janczura, K. J., Ball, S. R., Madore, J. C., Lavin, K. M., Lee, J. C. M., Lee, M. J., Der, E. K., Hark, T. J., Farago, P. R., Profaci, C. P., Bzdega, T., and Neale, J. H. (2012). 'NAAG peptidase inhibitors block cognitive deficit induced by MK-801 and motor activation induced by d-amphetamine in animal models of schizophrenia', *Translational Psychiatry*, **2**.
- Pangalos, M. N., Neefs, J. M., Somers, M., Verhasselt, P., Bekkers, M., van der Helm, L., Fraiponts, E., Ashton, D., and Gordon, R. D. (1999). 'Isolation and expression of novel human glutamate carboxypeptidases with N-acetylated alpha-linked acidic dipeptidase and dipeptidyl peptidase IV activity', *Journal of Biological Chemistry*, **274**(13): 8470-83.
- Patanwala, I., King, M. J., Barrett, D. A., Rose, J., Jackson, R., Hudson, M., Philo, M., Dainty, J. R., Wright, A. J., Finglas, P. M., and Jones, D. E. (2014). 'Folic acid handling by the human gut: implications for food fortification and supplementation', *Am J Clin Nutr*, **100**(2): 593-9.
- Patterson, J. T., Isaacson, J., Kerwin, L., Atassi, G., Duggal, R., Bresson, D., Zhu, T., Zhou, H., Fu, Y., and Kaufmann, G. F. (2017). 'PSMA-targeted bispecific Fab conjugates that engage T cells', *Bioorg Med Chem Lett*, **27**(24): 5490-95.

- Pauwels, K., Podevin, N., Breyer, D., Carroll, D., and Herman, P. (2014). 'Engineering nucleases for gene targeting: safety and regulatory considerations', *N Biotechnol*, **31**(1): 18-27.
- Perner, S., Hofer, M. D., Kim, R., Shah, R. B., Li, H., Moller, P., Hautmann, R. E., Gschwend, J. E., Kuefer, R., and Rubin, M. A. (2007). 'Prostate-specific membrane antigen expression as a predictor of prostate cancer progression', *Hum Pathol*, **38**(5): 696-701.
- Pettan-Brewer, C., and Treuting, P. M. (2011). 'Practical pathology of aging mice', *Pathobiol Aging Age Relat Dis*, **1**.
- Pham, C. T., MacIvor, D. M., Hug, B. A., Heusel, J. W., and Ley, T. J. (1996). 'Long-range disruption of gene expression by a selectable marker cassette', *Proc Natl Acad Sci U S A*, **93**(23): 13090-5.
- Pinto, J. T., Suffoletto, B. P., Berzin, T. M., Qiao, C. H., Lin, S., Tong, W. P., May, F., Mukherjee, B., and Heston, W. D. (1996). 'Prostate-specific membrane antigen: a novel folate hydrolase in human prostatic carcinoma cells', *Clin Cancer Res*, **2**(9): 1445-51.
- Psimadas, D., Valotassiou, V., Alexiou, S., Tsougos, I., and Georgoulas, P. (2018). 'Radiolabeled mAbs as Molecular Imaging and/or Therapy Agents Targeting PSMA', *Cancer Invest*, **36**(2): 118-28.
- Qiu, A., Jansen, M., Sakaris, A., Min, S. H., Chattopadhyay, S., Tsai, E., Sandoval, C., Zhao, R., Akabas, M. H., and Goldman, I. D. (2006). 'Identification of an intestinal folate transporter and the molecular basis for hereditary folate malabsorption', *Cell*, **127**(5): 917-28.
- Qiu, A., Min, S. H., Jansen, M., Malhotra, U., Tsai, E., Cabelof, D. C., Matherly, L. H., Zhao, R., Akabas, M. H., and Goldman, I. D. (2007). 'Rodent intestinal folate transporters (SLC46A1): secondary structure, functional properties, and response to dietary folate restriction', *Am J Physiol Cell Physiol*, **293**(5): C1669-78.
- Rahbar, K., Ahmadzadehfar, H., Kratochwil, C., Haberkorn, U., Schafers, M., Essler, M., Baum, R. P., Kulkarni, H. R., Schmidt, M., Drzezga, A., Bartenstein, P., Pfestroff, A., Luster, M., Lutzen, U., Marx, M., Prasad, V., Brenner, W., Heinzl, A., Mottaghy, F. M., Ruf, J., Meyer, P. T., Heuschkel, M., Eveslage, M., Bogemann, M., Fendler, W. P., and Krause, B. J. (2017). 'German Multicenter Study Investigating ¹⁷⁷Lu-PSMA-617 Radioligand Therapy in Advanced Prostate Cancer Patients', *J Nucl Med*, **58**(1): 85-90.
- Rahn, K. A., Watkins, C. C., Alt, J., Rais, R., Stathis, M., Grishkan, I., Crainiceau, C. M., Pomper, M. G., Rojas, C., Pletnikov, M. V., Calabresi, P. A., Brandt, J., Barker, P. B., Slusher, B. S., and Kaplin, A. I. (2012). 'Inhibition of glutamate carboxypeptidase II (GCPII) activity as a treatment for cognitive impairment in multiple sclerosis', *Proc Natl Acad Sci U S A*, **109**(49): 20101-6.
- Rais, R., Jiang, W., Zhai, H., Wozniak, K. M., Stathis, M., Hollinger, K. R., Thomas, A. G., Rojas, C., Vornov, J. J., Marohn, M., Li, X., and Slusher, B. S. (2016). 'FOLH1/GCPII is elevated in IBD patients, and its inhibition ameliorates murine IBD abnormalities', *JCI Insight*, **1**(12): e88634.

- Rajasekaran, S. A., Anilkumar, G., Oshima, E., Bowie, J. U., Liu, H., Heston, W., Bander, N. H., and Rajasekaran, A. K. (2003). 'A novel cytoplasmic tail MXXXL motif mediates the internalization of prostate-specific membrane antigen', *Mol Biol Cell*, **14**(12): 4835-45.
- Rawlings, N. D., and Barrett, A. J. (1997). 'Structure of membrane glutamate carboxypeptidase', *Bba-Protein Struct M*, **1339**(2): 247-52.
- Rawlings, N. D., Barrett, A. J., and Finn, R. (2016). 'Twenty years of the MEROPS database of proteolytic enzymes, their substrates and inhibitors', *Nucleic Acids Res*, **44**(D1): D343-50.
- Ren, H., Zhang, H., Wang, X., Liu, J., Yuan, Z., and Hao, J. (2014). 'Prostate-specific membrane antigen as a marker of pancreatic cancer cells', *Med Oncol*, **31**(3): 857.
- Renneberg, H., Friedetzky, A., Konrad, L., Kurek, R., Weingartner, K., Wennemuth, G., Tunn, U. W., and Aumuller, G. (1999). 'Prostate specific membrane antigen (PSM) is expressed in various human tissues: implication for the use of PSM reverse transcription polymerase chain reaction to detect hematogenous prostate cancer spread', *Urol Res*, **27**(1): 23-7.
- Rinkerschaeffter, C. W., Hawkins, A. L., Su, S. L., Israeli, R. S., Griffin, C. A., Isaacs, J. T., and Heston, W. D. W. (1995). 'Localization and Physical Mapping of the Prostate-Specific Membrane Antigen (Psm) Gene to Human-Chromosome-11', *Genomics*, **30**(1): 105-08.
- Robinson, M. B., Blakely, R. D., and Coyle, J. T. (1986). 'Quisqualate selectively inhibits a brain peptidase which cleaves N-acetyl-L-aspartyl-L-glutamate in vitro', *Eur J Pharmacol*, **130**(3): 345-7.
- Robinson, M. B., Blakely, R. D., Couto, R., and Coyle, J. T. (1987). 'Hydrolysis of the Brain Dipeptide N-Acetyl-L-Aspartyl-L-Glutamate - Identification and Characterization of a Novel N-Acetylated Alpha-Linked Acidic Dipeptidase Activity from Rat-Brain', *Journal of Biological Chemistry*, **262**(30): 14498-506.
- Rochon, Y. P., Horoszewicz, J. S., Boynton, A. L., Holmes, E. H., Barren, R. J., 3rd, Erickson, S. J., Kenny, G. M., and Murphy, G. P. (1994). 'Western blot assay for prostate-specific membrane antigen in serum of prostate cancer patients', *Prostate*, **25**(4): 219-23.
- Roffman, J. L., Lamberti, J. S., Achtyes, E., Macklin, E. A., Galendez, G. C., Raeke, L. H., Silverstein, N. J., Smoller, J. W., Hill, M., and Goff, D. C. (2013). 'Randomized multicenter investigation of folate plus vitamin B12 supplementation in schizophrenia', *JAMA Psychiatry*, **70**(5): 481-9.
- Romei, C., Raiteri, M., and Raiteri, L. (2013). 'Glycine release is regulated by metabotropic glutamate receptors sensitive to mGluR2/3 ligands and activated by N-acetylaspartylglutamate (NAAG)', *Neuropharmacology*, **66**: 311-16.
- Rovenska, M., Hlouchova, K., Sacha, P., Mlcochova, P., Horak, V., Zamecnik, J., Barinka, C., and Konvalinka, J. (2008). 'Tissue expression and enzymologic

characterization of human prostate specific membrane antigen and its rat and pig orthologs', *Prostate*, **68**(2): 171-82.

Ruberte Jose, Carretero Ana, Navarro Marc. 2017. *Morphological mouse phenotyping: anatomy, histology and imaging* (Medica Panamericana: Madrid).

Rueden, C. T., Schindelin, J., Hiner, M. C., DeZonia, B. E., Walter, A. E., Arena, E. T., and Eliceiri, K. W. (2017). 'ImageJ2: ImageJ for the next generation of scientific image data', *BMC Bioinformatics*, **18**(1): 529.

Ruocco, A., Nicole, O., Docagne, F., Ali, C., Chazalviel, L., Komesli, S., Yablonsky, F., Roussel, S., MacKenzie, E. T., Vivien, D., and Buisson, A. (1999). 'A transforming growth factor-beta antagonist unmasks the neuroprotective role of this endogenous cytokine in excitotoxic and ischemic brain injury', *Journal of Cerebral Blood Flow and Metabolism*, **19**(12): 1345-53.

Sacha, P., Zamecnik, J., Barinka, C., Hlouchova, K., Vicha, A., Mlcochova, P., Hilgert, I., Eckschlager, T., and Konvalinka, J. (2007). 'Expression of glutamate carboxypeptidase II in human brain', *Neuroscience*, **144**(4): 1361-72.

Salas Fragomeni, R. A., Menke, J. R., Holdhoff, M., Ferrigno, C., Laterra, J. J., Solnes, L. B., Javadi, M. S., Szabo, Z., Pomper, M. G., and Rowe, S. P. (2017). 'Prostate-Specific Membrane Antigen-Targeted Imaging With [18F]DCFPyL in High-Grade Gliomas', *Clin Nucl Med*, **42**(10): e433-e35.

Salas Fragomeni, R. A., Amir, T., Sheikhabaei, S., Harvey, S. C., Javadi, M. S., Solnes, L. B., Kiess, A. P., Allaf, M. E., Pomper, M. G., Gorin, M. A., and Rowe, S. P. (2018). 'Imaging of Nonprostate Cancers Using PSMA-Targeted Radiotracers: Rationale, Current State of the Field, and a Call to Arms', *J Nucl Med*, **59**(6): 871-77.

Samplaski, M. K., Heston, W., Elson, P., Magi-Galluzzi, C., and Hansel, D. E. (2011). 'Folate hydrolase (prostate-specific membrane [corrected] antigen) 1 expression in bladder cancer subtypes and associated tumor neovasculature', *Mod Pathol*, **24**(11): 1521-9.

Sanabria, E. R. G., Wozniak, K. M., Slusher, B. S., and Keller, A. (2004). 'GCP II (NAALADase) inhibition suppresses mossy fiber-CA3 synaptic neurotransmission by a presynaptic mechanism', *Journal of Neurophysiology*, **91**(1): 182-93.

Santoro, S. P., Kim, S., Motz, G. T., Alatzoglou, D., Li, C., Irving, M., Powell, D. J., Jr., and Coukos, G. (2015). 'T cells bearing a chimeric antigen receptor against prostate-specific membrane antigen mediate vascular disruption and result in tumor regression', *Cancer Immunol Res*, **3**(1): 68-84.

Schmidt, L. H., Heitkotter, B., Schulze, A. B., Schliemann, C., Steinestel, K., Trautmann, M., Marra, A., Hillejan, L., Mohr, M., Evers, G., Wardelmann, E., Rahbar, K., Gorlich, D., Lenz, G., Berdel, W. E., Hartmann, W., Wiewrodt, R., and Huss, S. (2017). 'Prostate specific membrane antigen (PSMA) expression in non-small cell lung cancer', *PLoS One*, **12**(10): e0186280.

- Schmittgen, T. D., Tiske, S., Vessella, R. L., True, L. D., and Zakrajsek, B. A. (2003). 'Expression of prostate specific membrane antigen and three alternatively spliced variants of PSMA in prostate cancer patients', *International Journal of Cancer*, **107**(2): 323-29.
- Schwartzberg, P. L., Goff, S. P., and Robertson, E. J. (1989). 'Germ-line transmission of a c-abl mutation produced by targeted gene disruption in ES cells', *Science*, **246**(4931): 799-803.
- Seong, E., Saunders, T. L., Stewart, C. L., and Burmeister, M. (2004). 'To knockout in 129 or in C57BL/6: that is the question', *Trends Genet*, **20**(2): 59-62.
- Serganova, I., Moroz, E., Cohen, I., Moroz, M., Mane, M., Zurita, J., Shenker, L., Ponomarev, V., and Blasberg, R. (2017). 'Enhancement of PSMA-Directed CAR Adoptive Immunotherapy by PD-1/PD-L1 Blockade', *Mol Ther Oncolytics*, **4**: 41-54.
- Shafizadeh, T. B., and Halsted, C. H. (2007). 'gamma-Glutamyl hydrolase, not glutamate carboxypeptidase II, hydrolyzes dietary folate in rat small intestine', *J Nutr*, **137**(5): 1149-53.
- Shane, B. (2010). 'Folate Chemistry and Metabolism.' in L. B. Bailey (ed.) *Folate in health and disease*. Taylor & Francis Group: Boca Raton, US (p. 1-24).
- Silver, D. A., Pellicer, I., Fair, W. R., Heston, W. D. W., and CordonCardo, C. (1997). 'Prostate-specific membrane antigen expression in normal and malignant human tissues', *Clinical Cancer Research*, **3**(1): 81-85.
- Slusher, B. S., Vornov, J. J., Thomas, A. G., Hurn, P. D., Harukuni, I., Bhardwaj, A., Traystman, R. J., Robinson, M. B., Britton, P., Lu, X. C., Tortella, F. C., Wozniak, K. M., Yudkoff, M., Potter, B. M., and Jackson, P. F. (1999). 'Selective inhibition of NAALADase, which converts NAAG to glutamate, reduces ischemic brain injury', *Nature Medicine*, **5**(12): 1396-402.
- Sokoloff, R. L., Norton, K. C., Gasior, C. L., Marker, K. M., and Grauer, L. S. (2000). 'A dual-monoclonal sandwich assay for prostate-specific membrane antigen: Levels in tissues, seminal fluid and urine', *Prostate*, **43**(2): 150-57.
- Spatz, S., Tolkach, Y., Jung, K., Stephan, C., Busch, J., Ralla, B., Rabien, A., Feldmann, G., Brossart, P., Bundschuh, R. A., Ahmadzadehfar, H., Essler, M., Toma, M., Muller, S. C., Ellinger, J., Hauser, S., and Kristiansen, G. (2018). 'Comprehensive Evaluation of Prostate Specific Membrane Antigen Expression in the Vasculature of Renal Tumors: Implications for Imaging Studies and Prognostic Role', *J Urol*, **199**(2): 370-77.
- Speno, H. S., Luthi-Carter, R., Macias, W. L., Valentine, S. L., Joshi, A. R., and Coyle, J. T. (1999). 'Site-directed mutagenesis of predicted active site residues in glutamate carboxypeptidase II', *Mol Pharmacol*, **55**(1): 179-85.
- Srinivasarao, M., and Low, P. S. (2017). 'Ligand-Targeted Drug Delivery', *Chem Rev*, **117**(19): 12133-64.
- Stover, P.J. (2010). 'Folate Biochemical Pathways and Their Regulation.' in L. B. Bailey (ed.) *Folate in health and disease*. Taylor & Francis Group: Boca Raton, US (p. 49-74).

- Su, S. L., Huang, I. P., Fair, W. R., Powell, C. T., and Heston, W. D. (1995). 'Alternatively spliced variants of prostate-specific membrane antigen RNA: ratio of expression as a potential measurement of progression', *Cancer Res*, **55**(7): 1441-3.
- Sung, Y. H., Baek, I. J., Kim, D. H., Jeon, J., Lee, J., Lee, K., Jeong, D., Kim, J. S., and Lee, H. W. (2013). 'Knockout mice created by TALEN-mediated gene targeting', *Nat Biotechnol*, **31**(1): 23-4.
- Tagawa, S. T., Beltran, H., Vallabhajosula, S., Goldsmith, S. J., Osborne, J., Matulich, D., Petrillo, K., Parmar, S., Nanus, D. M., and Bander, N. H. (2010). 'Anti-prostate-specific membrane antigen-based radioimmunotherapy for prostate cancer', *Cancer*, **116**(4 Suppl): 1075-83.
- Tagawa, S. T., Milowsky, M. I., Morris, M., Vallabhajosula, S., Christos, P., Akhtar, N. H., Osborne, J., Goldsmith, S. J., Larson, S., Taskar, N. P., Scher, H. I., Bander, N. H., and Nanus, D. M. (2013). 'Phase II study of Lutetium-177-labeled anti-prostate-specific membrane antigen monoclonal antibody J591 for metastatic castration-resistant prostate cancer', *Clin Cancer Res*, **19**(18): 5182-91.
- Thomas, A. G., Liu, W. L., Olkowski, J. L., Tang, Z. C., Lin, Q., Lu, X. C. M., and Slusher, B. S. (2001). 'Neuroprotection mediated by glutamate carboxypeptidase II (NAALADase) inhibition requires TGF-beta', *European Journal of Pharmacology*, **430**(1): 33-40.
- Tolkach, Y., Gevensleben, H., Bundschuh, R., Koyun, A., Huber, D., Kehrer, C., Hecking, T., Keyver-Paik, M. D., Kaiser, C., Ahmadzadehfar, H., Essler, M., Kuhn, W., and Kristiansen, G. (2018). 'Prostate-specific membrane antigen in breast cancer: a comprehensive evaluation of expression and a case report of radionuclide therapy', *Breast Cancer Res Treat*, **169**(3): 447-55.
- Tortella, F. C., Lin, Y., Ved, H., Slusher, B. S., and Dave, J. R. (2000). 'Neuroprotection produced by the NAALADase inhibitor 2-PMPA in rat cerebellar neurons', *Eur J Pharmacol*, **402**(1-2): 31-7.
- Troyer, J. K., Beckett, M. L., and Wright, G. L., Jr. (1995). 'Detection and characterization of the prostate-specific membrane antigen (PSMA) in tissue extracts and body fluids', *Int J Cancer*, **62**(5): 552-8.
- Tsai, G., Dunham, K. S., Drager, U., Grier, A., Anderson, C., Collura, J., and Coyle, J. T. (2003). 'Early embryonic death of glutamate carboxypeptidase II (NAALADase) homozygous mutants', *Synapse*, **50**(4): 285-92.
- Tykvart, J., Sacha, P., Barinka, C., Knedlik, T., Starkova, J., Lubkowski, J., and Konvalinka, J. (2012). 'Efficient and versatile one-step affinity purification of in vivo biotinylated proteins: Expression, characterization and structure analysis of recombinant human glutamate carboxypeptidase II', *Protein Protein Expres Purif*, **82**(1): 106-15.
- Tykvart, J., Navratil, V., Sedlak, F., Corey, E., Colombatti, M., Fracasso, G., Koukolik, F., Barinka, C., Sacha, P., and Konvalinka, J. (2014). 'Comparative analysis of monoclonal antibodies against prostate-specific membrane antigen (PSMA)', *Prostate*, **74**(16): 1674-90.

- Tykvart, J., Barinka, C., Svoboda, M., Navratil, V., Soucek, R., Hubalek, M., Hradilek, M., Sacha, P., Lubkowski, J., and Konvalinka, J. (2015). 'Structural and Biochemical Characterization of a Novel Aminopeptidase from Human Intestine', *Journal of Biological Chemistry*.
- Vargas-Martinez, C., Ordovas, J. M., Wilson, P. W., and Selhub, J. (2002). 'The glutamate carboxypeptidase gene II (C>T) polymorphism does not affect folate status in the Framingham Offspring cohort', *J Nutr*, **132**(6): 1176-9.
- Vorlova, B., Sedlak, F., Kasperek, P., Sramkova, K., Maly, M., Zamecnik, J., Sacha, P., and Konvalinka, J. (2018). 'A novel PSMA/GCPII-deficient mouse model shows enlarged seminal vesicles upon aging', *Prostate*, **In press**(doi: 10.1002/pros.23717).
- Wang, H. L., Wang, S. S., Song, W. H., Pan, Y., Yu, H. P., Si, T. G., Liu, Y., Cui, X. N., and Guo, Z. (2015). 'Expression of prostate-specific membrane antigen in lung cancer cells and tumor neovasculature endothelial cells and its clinical significance', *PLoS One*, **10**(5): e0125924.
- Wernicke, A. G., Varma, S., Greenwood, E. A., Christos, P. J., Chao, K. S., Liu, H., Bander, N. H., and Shin, S. J. (2014). 'Prostate-specific membrane antigen expression in tumor-associated vasculature of breast cancers', *APMIS*, **122**(6): 482-9.
- Westbrook, G. L., Mayer, M. L., Namboodiri, M. A., and Neale, J. H. (1986). 'High concentrations of N-acetylaspartylglutamate (NAAG) selectively activate NMDA receptors on mouse spinal cord neurons in cell culture', *J Neurosci*, **6**(11): 3385-92.
- Williams, T., and Kole, R. (2006). 'Analysis of prostate-specific membrane antigen splice variants in LNCap cells', *Oligonucleotides*, **16**(2): 186-95.
- Wolf, P., Freudenberg, N., Buhler, P., Alt, K., Schultze-Seemann, W., Wetterauer, U., and Elsasser-Beile, U. (2010). 'Three conformational antibodies specific for different PSMA epitopes are promising diagnostic and therapeutic tools for prostate cancer', *Prostate*, **70**(5): 562-9.
- Wright, G. L., Jr., Haley, C., Beckett, M. L., and Schellhammer, P. F. (1995). 'Expression of prostate-specific membrane antigen in normal, benign, and malignant prostate tissues', *Urol Oncol*, **1**(1): 18-28.
- Wroblewska, B., Wroblewski, J. T., Saab, O. H., and Neale, J. H. (1993). 'N-Acetylaspartylglutamate Inhibits Forskolin-Stimulated Cyclic-Amp Levels Via a Metabotropic Glutamate-Receptor in Cultured Cerebellar Granule Cells', *Journal of Neurochemistry*, **61**(3): 943-48.
- Wroblewska, B., Wroblewski, J. T., Pshenichkin, S., Surin, A., Sullivan, S. E., and Neale, J. H. (1997). 'N-acetylaspartylglutamate selectively activates mGluR3 receptors in transfected cells', *Journal of Neurochemistry*, **69**(1): 174-81.
- Wroblewska, B., Santi, M. R., and Neale, J. H. (1998). 'N-acetylaspartylglutamate activates cyclic AMP-coupled metabotropic glutamate receptors in cerebellar astrocytes', *Glia*, **24**(2): 172-9.

- Wroblewska, B., Wegorzewska, I. N., Bzdega, T., Olszewski, R. T., and Neale, J. H. (2006). 'Differential negative coupling of type 3 metabotropic glutamate receptor to cyclic GMP levels in neurons and astrocytes', *Journal of Neurochemistry*, **96**(4): 1071-77.
- Wustemann, T., Haberkorn, U., Babich, J., and Mier, W. (2018). 'Targeting prostate cancer: Prostate-specific membrane antigen based diagnosis and therapy', *Med Res Rev*.
- Xi, H. B., Wang, G. X., Fu, B., Liu, W. P., and Li, Y. (2015). 'Survivin and PSMA Loaded Dendritic Cell Vaccine for the Treatment of Prostate Cancer', *Biol Pharm Bull*, **38**(6): 827-35.
- Xiao, Z., Adam, B. L., Cazares, L. H., Clements, M. A., Davis, J. W., Schellhammer, P. F., Dalmaso, E. A., and Wright, G. L., Jr. (2001). 'Quantitation of serum prostate-specific membrane antigen by a novel protein biochip immunoassay discriminates benign from malignant prostate disease', *Cancer Res*, **61**(16): 6029-33.
- Yamamoto, T., Nozaki-Taguchi, N., Sakashita, Y., and Inagaki, T. (2001). 'Inhibition of spinal N-acetylated-alpha-linked acidic dipeptidase produces an antinociceptive effect in the rat formalin test', *Neuroscience*, **102**(2): 473-9.
- Yamamoto, T., Hirasawa, S., Wroblewska, B., Grajkowska, E., Zhou, J., Kozikowski, A., Wroblewski, J., and Neale, J. H. (2004). 'Antinociceptive effects of N-acetylaspartylglutamate (NAAG) peptidase inhibitors ZJ-11, ZJ-17 and ZJ-43 in the rat formalin test and in the rat neuropathic pain model', *Eur J Neurosci*, **20**(2): 483-94.
- Yao, V., Parwani, A., Maier, C., Heston, W. D., and Bacich, D. J. (2008). 'Moderate expression of prostate-specific membrane antigen, a tissue differentiation antigen and folate hydrolase, facilitates prostate carcinogenesis', *Cancer Res*, **68**(21): 9070-7.
- Yao, V., Berkman, C. E., Choi, J. K., O'Keefe, D. S., and Bacich, D. J. (2010). 'Expression of Prostate-Specific Membrane Antigen (PSMA), Increases Cell Folate Uptake and Proliferation and Suggests a Novel Role for PSMA in the Uptake of the Non-Polyglutamated Folate, Folic Acid', *Prostate*, **70**(3): 305-16.
- Yoshiki, A., and Moriwaki, K. (2006). 'Mouse phenome research: implications of genetic background', *ILAR J*, **47**(2): 94-102.
- Zeng, C., Ke, Z. F., Yang, Z., Wang, Z., Yang, S. C., Luo, C. Q., and Wang, L. T. (2012). 'Prostate-specific membrane antigen: a new potential prognostic marker of osteosarcoma', *Med Oncol*, **29**(3): 2234-9.
- Zhang, Q., Helfand, B. T., Carneiro, B. A., Qin, W., Yang, X. J., Lee, C., Zhang, W., Giles, F. J., Cristofanilli, M., and Kuzel, T. M. (2018). 'Efficacy Against Human Prostate Cancer by Prostate-specific Membrane Antigen-specific, Transforming Growth Factor-beta Insensitive Genetically Targeted CD8(+) T-cells Derived from Patients with Metastatic Castrate-resistant Disease', *Eur Urol*, **73**(5): 648-52.
- Zhang, S., Zhang, H. S., Reuter, V. E., Slovin, S. F., Scher, H. I., and Livingston, P. O. (1998). 'Expression of potential target antigens for immunotherapy on primary and metastatic prostate cancers', *Clin Cancer Res*, **4**(2): 295-302.

- Zhang, T., Song, B., Zhu, W., Xu, X., Gong, Q. Q., Morando, C., Dassopoulos, T., Newberry, R. D., Hunt, S. R., and Li, E. (2012). 'An ileal Crohn's disease gene signature based on whole human genome expression profiles of disease unaffected ileal mucosal biopsies', *PLoS One*, **7**(5): e37139.
- Zhao, J., Ramadan, E., Cappiello, M., Wroblewska, B., Bzdega, T., and Neale, J. H. (2001). 'NAAG inhibits KCl-induced [H-3]-GABA release via mGluR3, cAMP, PKA and L-type calcium conductance', *European Journal of Neuroscience*, **13**(2): 340-46.
- Zhao, R., Matherly, L. H., and Goldman, I. D. (2009). 'Membrane transporters and folate homeostasis: intestinal absorption and transport into systemic compartments and tissues', *Expert Rev Mol Med*, **11**e4.
- Zhong, C., Zhao, X., Sarva, J., Kozikowski, A., Neale, J. H., and Lyeth, B. G. (2005). 'NAAG peptidase inhibitor reduces acute neuronal degeneration and astrocyte damage following lateral fluid percussion TBI in rats', *J Neurotrauma*, **22**(2): 266-76.
- Zhong, C., Zhao, X., Van, K. C., Bzdega, T., Smyth, A., Zhou, J., Kozikowski, A. P., Jiang, J., O'Connor, W. T., Berman, R. F., Neale, J. H., and Lyeth, B. G. (2006). 'NAAG peptidase inhibitor increases dialysate NAAG and reduces glutamate, aspartate and GABA levels in the dorsal hippocampus following fluid percussion injury in the rat', *J Neurochem*, **97**(4): 1015-25.
- Zhong, C., Luo, Q., and Jiang, J. (2014). 'Blockade of N-acetylaspartylglutamate peptidases: a novel protective strategy for brain injuries and neurological disorders', *Int J Neurosci*, **124**(12): 867-73.
- Zijlstra, M., Li, E., Sajjadi, F., Subramani, S., and Jaenisch, R. (1989). 'Germ-line transmission of a disrupted beta 2-microglobulin gene produced by homologous recombination in embryonic stem cells', *Nature*, **342**(6248): 435-8.

APPENDICES

| | |
|-----------------|-----|
| APPENDIX 1..... | 138 |
|-----------------|-----|

Knedlík T., Vorlová B., Navrátil V., Tykvart J., Sedlák F., Vaculín Š., Franěk M., Šácha P., Konvalinka J.: Mouse glutamate carboxypeptidase II (GCPII) has a similar enzyme activity and inhibition profile but a different tissue distribution to human GCPII. *FEBS Open Bio*, 2017; 7(9): 1362-78.

| | |
|-----------------|-----|
| APPENDIX 2..... | 155 |
|-----------------|-----|

Vorlová B., Sedlák F., Kašpárek P., Šrámková K., Malý M., Zámečník J., Šácha P., Konvalinka J.: A novel PSMA/GCPII-deficient mouse model shows enlarged seminal vesicles upon aging. *Prostate*, 2018; In press, doi: 10.1002/pros.23717.

| | |
|-----------------|-----|
| APPENDIX 3..... | 169 |
|-----------------|-----|

List of metabolites and their abbreviations used in targeted metabolomic analysis

APPENDIX 1

Mouse glutamate carboxypeptidase II (GCPII) has a similar enzyme activity and inhibition profile but a different tissue distribution to human GCPII

Tomáš Knedlík^{1,2}, Barbora Vorlová^{1,3}, Václav Navrátil^{1,2}, Jan Tykvart^{1,2,†}, František Sedlák^{1,3,4}, Šimon Vaculín⁵, Miloslav Franěk⁵, Pavel Sácha¹ and Jan Konvalinka^{1,2}

1 Institute of Organic Chemistry and Biochemistry of the Czech Academy of Sciences, Prague, Czech Republic

2 Department of Biochemistry, Faculty of Science, Charles University, Prague, Czech Republic

3 First Faculty of Medicine, Charles University, Prague, Czech Republic

4 Department of Genetics and Microbiology, Faculty of Science, Charles University, Prague, Czech Republic

5 Department of Normal, Pathological and Clinical Physiology, Third Faculty of Medicine, Charles University, Prague, Czech Republic

Keywords

glutamate carboxypeptidase II; mouse animal model; neuronal disorders; prostate cancer; prostate-specific membrane antigen

Correspondence

J. Konvalinka, Institute of Organic Chemistry and Biochemistry of the CAS, v.v.i., Flemingovo n. 2, Prague 6, 16610, Czech Republic
Fax: +420 220 183 578
Tel: +420 220 183 218
E-mail: konval@uochb.cas.cz

†Present address

Donnelly Centre for Cellular and Biomolecular Research, University of Toronto, Toronto, ON, Canada

(Received 18 April 2017, revised 23 June 2017, accepted 19 July 2017)

doi:10.1002/2211-5463.12276

Glutamate carboxypeptidase II (GCPII), also known as prostate-specific membrane antigen (PSMA) or folate hydrolase, is a metallopeptidase expressed predominantly in the human brain and prostate. GCPII expression is considerably increased in prostate carcinoma, and the enzyme also participates in glutamate excitotoxicity in the brain. Therefore, GCPII represents an important diagnostic marker of prostate cancer progression and a putative target for the treatment of both prostate cancer and neuronal disorders associated with glutamate excitotoxicity. For the development of novel therapeutics, mouse models are widely used. However, although mouse GCPII activity has been characterized, a detailed comparison of the enzymatic activity and tissue distribution of the mouse and human GCPII orthologs remains lacking. In this study, we prepared extracellular mouse GCPII and compared it with human GCPII. We found that mouse GCPII possesses lower catalytic efficiency but similar substrate specificity compared with the human protein. Using a panel of GCPII inhibitors, we discovered that inhibition constants are generally similar for mouse and human GCPII. Furthermore, we observed highest expression of GCPII protein in the mouse kidney, brain, and salivary glands. Importantly, we did not detect GCPII in the mouse prostate. Our data suggest that the differences in enzymatic activity and inhibition profile are rather small; therefore, mouse GCPII can approximate human GCPII in drug development and testing. On the other hand, significant differences in GCPII tissue expression must be taken into account when developing novel GCPII-based anticancer and therapeutic methods, including targeted anticancer drug delivery systems, and when using mice as a model organism.

Glutamate carboxypeptidase II (GCPII; EC 3.4.17.21) is a membrane metalloprotease that has been studied intensively over the past 20 years in three different

scientific fields: neuroscience, prostate oncology, and dietology. In humans, GCPII is expressed predominantly in the brain [1,2], prostate [3,4], small intestine

Abbreviations

Avi-hGCPII, recombinant extracellular human GCPII; Avi-mGCPII, recombinant extracellular mouse GCPII; GCPII, glutamate carboxypeptidase II; GCPIII, glutamate carboxypeptidase III; NAAG, *N*-acetyl-L-aspartyl-L-glutamate; PSMA, prostate-specific membrane antigen.

[5], and kidney [4,6]. Because GCPII plays different physiological roles in these tissues, three alternative names for the enzyme have historically been used: *N*-acetylated alpha-linked acidic dipeptidase (NAALADase) [7], prostate-specific membrane antigen (PSMA) [8], and folate hydrolase [5]. The close GCPII homolog GCPIII [9,10], recently identified as β -citrull-glutamate hydrolase [11], is also expressed in human tissues.

In the human central nervous system, GCPII hydrolyzes the most abundant peptide neurotransmitter, *N*-acetyl-L-aspartyl-L-glutamate (NAAG), into *N*-acetyl-L-aspartate and glutamate [7]. Inhibition of this proteolytic activity with selective GCPII inhibitors has been shown to be neuroprotective in experiments with mouse models [12]; NAAG activation of metabotropic glutamate type 3 receptors exerts neuroprotective effects toward glutamate-mediated excitotoxicity caused by elevated levels of glutamate released during stroke, traumatic brain injury, and other pathological conditions [13–15]. In addition to the brain, GCPII is expressed on the human jejunal brush border [5,16], where it cleaves the terminal glutamates from poly- γ -glutamylated folates, enabling their transport across the intestinal mucosa (folate absorption) [17]. On the other hand, the function of GCPII in the human prostate is unknown. GCPII is overexpressed in prostate cancer [3,18]; therefore, it has been suggested as a promising target for prostate cancer diagnosis and treatment using targeted strategies [19–21].

An appropriate animal model is necessary for the development and testing of novel therapeutics. Mice, rats, and pigs are among the most promising candidates to become such a model for GCPII research. Several years ago, our laboratory conducted a study comparing human GCPII with its porcine and rat orthologs [22]. The orthologs showed similarity in their enzymatic properties, but considerable differences in terms of their tissue distribution [22]. However, mouse GCPII was not included in the study, even though mice now are the most widely used preclinical models for GCPII-targeted research (stroke [12], traumatic brain injury [23,24], amyotrophic lateral sclerosis [25], inflammatory, and neuropathic pain [26,27], reviewed in Refs [13,28]). Therefore, a comparative analysis of mouse GCPII characterization is needed.

Mouse GCPII shares 91% amino acid similarity with human GCPII and preserves the internalization signal MXXXL, despite low similarity in the intracellular domain [29]. Mouse GCPII also possesses both NAAG-hydrolyzing and folate hydrolase activities [29]. In contrast to the expression pattern of human GCPII, mouse GCPII is expressed in largest amounts in the kidney and, surprisingly, is absent in the mouse

prostate [29]. Results from studies with GCPII-knock-out mice have been contradictory: some reports have described normal development to adulthood [9,30] and others have noted early embryonic death [31,32].

In the current study, we prepared and characterized recombinant mouse GCPII and compared it with its human counterpart. We put a strong focus on distribution of GCPII in mouse tissues, as this information is highly relevant for the development of novel GCPII-based anticancer and neuroprotective therapies using mouse models.

Results

Efficient one-step purification method yields purified recombinant mouse GCPII (Avi-mGCPII)

As recombinant extracellular human GCPII was shown to correctly represent the endogenous full-length GCPII [33,34], we prepared the recombinant extracellular part of mouse GCPII (Avi-mGCPII) using a *Drosophila* S2 expression system, according to the protocol previously established in our laboratory [34]. Avi-mGCPII has a TEV cleavable Avi-tag sequence attached to the N terminus of the mouse GCPII extracellular domain (amino acids 45–752), enabling fast one-step purification (Fig. 1A).

Avi-mGCPII was purified from the conditioned medium of cells stably transfected with Avi-mGCPII by affinity chromatography based on the biotin–streptavidin interaction [34], yielding 3 mg of pure protein from 1 L conditioned medium (Fig. 1B).

Mouse GCPII has lower catalytic efficiency than human GCPII

To characterize the enzyme activity of Avi-mGCPII, we determined kinetic parameters (K_M and k_{cat}) for cleavage of both substrates: *N*-acetyl-L-aspartyl-L-glutamate (NAAG) and pteroyl-di-L-glutamate (Table 1). The data revealed that the catalytic efficiency of Avi-mGCPII is lower than that of its human counterpart. The enzymes had similar turnover numbers but differed in their K_M values. The differences were more pronounced for pteroyl-di-L-glutamate than for NAAG. Surprisingly, both enzymes had higher catalytic efficiencies for cleavage of pteroyl-di-L-glutamate than for NAAG (Table 1).

Furthermore, to analyze the inhibition profile of Avi-mGCPII, we determined K_i values for several commonly used GCPII inhibitors (using pteroyl-di-L-glutamate as a substrate). The set of GCPII inhibitors included 2-(phosphonomethyl)pentanedioic acid

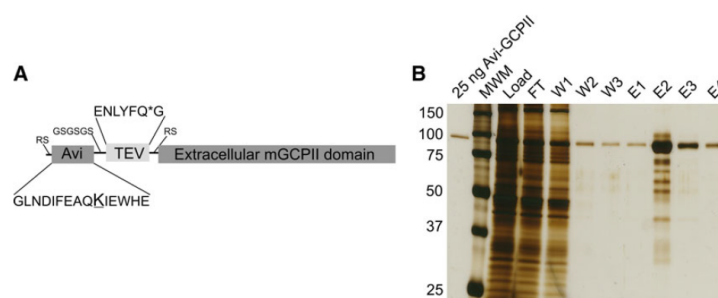


Fig. 1. Schematic structure of Avi-mGCPII and affinity purification. (A) Schematic structure of Avi-mGCPII containing an Avi sequence (the biotinylated lysine residue is enlarged and underlined) and TEV protease cleavage sequence (the cleavage site is marked with an asterisk). (B) Silver-stained SDS/PAGE gel showing affinity purification of Avi-mGCPII expressed in *Drosophila* S2 cells. MWM, molecular weight marker; load, concentrated S2 cell medium; FT, flow-through; W1–W3, wash fractions; E1–E4, elution fractions. Ten microliter samples was loaded onto the gel, except for the E2 fraction (1 μ L was loaded).

Table 1. Kinetic parameters of recombinant mouse and human GCPII (Avi-mGCPII and Avi-hGCPII, respectively) for their substrates. Kinetic parameters (K_M and k_{cat}) of *N*-acetyl-L-aspartyl-L-glutamate (NAAG) and pteroyl-di-L-glutamate cleavage were determined using radioenzymatic [34] and HPLC assays [39], respectively. The values shown are mean \pm standard deviation of duplicate measurements.

| Enzymes | NAAG | | | Pteroyl-di-L-glutamate | | |
|------------|----------------|------------------------|--|------------------------|------------------------|--|
| | K_M [nM] | k_{cat} [s^{-1}] | k_{cat}/K_M [$\times 10^7 s^{-1} M$] | K_M [nM] | k_{cat} [s^{-1}] | k_{cat}/K_M [$\times 10^7 s^{-1} M$] |
| Avi-mGCPII | 1900 \pm 100 | 1.44 \pm 0.02 | 0.077 \pm 0.001 | 290 \pm 20 | 3.63 \pm 0.09 | 1.26 \pm 0.08 |
| Avi-hGCPII | 550 \pm 60 | 1.45 \pm 0.04 | 0.265 \pm 0.007 | 39 \pm 2 | 5.09 \pm 0.09 | 13.2 \pm 0.8 |

(2-PMPA) [35], (S)-2-(3-((S)-1-carboxy-3-methylbutyl)ureido)pentanedioic acid (ZJ-43) [36], (S)-2-(3-((S)-1-carboxy-(4-iodobenzamido)pentyl)ureido)pentanedioic acid (DCIBzL) [37], quisqualate, DKFZ-PSMA-11 [38], and beta-citryl-L-glutamate (Table 2). We also tested three compounds recently prepared in our laboratory: JB-352 and JB-277 (originally reported as compounds **3** and **22a** [39]) and JS-686 (originally compound **7** [40]).

Mouse and human GCPII exhibit similar substrate specificities

To obtain information about the substrate specificity of Avi-mGCPII, we screened 19 different dipeptide libraries of the general formula *N*-Ac-A-X [where A represents a given single N-terminal amino acid and X represents a mixture of 19 proteinogenic amino acids (all except for cysteine)]. The *N*-acetylated dipeptide libraries were incubated with the enzymes, and the cleaved amino acids were analyzed by HPLC [41]. As a negative control, the potent and selective GCPII inhibitor 2-PMPA was used to block the specific enzyme activity.

Overall, we found no significant differences in hydrolysis of dipeptide substrates between mouse and

human GCPII, as illustrated by heat maps showing mouse and human GCPII processing of individual *N*-acetylated dipeptides (Fig. 2). The enzymes exhibited a clear preference for glutamate in the C-terminal position (i.e., glutamate carboxypeptidase activity); mouse GCPII possesses higher selectivity toward the C-terminal glutamate.

GCPII is highly expressed in mouse kidney, brain, and major salivary glands

To analyze GCPII distribution in mouse tissues, we collected tissues samples from six mice (three females and three males) and analyzed them by western blot using the anti-GCPII antibody GCP-04 [2,42].

Mouse GCPII was expressed predominantly in the mouse kidney and brain (Fig. 3), which is in agreement with previous data [9]. Interestingly, we observed high and variable expression in the mouse major salivary glands. The different apparent molecular weights are likely caused by different glycosylation of GCPII in the tissues.

We also determined the NAAG-hydrolyzing activity in the tissue lysate samples using tritium-labeled NAAG as a substrate and compared these results with

Table 2. Inhibition of recombinant mouse and human GCPII (Avi-mGCPII and Avi-hGCPII, respectively) by a panel of GCPII inhibitors. Inhibition constants (K_i values) were determined using an HPLC-based assay using pteroyl-di-L-glutamate as a substrate. The values shown are mean \pm standard deviation of duplicate measurements.

| Compound | K_i (Avi-mGCPII) (nM) | K_i (Avi-hGCPII) (nM) |
|-----------------------------|-------------------------|-------------------------|
| Quisqualate | 580 \pm 60 | 520 \pm 80 |
| 2-PMPA | 0.56 \pm 0.05 | 0.26 \pm 0.03 |
| ZJ-43 | 5.9 \pm 0.9 | 0.58 \pm 0.07 |
| JB-352 | 0.66 \pm 0.06 | 0.17 \pm 0.04 |
| β -citryl-L-glutamate | 24 000 \pm 3000 | 16 000 \pm 5000 |
| DCIBzL | 0.028 \pm 0.003 | 0.017 \pm 0.002 |
| JB-277 | 0.68 \pm 0.07 | 0.05 \pm 0.02 |
| DKFZ-PSMA-11 | 0.10 \pm 0.01 | 0.018 \pm 0.002 |
| JS-686 | 0.049 \pm 0.005 | 0.021 \pm 0.004 |

the data obtained by western blot analysis. Recombinant mouse GCPII was used as a standard, and the observed levels of NAAG-hydrolyzing activity were

converted to amounts of GCPII, which were then normalized to the total protein concentrations in the homogenates (Fig. 4).

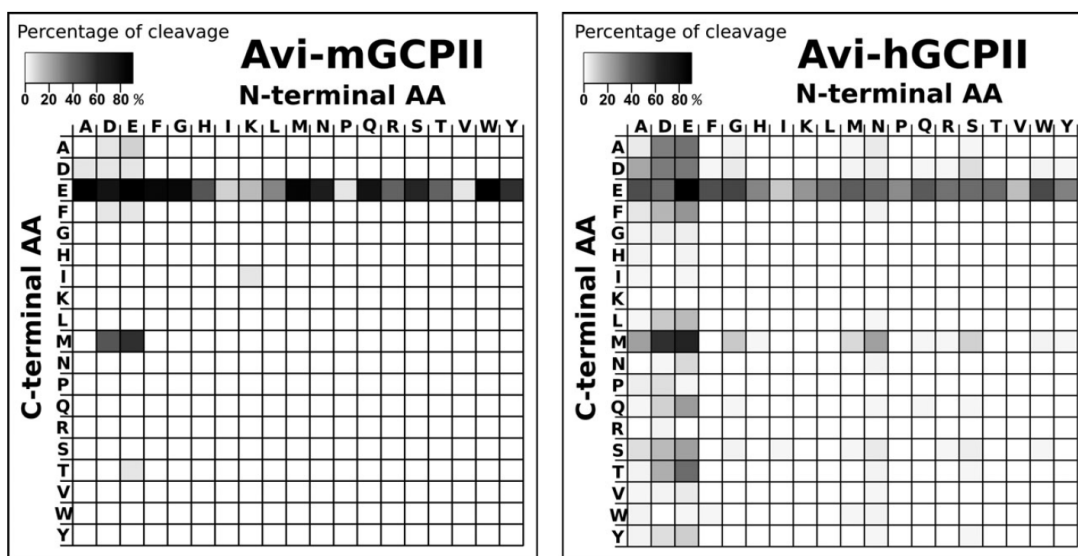


Fig. 2. Heat maps representing the substrate specificities of mouse and human GCPII. Recombinant mouse and human GCPII (Avi-mGCPII and Avi-hGCPII, respectively) were incubated with 19 dipeptide libraries of the general formula *N*-Ac-A-X-OH [where A represents a given single N-terminal amino acid and X represents a mixture of 19 proteinogenic amino acids (all except for cysteine)]. The samples were incubated for 1.5 h at 37 °C, and the cleaved C-terminal amino acids were quantified using HPLC. As negative controls, experiments either with the GCPII-specific inhibitor 2-PMPA or without Avi-mGCPII/Avi-hGCPII were performed. The grayscale key represents the percentage of conversion of the particular amino acid in the reaction mixture.

The results confirmed high expression of GCPII in the kidney, brain, and major salivary glands. We did not detect GCPII in the mouse prostate (Fig. 4).

To further examine the location of GCPII in the highly expressing tissues, we performed immunohistochemistry using the anti-GCPII antibody GCP-04 [2,42]. We found relatively high expression in the white matter in the brain, on luminal side of proximal tubules in the kidney and in the abluminal cells in the major salivary glands (mainly in the sublingual gland) (Fig. 5).

mRNA expression profile differentiates GCPII and GCPIII expression levels in mouse tissues

The GCP-04 antibody cross-reacts with GCPIII, which also cleaves NAAG [11,43]. Therefore, we decided to further analyze the tissue distribution of both homologs by quantitative RNA determination (qPCR). For these analyses, we used either commercially available panels of mouse tissue cDNA libraries (Fig. 6A) or cDNA libraries prepared from mouse tissues (female 1 and male 1; Fig. 6B,C).

The results from commercial cDNA libraries represent the average tissue distribution of both transcripts

in the mouse population. Each library was pooled from several hundred mice and normalized by the vendor to several different housekeeping genes (beta-actin, G3PDH, phospholipase A2, and ribosomal protein S29). The highest expression of mouse GCPII mRNA was in the kidney, brain, and testis, while mouse GCPIII mRNA was predominantly expressed in the testis, heart, lung, and skeletal muscle (Fig. 6A).

To gain insight into expression of both transcripts in individual mice, we also quantified mRNA transcripts in cDNA libraries prepared from mouse tissues dissected from one female and one male mouse. The results were normalized to the starting amount of total RNA and are in good agreement with findings from the pooled libraries (Fig. 6B,C).

Discussion

GCPII is a potential pharmaceutical target for a number of pathological conditions caused by glutamate excitotoxicity in the central nervous system, including stroke and traumatic brain injury. Moreover, GCPII has been intensively studied as a target for diagnosis and treatment of prostate cancer, as it is overexpressed in the malignant prostate. In last two decades, a large

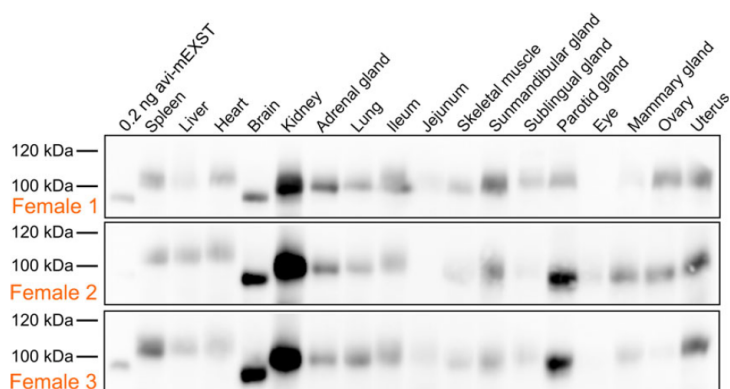


Fig. 3. Western blot analysis of GCPII expression in a panel of mouse tissues. Mouse tissue samples (from three males and three females) were homogenized, and lysates were resolved by SDS/PAGE (50 μ g of total protein per lane). Mouse GCPII was visualized using the anti-GCPII primary antibody GCP-04 [2] and HRP-conjugated goat anti-mouse secondary antibody.

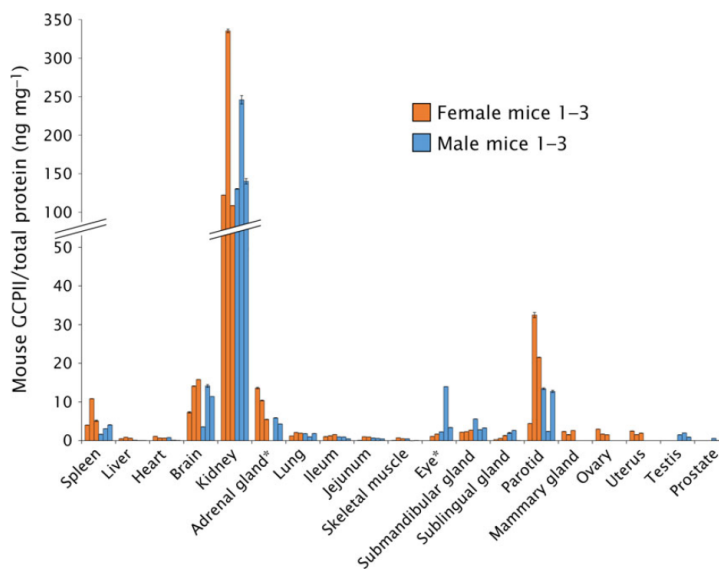
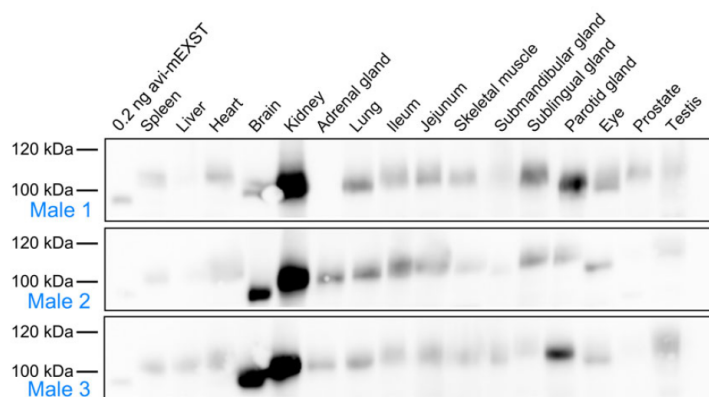


Fig. 4. GCPII expression in mouse tissues determined by radioenzymatic assay. The amount of GCPII in mouse tissues was determined by radioenzymatic assay using [3 H]NAAG as a substrate and recombinant mouse GCPII (Avi-mGCPII) as a standard. Each tissue sample was measured in duplicate using 1–50 μ g total protein in the reaction; the amount of mouse GCPII was normalized to total protein concentration (ng GCPII per mg total protein). The assay was performed with the same tissue samples used in the western blot analysis. *Not determined (adrenal gland: sample M1; eye: sample F1).

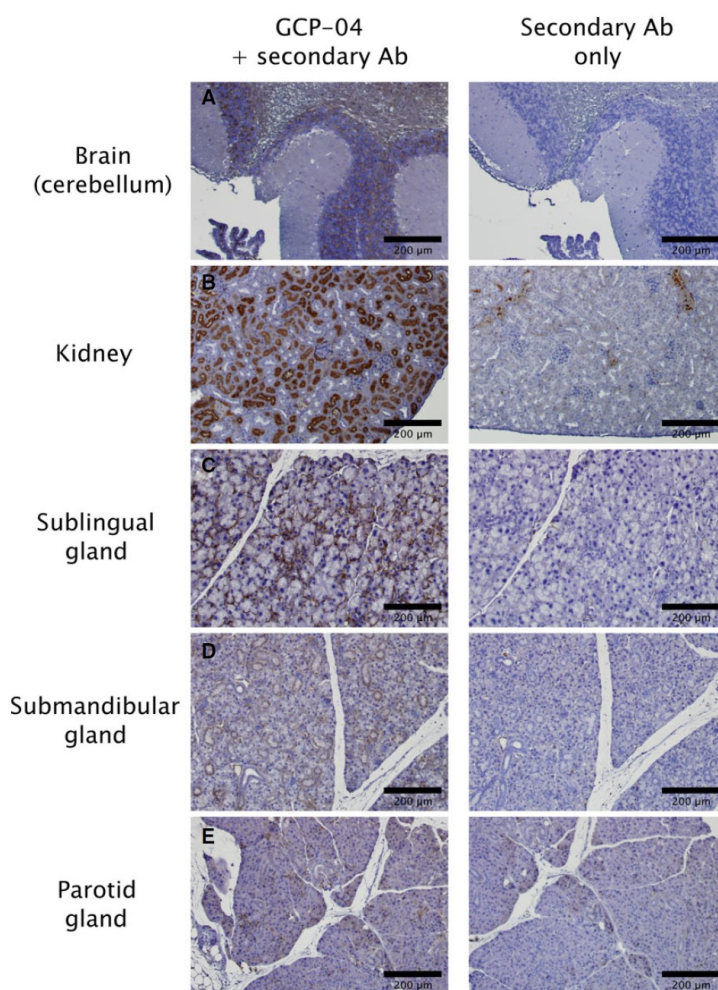


Fig. 5. Immunohistochemical staining of chosen mouse tissue sections. Formalin-fixed, paraffin-embedded mouse tissue sections were incubated with anti-GCPII antibody GCP-04 (at $10 \mu\text{g}\cdot\text{mL}^{-1}$ concentration) to visualize and localize mouse GCPII expression [42]. (A) Brain (cerebellum): positive choroid plexus, stratum granulare, white matter. (B) Kidney: positive luminal side of proximal tubules, Bowman capsule; little crossreactivity of secondary anti-mouse antibody with capillaries and blood vessels could be seen in the negative control. (C) Sublingual gland: positive staining of abluminal cells (probably myoepithelial cells). (D) Submandibular gland: faint staining of intercalated ducts and some non-glandular abluminal cells. (E) Parotid gland: faint staining of some non-glandular abluminal cells.

number of papers have been published describing novel GCPII inhibitors acting as neuroprotective drugs [28,44] and GCPII inhibitor-based tools for imaging and/or treating prostate cancer [19,20,45–47]. Most of these compounds and methods were evaluated using mouse models. However, there has been no direct comparison of mouse and human GCPII, which would provide important information to assess the usefulness of such mouse models. Therefore, we set out to perform a systematic and detailed study to compare the enzymatic properties of mouse and human GCPII, as well as tissue distributions on both the mRNA and protein levels.

We expressed the recombinant extracellular part of mouse GCPII with an N-terminal Avi-tag

(Avi-mGCPII), which enables fast and efficient one-step purification [34]. Even though GCPII is a transmembrane enzyme, its extracellular domain is the catalytically active portion and correctly represents endogenous full-length GCPII [33]. To compare the enzymatic properties of mouse and human GCPII, we analyzed the cleavage of their substrates: *N*-acetyl-L-aspartyl-L-glutamate (NAAG), which is cleaved by GCPII in the brain, and pteroyl-di-L-glutamate, which is a model substrate for poly-gamma-glutamylated folates hydrolyzed by GCPII in the small intestine. Because mouse and human GCPII have high sequence similarity (86% identity and 97% similarity in the extracellular part; Fig. 7), we did not expect to find any significant differences in their enzymatic

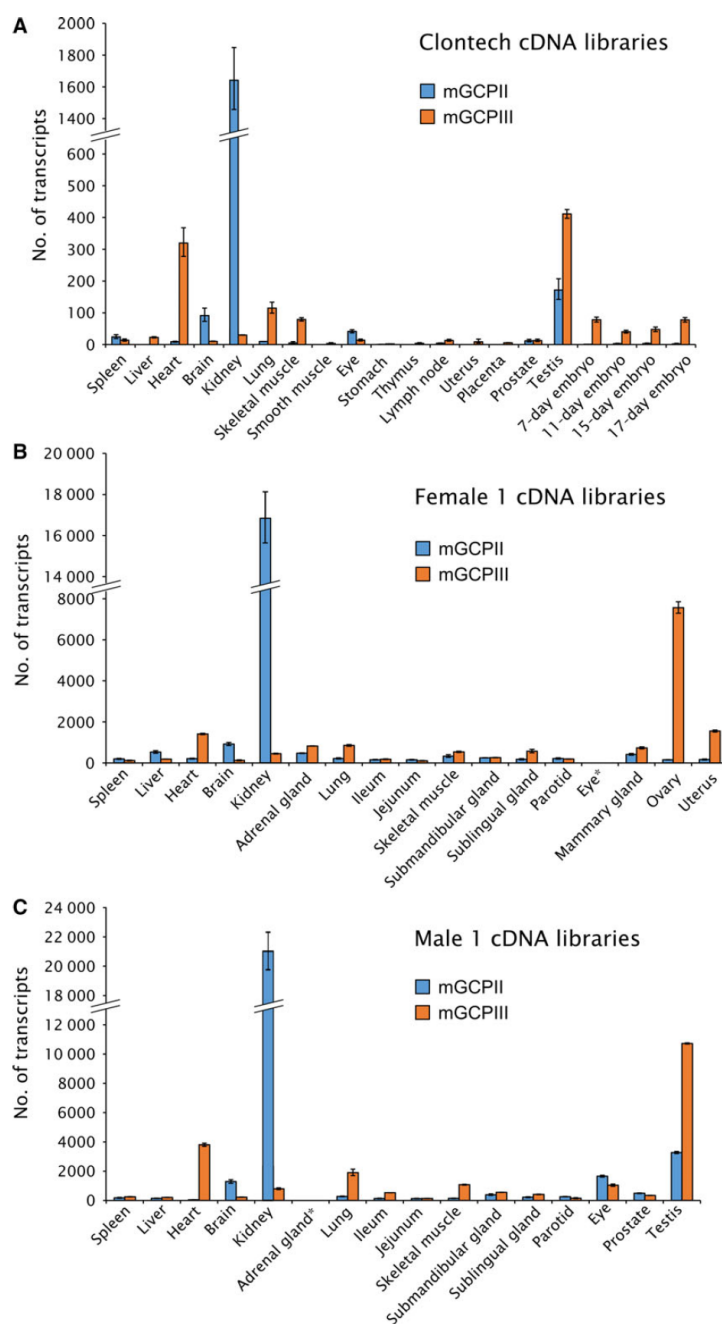


Fig. 6. Quantification of mouse GCPII and GCPIII (mGCPII and mGCPIII, respectively) transcripts using qPCR. (A) Quantification of mGCPII and mGCPIII transcripts using qPCR in commercial mouse tissue cDNA libraries from Clontech. The 'number of transcripts' corresponds to the amount of transcripts in 1.0 μ L of 10-fold diluted cDNA libraries (for experimental details, see Experimental procedures). Error bars show standard deviations from triplicate measurements. (B, C) Quantification of mGCPII and mGCPIII transcripts using qPCR in cDNA libraries prepared from mouse tissues dissected from one female (B) and one male mouse (C). The 'number of transcripts' corresponds to the amount of transcripts per 10 ng of total RNA as a starting material for cDNA synthesis (for experimental details, see Experimental procedures). Error bars show standard deviations from triplicate measurements. *Not determined.

properties. In fact, we found that while the enzymes are quite similar in NAAG-hydrolyzing activity, there is an order-of-magnitude difference in their catalytic

efficiencies for cleavage of pteroyl-di-L-glutamate. This difference lies in the K_M values of mouse and human GCPII (290 vs. 39 nM for pteroyl-di-L-glutamate and

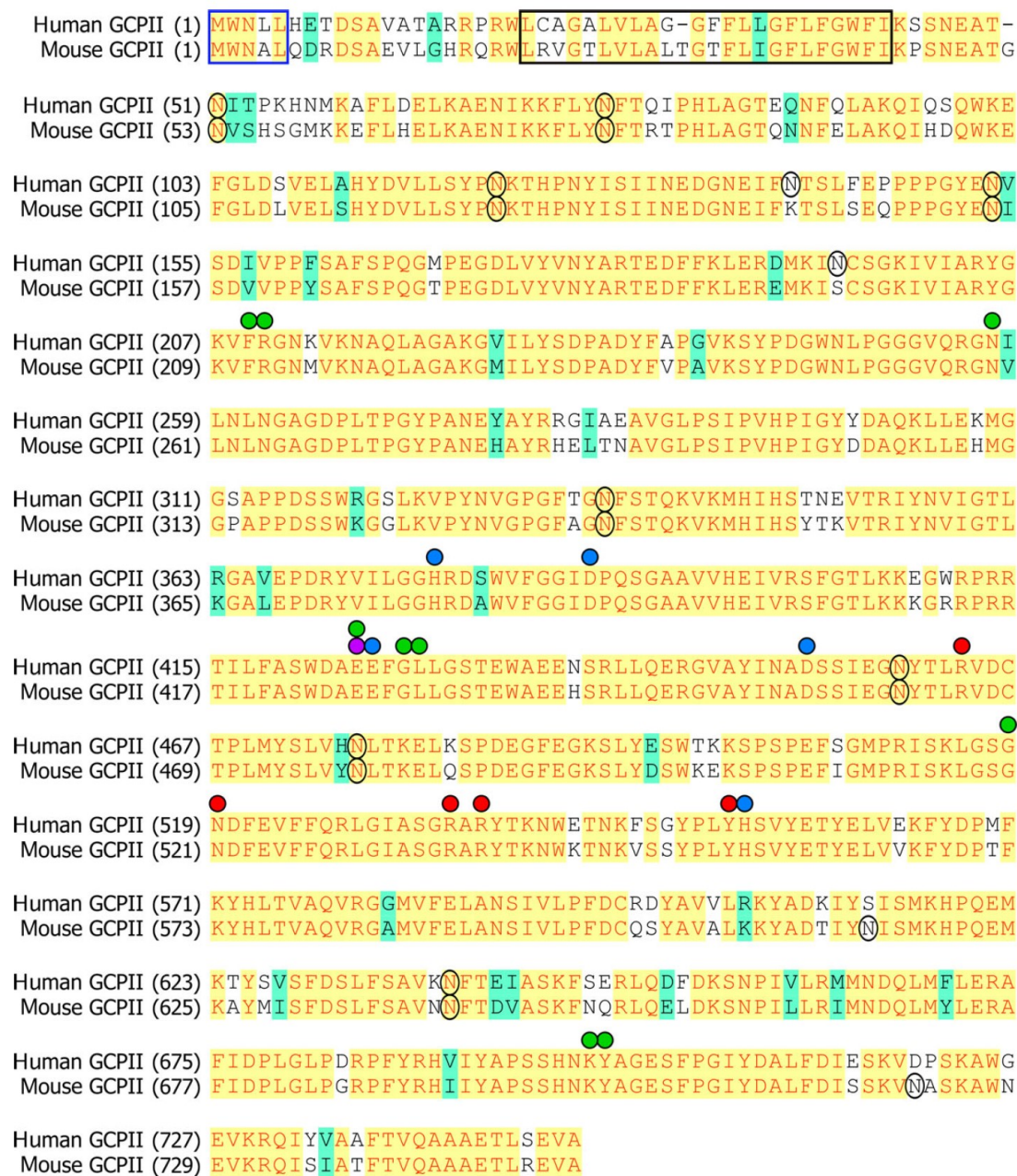


Fig. 7. Sequence alignment of the mouse and human GCPII proteins. Identical amino acid residues are highlighted in yellow, similar residues in green, and different residues in white. A blue frame marks the internalization signal MXXXL [54], and a black frame corresponds to predicted GCPII transmembrane domain (predicted by TMHMM Server v. 2.0). Black circles denote potential N-glycosylation sites ('N-X-S/T'). Green spheres: residues defining the S1' pocket [49]; red spheres: residues forming the S1 pocket [48]; purple sphere: proton shuttle catalytic base [55]; blue spheres: zinc ligands [56,57].

1900 vs. 550 nm for NAAG). Their turnover numbers are quite similar (3.6 vs. 5.1 s⁻¹ and 1.4 vs. 1.5 s⁻¹, respectively) (see Table 1). Slightly surprisingly, our data revealed that the catalytic efficiency of NAAG cleavage by mouse and human GCPII is significantly lower than that of pteroyl-di-L-glutamate cleavage (20-fold and 50-fold, respectively) (see Table 1).

Additionally, we analyzed the inhibition profile of Avi-mGCPII using several GCPII inhibitors commonly used in research, including 2-PMPA, ZJ-43, DCIBzL, DKFZ-PSMA-11, and quisqualate. We also tested several other inhibitors that were prepared in our laboratory. Generally, we did not observe considerable differences in the K_i values obtained for mouse and human GCPII. However, inhibitors ZJ-43 and JB-277 were exceptions; the K_i values for Avi-mGCPII were 10-fold higher (Table 2). Both compounds belong to the urea-based group of GCPII inhibitors, together with DCIBzL. Surprisingly, the K_i value of DCIBzL was identical for both enzymes. As seen in Fig. 7, mouse and human GCPII are highly similar and key amino acid residues participating in substrate binding and hydrolysis are identical [48–50]. Thus, in the absence of an experimentally determined structure of mouse GCPII, it is difficult to explain the observed differences in inhibitor binding and catalytic efficiency.

Next, we assessed the substrate specificity of Avi-mGCPII. We screened dipeptide libraries covering almost all *N*-acetylated dipeptide substrates, not including cysteine-containing dipeptides. Unsurprisingly, mouse GCPII exhibited a strong preference for glutamate in the P1' position, cleaving almost any dipeptide with a C-terminal glutamate (i.e., glutamate carboxypeptidase activity). It also cleaves dipeptides with methionine in the P1' position and an acidic amino acid (aspartate or glutamate) in the P1 position. Dipeptides containing any other C-terminal amino acid were not hydrolyzed by mouse GCPII. The substrate specificity of mouse GCPII thus seems to be even more pronounced than that of the human enzyme (Fig. 2).

In addition to the enzymatic properties of mouse GCPII, its tissue distribution is a relevant aspect both to understand the physiological function of the enzyme and to assess the use of mouse models for targeted drug delivery and GCPII inhibition experiments. Therefore, we set out to elucidate GCPII expression in mouse tissues. To see individual differences, we collected tissue samples from six mice (three females and three males).

To assess GCPII expression on the protein level, we prepared mouse tissue lysates and detected mouse GCPII by western blot using the anti-GCPII antibody GCP-04, which was raised against human GCPII

[2,42]. Because GCP-04 recognizes a linear epitope in the GCPII primary structure (amino acids 100–104: WKEFG [22]), which is conserved in the mouse GCPII sequence, the antibody can be used for selective and sensitive detection of mouse GCPII as well. We confirmed very high expression of GCPII in the mouse kidney and high expression in the mouse brain, which is in agreement with high GCPII expression in the corresponding human tissues [22]. Furthermore, we observed high expression of GCPII in the mouse major salivary glands. Relatively high variability among individual samples of major salivary glands is probably caused by close association of salivary glands that are macroscopically quite similar. This makes the proper dissection of topographically complicated ventral cervical region particularly cumbersome and might lead to cross-contamination. Therefore, we localized GCPII expression by immunohistochemistry using anti-GCPII antibody GCP-04. We observed GCPII expression in all three salivary glands (sublingual, submandibular, and parotid); however, GCPII is expressed predominantly in the sublingual gland, while the expression in the submandibular and parotid glands is lower (Fig. 5).

Mouse prostate contains negligible levels of GCPII, which is consistent with previous findings [9] and in contrast with human prostate, which expresses large amounts of GCPII [6,22,51]. Additionally, as human and mouse prostates differ considerably in their morphology, we dissected a mouse prostate into its individual parts (anterior, dorsal, and lateral prostate) and searched for potential GCPII expression in each part separately. Nevertheless, we did not detect GCPII expression in any of the tested parts of mouse prostate. Our data suggest that GCPII might also be absent in the mouse jejunum, a tissue where human GCPII cleaves off glutamates from glutamylated folates [17]. Rat jejunum and ileum were shown not to contain GCPII, in contrast to the corresponding human tissues, which express large amounts of GCPII [22]. Folates in rat intestine are hydrolyzed by γ -glutamyl hydrolase, not GCPII [52], and the situation in mice may be thus similar.

Furthermore, we verified GCPII tissue distribution obtained by western blot analysis by quantification of NAAG-hydrolyzing activity in mouse tissues. The activity-based GCPII expression profile correlated well with the western blot results, confirming strong GCPII expression in the mouse kidney, brain, and salivary glands and no expression in mouse prostate and jejunum.

GCPIII is a close GCPII homolog found both in humans and in mouse. The GCP-04 antibody also

recognizes GCPIII but is roughly 10-fold less sensitive toward GCPIII than toward GCPII [42]. Moreover, GCPIII also hydrolyzes NAAG, although with a lower catalytic efficiency [10,11,43]. Therefore, GCPII distribution in mouse tissues obtained by western blot analysis with GCP-04 and activity assay based on NAAG hydrolysis could be distorted by a high amount of GCPIII and low amount of GCPII in a particular tissue. Because there is no specific antibody against GCPIII, we explored GCPII/GCPIII expression in mouse tissues on the mRNA level to differentiate between the two homologs. We quantified GCPII and GCPIII transcripts in both commercially available mouse tissue cDNA libraries and cDNA libraries we prepared from isolated mouse tissues (Fig. 6). Taking these qPCR data into account, GCPIII appears to be the source of the NAAG-hydrolyzing activity in the mouse ovary, uterus, and heart. GCPIII was most strongly expressed in the testis but was accompanied by rather high quantities of GCPII.

To conclude, we prepared and characterized recombinant mouse GCPII and compared it with human GCPII. We found that the differences in enzymatic activity, inhibition profile, and substrate specificity between mouse and human GCPII are rather small; therefore, mouse GCPII can serve as a suitable substitute for human GCPII in enzymological studies.

Due to the observed lack of GCPII expression in the mouse prostate, mouse might not seem to be an ideal model for the development of prostate cancer diagnostic/therapeutic agents. However, most such studies employ human tumor xenografts in mouse models. For this purpose, mice are generally suitable, because the distribution of GCPII in other tissues is quite similar to that in humans. Therefore, mouse GCPII appears to be a good model for the development of GCPII-targeted drugs for treatment of prostate cancer and neuronal disorders.

Experimental procedures

Cloning of mouse GCPII (Avi-mGCPII)

The pIRES/mGCPII plasmid encoding full-length mouse GCPII (amino acids 1-752) was a kind gift from Warren Heston (Cleveland Clinic, USA).

Because the sequence contained two conflicts compared to the annotated mouse GCPII sequence, we performed site-directed mutagenesis to remove them (G240A and E287N). The primers 5'-gctgactactttgttctcGCGgtgaagtcctatcc-3' and 5'-ggataggactcacCGCaggaacaagtagtcagc-3' were used to remove the sequence conflict at position 240,

and the primers 5'-catgagttgacaAACgctgttgccctc-3' and 5'-gaaggccaacagcGTTgtcaactcatg-3' to remove the sequence conflict at position 287 (changed deoxyribonucleotides are underlined, changed codons capitalized). The mutagenesis was carried out according to the manufacturer's protocol (QuikChange™ Site-Directed Mutagenesis; Stratagene, San Diego, CA, USA).

Then, the sequence corresponding to the extracellular part of mouse GCPII (amino acids 45-752) was amplified by PCR using primers 5'-aaaagatctaaacctccaatgaagctactgg-3' and 5'-aaactcgagttaagctactcctcagagtc-3' (restriction sites introduced into the sequence are underlined; the primers introduced a *Bgl*II site at the 5' end and an *Xho*I site at the 3' end). The resulting DNA fragment was cleaved with *Bgl*II and *Xho*I and ligated into pMT/BiP/AviTEV/rhGCPII plasmid [34] cleaved with the same endonucleases. The correct sequence of the resulting plasmid pMT/BiP/Avi-mGCPII was verified by DNA sequencing.

Transfection of *Drosophila* S2 cells and expression of Avi-mGCPII

Drosophila S2 cells expressing BirA biotin-protein ligase localized in the endoplasmic reticulum (described in Ref. [34]) were used to prepare stable Avi-mGCPII transfectants. The cells were transfected using Calcium Phosphate Transfection Kit (Invitrogen, Waltham, MA, USA) with 9 µg of pMT/BiP/Avi-mGCPII together with 0.5 µg of pCoBlast (Invitrogen), as previously described [10]. The transfected cells were cultivated in the presence of both blasticidin (5 µg·mL⁻¹, Invitrogen) and hygromycin B (300 µg·mL⁻¹; Invitrogen).

To express Avi-mGCPII, approximately 2 × 10⁶ stably transfected cells was transferred into a 35-mm Petri dish supplemented with 2 mL SF900II medium (Invitrogen). The following day, protein expression was induced by adding CuSO₄ (Sigma-Aldrich, St. Louis, MO, USA) to a final concentration of 1 mM. After three days, cells were harvested by centrifugation, and the medium was analyzed by western blot.

The large-scale expression of Avi-mGCPII was performed as previously described [33]. The final volume of cell suspension was 1000 mL.

Purification of Avi-mGCPII

Purification of Avi-mGCPII was performed as previously described [34]. Briefly, cell medium (1000 mL) containing secreted biotinylated Avi-mGCPII was centrifuged at 3400 g for 45 min. Then, it was concentrated 10-fold using a LabScale TFF System (Merck Millipore, Billerica, MA, USA) with a Pellicon® XL 50 Cassette, Biomax 100. The concentrated medium was centrifuged again at 3400 g for 20 min and equilibrated with 300 mM Tris/HCl, 450 mM NaCl, pH 7.2 in a 2 : 1 ratio. The equilibrated

concentrated Avi-mGCPII medium was then mixed with 1 mL Streptavidin Mutein Matrix (Roche, Basel, Switzerland) and incubated with gentle shaking at 6 °C for 15 h. Afterward, the resin was washed with 50 column volumes of 100 mM Tris/HCl, 150 mM NaCl, pH 7.2. Bound biotinylated proteins were eluted with 5 mL of 100 mM Tris/HCl, 150 mM NaCl, 2 mM D-biotin, pH 7.2, in five consecutive elution fractions (after the first elution fraction, the resin was incubated with elution buffer for 1 h). After regeneration of the resin, the flow-through fraction was again mixed with the resin, and the purification procedure was repeated.

Determination of kinetic parameters by radioenzymatic assay

Kinetic parameters (K_M and k_{cat}) of *N*-acetyl-L-aspartyl-L-glutamate (NAAG) cleavage by Avi-mGCPII were determined as previously described [34], with a minor modification: The reactions were performed in a 96-well plate, and appropriate amounts of Avi-mGCPII were mixed with 25 mM Bis-Tris propane, 150 mM NaCl, 0.001% octaethylene glycol monododecyl ether (Affymetrix, Santa Clara, CA, USA), pH 7.4.

Determination of kinetic and inhibition constants by HPLC

Kinetic parameters (K_M and k_{cat}) of pteroyl-di-L-glutamate cleavage by Avi-mGCPII, as well as K_i values for all inhibitors, were determined as previously described [39]. Briefly, in a 96-well plate, Avi-mGCPII was mixed with 25 mM Bis-Tris propane, 150 mM NaCl, 0.001% octaethylene glycol monododecyl ether (Affymetrix), pH 7.4 (and tested inhibitor, if used), into a final volume of 90 μ L. Reactions were started by adding 10 μ L of 4 μ M pteroyl-di-L-glutamate and incubated at 37 °C for 20 min. The reactions were stopped with 20 μ L of 25 μ M 2-PMPA and subsequently analyzed on an Agilent 1200 Series system using an Acquity UPLC HSS T3 1.8 μ m column (2.1 \times 100 mm; Waters, Milford, MA, USA).

Animals and tissue isolation

Six C57BL/GJ mice (three males (M) and three females (F)) were sacrificed by cervical dislocation with agreement of the local ethical commission. The ages of the mice were as follows: M1: 5 months; M2: 8 months; M3: 12 months; F1: 8 months; F2 and F3: 12 months. Samples of tissues (for preparation of tissue lysates) were immediately transferred into microtubes and frozen at -80 °C. Samples of tissues (for qPCR quantification) were immediately transferred into RNAlater, impregnated with it for 2 days at 4 °C, and then stored at -80 °C.

Tissue lysate sample preparation

A small piece of tissue (approx. 30 mg) was transferred into 250 μ L of 50 mM Tris/HCl, 100 mM NaCl, pH 7.4, in a 2-mL microtube. Tissue samples were homogenized using TissueLyser II (30 Hz, 3 min). The homogenates were then diluted with 250 μ L of the lysis buffer. Octaethylene glycol monododecyl ether (Affymetrix) was added to reach 1% final concentration, and the homogenate was sonicated in a water bath for 5 min at 0 °C. Finally, the samples were centrifuged at 600 *g* for 15 min, and the resulting supernatant was stored at -80 °C until further use. The lysate protein concentration was determined using Bradford 1 \times Dye Reagent (Bio-Rad, Hercules, CA, USA).

Radioenzymatic determination of NAAG-hydrolyzing activity in mouse tissues

The determination of NAAG-hydrolyzing activity in mouse tissues was performed as previously described [53]. A sample of tissue lysate was mixed with 20 mM Tris/HCl, 150 mM NaCl, 0.1% Tween 20, pH 7.4, to a final volume of 90 μ L. Reactions were started by adding 10 μ L of 1 μ M NAAG (containing 50 nM tritium-labeled NAAG), and incubated at 37 °C for 15 h. The reactions were stopped with 100 μ L of ice-cold 200 mM KH_2PO_4 , 2 mM 2-mercaptoethanol, pH 7.4. The released glutamate was separated from the unreacted substrate using ion-exchange AG1-X resin (Bio-Rad). The radioactivity of the sample was quantified by liquid scintillation using the Rotiszint ECO Plus scintillation cocktail (Roth) in a Tri-Carb Liquid Scintillation Counter (Perkin-Elmer, Waltham, MA, USA). The samples were measured in duplicate.

SDS/PAGE and western blotting

Protein samples were resolved by reducing SDS/PAGE. Proteins were electroblotted onto a nitrocellulose membrane (wet blotting: 100 V/1 h). After blotting, the membrane was blocked with 0.55% (w/v) casein solution in PBS (Casein Buffer 20X-4X Concentrate, SDT, Baesweiler, Germany) at room temperature for 1 h. To visualize GCPII, the blots were probed with the antibody GCP-04 (described in [2]) for 12 h at 4 °C (200 ng·mL⁻¹; diluted in 0.55% casein solution), washed three times with PBS containing 0.05% Tween 20 (PBST buffer), and incubated with goat anti-mouse antibody conjugated with horseradish peroxidase (Thermo Scientific, Waltham, MA, USA; diluted in 0.55% casein solution, 1 : 25 000). The blots were then washed three times with PBST to remove unbound antibodies and developed with SuperSignal West Femo Chemiluminescent Substrate (Thermo Scientific).

Chemiluminescence was captured with a ChemiDoc-It™ 600 Imaging System (UVP, Upland, CA, USA).

Immunohistochemistry

Immunohistochemistry was performed according to the protocol described previously using anti-GCPII antibody GCP-04 [2] with minor modifications [42]. Briefly, after standard histological processing (fixation, dehydration, embedding into paraffin, cutting, paraffin removal, rehydration), heat antigen retrieval was performed using 10 mM sodium citrate, 0.1% Tween 20, pH 6.0 buffer and heating to 110 °C for 15 min in an autoclave. Afterward, samples were incubated in 1.5% hydrogen peroxide solution for 20 min to reduce endogenous peroxidase activity and in 10% fetal bovine serum in PBS to block unspecific interactions. The slides were then stained by primary anti-GCPII antibody GCP-04 (10 µg·mL⁻¹ in 4 °C, overnight), followed by extensive washing (five times with PBS containing 0.1% Tween 20) and incubation with secondary antibody Histofine® Simple Stain™ MAX PO (MULTI) (Nichirei Bioscience Inc., Tokyo, Japan) diluted 1 : 2 with 10% fetal bovine serum in PBS at room temperature for 1 h. After further extensive washing (five times with PBS containing 0.1% Tween 20), GCPII was visualized using DAB/Plus kit (Diagnostic BioSystems, Pleasanton, CA, USA, 60 s). The slides were counterstained with Harris' hematoxylin and mounted in polyvinyl alcohol-based media.

Carboxypeptidase activity assay

Carboxypeptidase activity (i.e., substrate specificity) of mouse GCPII was determined using *N*-Ac-A-X peptide libraries according to a previously published method [41]. Briefly, 1.2 µg Avi-mGCPII was diluted into 25 mM Bis-Tris propane, 150 mM NaCl, 0.001% octaethylene glycol monododecyl ether (Affymetrix), pH 7.4, and incubated in the presence of 25 µM dipeptide for 1.5 h at 37 °C. As negative controls, reactions without the enzyme and in the presence of 1 mM 2-PMPA, a highly selective GCPII inhibitor, were performed. The reaction mixture was then analyzed using HPLC, as previously described [41].

Total RNA isolation and reverse transcription

First, tissue samples were transferred from RNA later solution (Invitrogen, #AM7021) to RLT buffer (part of the RNEasy Mini Kit, Qiagen, Hilden, Germany, #74106) supplied with β-mercaptoethanol and homogenized with 5-mm steel beads (Qiagen; #69989) using TissueLyser II (#85300; Qiagen). Total RNA was isolated using RNEasy Mini Kit according to the manufacturer's instructions. The concentration and purity of isolated RNA were determined spectrophotometrically using a Nanodrop ND-1000 spectrophotometer. The integrity of each RNA sample was

analyzed using the Agilent RNA 6000 Nano kit run on an Agilent 2100 Bioanalyzer. Only samples without significant degradation were used for subsequent steps.

RNA was then reverse-transcribed using M-MLV (#28025013; Invitrogen) according to the manufacturer's instructions. Each 20 µL reaction contained up to 2 µg total RNA, 2.5 µM oligo(dT)₂₀ primers (#18418020; Invitrogen), 50 ng random hexamers (100 ng if more than 1 µg RNA was transcribed), 40 units of RNaseOUT, 200 units of M-MLV reverse transcriptase, and other components as specified by the manufacturer.

Quantitative PCR (qPCR) analysis

All qPCRs were carried out in triplicate in FrameStar 480/96 multiwell plates (#4ti-0951; 4titude, Wotton, UK) sealed with adhesive optical foil (#4729692001; Roche) using a LightCycler 480 II instrument (Roche) in a total volume of 10 µL. Each reaction consisted of LightCycler 480 Probe Master (Roche) diluted according to the manufacturer's instructions, forward and reverse primers (1 µM final concentration each), fluorescent probe (see description of individual assays for final concentration), and 1 µL of sample or template DNA (positive and nontemplate controls as well as interplate calibrators were included on each plate). Initial denaturation for 3 min at 95 °C was followed by 45 cycles of 10 s at 95 °C, 30 s at 66 °C, and 30 s at 72 °C. The threshold cycle numbers (*C_q*) were then determined from fluorescence intensities acquired during the qPCR runs by the second-derivative maximum method using LightCycler 480 software (Roche). The presence and size of PCR products were analyzed by agarose gel electrophoresis.

The amount of mouse GCPII (encoded by the gene *Folh1*) was quantified by an assay set of forward and reverse primers (sequences 5'-gattgccagatatgggaaagtg-3' and 5'-ctgccagtggagctttt-3') and fluorescent hydrolysis probe #6 from the Roche Universal Probe Library (LNA octamer sequence 5'-cagaggaa-3'; final concentration 100 nM). This set was designed to amplify nucleotides 714–773 in mouse GCPII transcript NM_016770 to yield an amplified product of 60 bps, which spans the region of exons 5 and 6 and corresponds to amino acids 202–223 in the longest open reading frame (ORF). This assay should not amplify genomic sequence because it spans a 1029-bp intron.

The amount of mouse GCPIII transcript (encoded by the gene *Naalad2*) was quantified by an assay set of forward and reverse primers (sequences 5'-aatgatcagagagacattaccg-3' and 5'-ccagctttgtctggtggag-3') and fluorescent hydrolysis probe #52 from the Roche Universal Probe Library (LNA octamer sequence 5'-gggaggag-3'; final concentration 50 nM). This set was designed to amplify nucleotides 922–981 in mouse GCPIII transcript NM_028279 to yield an amplified product of 60 bps, which spans the region of exons 7 and 8 and corresponds to

amino acids 289–309 in the longest ORF. This assay should not amplify genomic sequence because it spans a 880-bp intron.

As a standard for absolute quantification, serial 10-fold dilutions covering concentrations from 10^8 to 10^2 copies per reaction of either pcDNA4 plasmid with subcloned coding sequence of full-length mouse GCPII (longest ORF from NM_016770 coding amino acids 1–752) or pMT/BiP plasmid with subcloned coding sequence of extracellular part of mouse GCPIII (part of longest ORF from NM_028279 coding amino acids 36–740) were amplified with the corresponding assay set. The initial concentration of plasmid DNA (purified by QIAprep Spin Miniprep Kit, #27106; Qiagen) prior to dilution was determined spectrophotometrically at 260 nm (Nanodrop ND-1000; Thermo Scientific).

To enable precise absolute comparison between the determined amounts of both transcripts, obtained calibration curves were further normalized against each other by quantification of a common region of both plasmids. The region containing the ampicillin resistance gene was quantified by a set of primers with sequences 5'-gcagaagtgtctgccaact-3' and 5'-agcttcccggcaacaatta-3' and fluorescent hydrolysis probe #58 from the Roche Universal Probe Library (final concentration 50 nM). In this way, two calibration curves were obtained for each plasmid, one for the amplification of target transcript and one for the common sequence. Finally, the slope and intercept values of both curves were transformed for each plasmid so that the transformed slope and intercept values of the curves for the common sequence were equal between the two plasmids and corresponded to the average value between the two plasmids.

The amount of both transcripts was determined in the prepared tissue cDNA libraries. In each qPCR, an amount of cDNA corresponding to the starting amount of total RNA of 5–10 ng was used, and the amount of GCPII and GCPIII transcripts were normalized to the total amount of RNA. Both transcripts were also quantified in 1.0 μ L of 10-fold diluted commercial tissue cDNA libraries (Mouse MTC Panels I and III supplied by Clontech, Mountain View, CA, USA, #636745 and 636757), which had been normalized to several control genes by the vendor (beta-actin, G3PDH, phospholipase A2, and ribosomal protein S29).

Statistical analysis

All values are presented as the mean \pm standard deviation.

Acknowledgements

We would like to thank Warren Heston (Lerner Research Institute, Cleveland Clinic) for providing us with a plasmid encoding mouse GCPII, Jana Starková

and Karolína Šrámková for their excellent technical support, Radko Souček for HPLC analyses, and Hillary Hoffman for language editing. This work was supported by Grant No. GA16-02938S from the Grant Agency of the Czech Republic and InterBioMed Project LO 1302 from the Ministry of Education of the Czech Republic.

Author contributions

The manuscript was written through contributions of all authors. All authors have given approval to the final version of the manuscript. JK and PS conceived the project and analyzed data, TK, BV, JT, VN, PS and JK wrote the manuscript, TK, BV, VN, JT, FS, SV and MF designed, performed and interpreted the experiments.

References

- Berger UV, Carter RE, Mckee M and Coyle JT (1995) N-acetylated alpha-linked acidic dipeptidase is expressed by non-myelinating Schwann-cells in the peripheral nervous-system. *J Neurocytol* **24**, 99–109.
- Sacha P, Zamecnik J, Barinka C, Hlouchova K, Vicha A, Mlcochova P, Hilgert I, Eckschlager T and Konvalinka J (2007) Expression of glutamate carboxypeptidase II in human brain. *Neuroscience* **144**, 1361–1372.
- Bostwick DG, Pacelli A, Blute M, Roche P and Murphy GP (1998) Prostate specific membrane antigen expression in prostatic intraepithelial neoplasia and adenocarcinoma: a study of 184 cases. *Cancer* **82**, 2256–2261.
- Silver DA, Pellicer I, Fair WR, Heston WD and Cordon-Cardo C (1997) Prostate-specific membrane antigen expression in normal and malignant human tissues. *Clin Cancer Res* **3**, 81–85.
- Pinto JT, Suffoletto BP, Berzin TM, Qiao CH, Lin SL, Tong WP, May F, Mukherjee B and Heston WDW (1996) Prostate-specific membrane antigen: a novel folate hydrolase in human prostatic carcinoma cells. *Clin Cancer Res* **2**, 1445–1451.
- Kinoshita Y, Kuratsukuri K, Landas S, Imaida K, Rovito PM Jr, Wang CY and Haas GP (2006) Expression of prostate-specific membrane antigen in normal and malignant human tissues. *World J Surg* **30**, 628–636.
- Robinson MB, Blakely RD, Couto R and Coyle JT (1987) Hydrolysis of the brain dipeptide N-acetyl-L-aspartyl-L-glutamate. Identification and characterization of a novel N-acetylated alpha-linked acidic dipeptidase activity from rat brain. *J Biol Chem* **262**, 14498–14506.

- 8 Horoszewicz JS, Kawinski E and Murphy GP (1987) Monoclonal-antibodies to a new antigenic marker in epithelial prostatic cells and serum of prostatic-cancer patients. *Anticancer Res* **7**, 927–936.
- 9 Bacich DJ, Ramadan E, O’Keefe DS, Bukhari N, Wegorzewska I, Ojeifo O, Olszewski R, Wrenn CC, Bzdega T, Wroblewska B *et al.* (2002) Deletion of the glutamate carboxypeptidase II gene in mice reveals a second enzyme activity that hydrolyzes N-acetylaspartylglutamate. *J Neurochem* **83**, 20–29.
- 10 Hlouchova K, Barinka C, Klusak V, Sacha P, Mlcochova P, Majer P, Rulisek L and Konvalinka J (2007) Biochemical characterization of human glutamate carboxypeptidase III. *J Neurochem* **101**, 682–696.
- 11 Collard F, Vertommen D, Constantinescu S, Buts L and Van Schaftingen E (2011) Molecular identification of beta-citrylglutamate hydrolase as glutamate carboxypeptidase 3. *J Biol Chem* **286**, 38220–38230.
- 12 Slusher BS, Vornov JJ, Thomas AG, Hurn PD, Harukuni I, Bhardwaj A, Traystman RJ, Robinson MB, Britton P, Lu XCM *et al.* (1999) Selective inhibition of NAALADase, which converts NAAG to glutamate, reduces ischemic brain injury. *Nat Med* **5**, 1396–1402.
- 13 Neale JH, Olszewski RT, Gehl LM, Wroblewska B and Bzdega T (2005) The neurotransmitter N-acetylaspartylglutamate in models of pain, ALS, diabetic neuropathy, CNS injury and schizophrenia. *Trends Pharmacol Sci* **26**, 477–484.
- 14 Wroblewska B, Wroblewski JT, Pshenichkin S, Surin A, Sullivan SE and Neale JH (1997) N-acetylaspartylglutamate selectively activates mGluR3 receptors in transfected cells. *J Neurochem* **69**, 174–181.
- 15 Bruno V, Wroblewska B, Wroblewski JT, Fiore L and Nicoletti F (1998) Neuroprotective activity of N-acetylaspartylglutamate in cultured cortical cells. *Neuroscience* **85**, 751–757.
- 16 Halsted CH, Ling EH, Luthi-Carter R, Villanueva JA, Gardner JM and Coyle JT (1998) Folylpoly-gamma-glutamate carboxypeptidase from pig jejunum – molecular characterization and relation to glutamate carboxypeptidase II. *J Biol Chem* **273**, 20417–20424.
- 17 Chandler CJ, Wang TT and Halsted CH (1986) Pteroylpolyglutamate hydrolase from human jejunal brush borders. Purification and characterization. *J Biol Chem* **261**, 928–933.
- 18 Mhaweck-Fauceglia P, Zhang S, Terracciano L, Sauter G, Chadhuri A, Herrmann FR and Penetrante R (2007) Prostate-specific membrane antigen (PSMA) protein expression in normal and neoplastic tissues and its sensitivity and specificity in prostate adenocarcinoma: an immunohistochemical study using multiple tumour tissue microarray technique. *Histopathology* **50**, 472–483.
- 19 Chen Z, Penet MF, Nimmagadda S, Li C, Banerjee SR, Winnard PT Jr, Artemov D, Glunde K, Pomper MG and Bhujwala ZM (2012) PSMA-targeted theranostic nanoplex for prostate cancer therapy. *ACS Nano* **6**, 7752–7762.
- 20 Heck MM, Retz M, D’Alessandria C, Rauscher I, Scheidhauer K, Maurer T, Storz E, Janssen F, Schottelius M, Wester HJ *et al.* (2016) Systemic radioligand therapy with (177)Lu labeled prostate specific membrane antigen ligand for imaging and therapy in patients with metastatic castration resistant prostate cancer. *J Urol* **196**, 382–391.
- 21 Hrkach J, Von Hoff D, Ali MM, Andrianova E, Auer J, Campbell T, De Witt D, Figa M, Figueiredo M, Horhota A *et al.* (2012) Preclinical development and clinical translation of a PSMA-targeted docetaxel nanoparticle with a differentiated pharmacological profile. *Sci Transl Med* **4**, 128ra39.
- 22 Rovenska M, Hlouchova K, Sacha P, Mlcochova P, Horak V, Zamecnik J, Barinka C and Konvalinka J (2008) Tissue expression and enzymologic characterization of human prostate specific membrane antigen and its rat and pig orthologs. *Prostate* **68**, 171–182.
- 23 Zhong C, Zhao X, Van KC, Bzdega T, Smyth A, Zhou J, Kozikowski AP, Jiang J, O’Connor WT, Berman RF *et al.* (2006) NAAG peptidase inhibitor increases dialysate NAAG and reduces glutamate, aspartate and GABA levels in the dorsal hippocampus following fluid percussion injury in the rat. *J Neurochem* **97**, 1015–1025.
- 24 Zhong CL, Zhao XR, Sarva J, Kozikowski A, Neale JH and Lyeth BG (2005) NAAG peptidase inhibitor reduces acute neuronal degeneration and astrocyte damage following lateral fluid percussion TBI in rats. *J Neurotraum* **22**, 266–276.
- 25 Ghadge GD, Slusher BS, Bodner A, Canto MD, Wozniak K, Thomas AG, Rojas C, Tsukamoto T, Majer P, Miller RJ *et al.* (2003) Glutamate carboxypeptidase II inhibition protects motor neurons from death in familial amyotrophic lateral sclerosis models. *Proc Natl Acad Sci USA* **100**, 9554–9559.
- 26 Chen SR, Wozniak KM, Slusher BS and Pan HL (2002) Effect of 2-(phosphono-methyl)-pentanedioic acid on allodynia and afferent ectopic discharges in a rat model of neuropathic pain. *J Pharmacol Exp Ther* **300**, 662–667.
- 27 Nagel J, Belozertseva I, Greco S, Kashkin V, Malyshkin A, Jirgensons A, Shekunova E, Eilbacher B, Bepalov A and Danysz W (2006) Effects of NAAG peptidase inhibitor 2-PMPA in model chronic pain – relation to brain concentration. *Neuropharmacology* **51**, 1163–1171.
- 28 Zhou J, Neale JH, Pomper MG and Kozikowski AP (2005) NAAG peptidase inhibitors and their potential

- for diagnosis and therapy. *Nat Rev Drug Discov* **4**, 1015–1026.
- 29 Bacich DJ, Pinto JT, Tong WP and Heston WD (2001) Cloning, expression, genomic localization, and enzymatic activities of the mouse homolog of prostate-specific membrane antigen/NAALADase/folate hydrolase. *Mamm Genome* **12**, 117–123.
- 30 Gao Y, Xu SY, Cui ZW, Zhang MK, Lin YY, Cai L, Wang ZG, Luo XG, Zheng Y, Wang Y *et al.* (2015) Mice lacking glutamate carboxypeptidase II develop normally, but are less susceptible to traumatic brain injury. *J Neurochem* **134**, 340–353.
- 31 Tsai G, Dunham KS, Drager U, Grier A, Anderson C, Collura J and Coyle JT (2003) Early embryonic death of glutamate carboxypeptidase II (NAALADase) homozygous mutants. *Synapse* **50**, 285–292.
- 32 Han LQ, Picker JD, Schaevitz LR, Tsai GC, Feng JM, Jiang ZC, Chu HC, Basu AC, Berger-Sweeney J and Coyle JT (2009) Phenotypic characterization of mice heterozygous for a null mutation of glutamate carboxypeptidase II. *Synapse* **63**, 625–635.
- 33 Barinka C, Rinnova M, Sacha P, Rojas C, Majer P, Slusher BS and Konvalinka J (2002) Substrate specificity, inhibition and enzymological analysis of recombinant human glutamate carboxypeptidase II. *J Neurochem* **80**, 477–487.
- 34 Tykvar J, Sacha P, Barinka C, Knedlík T, Starkova J, Lubkowski J and Konvalinka J (2012) Efficient and versatile one-step affinity purification of in vivo biotinylated proteins: expression, characterization and structure analysis of recombinant human glutamate carboxypeptidase II. *Protein Expr Purif* **82**, 106–115.
- 35 Jackson PF, Cole DC, Slusher BS, Stetz SL, Ross LE, Donzanti BA and Trainor DA (1996) Design, synthesis, and biological activity of a potent inhibitor of the neuropeptidase N-acetylated alpha-linked acidic dipeptidase. *J Med Chem* **39**, 619–622.
- 36 Kozikowski AP, Zhang J, Nan FJ, Petukhov PA, Grajkowska E, Wroblewski JT, Yamamoto T, Bzdega T, Wroblewska B and Neale JH (2004) Synthesis of urea-based inhibitors as active site probes of glutamate carboxypeptidase II: efficacy as analgesic agents. *J Med Chem* **47**, 1729–1738.
- 37 Chen Y, Foss CA, Byun Y, Nimmagadda S, Pullambhatla M, Fox JJ, Castaneres M, Lupold SE, Babich JW, Mease RC *et al.* (2008) Radiohalogenated prostate-specific membrane antigen (PSMA)-based ureas as imaging agents for prostate cancer. *J Med Chem* **51**, 7933–7943.
- 38 Eder M, Schafer M, Bauder-Wust U, Hull WE, Wangler C, Mier W, Haberkorn U and Eisenhut M (2012) Ga-68-complex lipophilicity and the targeting property of a urea-based PSMA inhibitor for PET imaging. *Bioconjug Chem* **23**, 688–697.
- 39 Tykvar J, Schimer J, Barinkova J, Pacht P, Postova-Slavetinska L, Majer P, Konvalinka J and Sacha P (2014) Rational design of urea-based glutamate carboxypeptidase II (GCPII) inhibitors as versatile tools for specific drug targeting and delivery. *Bioorg Med Chem* **22**, 4099–4108.
- 40 Tykvar J, Schimer J, Jancarik A, Barinkova J, Navratil V, Starkova J, Sramkova K, Konvalinka J, Majer P and Sacha P (2015) Design of highly potent urea-based, exosite-binding inhibitors selective for glutamate carboxypeptidase II. *J Med Chem* **58**, 4357–4363.
- 41 Tykvar J, Barinka C, Svoboda M, Navratil V, Soucek R, Hubalek M, Hradilek M, Sacha P, Lubkowski J and Konvalinka J (2015) Structural and biochemical characterization of a novel aminopeptidase from human intestine. *J Biol Chem* **290**, 11321–11336.
- 42 Tykvar J, Navratil V, Sedlak F, Corey E, Colombatti M, Fracasso G, Koukolik F, Barinka C, Sacha P and Konvalinka J (2014) Comparative analysis of monoclonal antibodies against prostate-specific membrane antigen (PSMA). *Prostate* **74**, 1674–1690.
- 43 Navratil M, Tykvar J, Schimer J, Pacht P, Navratil V, Rokob TA, Hlouchova K, Rulisek L and Konvalinka J (2016) Comparison of human glutamate carboxypeptidases II and III reveals their divergent substrate specificities. *FEBS J* **283**, 2528–2545.
- 44 Majer P, Jancarik A, Krecmerova M, Tichy T, Tenora L, Wozniak K, Wu Y, Pommier E, Ferraris D, Rais R *et al.* (2016) Discovery of orally available prodrugs of the glutamate carboxypeptidase II (GCPII) inhibitor 2-phosphonomethylpentanedioic acid (2-PMPA). *J Med Chem* **59**, 2810–2819.
- 45 Chen Y, Dhara S, Banerjee SR, Byun Y, Pullambhatla M, Mease RC and Pomper MG (2009) A low molecular weight PSMA-based fluorescent imaging agent for cancer. *Biochem Biophys Res Commun* **390**, 624–629.
- 46 Gorin MA, Pomper MG and Rowe SP (2016) PSMA-targeted imaging of prostate cancer: the best is yet to come. *BJU Int* **117**, 715–716.
- 47 Yang X, Mease RC, Pullambhatla M, Lisok A, Chen Y, Foss CA, Wang Y, Shallal H, Edelman H, Hoye AT *et al.* (2016) [(18)F]Fluorobenzoyllysinepentanedioic acid carbamates: new scaffolds for positron emission tomography (PET) imaging of prostate-specific membrane antigen (PSMA). *J Med Chem* **59**, 206–218.
- 48 Barinka C, Hlouchova K, Rovenska M, Majer P, Dauter M, Hin N, Ko YS, Tsukamoto T, Slusher BS, Konvalinka J *et al.* (2008) Structural basis of interactions between human glutamate carboxypeptidase II and its substrate analogs. *J Mol Biol* **376**, 1438–1450.
- 49 Barinka C, Rovenska M, Mlcochova P, Hlouchova K, Plechanovova A, Majer P, Tsukamoto T, Slusher BS, Konvalinka J and Lubkowski J (2007) Structural

- insight into the pharmacophore pocket of human glutamate carboxypeptidase II. *J Med Chem* **50**, 3267–3273.
- 50 Mlcochova P, Plechanovova A, Barinka C, Mahadevan D, Saldanha JW, Rulisek L and Konvalinka J (2007) Mapping of the active site of glutamate carboxypeptidase II by site-directed mutagenesis. *FEBS J* **274**, 4731–4741.
- 51 O’Keefe DS, Bacich DJ and Heston WD (2004) Comparative analysis of prostate-specific membrane antigen (PSMA) versus a prostate-specific membrane antigen-like gene. *Prostate* **58**, 200–210.
- 52 Shafizadeh TB and Halsted CH (2007) Gamma-glutamyl hydrolase, not glutamate carboxypeptidase II, hydrolyzes dietary folate in rat small intestine. *J Nutr* **137**, 1149–1153.
- 53 Knedlík T, Navrátil V, Vík V, Pacík D, Saha P and Konvalinka J (2014) Detection and quantitation of glutamate carboxypeptidase II in human blood. *Prostate* **74**, 768–780.
- 54 Rajasekaran SA, Anilkumar G, Oshima E, Bowie JU, Liu H, Heston W, Bander NH and Rajasekaran AK (2003) A novel cytoplasmic tail MXXXL motif mediates the internalization of prostate-specific membrane antigen. *Mol Biol Cell* **14**, 4835–4845.
- 55 Klusak V, Barinka C, Plechanovova A, Mlcochova P, Konvalinka J, Rulisek L and Lubkowski J (2009) Reaction mechanism of glutamate carboxypeptidase II revealed by mutagenesis, X-ray crystallography, and computational methods. *Biochemistry* **48**, 4126–4138.
- 56 Mesters JR, Barinka C, Li WX, Tsukamoto T, Majer P, Slusher BS, Konvalinka J and Hilgenfeld R (2006) Structure of glutamate carboxypeptidase II, a drug target in neuronal damage and prostate cancer. *EMBO J* **25**, 1375–1384.
- 57 Speno HS, Luthi-Carter R, Macias WL, Valentine SL, Joshi ART and Coyle JT (1999) Site-directed mutagenesis of predicted active site residues in glutamate carboxypeptidase II. *Mol Pharmacol* **55**, 179–185.


APPENDIX 2

Received: 8 June 2018 | Accepted: 21 August 2018
DOI: 10.1002/pros.23717

ORIGINAL ARTICLE

WILEY **The Prostate**

A novel PSMA/GCPII-deficient mouse model shows enlarged seminal vesicles upon aging

Barbora Vorlová MSc^{1,2} | František Sedlák MD^{1,2,3} | Petr Kašpárek PhD^{4,5} |
Karolína Šrámková MSc¹ | Marek Malý PhD⁶ | Josef Zámečník MD, PhD⁷ |
Pavel Šácha PhD¹ | Jan Konvalinka PhD^{1,8} 

¹Institute of Organic Chemistry and Biochemistry of the Czech Academy of Sciences, Prague 6, Czech Republic

²First Faculty of Medicine, Charles University, Prague 2, Czech Republic

³Faculty of Science, Department of Genetics and Microbiology, Charles University, Prague 2, Czech Republic

⁴Laboratory of Transgenic Models of Diseases, Institute of Molecular Genetics of the Czech Academy of Sciences, Vestec, Czech Republic

⁵Czech Centre for Phenogenomics, Institute of Molecular Genetics of the Czech Academy of Sciences, Vestec, Czech Republic

⁶National Institute of Public Health, Prague 10, Czech Republic

⁷Department of Pathology and Molecular Medicine, Second Faculty of Medicine, Charles University and Motol University Hospital, Prague 5, Czech Republic

⁸Department of Biochemistry, Faculty of Science, Charles University, Prague 2, Czech Republic

Correspondence

Jan Konvalinka, Institute of Organic Chemistry and Biochemistry of the CAS, v.v.i. Flemingovo n. 2, 16610 Prague 6, Czech Republic.
Email: konval@uochb.cas.cz

Funding information

Czech Republic, Grant number: GA16-02938S; Ministry of Education, Youth and Sports of the Czech Republic, Grant numbers: LO1302, LM20150400; Academy of Sciences of the Czech Republic, Grant number: RVO 68378050

Background: Prostate-specific membrane antigen (PSMA), also known as glutamate carboxypeptidase II (GCPII), is an important diagnostic and therapeutic target in prostate cancer. PSMA/GCPII is also expressed in many healthy tissues, but its function has only been established in the brain and small intestine. Several research groups have attempted to produce PSMA/GCPII-deficient mice to study the physiological role of PSMA/GCPII in detail. The outcomes of these studies differ dramatically, ranging from embryonic lethality to production of viable PSMA/GCPII-deficient mice without any obvious phenotype.

Methods: We produced PSMA/GCPII-deficient mice (hereafter also referred as Folh1^{-/-} mice) by TALEN-mediated mutagenesis on a C57BL/6NCrI background. Using Western blot and an enzyme activity assay, we confirmed the absence of PSMA/GCPII in our Folh1^{-/-} mice. We performed anatomical and histopathological examination of selected tissues with a focus on urogenital system. We also examined the PSMA/GCPII expression profile within the mouse urogenital system using an enzyme activity assay and confirmed the presence of PSMA/GCPII in selected tissues by immunohistochemistry.

Results: Our Folh1^{-/-} mice are viable, breed normally, and do not show any obvious phenotype. Nevertheless, aged Folh1^{-/-} mice of 69–72 weeks exhibit seminal vesicle dilation, which is caused by accumulation of luminal fluid. This phenotype was also observed in Folh1^{+/-} mice; the overall difference between our three cohorts (Folh1^{-/-}, Folh1^{+/-}, and Folh1^{+/+}) was highly significant ($P < 0.002$). Of all studied tissues of the mouse urogenital system, only the epididymis appeared to have a physiologically relevant level of PSMA/GCPII expression. Additional experiments demonstrated that PSMA/GCPII is also present in the human epididymis.

Conclusions: In this study, we provide the first evidence characterizing the reproductive tissue phenotype of PSMA/GCPII-deficient mice. These findings will help lay the groundwork for future studies to reveal PSMA/GCPII function in human reproduction.

KEYWORDS

dilated seminal vesicles, Folh1, glutamate carboxypeptidase II, knockout mice, prostate-specific membrane antigen

1 | INTRODUCTION

Prostate-specific membrane antigen (PSMA),¹ also known as glutamate carboxypeptidase II (GCPII),^{2,3} is a transmembrane glycoprotein that is overexpressed in prostate cancer^{4,5} and is regarded as an important diagnostic target and suitable molecular address for anticancer drug delivery.^{6,7} PSMA/GCPII consists of short intracellular and transmembrane domains and a large extracellular domain with carboxypeptidase activity.^{8,9} Under physiological conditions, PSMA/GCPII is primarily expressed in the prostate, brain, small intestine, and kidney.^{4,10–14} However, the function of the enzyme has only been established in the brain and small intestine. In the brain, it cleaves the most abundant peptide neurotransmitter, N-acetyl-L-aspartyl-L-glutamate (NAAG), to yield N-acetyl-L-aspartate and L-glutamate, an important neurotransmitter.^{15,16} In the small intestine, PSMA/GCPII cleaves poly-gamma-glutamylated folates and thus enables folate absorption.^{1,17} The role of PSMA/GCPII in other tissues, most notably in the urogenital system, remains enigmatic.

PSMA/GCPII has several homologues in the human genome.¹⁸ The only one with similar enzymatic activity is glutamate carboxypeptidase III (GCPIII),^{19,20} which shares 67% amino acid identity and 81% amino acid similarity with PSMA/GCPII.^{19,21} While the protein expression profile of GCPIII in human tissues has been addressed in only one report, it seems to be similar to that of PSMA/GCPII.²² The most notable differences were found in the urogenital system. While GCPIII was detected in the highest amounts in human testis, its expression level in the prostate was much lower than that of PSMA/GCPII.

To understand the physiological role of PSMA/GCPII in more detail, several independent research groups have studied the consequences of inactivating the PSMA/GCPII-encoding gene *Folh1* in mice.^{23–26} Surprisingly, the outcomes of these studies differ markedly. While some studies concluded that the PSMA/GCPII knockout is embryonically lethal,^{24,25} others found that inactivating *Folh1* results in viable PSMA/GCPII-deficient mice with normal breeding performance and no obvious phenotype.^{23,26}

Viable PSMA/GCPII-deficient mice have been used in studies to evaluate PSMA/GCPII function in the nervous system.^{23,26–28} Although no significant differences between PSMA/GCPII-deficient and wild-type (WT) mice were observed in standard neurological behavioral tests, PSMA/GCPII-deficient mice showed lower susceptibility to peripheral neuropathies and traumatic brain injury, as well as improved long-term behavioral outcomes after traumatic brain injury.^{26,27} Recently, the International Mouse Phenotyping Consortium (IMPC) incorporated PSMA/GCPII-deficient mice into the primary phenotyping pipeline and published the first results.²⁹ No clear phenotype has been revealed to date, but the set of phenotyping data is still not complete.

It remains unclear why such different outcomes of *Folh1* gene inactivation in mice have been observed. All attempts to date to prepare transgenic animals with impaired PSMA/GCPII have been performed by embryonic stem (ES) cell manipulation. The main methodological differences lie in the design of the targeting cassette. Embryonic lethality resulted after deletion of either exons 1 and 2 or

exons 9 and 10 within the *Folh1* gene.^{24,25} On the other hand, insertion of three stop codons between exons 1 and 2, deletion of exons 3–5, or deletion of exon 3 within the *Folh1* gene led to production of viable mice.^{23,26,29} Of all the *Folh1* inactivation attempts, only one study has aimed to disrupt the active site of PSMA/GCPII (by deletion of exons 9 and 10) and thus avoid possible preservation of PSMA/GCPII enzyme activity by alternative mRNA splicing.²⁴ However, this attempt did not result in production of viable PSMA/GCPII-deficient mice.

Here, we describe production of PSMA/GCPII-deficient mice (hereafter also referred as *Folh1*^{-/-} mice) by disrupting the PSMA/GCPII active site using a strategy different than ES cell manipulation—manipulation of mouse zygotes by targeted nucleases. We designed transcription activator-like effector nucleases (TALENs) that specifically cleave exon 11 of the *Folh1* gene within the sequence encoding the PSMA/GCPII active site. This strategy led to full loss of PSMA/GCPII protein expression in *Folh1*^{-/-} mice. Our *Folh1*^{-/-} mice were viable, able to breed normally, and did not show any obvious phenotype. As PSMA/GCPII function in the brain has been thoroughly studied using PSMA/GCPII-deficient mice by others, we focused on the mouse urogenital system. We found that aged *Folh1*^{-/-} mice have an increased propensity for enlarged seminal vesicles compared with their WT littermates, and we explored the possible source of this phenomenon.

2 | MATERIALS AND METHODS

2.1 | Generation of *Folh1*^{-/-} mice

All animal procedures were ethically reviewed and performed in accordance with European directive 2010/63/EU and were approved by the Czech Central Commission for Animal Welfare. *Folh1*^{-/-} mice were generated by TALEN-mediated genome editing. TALENs were designed to target exon 11 of the *Folh1* gene, which encodes PSMA/GCPII. The following TALEN-repeat domain sequences were used: Left TALEN, NG NG NN HD NI NI NN HD NG NN NN NI NG NN; right TALEN, HD NI NN NG NI NN NI NI HD HD NI NI NN NI NI. TALEN RNA precursors were generated and microinjected into male nucleoli of zygotes isolated from C57BL/6NcrI mice as previously described.³⁰ These zygotes were subsequently implanted into pseudopregnant females. Tail biopsies from newborn pups were analyzed for the presence of TALEN-mediated mutations using Sanger sequencing. Briefly, chromosomal DNA was first isolated from tail biopsies using phenol-chloroform extraction. PCR with the primers F1 (5'-GGGCTATGCATTTTCAGGA-3') and R1 (5'-GCAGCAAGTGCCT-TAACCAG-3') was performed, generating fragments of approximately 500 bp (546 bp for the WT allele). PCR products were separated by agarose electrophoresis, isolated from the gel and ligated into pCRII-TOPO vector using TOPO TA Cloning Kit (Invitrogen, Carlsbad, CA). The resulting plasmids were sequenced using M13 Reverse primer supplied in the TOPO TA Cloning Kit. Founder mice carrying deletions of 3 bp (del3), 4 bp (del4), and 17 bp (del17) within exon 11 of the *Folh1* gene were bred with a WT C57BL/6NcrI mice to obtain the F1 generation. The mice used in this study were offspring of the F2 generation or subsequent generations.

2.2 | Folh1^{-/-} mice genotyping

Chromosomal DNA was isolated from tail biopsies using QuickExtract DNA Extraction Solution (Epicentre, Madison, WI). Genotyping was performed by nested PCR, which consisted of two successive rounds of PCR. In the first round, primers F1 and R1 (see above for sequences) were used to amplify a fragment of approximately 540 bp (546 bp for WT allele, 543 bp for del3 allele, 542 bp for del4 allele, and 529 bp for del17 allele). Reactions from the first round of PCR were diluted 200-fold and served as templates for the second round of PCR using primers F2 (5'-ATTTGTTTGAAGCTGG-3') and R2 (5'-CACTACTAGAACCAAGAAGG-3'). Amplified fragments of specific length (56 bp for WT allele, 53 bp for del3 allele, 52 bp for del4 allele, 39 bp for del17 allele) were analyzed by DNA polyacrylamide gel electrophoresis in TBE followed by GelRed post-staining (Biotinum, Fremont, CA).

2.3 | Preparation of rm-GCPII

The extracellular portion of mouse GCPII (rm-GCPII) was prepared as previously described.³¹ Briefly, large scale expression was performed using *Drosophila* S2 (BiP-BirA-KDEL) cells³² stably transfected with a plasmid encoding rm-GCPII (pMT/BiP/AvimGCPII).³¹ Biotinylated rm-GCPII was purified from S2 cell media using Streptavidin Mutein Matrix (Roche, Basel, Switzerland).³² rm-GCPII protein solution containing D-biotin was subsequently purified by size-exclusion chromatography using a HiLoad™ Superdex™ 200 10/300 GL column (GE-Healthcare, Chicago, IL) as a solid phase and buffer consisting of 10 mM Tris-HCl, pH 7.4, 150 mM NaCl as a mobile phase. The protein concentration was determined using quantitative amino acid analysis (Biochrom, Cambridge, UK) following the manufacturer's protocol.

2.4 | Cloning of vector encoding rm-GCPII^{del17}

Site-directed mutagenesis was carried out using pMT/BiP/AvimGCPII³¹ as a template according to the manufacturer's protocol (Phusion Site-Directed Mutagenesis Kit, Thermo Fisher Scientific, Waltham, MA). Four consecutive mutageneses were performed. First, a deletion of 6 bp within pMT/BiP/AvimGCPII (pMT/BiP/AvimGCPII^{del6}) was introduced using primers 5'-TGCAAGCTGGGATGCAGAAGGCCTTCTGGTCTACTG-3' and 5'-CAGTAGAACCAAGAAGGCCTTCTGCATCCAGCTTGCA-3'. Subsequently, pMT/BiP/AvimGCPII with a 9-bp deletion of was prepared from pMT/BiP/AvimGCPII^{del6} using primers 5'-TTTGTGGCAA GCTGGATGAAGGCCTTCTGGTCTACT-3' and 5'-AGTAGAAC-CAAGAAGGCCTTCTGCATCCAGCTTGCAACAAA-3' followed by preparation of pMT/BiP/AvimGCPII with a deletion of 12 bp using primers 5'-TTTGTGGCAAAGCTGGGATGGCCTTCTGGTCTACTGAG-3' and 5'-CTCAGTAGAACCAAGAAGGCATCCAGCTTGCAACAAA-3'. Finally, deletion of 17 bp within pMT/BiP/AvimGCPII (pMT/BiP/AvimGCPII^{del17}) was prepared using pMT/BiP/AvimGCPII^{del12} as a template with primers 5'-CAATTTTGTGGCAAGCTGGCCTTCTGGTCTACTGAGT-3' and 5'-ACTCAGTAGAACCAAGAAGGC-CAGCTTGCAACAAAATTG-3'. To ensure that no other mutation was introduced into the vector during mutagenesis, the sequence of the resulting pMT/BiP/AvimGCPII^{del17} plasmid was verified by sequencing.

2.5 | Preparation of rm-GCPII^{del17}

The recombinant protein rm-GCPII^{del17} was prepared similarly as previously described for rm-GCPII.³¹ Briefly, *Drosophila* S2 (BiP-BirA-KDEL) cells³² were co-transfected with the plasmids pMT/BiP/AvimGCPII^{del17} and pCoBlast (Invitrogen), followed by cell culture selection using cultivation of the transfectants in the presence of blasticidin (Invitrogen) and hygromycin B (Invitrogen). Prepared stably transfected cultures of S2 cells were tested for their ability to express rm-GCPII^{del17} using Western blot, and the cell culture expressing the highest amount of rm-GCPII^{del17} was used for large-scale expression. Large-scale expression was performed in a similar fashion as previously described for rh-GCPII.³³ Biotinylated rm-GCPII^{del17} was purified from S2 cell media by one-step purification using Streptavidin Mutein Matrix (Roche).³² The protein concentration was determined using Bradford 1× Dye Reagent (Bio-Rad, Hercules, CA).

2.6 | Tissue lysate preparation

Mice were sacrificed by intraperitoneal anesthetic injection followed by cervical dislocation. The anesthetics used were a combination of either tiletamine (125 mg/kg), zolazepam (125 mg/kg), and xylazine (10 mg/kg) or ketamine (125 mg/kg), and xylazine (20 mg/kg). Tissues intended for Western blot and enzyme activity analysis were frozen on dry ice immediately after collection and stored at -80°C until further processing.

To ensure homogeneity during tissue lysis, whole organs were processed. The only exception was the brains, which were first split into two identical hemispheres, only one of which was subsequently used for the tissue lysis.

The mouse tissues were weighed and homogenized in lysis buffer (50 mM Tris-HCl, pH 7.4, 100 mM NaCl, 1× Roche cOmplete protease inhibitor cocktail; 3 µL of lysis buffer added per 1 mg of tissue) using TissueLyser II (Qiagen, Hilden, Germany). The homogenization process slightly differed between tissues. The kidneys and brains were first homogenized with TissueLyser II at 30 Hz for 3 min. A 120 µL aliquot of the tissue homogenate was subsequently diluted with 180 µL lysis buffer and further homogenized using TissueLyser II (30 Hz, 3 min). In contrast, tissues of the urogenital system were homogenized with TissueLyser II at 30 Hz once for 5 min.

All homogenates were mixed with lysis buffer containing an appropriate amount of Igepal CA-630 (Sigma-Aldrich, St. Louis, MO) to reach a final detergent concentration of 1%. The samples were sonicated in a water bath 4 × 1 min at 0°C. Finally, the samples were centrifuged at 16 000g for 30 min, and the supernatants were stored at -80°C until further use. The concentration of total protein in the lysates was determined right before Western blot or enzyme activity analysis using Bradford 1× Dye Reagent (Bio-Rad).

2.7 | Western blot analysis

A combination of reducing sodium dodecyl sulfate polyacrylamide gel electrophoresis (SDS-PAGE, Bio-Rad) and wet electroblotting (Bio-Rad)

was used for Western blot analysis. A total amount of protein per line was 100 µg. The antibody mixture consisted of the anti-mouse PSMA/GCPII GCP-04 (Exbio, Prague, Czechia) labeled with HRP and an anti-β-actin antibody (Mouse monoclonal anti-β-actin antibody, clone AC-15, Sigma-Aldrich) diluted in 0.55% casein solution. Conjugation of GCP-04 with HRP was performed at pH 9.4 using the EZ-Link™ Plus Activated Peroxidase Kit (Thermo Fisher Scientific) according to the manufacturer's protocol. To visualize PSMA/GCPII, the blots were incubated with SuperSignal West Femto Chemiluminescent Substrate (Thermo Fisher Scientific), and chemiluminescence was captured with a LAS-3000 CCD Camera (Fujifilm, Tokyo, Japan). To visualize β-actin, the blots were incubated with IRDye 680 RD goat anti-mouse antibody (LI-COR Biosciences, Lincoln, NE) and developed by an Odyssey CLx Infrared Imaging System (LI-COR Biosciences).

2.8 | Radioenzymatic assay

NAAG-hydrolyzing activity in mouse tissues was determined using ³H-NAAG (radiolabeled on the terminal glutamate) as previously described³¹ with minor modifications. A volume of tissue lysate corresponding to a selected amount of total protein was adjusted by addition of lysis buffer to 20 µL and mixed with 70 µL reaction buffer (20 mM Tris-HCl, pH 7.4, 150 mM NaCl, 0.1% Tween 20). Reactions were incubated with 10 µL of 1 µM NAAG (containing 50 nM ³H-NAAG) at 37°C for 17 h (ie, overnight) or 6 h. The reactions were stopped by addition of 100 µL ice-cold stopping buffer (200 mM KH₂PO₄, 2 mM 2-mercaptoethanol, pH 7.4), and the released glutamate was separated from the uncleaved NAAG using AG1-X ion exchange resin (Bio-Rad). The eluate containing radioactive glutamate was mixed with Rotiszint ECO Plus scintillation cocktail (Roth), and the radioactivity of each sample was quantified by liquid scintillation using a Tri-Carb Liquid Scintillation Counter (PerkinElmer, Waltham, MA). The samples were measured in either duplicates or triplicates. A calibration curve of rm-GCPII (10 pg, 25 pg, 50 pg, 100 pg, 125 pg, and 250 pg of rm-GCPII per reaction) was included in each sample set.

2.9 | Gross anatomy of the urogenital system

Mice were sacrificed by intraperitoneal anesthetic injection followed by cervical dislocation. Ketamine (125 mg/kg) and xylazine (20 mg/kg) were used as anesthetics. The abdominal cavity was opened by midline laparotomy extending from the xiphoid process to the pubic symphysis. Seminal vesicles were localised, gently inverted, and pulled out of the abdominal cavity. Images of the seminal vesicles in front view with length scale were recorded. The seminal vesicle area was measured with ImageJ software³⁴ using the length scale as an internal standard.

2.10 | Histopathology and immunohistochemistry

Selected tissues from the mouse urogenital system were collected following gross anatomy examination. Unaffected human epididymis tissue samples were obtained from specimen surgically resected for

testicular cancer ($n = 3$, average age—39 years). Tissues were immersed in 10% buffered formalin immediately after collection and stored at 4°C before further processing.

A standard histopathological examination of the seminal vesicles was performed. Briefly, after fixation in 10% buffered formalin, transverse sections of the tissues were dehydrated using graded ethanol followed by xylene immersion and embedded in paraffin. Five-micrometer slices were subsequently prepared and stained with hematoxylin-eosin.

Immunohistochemistry of human and mouse samples was performed as previously described³⁵ with minor modifications. After fixation in 10% buffered formalin, tissues were dehydrated using graded ethanol followed by xylene immersion and paraffin embedding. Five-micrometer serial slices were prepared, deparaffinized in xylene and rehydrated in graded ethanol. Heat antigen retrieval was performed in buffer containing 10 mM sodium citrate, pH 6.0, and 0.1% Tween 20 using an autoclave (110°C, 15 min). Endogenous peroxidase activity was blocked by incubation in a 1.5% hydrogen peroxide solution in PBS for 20 min at room temperature followed by incubation in 10% fetal bovine serum (FBS) in PBS for 1 h at room temperature to reduce nonspecific interactions. To block endogenous immunoglobulins in the mouse samples, the slices were incubated with AffiniPure Fab Fragment Goat Anti-Mouse IgG (H + L) (Jackson ImmunoResearch Laboratories, West Grove, PA, diluted to 50 µg/mL by 10% FBS in PBS) for 1 h at room temperature. The slides were then washed four times with PBS, and a solution of primary antibodies against mGCPII/hGCPII (GCP-04, Exbio, or GCP-02³⁶) or hGCPII (YPSMA-1, Anogen, Toronto, Canada) diluted in 10% FBS in PBS to a concentration of 10 µg/mL was added to each slice. After overnight incubation at 4°C, the slides were washed five times with PBS containing 0.1% Tween 20, and each slice was incubated for 1 h at room temperature with the secondary antibody Histofine Simple Stain™ MAX PO (MULTI) (Nichirei Biosciences Inc., Tokyo, Japan), either undiluted (human samples) or diluted 1:2 with 10% FBS in PBS (mouse samples). Finally, the slides were washed five times with PBS containing 0.1% Tween 20, and mGCPII was visualized using the DAB/Plus kit (Diagnostic BioSystems, Pleasanton, CA). The slides were counterstained with Harris' hematoxylin and mounted in polyvinylalcohol-based media.

2.11 | Statistical analysis

All data from radioactive assays are presented as the mean of biological replicates ± standard deviation. Statistical analysis of mouse seminal vesicle enlargements was performed with the statistical software Stata, release 9.2 (Stata Corp LP, College Station, TX). A random-effects linear regression model with generalized least squares technique for estimating parameters was used to analyze the data. This approach allows estimation of within-animal variation as well as between-animal variation. It also takes into account the correlation between responses on paired organs from the same individual. Based on the result of the Shapiro-Wilk test for normality, the dependent variable (ie, area) was log-transformed to bring its distribution closer to normal. Group (Folh1^{-/-} vs Folh1^{+/-} vs Folh1^{+/+}) or age (<72 weeks old

vs >72 weeks old) entered the model as independent variables. All statistical tests were evaluated at a significance level of 0.05.

3 | RESULTS

3.1 | *Folh1*^{-/-} mice generated by TALEN-mediated gene disruption are viable and devoid of PSMA/GCPII specific activity

To generate *Folh1*^{-/-} mice, we designed TALENs that specifically cleaved exon 11 of the *Folh1* gene within the sequence encoding the PSMA/GCPII active site (Figure 1A). Two independent TALEN microinjections into male nuclei of C57BL/6NCRl zygotes were performed, resulting in 65 transgenic mice of the F0 generation. Gene sequencing was carried out on all F0 transgenic mice, and the chosen founder mice carrying deletions of 3 bp (del3), 4 bp (del4), and 17 bp (del17) within exon 11 of the *Folh1* gene were bred with WT C57BL/6NCRl mice to obtain the F1 generation. For facile monitoring of resulting genotypes, we established a reliable genotyping method based on nested PCR (Figure 1B).

Heterozygous mice bearing the *Folh1-del3*, *Folh1-del4*, or *Folh1-del17* variant bred normally and did not show any obvious

phenotype. PSMA/GCPII mutant mice (mice homozygous for either *Folh1-del3* or *Folh1-del4* or *Folh1-del17*) were generated by intercrossing heterozygous mice of at least the F2 generation. Neither embryonic lethality nor any obvious phenotype was observed for the PSMA/GCPII mutant mice. Subsequent intercrossing of PSMA/GCPII mutant mice was consistent with the usual breeding performance of C57BL/6NCRl mice.

To confirm that the generated mutants could be considered as knockout, that is, possess functional gene ablations, we examined at first the PSMA/GCPII protein expression in the kidney and brain using Western blot (Figures 2A and 2C). No band corresponding to either full-length PSMA/GCPII or any truncated form of PSMA/GCPII was detected by Western blot, although the antibody against mouse PSMA/GCPII is able to recognize the potential protein products of *Folh1-del3*, *Folh1-del4*, and *Folh1-del17* gene expression. In addition, no version of PSMA/GCPII was detected in the insoluble fractions of lysates from PSMA/GCPII mutant mice (data not shown). Since all three mutants were devoid of PSMA/GCPII protein expression, they are hereafter collectively referred as *Folh1*^{-/-} mice.

Next, we set out to determine if the *Folh1*^{-/-} mice were devoid of specific PSMA/GCPII activity. We performed enzymatic activity assays with the brain and kidney lysates using NAAG, a physiologic substrate

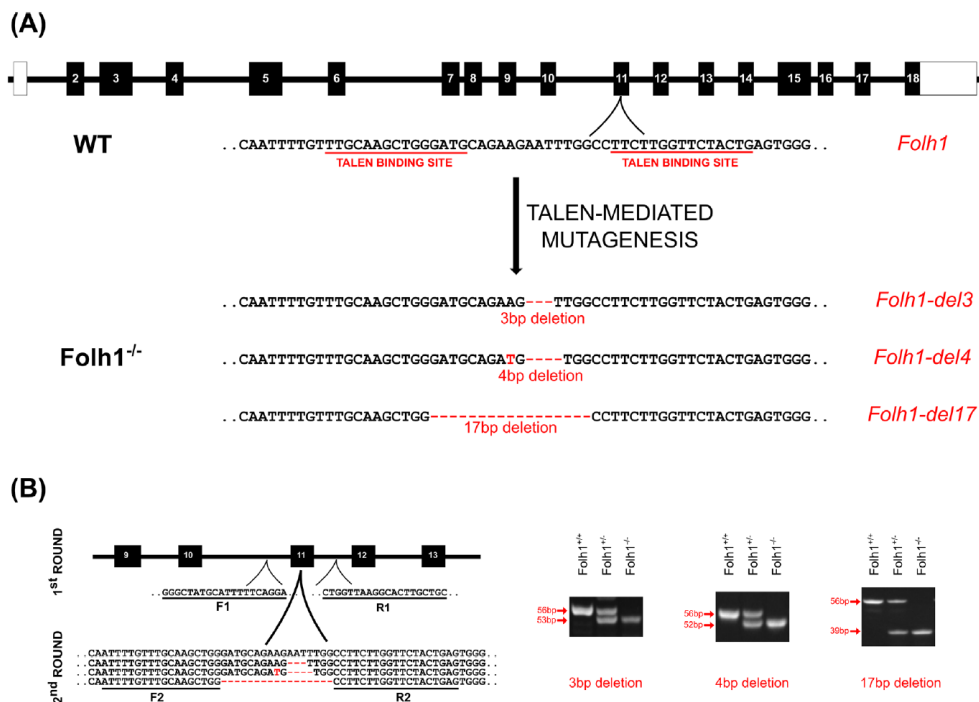


FIGURE 1 Generation and genotyping of *Folh1*^{-/-} mice. A, *Folh1*^{-/-} mice were generated on a C57BL/6NCRl background using TALEN technology. TALEN activity followed by non-homologous end joining generated several different mutations. Founder mice with deletions of 3 bp (*Folh1-del3*), 4 bp (*Folh1-del4*), and 17 bp (*Folh1-del17*) were chosen to establish PSMA/GCPII mutant mouse colonies. B, Mice were genotyped using nested PCR. The first round of PCR using F1 and R1 primers generated fragments of approximately 540 bp. The second round using F2 and R2 primers generated fragments with length depending on genotype. [Color figure can be viewed at wileyonlinelibrary.com]

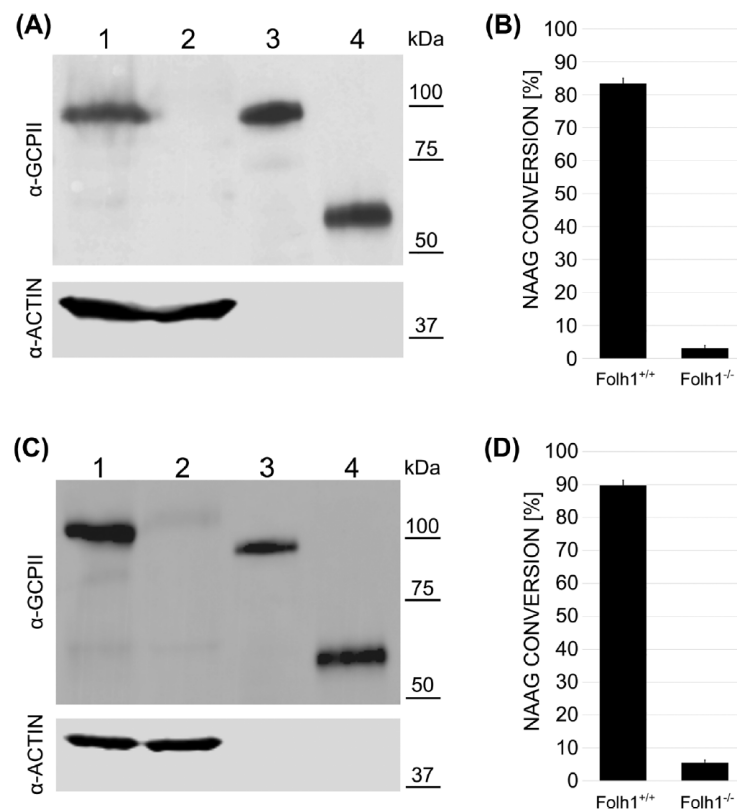


FIGURE 2 Characterization of Folh1^{-/-} mice using brain and kidney lysates. A and C, Representative Western blot analysis of brain lysates (A) and kidney lysates (C). Western blot were performed with the anti-PSMA/GCPII antibody GCPII-04 (designated α-GCPII) and anti-β-actin antibody (designated α-ACTIN). Recombinant mouse GCPII (rm-GCPII)³¹ and a truncated version corresponding to the extracellular part of the potential protein product of *Folh1-del17* gene expression (rm-GCPIIdel17) were used as mGCPII standards. 1-Folh1^{+/+}, 2-Folh1^{-/-}, 3-rm-GCPII WT, 4-rm-GCPII del17. B and D, NAAG cleavage activity analysis of brain lysates (B) and kidney lysates (D). Reactions were performed in 100 μg of total protein overnight. Error bars represent standard deviation of six biological replicates (8-week-old males)

of PSMA/GCPII (Figures 2B and 2D). Indeed, NAAG conversion after overnight incubation with Folh1^{-/-} lysates did not exceed 6%.

3.2 | Aged Folh1^{-/-} mice have an increased propensity for enlarged seminal vesicles

We focused on the urogenital system of aged mice to further examine possible phenotypic differences between Folh1^{-/-} and Folh1^{+/+} mice. We first performed gross anatomy analysis of the urogenital system of aged WT mice. Age-related changes were observed only in the seminal vesicles, which showed a tendency toward bilateral enlargement. Based on preliminary observations of a small cohort consisting of mice aged 63-82 weeks, we further studied two age groups—mice aged 69-72 weeks and mice aged 72.1-81 weeks. While the seminal vesicles of all WT mice aged 69-72 weeks were of a normal size (average stretched length of 1.5 cm and average area of 1 cm²), the propensity for bilaterally enlarged seminal vesicles increased significantly in WT mice older than 72 weeks ($P < 0.001$, see Figure 3).

Based on these observations, we investigated possible PSMA/GCPII-mediated changes in the urogenital system in mice aged 69-72 weeks. Interestingly, we observed a higher prevalence of bilaterally enlarged seminal vesicles in Folh1^{-/-} mice compared with Folh1^{+/+} mice. Typical gross anatomy of the seminal vesicles of both Folh1^{+/+} and Folh1^{-/-} mice is depicted in Figure 4A. Histopathological examination using hematoxylin-eosin staining did not show any substantial differences between the seminal vesicles of Folh1^{+/+} and Folh1^{-/-} mice (Figures 4B and 4C). Nevertheless, “dilated” parts of the seminal vesicles were present to a greater extent in Folh1^{-/-} mice than in their WT counterparts. Moreover, loosening of mucosal folds and decreasing epithelial thickness were also more prominent in Folh1^{-/-} seminal vesicles. No epithelial hyperplasia, tumor or infection was observed.

To investigate the statistical significance of our observations, we performed gross anatomy analysis of a sufficient number of Folh1^{-/-}, Folh1^{-/-}, and Folh1^{+/+} mice (at least nine mice per group, Figure 5A). Linear regression analysis of logarithmically transformed seminal

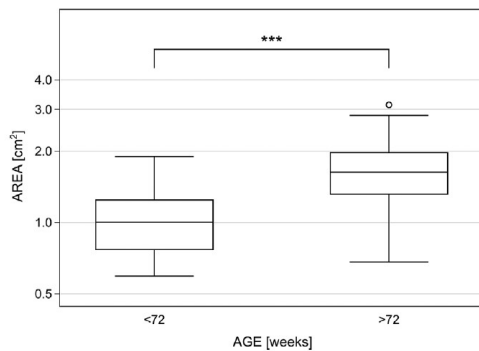


FIGURE 3 Age-related enlargement of mouse seminal vesicles. The WT mice were divided into two age groups based on preliminary observations of a small cohort consisting of mice aged 63–82 weeks. The group designated as <72 consisted of 20 mice aged 69–72 weeks. The group designated as >72 consisted of 11 mice aged 72.1–81 weeks. The difference in seminal vesicle area between the two groups was statistically significant ($P < 0.001$ as designated by ***)

vesicle areas showed that the overall difference between the three groups was highly statistically significant ($P < 0.002$). Comparisons of group pairs revealed a highly statistically significant difference between $Folh1^{-/-}$ and $Folh1^{+/+}$ mice ($P < 0.001$) and a statistically significant difference between $Folh1^{-/-}$ and $Folh1^{+/-}$ mice ($P = 0.028$). These data suggest that the propensity for enlarged seminal vesicles tends to increase with a decreasing number of PSMA/GCPII-expressing alleles.

We next investigated whether the amount of expressed PSMA/GCPII depends on the number of functional *Folh1* alleles in the aged mice. We prepared lysates from kidneys collected from 70-week-old mice with the three genotypes ($Folh1^{-/-}$, $Folh1^{+/-}$, $Folh1^{+/+}$) and analyzed them using two independent methods—Western blot and NAAG-hydrolyzing activity analysis (Figure 5B). Interestingly, the amount of PSMA/GCPII expressed in $Folh1^{+/-}$ mice was close to half that expressed in $Folh1^{+/+}$ mice, as determined by Western blot (Figure 5B). No PSMA/GCPII was detected in lysates from $Folh1^{-/-}$ mice. Moreover, NAAG conversion after incubation with kidney lysates from $Folh1^{+/-}$ mice was half of that observed after incubation

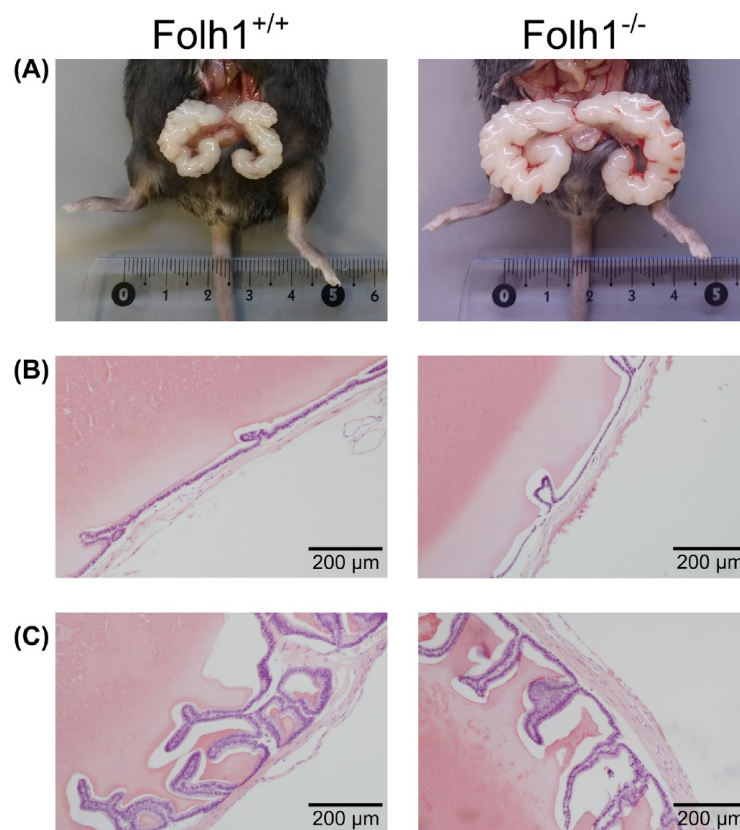


FIGURE 4 Images and histopathology of the seminal vesicles of typical $Folh1^{+/+}$ mice and some $Folh1^{-/-}$ mice. A, Images of mouse abdominal part. B, Histopathological images of mouse seminal vesicles showing “dilated” parts. C, Histopathological images of mouse seminal vesicles showing parts with normal seminal vesicle histology. [Color figure can be viewed at wileyonlinelibrary.com]

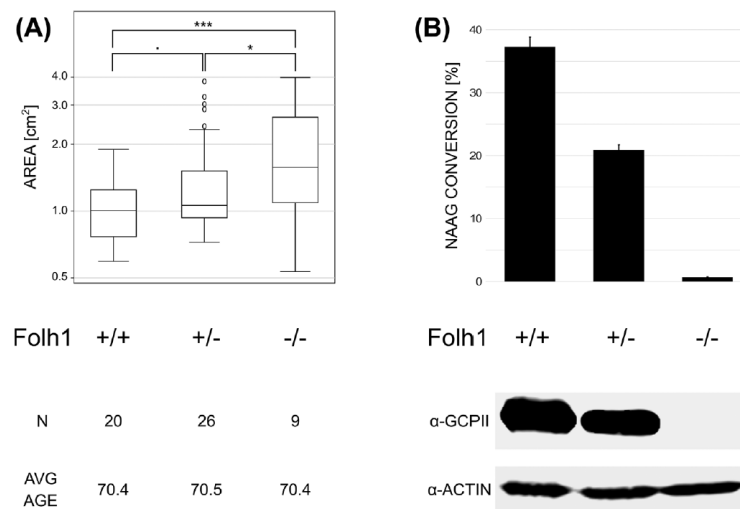


FIGURE 5 Statistical analysis of enlarged seminal vesicles and expression of PSMA/GCPII protein in kidneys of 70-week-old mice with distinct genotypes. A, Comparison of seminal vesicle areas of Folh1^{+/+}, Folh1^{+/-}, and Folh1^{-/-} mice. AVG AGE indicates the average age of the mice in weeks. The difference in seminal vesicle area was highly statistically significant between Folh1^{-/-} and Folh1^{+/+} mice ($P < 0.001$, designated by ***), statistically significant between Folh1^{-/-} and Folh1^{+/-} mice ($P = 0.028$, designated by *) and on the border of significance between Folh1^{+/-} and Folh1^{+/+} mice ($P = 0.052$, designated by ·). B, NAAG cleavage and Western blot analysis of kidney lysates from Folh1^{+/+}, Folh1^{+/-}, and Folh1^{-/-} mice. NAAG cleavage analysis was performed in 0.5 μ g total protein for 6 h. Error bars represent standard deviation of 2 (for Folh1^{-/-}) or 3 (for Folh1^{+/+} and Folh1^{+/-}) biological replicates. Western blot analysis of kidney lysates was performed using the anti-PSMA/GCPII antibody GCPII-04 (designated α -GCPII) and anti- β -actin antibody (designated α -ACTIN)

with kidney lysates from Folh1^{+/+} mice (Figure 5B). As expected, almost no NAAG cleavage activity was observed in lysates from the kidneys of Folh1^{-/-} mice.

3.3 | PSMA/GCPII is highly expressed in the epididymis

To investigate whether a possible source of seminal vesicle enlargement could be located within or close to the seminal vesicles, we examined the expression profile of PSMA/GCPII in male mouse urogenital tissues using the NAAG cleavage assay (Figure 6A). Among the tissues tested (30 μ g total protein per reaction), only the kidney, spermatic cord, and epididymis reached at least 50% NAAG conversion after overnight incubation. Other tissues, including all four prostate glands and seminal vesicles, showed less than 25% NAAG conversion (Figure 6A). Assuming PSMA/GCPII is the only enzyme responsible for NAAG cleavage, this would correspond to less than 2.5 pg PSMA/GCPII per 1 μ g total protein (as determined from our calibration curve, which was linear from 4% to 42% NAAG conversion, corresponding to 10 pg to 125 pg recombinant mouse GCPII). In addition, we examined PSMA/GCPII expression in the seminal vesicles using Western blot analysis. Even though a weak band of molecular weight similar to that of PSMA/GCPII was detected in the seminal vesicles of Folh1^{+/+} mice, the same signal was also observed in the seminal vesicles of Folh1^{-/-} mice (Figure 6B), suggesting possible cross-reactivity of the antibody.

We thus further investigated only the spermatic cord and epididymis.

To filter out the possible contribution of other enzymes (such as mouse GCPIII) to NAAG hydrolysis, we analyzed lysates from the epididymis and spermatic cord of both Folh1^{+/+} and Folh1^{-/-} mice. While NAAG hydrolysis in the epididymis of Folh1^{-/-} mice was negligible, NAAG conversion after incubation with spermatic cord lysates from Folh1^{-/-} mice was more than half the WT value (Figure 6C). After taking into account the conversion from Folh1^{-/-} mice, the amount of PSMA/GCPII in the spermatic cord appeared to be within the range of other tissues expressing low levels of PSMA/GCPII (Figure 6C). On the other hand, the amount of PSMA/GCPII in the epididymis was as high as 180 pg per 1 μ g total protein. In comparison, we previously showed that the amount of PSMA/GCPII in the male kidney and brain is 100–250 pg and 2.5–10 pg in 1 μ g total protein, respectively.³¹ We thus visualized and localized PSMA/GCPII in the epididymis by immunohistochemistry using two different antibodies against mouse PSMA/GCPII—GCPII-02 and GCPII-04 (Figure 7). Cells expressing the protein were detected in all three parts of the epididymis—head, body, and tail.

Finally, we investigated whether PSMA/GCPII could be also detected in the human epididymis. For this purpose, we performed immunohistochemistry with tissue sections of the body of the epididymis collected from three patients using three different antibodies against human PSMA/GCPII—GCPII-02, GCPII-04, and YPSMA1. Interestingly, PSMA/GCPII-expressing cells were detected in all cases (Figure 8).

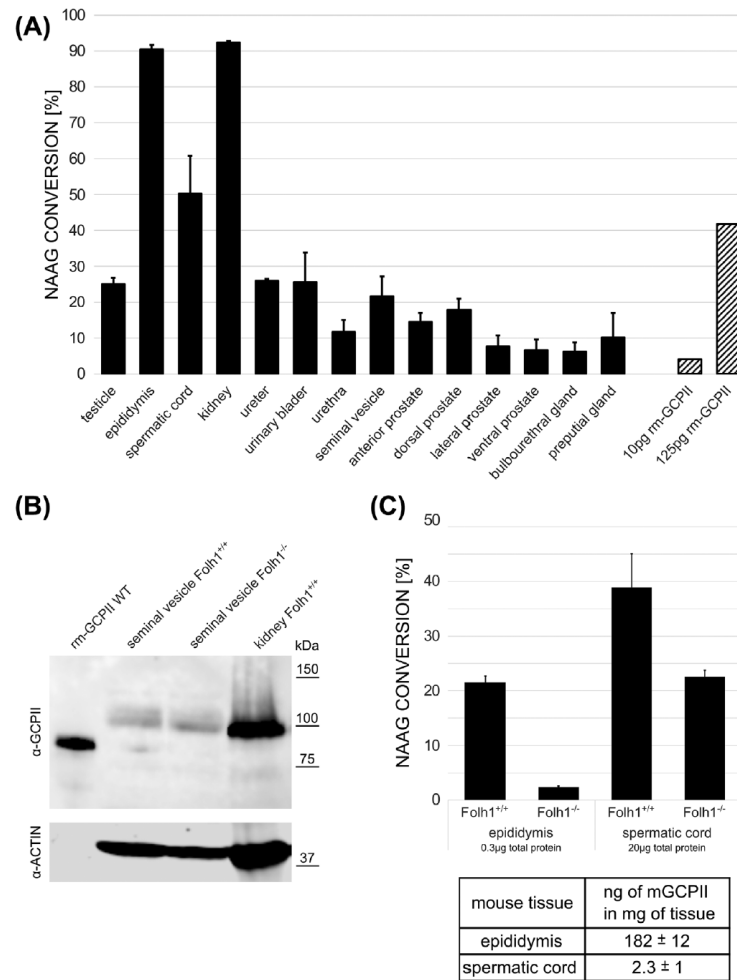


FIGURE 6 NAAG cleavage activity in the male mouse urogenital system and Western blot analysis of the seminal vesicles. A, NAAG conversion performed overnight in 30 µg total protein of WT lysates compared to NAAG conversion performed overnight with 10 pg and 125 pg of recombinant mouse GCPII (rm-GCPII). Error bars of tissue lysate conversions represent standard deviations of biological replicates (from 3 to 5 mice of at least 2 of 3 different ages: 8 weeks, 17 weeks, and 30 weeks). Error bars of NAAG conversions by rm-GCPII represent standard deviations of 6 independent measurements. B, Representative Western blot analysis of seminal vesicle lysates. Western blots were performed with the anti-PSMA/GCPII antibody GCPII-04 (designated α-GCPII) and anti-β-actin antibody (designated α-ACTIN). Recombinant mouse GCPII (designated rm-GCPII WT)³¹ was used as mGCPII standard. C, Comparison of overnight NAAG cleavage activity in selected reproductive tissues of Folh1^{+/+} and Folh1^{-/-} mice together with calculated amount of PSMA/GCPII (mGCPII) in mouse epididymis and spermatic cord after taking into account NAAG conversion in tissues from Folh1^{-/-} mice. Error bars represent standard deviation of 4 biological replicates (8-week-old mice)

4 | DISCUSSION

Despite more than three decades of extensive research, the physiological function of PSMA/GCPII is still not fully understood. Several independent research groups have attempted to produce and characterize mice with disrupted PSMA/GCPII. However, the outcomes of these studies differ dramatically, ranging from embryonic lethality^{24,25} to generation of viable mice without any obvious

phenotype.^{23,26} Viable PSMA/GCPII-deficient mice have been used to investigate PSMA/GCPII function in the nervous system^{26–28} but not in other PSMA/GCPII-expressing tissues such as the urogenital system. In this study, we explored several issues that have not been addressed in the reports published to date.

First, in contrast to previous studies, which used ES cell manipulation to generate PSMA/GCPII-deficient mice, we inactivated the *Folh1* gene in mice using TALEN technology.^{37,38} This strategy

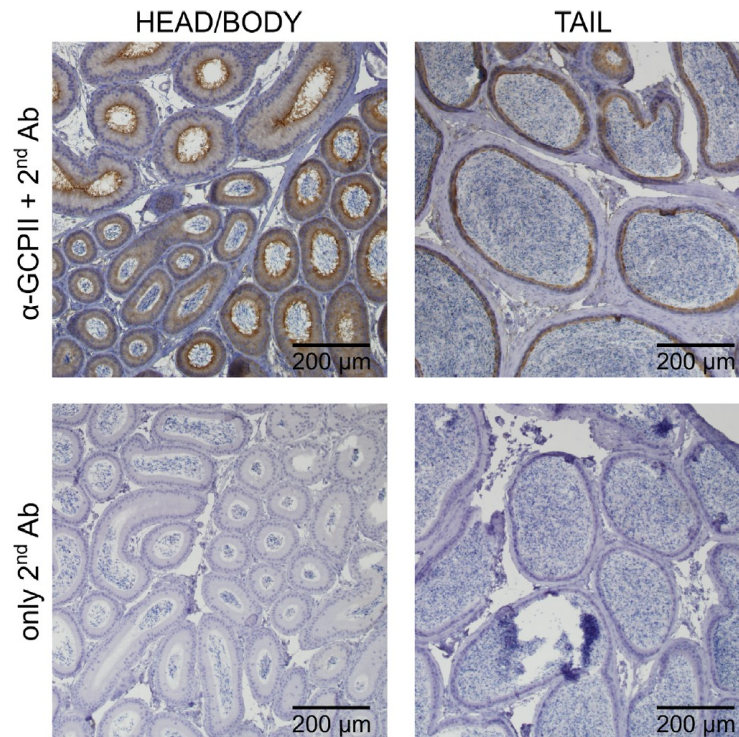


FIGURE 7 Representative immunohistochemical staining of the head, body, and tail of mouse epididymis. Formalin-fixed paraffin-embedded mouse epididymis tissue sections were incubated with the anti-PSMA/GCPII (α -GCPII) antibody GCP-04 (Exbio) to localize mouse PSMA/GCPII expression. As a negative control, immunohistochemistry using only secondary antibody (2nd Ab) Histofine Simple Stain™ MAX PO (MULTI) (Nichirei Biosciences Inc.) was performed. [Color figure can be viewed at wileyonlinelibrary.com]

enabled us to manipulate mouse zygotes with the same genetic background as the knockout colony that was being established. Therefore, potential phenotypic variations that could be caused by mixed genetic backgrounds³⁹ were eliminated. Moreover, our PSMA/GCPII-deficient mice do not contain the PGK-Neo cassette because TALEN technology does not require a selectable marker. When retained in the targeted loci, selectable marker cassettes such as PGK-Neo have been repeatedly shown to greatly influence the expression of neighboring genes within the locus, leading to unexpected phenotypes of null mutant mice.^{40,41} Out of three PSMA/GCPII-deficient colonies established to date, only one (IMPC) had the PGK-Neo cassette removed using the Cre-Lox system before the mice were characterized.²⁹ The other two PSMA/GCPII-deficient colonies,^{23,26} which are routinely used for diverse experiments,^{28,42,43} likely do not contain any LoxP sites, and PGK-Neo cassette removal is thus not possible.

Second, when using TALENs to inactivate the *Folh1* gene, we intended to disrupt the active site of PSMA/GCPII. Several reports have shown that novel alternative splice variants can be detected in some knockout mice, and these may serve to rescue a severe phenotype of complete gene inactivation.^{44,45} Modification of the *Folh1* gene within

the sequence encoding the active site of PSMA/GCPII ensures that no alternative splicing that would enable at least partial restoration of PSMA/GCPII activity can occur. A previous attempt to generate PSMA/GCPII-deficient mice through active site disruption led to embryonic lethality.²⁴ Here, we show that a small TALEN-mediated deletion within exon 11 of the *Folh1* gene leads to production of viable PSMA/GCPII-deficient mice with no obvious phenotype. In comparison with previous reports characterizing viable PSMA/GCPII-deficient mice,^{23,26} residual NAAG hydrolyzing activity in our *Folh1*^{-/-} mice seems to be negligible. Indeed, while NAAG conversion in saturation was as low as 3% in the brain lysates of our *Folh1*^{-/-} mice, others have reported that NAAG hydrolyzing activity measured in PSMA/GCPII-deficient mouse brains within the linear range of reaction velocity reached 6% to 18% of the WT values.

Finally, we focused on possible phenotypic differences between *Folh1*^{+/+} and *Folh1*^{-/-} mice in the urogenital system rather than the nervous system. We found that PSMA/GCPII-deficient mice aged 69–72 weeks have a higher propensity for bilaterally enlarged seminal vesicles. The dilation of seminal vesicles seems to be solely a result of the accumulation of luminal fluid, as we observed no other cause such as epithelial hyperplasia, cysts, tumors or infections. Interestingly, we

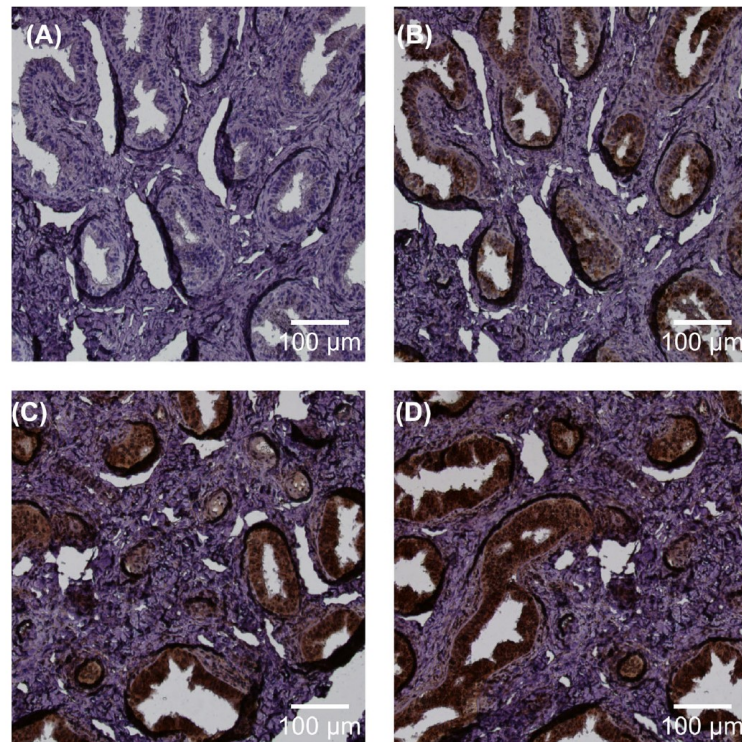


FIGURE 8 Representative immunohistochemical staining of the body of human epididymis. Formalin-fixed paraffin-embedded human epididymis tissue sections were incubated with several anti-PSMA/GCPII antibodies to specifically detect PSMA/GCPII. A, Negative control—immunohistochemistry using only the secondary antibody Histofine Simple Stain™ MAX PO (MULTI) (Nichirei Biosciences Inc.). B, Immunohistochemistry using the antibody GCP-04 (Exbio). C, Immunohistochemistry using the antibody GCP-02.³⁶ D, Immunohistochemistry using the antibody YPSMA1 (Anogen). [Color figure can be viewed at wileyonlinelibrary.com]

observed this increased propensity for seminal vesicle enlargement to a lesser extent in *Folh1*^{+/-} mice. It is thus possible that the seminal vesicle dilation is somehow associated with PSMA/GCPII activity, as the amount of PSMA/GCPII in the *Folh1*^{+/-} mice was roughly half the amount of PSMA/GCPII in *Folh1*^{+/+} mice, as determined by both Western blot and NAAG-hydrolyzing activity.

Previous studies have reported that enlarged seminal vesicles are one of the signs of aging in C57BL mice.^{46,47} In one of these studies, the mice, which had dilation of seminal vesicles caused by accumulation of luminal fluid, were at least 24 months old⁴⁶—much older than the mice investigated in our study. Dilated seminal vesicles have also been reported in aged C57BL mice with a lower age limit (16 months) but in connection with either an infection or the presence of an abdominal tumor,⁴⁷ neither of which we observed in our histopathological examination. In addition, several genetically modified mice with a phenotype association to enlarged seminal vesicles can be found in public databases or the literature.^{29,48} However, none of the reported genes seems to be connected with PSMA/GCPII.

To investigate the possible source of seminal vesicle enlargement in *Folh1*^{+/-} mice, we examined the expression profile of PSMA/

GCPII in the urogenital system of WT mice using a NAAG-hydrolyzing activity assay. Somewhat surprisingly, low levels of NAAG hydrolyzing activity were detected in the seminal vesicles and most surrounding tissues. In the case of seminal vesicles, we additionally performed Western blot analysis, which showed non-detectable expression of PSMA/GCPII. Indeed, no difference was seen between seminal vesicle lysates of *Folh1*^{+/+} and *Folh1*^{+/-} mice suggesting that if PSMA/GCPII is expressed in the seminal vesicles, its level is below the detection limit. In agreement with previous reports,^{31,49} almost no NAAG hydrolyzing activity was observed in any of the mouse prostate lobes. In contrast, high levels of NAAG hydrolyzing activity were detected in the mouse spermatic cord and epididymis.

The possibility that PSMA/GCPII is present in seminal vesicles or other urogenital tissues in an amount sufficient for execution of a specific function cannot be excluded. Indeed, the seminal vesicles contain seminal fluid, which represents 60–75% of the seminal vesicle mass.⁴⁶ As protein concentration in the seminal fluid can be as high as 86 mg/mL,⁵⁰ analysis of seminal vesicle lysates (ie, a mixture of seminal fluid and seminal vesicle cells) could result in dramatic underestimation

of PSMA/GCPII amount in the seminal vesicle cells. Similarly, male urogenital tissues such as the urethra consist of diverse types of cells.⁵¹ If PSMA/GCPII is expressed in only one cell type, the amount of PSMA/GCPII could be physiologically relevant.

Even though we performed the NAAG-hydrolyzing activity assay in reaction conditions highly specific for PSMA/GCPII,²² other enzymes such as GCPIII potentially could influence the outcome of the analysis. GCPIII is expressed in considerable amounts in the mouse testis and bladder,⁵² although no other urogenital system tissues have been examined. To account for the possible involvement of other enzymes including GCPIII, we performed the NAAG-hydrolyzing activity assay in the spermatic cord and epididymis (the tissues with highest levels of NAAG-hydrolyzing activity) of both *Folh1*^{+/+} and *Folh1*^{-/-} mice. We concluded that high amounts of PSMA/GCPII within the urogenital system can be only detected in epididymis. Interestingly, the amount of PSMA/GCPII in the epididymis is comparable to the amount in the kidney and 10-fold higher than the amount in the brain.³¹ Epididymis is thus one of the most PSMA/GCPII expressing tissue in mice.

Additionally, we found that PSMA/GCPII is expressed throughout all parts of the mouse epididymis, as determined by immunohistochemistry. This agrees with previous findings, in which the researchers saw a strong signal in mouse epididymis after intravenous injection of a low-molecular-weight fluorescent agent targeting PSMA/GCPII.^{53,54} To investigate whether our observations may also be applicable to humans, we examined tissue sections of human epididymis. The presence of PSMA/GCPII mRNA in human epididymis has been reported.⁵⁵ Using immunohistochemistry with three different antibodies against human PSMA/GCPII, we confirmed that PSMA/GCPII protein is also expressed in the human epididymis.

In humans, ejaculatory duct obstruction is relatively rare but has been shown to be one of the causes of male infertility.⁵⁶ It is a matter of speculation whether the absence of PSMA/GCPII in the epididymis is somehow connected with an increased propensity for dilated seminal vesicles. The association between inactivation of the *Folh1* gene and enlargement of seminal vesicles in aged PSMA/GCPII-deficient mice remains enigmatic, and further research is needed.

5 | CONCLUSIONS

We produced PSMA/GCPII-deficient mice by disrupting the PSMA/GCPII active site using TALEN-mediated mutagenesis. We confirmed that PSMA/GCPII protein is not expressed in these mice, and NAAG hydrolyzing activity is almost completely abolished. Young PSMA/GCPII-deficient mice breed normally and do not show any obvious phenotype. Based on investigation of the urogenital system of aged mice, we report that PSMA/GCPII-deficient mice have an increased propensity for enlarged seminal vesicles. The cause of this phenotype remains uncertain, as significant amounts of PSMA/GCPII within the mouse urogenital system were detected only in the epididymis. PSMA/GCPII was also shown to be present in the human epididymis. We thus

believe that our findings can set the direction for future work to reveal PSMA/GCPII function in human reproduction.

ACKNOWLEDGEMENTS

The authors would like to acknowledge Jana Starková for preparation of stably transfected cell cultures, Dr. Tomas Olejar for preparation of mouse seminal vesicle sections for histopathology examination and help with interpretation of the data, Adrian Cibula for preparation of human epididymis sections and Dr. Hillary Hoffman for language editing. This work was supported by grant no. GA16-02938S from the Grant Agency of the Czech Republic, InterBioMed project LO1302 and Czech Centre for Phenogenomics project LM2015040 from the Ministry of Education, Youth and Sports of the Czech Republic, and RVO 68378050 from Academy of Sciences of the Czech Republic.

CONFLICT OF INTEREST

The authors declare no conflicts of interest.

ORCID

Jan Konvalinka  <http://orcid.org/0000-0003-0695-9266>

REFERENCES

1. Pinto JT, Suffoletto BP, Berzin TM, et al. Prostate-specific membrane antigen: a novel folate hydrolase in human prostatic carcinoma cells. *Clin Cancer Res*. 1996;2:1445–1451.
2. Luthi-Carter R, Berger UV, Barczak AK, Enna M, Coyle JT. Isolation and expression of a rat brain cDNA encoding glutamate carboxypeptidase II. *Proc Natl Acad Sci USA*. 1998;95:3215–3220.
3. Luthi-Carter R, Barczak AK, Speno H, Coyle JT. Molecular characterization of human brain N-acetylated alpha-linked acidic dipeptidase (NAALADase). *J Pharmacol Exp Ther*. 1998;286:1020–1025.
4. Horoszewicz JS, Kawinski E, Murphy GP. Monoclonal antibodies to a new antigenic marker in epithelial prostatic cells and serum of prostatic cancer patients. *Anticancer Res*. 1987;7:927–935.
5. Bostwick DG, Pacelli A, Blute M, Roche P, Murphy GP. Prostate specific membrane antigen expression in prostatic intraepithelial neoplasia and adenocarcinoma: a study of 184 cases. *Cancer*. 1998; 82:2256–2261.
6. Evans JC, Malhotra M, Cryan JF, O'Driscoll CM. The therapeutic and diagnostic potential of the prostate specific membrane antigen/glutamate carboxypeptidase II (PSMA/GCPII) in cancer and neurological disease. *Br J Pharmacol*. 2016;173:3041–3079.
7. Barinka C, Rojas C, Slusher B, Pomper M. Glutamate carboxypeptidase II in diagnosis and treatment of neurologic disorders and prostate cancer. *Curr Med Chem*. 2012;19:856–870.
8. O'Keefe DS, Su SL, Bacich DJ, et al. Mapping, genomic organization and promoter analysis of the human prostate-specific membrane antigen gene. *Biochim Biophys Acta*. 1998;1443:113–127.
9. Rawlings ND, Barrett AJ. Structure of membrane glutamate carboxypeptidase. *Biochim Biophys Acta*. 1997;1339:247–252.
10. Silver DA, Pellicer I, Fair WR, Heston WDW, CordonCardo C. Prostate-specific membrane antigen expression in normal and malignant human tissues. *Clin Cancer Res*. 1997;3:81–85.

11. Liu H, Moy P, Kim S, et al. Monoclonal antibodies to the extracellular domain of prostate-specific membrane antigen also react with tumor vascular endothelium. *Cancer Res.* 1997;57:3629–3634.
12. Troyer JK, Beckett ML, Wright GL, Jr. Detection and characterization of the prostate-specific membrane antigen (PSMA) in tissue extracts and body fluids. *Int J Cancer.* 1995;62:552–558.
13. Rovenska M, Hlouchova K, Sacha P, et al. Tissue expression and enzymologic characterization of human prostate specific membrane antigen and its rat and pig orthologs. *Prostate.* 2008;68:171–182.
14. Sacha P, Zamecnik J, Barinka C, et al. Expression of glutamate carboxypeptidase II in human brain. *Neuroscience.* 2007;144:1361–1372.
15. Robinson MB, Blakely RD, Coyle JT. Quisqualate selectively inhibits a brain peptidase which cleaves N-acetyl-L-aspartyl-L-glutamate in vitro. *Eur J Pharmacol.* 1986;130:345–347.
16. Robinson MB, Blakely RD, Couto R, Coyle JT. Hydrolysis of the brain dipeptide N-acetyl-L-aspartyl-L-glutamate—identification and characterization of a novel N-acetylated alpha-linked acidic dipeptidase activity from rat-Brain. *J Biol Chem.* 1987;262:14498–14506.
17. Halsted CH, Ling EH, Luthi-Carter R, Villanueva JA, Gardner JM, Coyle JT. Folylpoly-gamma-glutamate carboxypeptidase from pig jejunum—molecular characterization and relation to glutamate carboxypeptidase II. *J Biol Chem.* 1998;273:20417–20424.
18. Hlouchova K, Navratil V, Tykvar J, Sacha P, Konvalinka J. GCPII variants, paralogs and orthologs. *Curr Med Chem.* 2012;19:1316–1322.
19. Pangalos MN, Neefs JM, Somers M, et al. Isolation and expression of novel human glutamate carboxypeptidases with N-acetylated alpha-linked acidic dipeptidase and dipeptidyl peptidase IV activity. *J Biol Chem.* 1999;274:8470–8483.
20. Bzdega T, Crowe SL, Ramadan ER, et al. The cloning and characterization of a second brain enzyme with NAAG peptidase activity. *J Neurochem.* 2004;89:627–635.
21. Hlouchova K, Barinka C, Konvalinka J, Lubkowski J. Structural insight into the evolutionary and pharmacologic homology of glutamate carboxypeptidases II and III. *FEBS J.* 2009;276:4448–4462.
22. Navratil M, Tykvar J, Schimer J, et al. Comparison of human glutamate carboxypeptidases II and III reveals their divergent substrate specificities. *FEBS J.* 2016;283:2528–2545.
23. Bacich DJ, Ramadan E, O'Keefe DS, et al. Deletion of the glutamate carboxypeptidase II gene in mice reveals a second enzyme activity that hydrolyzes N-acetyl-aspartylglutamate. *J Neurochem.* 2002;83:20–29.
24. Tsai G, Dunham KS, Drager U, et al. Early embryonic death of glutamate carboxypeptidase II (NAALADase) homozygous mutants. *Synapse.* 2003;50:285–292.
25. Han L, Picker JD, Schaevitz LR, et al. Phenotypic characterization of mice heterozygous for a null mutation of glutamate carboxypeptidase II. *Synapse.* 2009;63:625–635.
26. Gao Y, Xu S, Cui Z, et al. Mice lacking glutamate carboxypeptidase II develop normally, but are less susceptible to traumatic brain injury. *J Neurochem.* 2015;134:340–353.
27. Bacich DJ, Wozniak KM, Lu XCM, et al. Mice lacking glutamate carboxypeptidase II are protected from peripheral neuropathy and ischemic brain injury. *J Neurochem.* 2005;95:314–323.
28. Cao Y, Gao Y, Xu S, et al. Glutamate carboxypeptidase II gene knockout attenuates oxidative stress and cortical apoptosis after traumatic brain injury. *BMC Neurosci.* 2016;17:15.
29. Koscielny G, Yaikhom G, Iyer V, et al. The International Mouse Phenotyping Consortium Web Portal, a unified point of access for knockout mice and related phenotyping data. *Nucleic Acids Res.* 2014;42:D802–D809. Release 7.0.
30. Kasperek P, Krausova M, Haneckova R, et al. Efficient gene targeting of the Rosa26 locus in mouse zygotes using TALE nucleases. *FEBS Lett.* 2014;588:3982–3988.
31. Knedlik T, Vorlova B, Navratil V, et al. Mouse glutamate carboxypeptidase II (GCPII) has a similar enzyme activity and inhibition profile but a different tissue distribution to human GCPII. *FEBS Open Bio.* 2017;7:1362–1378.
32. Tykvar J, Sacha P, Barinka C, et al. Efficient and versatile one-step affinity purification of in vivo biotinylated proteins: expression, characterization and structure analysis of recombinant human glutamate carboxypeptidase II. *Protein Expr Purif.* 2012;82:106–115.
33. Barinka C, Rinnova M, Sacha P, et al. Substrate specificity, inhibition and enzymological analysis of recombinant human glutamate carboxypeptidase II. *J Neurochem.* 2002;80:477–487.
34. Rueden CT, Schindelin J, Hiner MC, et al. ImageJ2: ImageJ for the next generation of scientific image data. *BMC Bioinformatics.* 2017;18:529.
35. Tykvar J, Navratil V, Sedlak F, et al. Comparative analysis of monoclonal antibodies against prostate-specific membrane antigen (PSMA). *Prostate.* 2014;74:1674–1690.
36. Barinka C, Mlcochova P, Sacha P, et al. Amino acids at the N- and C-termini of human glutamate carboxypeptidase II are required for enzymatic activity and proper folding. *Eur J Biochem.* 2004;271:2782–2790.
37. Cermak T, Doyle EL, Christian M, et al. Efficient design and assembly of custom TALEN and other TAL effector-based constructs for DNA targeting. *Nucleic Acids Res.* 2011;39:e82.
38. Miller JC, Tan S, Qiao G, et al. A TALE nuclease architecture for efficient genome editing. *Nat Biotechnol.* 2011;29:143–148.
39. Yoshiki A, Moriwaki K. Mouse phenome research: implications of genetic background. *ILAR J.* 2006;47:94–102.
40. Olson EN, Arnold HH, Rigby PW, Wold BJ. Know your neighbors: three phenotypes in null mutants of the myogenic bHLH gene MRF4. *Cell.* 1996;85:1–4.
41. Pham CT, MacIvor DM, Hug BA, Heusel JW, Ley TJ. Long-range disruption of gene expression by a selectable marker cassette. *Proc Natl Acad Sci USA.* 1996;93:13090–13095.
42. Rais R, Jiang W, Zhai H, et al. FOLH1/GCPII is elevated in IBD patients, and its inhibition ameliorates murine IBD abnormalities. *JCI Insight.* 2016;1:e88634.
43. Caromile LA, Dortche K, Rahman MM, et al. PSMA redirects cell survival signaling from the MAPK to the PI3K-AKT pathways to promote the progression of prostate cancer. *Sci Signal.* 2017;10:eag3326.
44. Gros-Louis F, Kriz J, Kabashi E, et al. Als2 mRNA splicing variants detected in KO mice rescue severe motor dysfunction phenotype in Als2 knock-down zebrafish. *Hum Mol Genet.* 2008;17:2691–2702.
45. Kraemer N, Issa-Jahns L, Neubert G, et al. Novel alternative splice variants of mouse cdk5rap2. *PLoS ONE.* 2015;10:e0136684.
46. Finch CE, Girgis FG. Enlarged seminal vesicles of senescent C57BL-6J mice. *J Gerontol.* 1974;29:134–138.
47. Pettan-Brewer C, Treuting PM. Practical pathology of aging mice. *Pathobiol Aging Age Relat Dis.* 2011;1: 7202.
48. Donjacour AA, Thomson AA, Cunha GR. Enlargement of the ampullary gland and seminal vesicle, but not the prostate in int-2/Fgf-3 transgenic mice. *Differentiation.* 1998;62:227–237.
49. Bacich DJ, Pinto JT, Tong WP, Heston WD. Cloning, expression, genomic localization, and enzymatic activities of the mouse homolog of prostate-specific membrane antigen/NAALADase/folate hydroxylase. *Mamm Genome.* 2001;12:117–123.
50. Dyck MK, Gagne D, Ouellet M, et al. Seminal vesicle production and secretion of growth hormone into seminal fluid. *Nat Biotechnol.* 1999;17:1087–1090.
51. Ruberte Jose CA, Navarro M. *Morphological Mouse Phenotyping: Anatomy, Histology and Imaging.* Madrid: Medica Panamericana; 2017: 195–226.
52. Collard F, Vertommen D, Constantinescu S, Buts L, Van Schaftingen E. Molecular identification of beta-citrylglutamate hydrolase as glutamate carboxypeptidase 3. *J Biol Chem.* 2011;286:38220–38230.

53. Neuman BP, Eifler JB, Castaneres M, et al. Real-time, near-infrared fluorescence imaging with an optimized dye/light source/camera combination for surgical guidance of prostate cancer. *Clin Cancer Res*. 2015;21:771-780.
54. Kovar JL, Cheung LL, Simpson MA, Olive DM. Pharmacokinetic and biodistribution assessment of a near infrared-labeled PSMA-specific small molecule in tumor-bearing mice. *Prostate Cancer*. 2014;2014:104248.
55. Renneberg H, Friedetzky A, Konrad L, et al. Prostate specific membrane antigen (PSM) is expressed in various human tissues: implication for the use of PSM reverse transcription polymerase chain reaction to detect hematogenous prostate cancer spread. *Urol Res*. 1999;27:23-27.
56. Fisch H, Lambert SM, Goluboff ET. Management of ejaculatory duct obstruction: etiology, diagnosis, and treatment. *World J Urol*. 2006; 24:604-610.

How to cite this article: Vorlová B, Sedlák F, Kašpárek P, et al. A novel PSMA/GCPII-deficient mouse model shows enlarged seminal vesicles upon aging. *The Prostate*. 2018;1-14. <https://doi.org/10.1002/pros.23717>

APPENDIX 3

List of metabolites and their abbreviations used in targeted metabolomic analysis

| ABBREVIATION OF METABOLITE | FULL NAME OF METABOLITE |
|---|--|
| C01613_ST163...STACHYOSE | stachyose |
| C00149_ST039...MALATE | malate |
| C00021_ST253...SArhCYS | S-adenosylhomocysteine |
| C02378_ST095...6nh2HEXANOATE | 6-aminohexanoate |
| C3DC.C4OH | malonylcarnitine hydroxybutyrylcarnitine |
| C00026_ST310...oGLUTARATE | oxoglutarate |
| C00407_ST242...ILEU_ST241...aILE.II | isoleucine alloisoleucine |
| C00186_ST137...lactate | lactate |
| C02291_ST040...CYSTATHIONINE | cystathionine |
| C01157_ST236...hPRO | hydroxyproline |
| ST378...LEUCINATE | leucinate |
| C01152_ST134...mHIS_ST060...NmHIS | 3-methylhistidine N-methylhistidine |
| C03406_ST244...ARGSUCC | argininosuccinate |
| C00314_ST156...pyridoxine | pyridoxine |
| C16358_ST059...1mX | 1-methylxanthine |
| C00633_ST087...4ohBENZALDEHYDE | 4-hydroxybenzoate |
| C00158.C00311_ST051...CIT_ST184..iCIT | citrate isocitrate |
| C00357_ST361...NacGLCnh26P | N-acetylglucosamine 6-phosphate |
| C18 | octadecanoylcarnitine |
| C01152_ST060...NmHIS_ST134...3mHIS | N-methylhistidine 3-methylhistidine |
| C00042.C02170_ST023...SUCC_ST193...MMA | succinate methylmalonate |
| C18.1 | octadecenoylcarnitine |
| C01026.C03665_ST139 ...dimGLY_ST062...nh2isobutanoate | N,N-dimethylglycine 2-aminoisobutyric acid |
| C00103.C00446.C00092.C00085_ST334...GLC1P_ST402 ...GAL1P_ST333...GLC6P_ST369...FRU6P | glucose -1-phosphate galactose 1-phosphate glucose 6-phosphate fructose 6-phosphate |
| C00492.C01835.C08243_ST225...RAFFINOSE_ST185 ...MALTOTRIOSE_ST186...MELEZITOSE | raffinose maltotriose melezitose |
| C01456._ST027...TROPATE | tropate |
| C07086_ST428...PHEAC | phenylacetate |
| C00295_ST214...OA | orotic acid |
| C05607._ST414...PHELACT | phenyllactate |
| C00346_ST234...EtOHNH2P | ethanolamine phosphate |
| C00491_ST012...CYStine | cystine |

| ABBREVIATION OF METABOLITE | FULL NAME OF METABOLITE |
|---|--|
| C00334_ST025...4nh2BUTANOATE | 4-aminobutanoate |
| C01042_ST199...NAcASP | N-acetylaspartate |
| ST123...GLYALA | glycyl-alanine |
| C03299_C10 | decanoylcarnitine |
| C02630_ST375...ohGLUTARATE | hydroxyglutarate |
| C00122.C01585.C00141_ST048...FUM_ST283 ...CAPROATE_ST444...3m2oBUTANOATE | fumarate caproate 3-methyl-2-oxobutanoate |
| NAAG.I | N-acetyl-L-aspartyl-L-glutamate |
| ST391...phenylpropGly | phenylpropionylglycine |
| C08277_ST192...SEBACATE | sebacate |
| C00487_ST315...C0 | carnitine |
| C00114_ST308...CHOLINE | choline |
| C00073_ST010...MET | methionine |
| C02037_ST104...GLYGLY | glycyl-glycine |
| ST392...suberylGly | suberylglycine |
| C00099.C00041.C00213_ST005...bALA_ST022 ...ALA_ST237...sarcosine | beta-alanine alanine sarcosine |
| ST201...2ohisoVALERATE | 2-hydroxyisovalerate |
| C03017_C3 | propionylcarnitine |
| C01004_ST435...TRIGONELLINE | trigonelline |
| C08243.C00492.C01835_ST186...MELEZITOSE_ST225 ...RAFFINOSE_ST185...MALTOTRIOSE | melezitose raffinose maltotriose |
| C05402.C00089.C00243.C00208_ST151 ...MEL_ST177...SUC_ST231...LAC_ST162...MAL | melibiose sucrose lactose maltose |
| C16.2 | hexadecadienylcarnitine |
| C00093_ST069...GLYCEROL3P | glycerol 3-phosphate |
| ST393...hexGLY | hexanoylglycine |
| C02712_ST173...acMET | N-acetylmethionine |
| C00327_ST050...CITRUL | citrulline |
| C00906_ST254...dihydroT | dihydrothymine |
| C00153_ST224...NICOTINAMIDE | nicotinamide |
| C04677_STx04...AICAr | aminoimidazole carboxamide ribonucleoside |
| C5DC.C6OH | glutaryl carnitine hydroxyhexanoylcarnitine |
| ST395...tiglylGLY_ST390...3mCROTONYLGLY | tiglylglycine 3-methylcrotonylglycine |
| pABA.I | 4-Aminobenzoic acid |
| C4DC.C5OH | methylmalonylcarnitine 3-hydroxyisovalerylcarnitine |
| C02990_C16 | hexadecanoylcarnitine |
| C00294_ST209...Hr | inosine |
| C00170_ST304...5mthioAr | 5'-methylthioadenosine |
| C00020_ST135...AMP.pos | AMP |

| ABBREVIATION OF METABOLITE | FULL NAME OF METABOLITE |
|---|--|
| ST394...propGly | propionylglycine |
| C00148_ST007...PRO | proline |
| C01835.C00492.C08243_ST185...MALTRIOSE_ST225 ...RAFFINOSE_ST186...MELEZITOSE | maltotriose raffinose melezitose |
| ST442...LEULEU | leucyl-leucine |
| C04376_STx07...FGAr | N-formylglycinamide ribonucleoside |
| C00386_ST052...CARNOSINE | carnosine |
| ST412...NAcALA | N-acetylalanine |
| ST397_ST396...mbutGLY.ivalGLY | 2-methylbutyrylglycine isovalerylglycine |
| C00956_ST026...2nh2ADIPATE | 2-aminoadipate |
| C05984_ST325...ohBUTYRIC_ST143 ...ISOohBUTYRIC | hydroxybutyrate isohydroxybutyrate |
| C02862_C4 | butyrylcarnitine |
| C7DC.C8OH | pimelylcarnitine hydroxyoctanoylcarnitine |
| C00383.C01089_ST037...MALONATE_ST079 ...ohBUTANOATE | malonate 3-hydroxybutanoate |
| C02838_C8 | octanoylcarnitine |
| C00047_ST246...LYS | lysine |
| C01717_ST148...KYNURENATE | kynurenate |
| C05145_ST029...3nh2ISOBUTANOATE | 3-aminoisobutyrate |
| C01924_ST044...hARG | homoarginine |
| C03626_ST424...NNdimARG | N,N-dimethylarginine |
| C00526_ST249...dUR | deoxyuridine |
| PteGlu1.l | pteroylglutamate |
| C12.1 | dodecenoylcarnitine |
| C00019_ST252...sArMET | S-adenosylmethionine |
| C00475_ST286...Cr | cytidine |
| C10.1 | decenoylcarnitine |
| C00178_ST216...T | thymine |
| C00214_ST164...Tr | thymidine |
| ST389_ST388...ISObutGLY.butGLY | isobutyrylglycine butyrylglycine |
| C00262_ST208...HX | hypoxanthine |
| C02642_ST178...UREIDOPROPIONATE | ureidopropionate |
| C8.1 | octenoylcarnitine |
| C01620_ST433...THREONATE | threonate |
| C00559_ST205...dAr | deoxyadenosine |
| C00082_ST002...TYR | tyrosine |
| C00062_ST247...ARG | arginine |
| C00624_ST068...NacGLU | N-acetylglutamate |
| C00041.C00213.C00099_ST022...ALA_ST237 ...sarcosine_ST005...bALA | alanine sarcosine beta-alanine |
| C00898_ST030...TARTRATE | tartarate |
| C16.1 | hexadecenoylcarnitine |

| ABBREVIATION OF METABOLITE | FULL NAME OF METABOLITE |
|---|--|
| C00300.C00430_ST170...CREATINE_ _ST240 ...5nh2LEVULINATE | 5-aminolevulinate creatine |
| C5 | valerylcarnitine |
| C00931_ST351...PORPHOBILINOGEN | porphobilinogen |
| C00417_ST312...ACONITATE | aconitate |
| C00805.C00156_ST187...SALICYLATE_ _ST223 ...4ohBENZOATE | salicylate 4-hydroxybenzoate |
| C02571_C2 | acetylcarnitine |
| C05588_ST089...METANEPHRINE | metanephrine |
| C14.2OH | hydroxytetradecadienylcarnitine |
| C00330_ST204...dGr | deoxyguanosine |
| PSI198 | N-acetyl-p-aminobenzoylglutamate |
| C00847_ST440...4.pyridoxate | 4-pyridoxate |
| pABG | 4-Aminobenzoyl-glutamate |
| C00719_ST101...BET | betaine |
| BCG.I | β -citril-L-glutamate |
| C00255_ST189...RIBOFLAVIN | riboflavin |
| C00455_ST305...NAMN | nicotinamide mononucleotide |
| C00385_ST207...X | xanthine |
| C01762_ST198...Xr | xanthosine |
| C01035_ST063...GuaBUTANOATE | 4-guanidinobutanoate |
| C00123_ST243...LEU.II | leucine |
| C00299_ST218...UR | uridine |
| ST109...PHENYLSER | phenylserine |
| C00152_ST021...ASN | asparagine |
| C00993_ST111...ALAALA | alanyl-alanine |
| C00212_ST210...Ar.pos | adenosine |
| C00036.C00489_ST321...oxaloacetate_ _ST047 ...glutarate_ST080...ethylmalonate | oxaloacetate glutarate ethylmalonate |
| C6 | hexanoylcarnitine |
| C00137_ST171...MYOINOSITOL | myoinositol |
| C00864_ST008...PANTHOTENATE | panthotenate |
| C00884_ST248...hCARNOSINE | homocarnosine |
| C00031.C00095.C00124.C00159_ST096 ...GLC_ST097...FRU_ST195...GAL_ST197...MAN | glucose fructose galactose manose |
| C19910_ST232...SIALIC | sialic acid |
| C10.2 | decadienylcarnitine |
| STx01...SAR | succinyladenosine |
| C02714_ST057...NAcPut | N-acetylputrescine |
| C01697.C00392_ST302 ...GALACTITOL_ST420...MANITOL | galactitol manitol |
| C00128_ST301...CMPNAcNEURAMINATE | CMP-N-acetylneuraminate |
| C00532.C00474_ST158 ...ARABITOL_ST423...RIBITOL | arabitol ribitol |

| ABBREVIATION OF METABOLITE | FULL NAME OF METABOLITE |
|--|---|
| C00245_ST159...TAU | taurine |
| C00257_ST165...GLUCONATE | gluconate |
| C00380_ST153...C | cytosine |
| C00135_ST015...HIS | histidine |
| C05635_ST343...ohINDOLAc | 5-hydroxyindoleacetate |
| C00037_ST239...GLY | glycine |
| C12 | dodecanoylcarnitine |
| C14 | tetradecanoyl-L-carnitine |
| C00064_ST238...GLN | glutamine |
| ST425...INDOLEPROPIONATE | indolepropionate |
| C05589_ST035...NORMETANEPHRINE | normetanephine |
| C00352_ST355...GLCnh2P | glucosamine 6-phosphate |
| C00049_ST235...ASP | aspartate |
| C00147_ST206...A | adenine |
| C00581_ST251...GuaAc | guanidinoacetate |
| C01879.C00408_ST161 ...oPRO.l.a.II.pos_ST031...PIPECOLATE | oxorpoline pipecolate |
| C03479_ST152...5formylTHF | 5-formyltetrahydrofolate |
| C00078_ST003...TRP | tryptophan |
| C01019_ST146...FUCOSE | fucose |
| C00183_ST001...VAL | valine |
| C00144_ST262...GMP.pos | GMP |
| C00188.C00263_ST004...THR_ST160...hSER | threonine homoserine |
| C00065_ST006...SER | serine |
| C14.1 | tetradecenoyl-L-carnitine |
| ST413...furoylGly | furoylglycine |
| C00387_ST211...Gr | guanosine |
| C05587_ST368...METHOXYTYRAMINE | methoxytyramine |
| ST427...INDOXYLSULFATE | indoxylsulfate |
| C02242_ST439...7mG | 7-methylguanine |
| C00310_ST036...XYLULOSE | xylulose |
| C00121_ST138...RIB | ribose |
| C00079_ST245...PHE | phenylalanine |
| C4.1 | butenylcarnitine |
| C00429_ST183...dihydroU | dihydrouracil |
| C02348_ST437...ALLANTOIN | allantoin |
| C00191_ST092...GLUCURONATE | glucuronate |
| C00106_ST215...U | uracil |
| C00645.C01132.C00140_ST341...NAcMANnh2_ST028 ...NAcGALnh2_ST380...NAcGLCnh2 | N-acetylmannosamine N-acetylgalactosamine N-acetylglucosamine |
| C00025_ST018...GLU | glutamate |
| C00750_ST041...SPERMINE | spermine |
| C02067_ST217...pseuUR | pseudouridine |
| C01586_ST053...HIPPURATE | hippurate |

| ABBREVIATION OF METABOLITE | FULL NAME OF METABOLITE |
|-----------------------------------|---|
| C05629_ST415...hCINNAMATE | hydrocinnamate |
| C00440_ST353...5mTHF | 5-methyltetrahydrofolate |
| C04823_STx03...SAICAr | SAICA riboside |
| C08278_ST188...SUBERATE | suberate |
| C04734_STx05...FAICAr | 5-formamidoimidazole-4-carboxamide riboside |
| C00329_ST179...GLCnh2 | glucosamine 6-phosphate |
| C00791_ST219...CREATININE | creatinine |

